# Identification and characterization of genetic drivers of central nervous system primitive neuroectodermal tumors, medulloblastoma, and neuroblastoma.

A DISSERTATION
SUBMITTED TO THE FACULTY OF THE GRADUATE SCHOOL
OF THE UNIVERSITY OF MINNESOTA
BY

**Pauline Joanne Beckmann**

IN PARTIAL FULFILLMENT OF THE REQUIREMENTS
FOR THE DEGREE OF
DOCTOR OF PHILOSOPHY

Dr. David A. Largaespada

July 2018

**Acknowledgements**

In addition to Pauline J. Beckmann, the following people contributed to the work described in this thesis:

Jon D. Larson, Alex T. Larsson, Jason P. Ostergaard, Sandra Wagner, Eric P. Rahrmann, Ghaidan A. Shamsan, George M. Otto, Rory L. Williams, Barbara R. Tschida, Paramita Das, Adrian M. Dubuc, Branden S. Moriarity, Daniel Picard, Xiaochong Wu, Fausto J. Rodriguez, Quincy Rosemarie, Ryan D. Krebs, Amy M. Molan, Addison M. Demer, Michelle M. Frees, Anthony E. Rizzardi, Stephen C. Schmechel, Charles G. Eberhart, Robert B. Jenkins, Dave J. Odde, Annie A. Huang, Michael D. Taylor, Aaron L. Sarver, Gonzalo G. Lopez, Emily J. Pomeroy, John M. Maris, and David A. Largaespada.

Contributions:

PJB, JDL, ALS, and DAL contributed to the study concept in Chapter 2.

PJB and DAL contributed to the study concept in Chapter 3.

PJB, GGL, JMM, and DAL contributed to the study concept in Chapter 4.

PJB, JDL, ALS, BRT, and DAL obtained funding.

PJB wrote the thesis.

Data acquisition and analysis contributions by chapter:

Chapter 2

PJB and DAL contributed to Figures 2.1 to 2.18

JDL contributed to Figures 2.1 to 2.3, 2.6, 2.7, 2.9-2.11

ALS contributed to Figures 2.4, 2.6, 2.8, 2.9, 2.12, and 2.14

ATL contributed to Figures 2.12 to 2.16

JPO contributed to Figures 2.13, 2.14, 2.16, 2.17

GAS contributed to Figures 2.12 and 2.14

GMO and RLM contributed to Figure 2.17

DP contributed to Figure 2.5

Chapter 3

PJB and DAL contributed to Figures 3.1 to 3.7

ATL contributed to Figures 3.5 and 3.6

JPO and RDK contributed to Figure 3.7

Chapter 4

PJB and DAL contributed to Figures 4.1 to 4.7

GGL contributed to Figure 4.1 and 4.2

ATL contributed to Figures 4.3 and 4.5

EJP contributed to Figure 4.3

JPO contributed to Figure 4.5

This work was supported by the University of Minnesota Genomics Center, the University of Minnesota Biology Materials Procurements Network, the Research Animal Resources, and the University Imaging Centers that are supported by the National Cancer Institute.

**Dedication**

I dedicate the time and effort put into this work to my family. To my dad for always supporting me and being my biggest fan. To my mom for instilling a sense of confidence in me to get me through anything and being my constant friend. To my brother for being my partner in crime when we were young and helping to shape my love for science. To Dom for standing by me through all of the stress, weekend lab visits, and vacationless years. To Cindy and Paul, for your extra help with Jeffrey and support through this time. And finally, to my son Jeff, for the motivation you have given me. You make me want the world to be a better place for you.

**Abstract**

Medulloblastoma, central nervous system primitive neuroectodermal tumors (CNS-PNETs), and neuroblastoma are cancers that affect the nervous system primarily in children. Current treatment strategies with severe long-term treatment-related side effects and dismal survival rates warrant further study into therapies with increased efficacy and lower cost to the patient. Targeted therapy represents a route to better treatments, but a barrier to identifying novel targets is the lack of appropriate animal models. To fill this void, we created a mouse model of medulloblastoma and CNS-PNET using *Sleeping Beauty* (*SB*) mutagenesis of neural progenitor cells (Nestin+). Importantly, *SB*-induced tumors resembled human medulloblastoma and CNS-PNET in location and histology. Additionally, we used RNA-Sequencing to determine that they most closely resemble human Sonic Hedgehog (SHH), group 3, and group 4 medulloblastoma and a subgroup of CNS-PNET with *FOXR2* activation (CNS NB-*FOXR2*). Using both DNA and RNA analyses, we identified over 100 genes as candidate drivers in medulloblastoma and/or CNS-PNET. Of these genes, we focused on validating 3 proto-oncogenes, *Megf10*, *Arhgap36*, and *Foxr2*. All 3 drove soft agar colony formation and tumor formation in mice, suggesting they are bona fide oncogenes. In further studies of *ARHGAP36*, we found that it promoted Shh signaling, did not affect RhoA activation, and that its 5 isoforms had distinct effects both *in vitro* and *in vivo*. We found that FOXR2 bound C-MYC and N-MYC and increased C-MYC stability. Additionally, in the context of neuroblastoma, increased *FOXR2* expression was mutually exclusive with *MYCN* amplification, further suggesting an important interaction between FOXR2 and MYC family transcription factors. We also found a novel role for FOXR2 in activating the FAK/SRC signaling pathway. Increased FOXR2 drove FAK/SRC activation and *FOXR2* KO decreased FAK/SRC activation. Interestingly, increased FOXR2 expression conveyed resistance to a SRC family kinase inhibitor (Dasatinib) in a MYC-dependent manner, indicating overlap between these two apparently distinct effects. In conclusion, this study identifies several promising therapeutic targets for treatment of patients with medulloblastoma, CNS-PNET, and neuroblastoma.

**Table of contents** **Page**

**List of tables**

**List of figures**

Chapter 3. Page



Chapter 4. Page

**List of abbreviations**

| Term | Abbreviation |
|---|---|
| Adenomatosis polyposis coli | APC |
| Alpha thalassemia/mental retardation syndrome X-linked | ATRX |
| Amino acid | AA |
| Anaplastic lymphoma kinase | ALK |
| Athymic nude, nu/nu mice | NU/J |
| ATP binding cassette subfamily B member 1 | ABCB1 |
| Avian leucosis virus | ALV |
| Avian leucosis viral receptor | TV-A |
| Axin protein | AXIN |
| B cell leukemia/lymphoma 2 | BCL2 |
| B cell leukemia/lymphoma 6 | BCL6 |
| Baculoviral IAP repeat containing 5 | BIRC5 |
| BCL6 corepressor | BCOR |
| Brain lipid-binding protein | Blbp |
| Breast cancer 2 | Brca2 |
| Calmodulin binding transcription activator 1 | CAMTA1 |
| cAMP responsive element binding protein | CREB |
| Casein kinase 2 beta | CSNK2B |
| CASP8 and FADD like apoptosis regulator | CFLAR |
| Castor zinc finger 1 | CASZ1 |
| Catenin beta 1, β-Catenin | CTNNB1 |
| Cell division cycle 42 | CDC42 |
| Central nervous system | CNS |
| Central nervous system primitive neuroectodermal tumor | CNS-PNET |
| Chromodomain helicase DNA binding protein 5 | CHD5 |
| Chromosome 19 miRNA cluster | C19MC |
| Cluster of differentiation 109 | CD109 |
| Cluster of differentiation 133 | CD133 |

| | |
|---|---|
| Clustered regularly interspaced short palindromic repeats | CRISPR |
| CNS high-grade neuroepithelial tumor with BCOR alteration | CNS HGNET-BCOR |
| CNS high-grade neuroepithelial tumor with MN1 alteration | CNS HGNET-MN1 |
| Colorectal cancer | CRC |
| Common insertion site | CIS |
| CREB binding protein | CREBBP |
| CRISPR associated protein 9 | Cas9 |
| Cre recombinase | Cre |
| Cre recombinase linked to estrogen receptor | Cre-ER |
| Cyclic adenosine monophosphate, cyclic AMP | cAMP |
| Cyclin D1 | CCND1 |
| Cyclin D2 | CCND2 |
| Cyclin dependent kinase 4 | CDK4 |
| Cyclin dependent kinase 6 | CDK6 |
| Cyclin dependent kinase inhibitor 2A | CDKN2A |
| Cyclin dependent kinase inhibitor 2B | CDKN2B |
| Cyclin dependent kinase inhibitor 2C | CDKN2C, Ink4c |
| DEAD-box helicase 3 X-linked | DDX3X |
| Deoxyribonucleic acid | DNA |
| DNA ligase IV | Lig4 |
| Dominant negative p53 | DNp53 |
| Embryonal tumor with multilayered rosettes | ETMR |
| Embryonal tumors with abundant neuropil and true rosettes | ETANTR |
| Endometrial adenocarcinoma | EAC |
| Ependymoblastoma | EB |
| Epithelial mesenchymal transition | EMT |
| Eomesdermin | EOMES |
| External granule layer | EGL |
| Extracellular matrix | ECM |
| Ewing sarcoma family tumor with CIC alteration | CNS EFT-CIC |

| | |
|---|---|
| FK506 binding protein 1 | FKBP1A |
| Focal adhesion kinase | FAK |
| Forkhead box C2 | FOXC2 |
| Forkhead box M1 | FOXM1 |
| Forkhead box R1 | FOXR1 |
| Forkhead box R2 | FOXR2 |
| gamma-Aminobutyric acid | GABA |
| Gain of function | GOF |
| *Glt-1* driven MycN and luciferase mouse model | GTML |
| Glioma-associated oncogene family zinc finger 1 | GLI1 |
| Glioma-associated oncogene family zinc finger 2 | GLI2 |
| Glycogen synthase kinase 3 beta | GSK3β |
| Granule neuron precursor cells | GNPCs |
| Growth factor independent 1 | GFI1 |
| Growth factor independent 1B | GFI1B |
| GTPase activating protein | GAP |
| Guanine nucleotide exchange factor | GEF |
| Hepatocellular carcinoma | HCC |
| Hepatocyte growth factor | HGF |
| Histone acetyltransferase | HAT |
| Hypermethylated in cancer 1 | HIC1 |
| Hypoxia inducible factor 1 subunit alpha | HIF-1α |
| Hypoxia inducible factor 2 subunit alpha | HIF-2α |
| Insulin like growth factor 2 | IGF2 |
| Internal granule layer | IGL |
| Internal ribosomal entry site | IRES |
| Inverted repeat/directed terminal repeat | IR/DR |
| Isocitrate dehydrogenase 1 | IDH1 |
| Kinase inhibitor proteins | PKI |
| Kinesin family member 1B | KIF1B |

| | |
|---|---|
| Kirsten rat sarcoma viral oncogene homolog | KRAS |
| Knotted interacting protein 1 | Kip1 |
| Kynurenine-oxoglutarate transaminase 3 | KAT3 |
| LIM homeobox transcription factor 1 alpha | LMX1A |
| Lysine (K)-specific demethylase 6A | KDM6A |
| Malignant peripheral nerve sheath tumors | MPNSTs |
| Matrix metallopeptidase 7 | MMP7 |
| Matrix metallopeptidase 14 | MMP14 |
| Medulloblastoma | MB |
| Medulloepithelioma | ME |
| Mitogen activated kinase-like protein | MAPK |
| Mouse atonal homolog 1 | Math1 |
| Mouse double minute 2 homolog | MDM2 |
| Mouse double minute 4 homolog | MDM4 |
| mutL homolog 1 | MLH1 |
| mutS homolog 2 | MSH2 |
| Multiple EGF like domains 10 | Megf10 |
| MYC associated factor X | MAX |
| Myelocytomatosis oncogene, cellular | MYC, C-MYC |
| Myelocytomatosis oncogene, neuroblastoma derived | MYCN, N-MYC |
| Myelocytomatosis oncogene, lung carcinoma derived | MYCL, L-MYC |
| Myelocytomatosis oncogene, viral origin | v-myc |
| Non-small cell lung cancer | NSCLC |
| Neuroblastoma | NB |
| Neuroblastoma ras oncogene | NRAS |
| Nestin-driven avian leucosis viral receptor | Ntv-a |
| Nonobese diabetic/severe combined immunodeficiency | NOD-SCID |
| Not otherwise specified | NOS |
| Nuclear factor kappa B | NF-κB |
| Oligo-neural progenitor cells | OPCs |

| | |
|---|---|
| Orthodenticle homeobox 2 | OTX2 |
| Overexpression | OE |
| Paired like homeobox 2b | PHOX2B |
| Peroxisome proliferator activated receptor delta | PPARD |
| Phosphoinositol-4,5-bisphosphate-3-kinase | PI3K |
| Phosphoinositol-4,5-bisphosphate-3-kinase catalytic subunit | Pik3ca |
| Phosphatase and tensin homolog | PTEN |
| Plasmacytoma variant translocation 1 | PVT1 |
| PMS1 homolog 2 | PMS2 |
| Poly(ADP-ribose) polymerase 1 | Parp1 |
| PR/SET domain 6 | PRDM6 |
| Protein kinase A | PKA |
| Protein patched homolog 1 | PTCH1 |
| Protein patched homolog 2 | PTCH2 |
| Rac family small GTPase 1 | RAC1 |
| Ras homolog family member A | RHOA |
| Rho GTPase activating protein 36 | ARHGAP36 |
| Ribonucleic acid | RNA |
| Signal transducer and activator of transcription 1 | Stat1 |
| Signal transducer and activator of transcription 2 | Stat2 |
| Sleeping Beauty | SB |
| Snail family transcriptional repressor 1 | SNAI1 |
| Snail family transcriptional repressor 2 | SNAI2 |
| Smoothened | SMO |
| Sonic hedgehog | SHH |
| Suppressor of fused | SUFU |
| Switch/sucrose non-fermentable | SWI/SNF |
| Synuclein alpha interaction protein | SNCAIP |
| Replication-competent, avian retroviral vector | RCAS |
| Telomerase reverse transcriptase | TERT |

| | |
|---|---|
| Tumor protein p53 | TP53 |
| Transformation related protein 53 | Trp53 |
| Transforming growth factor beta | TGF-β |
| Twist basic helix-loop-helix transcription factor 2 | TWIST2 |
| Ubiquitin specific peptidase 4 | USP4 |
| Vascular endothelial growth factor | VEGF |
| Ventricular zone | VZ |
| Wingless | WNT |
| World Health Organization | WHO |
| X-ray repair cross complementing 2 | Xrcc2 |
| X-ray repair cross complementing 4 | Xrcc4 |
| Zinc finger E-box binding homeobox 1 | ZEB1 |
| Zinc finger E-box binding homeobox 2 | ZEB2 |

# Chapter 1: Introduction

Genetic drivers of medulloblastoma, central nervous system primitive neuroectodermal tumors, and neuroblastoma

1. Medulloblastoma
    a. Overview

Medulloblastoma (MB) is an embryonal tumor of the cerebellum and the most common malignant brain tumor to affect children(1). As is common with embryonal tumors, MB is rarely seen in adults. Most patients present with ataxia and symptoms corresponding to hydrocephalus due to the tumor obstructing the fourth ventricle and/or cerebral aqueduct. Current treatment involves maximal surgical resection of the tumor, chemotherapy, and radiation, resulting in approximately 65% disease free survival over 5 years(2). Embryonal tumors, like MB, are known to spread through the cerebrospinal fluid and re-attach on the brain and spinal cord. Thus, whole-brain and spinal irradiation became a standard component of post-operative treatment and significantly increased survival(3). However, long-term quality of life outcomes of children, particularly those under 3 years of age, with MB and radiation therapy are very poor(4). The cerebellum plays critical roles in motor skills, coordination, and cognition(5,6). Co-morbidities associated with MB treatment include secondary tumors, neurological and neuropsychological dysfunction, endocrine complications, growth retardation, spinal deformities, and social impairment(7-12). Development of chemotherapy strategies to delay or avoid radiation in infants (<3 years) have decreased neurocognitive loss in these young patients(13). Clinical trials are also underway to reduce or completely remove radiation in low risk MB (NCT02724579, NCT02212574), but more targeted therapy is needed to increase efficacy and decrease side effects.

MB was first described as a distinct tumor type in 1925, distinguished from glioma by cerebellar location and a very consistent histology of small, blue cells(14). In the 2007 revision, the WHO classified MB into 5 main subtypes by histology: classic(~70% of MB), large cell (10 to 22%), anaplastic (2 to 4%, large cell and anaplastic are often group together as large cell anaplastic), desmoplastic nodular (7%), and medulloblastoma with extensive nodularity(3%)(15,16). Of these groups, large cell anaplastic have been associated with the worst prognosis and desmoplastic nodular have the most favorable outcomes. Subsequently, MB has been classified into 4 distinct subgroups based on molecular characteristics(17) and the current 2017 WHO lists Sonic Hedgehog (SHH), Wingless (WNT), Group 3, and Group 4 as the 4 molecular subtypes

of MB(18). WNT and SHH subgroup MB are characterized by mutations activating those signaling pathways, while driver mutations in Group 3 and Group 4 are less known. Clinical outcome varies with subgroup; patients with WNT subgroup MB have an excellent prognosis, with over 90% survival over 5 years, Group 3 tumors carry the poorest prognosis (~45% 5 year overall survival), and SHH and Group 4 tumors are intermediate (60% and 75% for SHH and Group 4, respectively)(19,20). There is some overlap between the histologically and molecularly-driven subgroups; WNT subgroup MBs are typically classic, with rare presentation of large cell anaplastic histology(19). SHH tumors are almost always desmoplastic nodular, but can also present with classic or large cell anaplastic histology. Group 3 and group 4 both typically present with classic or large cell anaplastic histology(19).

b. Known drivers of medulloblastoma

i. Familial syndromes

Although inherited MB is extremely rare, four familial syndromes have been associated with increased MB development. Patients with inactivating mutations in *PTCH1*, known as Gorlin syndrome, have a resultant high level of SHH pathway activation(21,22). Activated SHH signaling predisposes patients with Gorlin syndrome to developing a number of tumor types, including MB, with a lifetime risk of developing MB of 4%(23,24). Over 400 unique mutations in the *PTCH1* locus have been identified in humans, ranging from single base missense or nonsense mutations to large deletions or duplications(25). The function of PTCH is to inhibit activation of the SHH signaling pathway through inhibition of Smoothened (SMO). When PTCH is mutated, SMO is able to translocate to the primary cilia and promote GLI-dependent transcription of SHH pathway effector genes including *GLI1*, *PTCH1*, *PTCH2*, *FOXM1*, *MYCN*, *CCND1* and *CCND2*(26). GLI1, PTCH1 and PTCH2 participate in fine-tuning of SHH signals as members of positive (GLI1) and negative (PTCH1 and PTCH2) feedback loops. Upregulation of N-MYC, Cyclin D/E and FOXM1 promotes cell proliferation. Other SHH-induced genes promote cellular survival (*BCL2* and *CFLAR*) and epithelial to mesenchymal transition (*SNAI1*, *SNAI2*, *ZEB1*, *ZEB2*, *TWIST2*, and *FOXC2*(26).

Turcot syndrome Type II, characterized by a germline mutation in *Adenomatous Polyposis Coli* (*APC*), results in uncontrolled WNT signaling and increased risk for

colorectal cancer and MB(27). APC is a negative regulator of the WNT signaling pathway; it forms a complex with AXIN and GSK3β to promote phosphorylation and degradation of β-Catenin(28). *APC* mutations typically lead to formation of a truncated protein lacking its native regulatory ability, resulting in accumulation of β-Catenin and increased β-Catenin-dependent transcription(29). Targets of β-Catenin include genes involved in several processes related to cancer, including proliferation (*MYC*, *CCND1*, *PPARD*), survival (*ABCB1*, *BIRC5*), migration (*MMP7*, *MMP14*), and angiogenesis (*VEGF*)(30-37).

Patients with Li-Fraumeni syndrome present with several cancer types, including MB, driven by germline mutation of the *TP53* gene(38,39). p53 plays a central role as a regulator in numerous cellular and developmental processes and is a well-established tumor suppressor gene. p53 senses signs of cellular stress, including DNA damage, oxidative stress, hypoxia and hyperproliferation(40) and is displaced from two negative regulators, MDM2 and MDM4, resulting in its stabilization and activation(41). When activated, p53 functions as a transcription factor, regulating expression of target gene sets involved in cell-cycle arrest, senescence, and apoptosis(42-44). Most *TP53* mutations are missense mutations (80%) affecting the DNA-binding domain and preventing its regulatory function.

Germline mutations in *CREBBP* (CREB-binding protein) result in Rubinstein-Taybi syndrome, a developmental disorder which predisposes affected individuals to central nervous system malignancies, including MB(45,46). CREBBP is a member of the KAT3 histone acetyltransferase (HAT) family and is involved in a wide variety of processes, although its mechanism of action is not completely understood. *CREBBP* is most commonly mutated in a heterozygous state (commonly truncating point mutations in the HAT domain), leaving a functional wild type allele. These mutations impair its ability to catalyze acetylation of its target genes, which include TP53, BCL6 and KRAS(47,48).

ii. Sporadic medulloblastoma

Somatic gene mutation contributes to a much larger portion of human MB development than familial forms, and several, sophisticated next-generation sequencing studies of human tumors have identified common changes in the MB genome(49-54).

The largest study also included epigenetic and transcriptomic data to further characterize changes in gene expression(55). In this study, WNT subgroup MB mostly commonly contained mutations in *CTNNB1*(86%), monosomy chromosome 6 (signature chromosomal alteration in WNT MB, 83%), *CSNK2B* (an activator of WNT signaling, 14%), and subunits of the SWI/SNF complex (33%)(55). Another common mutation in this subgroup is *DDX3X*, a putative RNA helicase involved in regulation of chromosomal segregation and cell cycle progression(53). *PTCH1* and *SUFU* (Suppressor of Fused, another negative regulator of SHH) are the most commonly mutated genes in SHH MB, along with activating mutations in *SMO* and focal amplifications of *GLI2* and *MYCN*(55). Homozygous loss of *PTEN* and *CDKN2A/B* are also frequent in SHH MB(54). Promoter mutations driving telomerase reverse transcriptase (*TERT*) expression and *IDH1* mutations are seen in SHH MB(55,56). Finally, *TP53* mutations are enriched in WNT and SHH MB (16% and 24%, respectively), with little occurrence in Group 3 and 4(57).

Although group 3 and 4 MB retain generic names as little is known about their true drivers, recent studies have implicated some important pathways in these cancers. Group 3 MBs commonly carry *MYC* amplifications (17%), while *MYCN* amplification is present equally in group 3 and 4 tumors (5 and 6%, respectively)(55). Translocation events resulting in fusion of the *PVT1* locus, a long noncoding RNA thought to stabilize the MYC protein, to the coding sequence of *MYC* accounts for the majority of these *MYC* amplifications(54). Overexpression of GFI1 family transcription factors is also present in a subset of group 3 MB(51). Several components and effectors of the TGF-β pathway, including *OTX2*, *CD109*, and *FKBP1A*, are also mutated in group 3 MB(54). Group 3 MB characteristically have unstable genomes, with frequent large chromosomal gains and losses; isochromosome 17q is a frequent example of this, with concurrent loss of chromosome 17p and gain of 17q. Isochromosome 17q is also extremely common in group 4 tumors. Homozygous deletions in *KDM6A,* a histone-lysine demethylase, have been associated with group 4 MB(54). NF-ϰB signaling has also been implicated in group 4 MB, as deletions in regulators of NF-ϰB signaling, *NFKBIA* and *USP4,* have been identified in this subgroup(54). Other common alterations include tandem duplication of *SNCAIP*, amplification of *CDK6*, and overexpression of *PRDM6*(55).

c. Targeted therapies for medulloblastoma

i. Overview

In an effort to increase the effectiveness of MB therapy and decrease side effects, targeted therapies have been sought for MB. As we continue to develop a more complete understanding of the molecular heterogeneity of MB, it becomes clear that targeted therapy is unlikely to work across the 4 distinct subgroups of MB. To date, targeted therapies have been identified and tested in patients with SHH MB.

ii. Targeted therapies for SHH medulloblastoma

Targeted therapies for SHH pathway activation represent the options for patients with MB. SMO is the principle target for the development of SHH pathway inhibitors. Cyclopamine, a natural steroidal alkaloid, was the first SMO inhibitor to be used in clinical trials for basal cell carcinoma(58). Although cyclopamine application resulted in rapid tumor regression, cyclopamine cannot be administrated orally due to poor solubility and toxicity(59). Several other SMO inhibitors have made it to clinical trials, including NVPLDE-225(Erismodegib), Cur61414, and GDC-0449(vismodegib)(60-63).

GDC-0449 was the first SHH inhibitor to reach clinic trials for brain tumors in 2008, which resulted in rapid MB regression followed by rapid disease progression(61). Subsequent studies by different groups were done with GDC-0449 to determine its appropriate dosage in adult and pediatric populations and determine effectiveness treating patients with recurrent or refractory MB (Table 1.1). In one phase 2 study, GDC-0449 was effective in 41% of SHH MB, but not in other subgroups(64). Those SHH MBs that were not responsive had activating mutations downstream from SMO. Currently, GDC-0449 is the only targeted SMO inhibitor in clinical trials for MB, either in combination with temozolomide or alone as a frontline therapy immediately after surgery.

Another well-studied SMO inhibitor is LDE225 (Sonidegib). Several phase 1 and 2 trials have been performed in adult and pediatric patients with recurrent or refractory MB (Table 1.1). A phase 2 trial carried out in children and adults with SHH MB saw a modest response in the majority of patients, but some patients did have durable responses (125 to 503 days)(65). Unfortunately, while SMO inhibitors often have low acute side effects due to a lack of SMO in most tissues(66), treatment of pediatric patients is likely to have long term side effects as the SHH pathway is very important during development. For example, GDC-0449 results in short stature and irreversible growth plate fusion(67).

Not all MB with activated SHH signaling will respond to SMO inhibitors, as activation of downstream pathway members, like GLI2 or SUFU, can result in immediate or secondary resistance to SMO inhibitors. One ongoing trial involves the use of a Gli1 antagonist, Genistein, in MB (NCT02624388). Other mechanisms of SMO resistance also occur, including mutations in SMO resulting in a conformational change or activation of other pathways, such as PI3K, to allow tumor cells to growth without SHH pathway activation(68,69).

d. Models of medulloblastoma in mice

i. Overview

Mouse models have been critical to the advancement of cancer biology research. As mammals, mice are similar to humans but much less expensive to house than other mammals. Mouse genetics are easily manipulated, which allows the study of how specific genetic alterations lead to tumor development within an intact microenvironment. More sophisticated mouse models allow evaluation of altered oncogene expression at different points in tumor development. Use of the tetracycline-inducible systems, for example, allows control of these time elements to modify the expression of an oncogene or tumor suppressor(70,71). Recombination-dependent transgene construction allows tissue-specific expression through promoter modification of the site-specific bacterial Cre recombinase enzyme. A modified version of Cre linked to a mutated binding domain of the human estrogen receptor (Cre-ER) is another method of controlling gene expression(72). These systems overcome some limitations associated with conventional genetically engineered mouse models, such as embryonic lethality. Mice with immune system deficiencies, like NU/J mice which lack T cells, allow for xenograft or cell line injection studies, facilitating expedited results and analysis of human tissues. As the most common malignant pediatric brain tumor, MB has been rather extensively studied in mice (Table 1.1).

In order to generate the most accurate mouse models of human tumors, it is necessary to identify the tumor's cell of origin and target that cell for transformation. The cell(s) of origin for MB has been long thought to be a transient member of the developing cerebellum, although the exact nature of these populations and how they vary remains to be fully elucidated. The cells of the cerebellum arise from two distinct germinal zones,

the primary germinal zone on the roof of the fourth ventricle (ventricular zone (VZ) cells), and granule neuron precursor cells (GNPCs) that arise within the rhombic lip. VZ cells give rise to GABAergic neurons, including Purkinje cells and GABAergic interneurons. GNPCs migrate from the rhombic lip across the cerebellum to form the external granule layer (EGL). Nestin, an intermediate filament protein used as a marker for central nervous system (CNS) progenitor cells, is expressed throughout the developing brain until EGL development(73). While in the EGL, GNPCs respond to SHH signaling activation and undergo proliferation followed by migration inward, through the Purkinje cell layer, to form the mature neurons of the internal granule layer (IGL)(74). While in the EGL, GNPCs express MATH1, a transcription factor, which ceases upon maturity and inclusion in the IGL. This process takes approximately 2 years for humans and 2 weeks for mice after birth(16).

The four subgroups of MB are thought to originate from distinct cell types(16,75,76). In mice, committed GNPCs are the cell of origin of SHH MB(77,78) and cells within the lower rhombic lip are the cell of origin for WNT MB(76). A third group of stem cells located in the white matter of the postnatal cerebellum was identified(79) and shown to give rise to group 3 MB(80). The cell of origin for group 4 MB is still undetermined, but analysis of superenhancers has suggested that group 4 tumors may originate from *EOMES* and *LMX1A* expressing precursor cells in the upper rhombic lip(81).

ii. Shh subgroup medulloblastoma

Shh subgroup MBs represent the large majority of mouse MB models by far (Table 1.1). There are several genetic models resulting in the loss of *Ptch1* activity and development of MB(78,82). *Ptch1* loss has also been combined with other mutations, including $Tp53^{-/-}$, $Ink4c^{-/-}$, $Kip1^{-/-}$, and $Hic1^{-/-}$, to increase MB penetrance(83-86). Mutations in other members of the Shh pathway also result in tumor predisposition in mice, including loss of Sufu(87) and constitutive activation of Smo(77,88-91). Combination of *Trp53* loss and mutations in DNA repair genes including *Lig4*, *Xrcc4*, *Xrcc2*, *Brca2*, *Parp1*and *Ku80* also results in Shh subgroup MB(92-97). Dysregulated Shh signaling also results in MB in genetic models of altered interferon and *Stat1/2* expression(98,99).

Shh MB has also been modeled through somatic gene editing *in vivo* using the RCAS/*tv-a*, CRISPR/Cas9, and *Sleeping Beauty* mutagenesis systems. The RCAS/*tv-a* system uses a replication-competent, avian retroviral vector (RCAS) derived from avian leucosis virus (ALV), and a transgenic mouse producing the receptor for ALV (TV-A) under control of the Nestin promoter (*Ntv-a*). Nestin is expressed in neural progenitor cells, allowing postnatal gene transfer in cells of the developing cerebellum(100). Cells producing the RCAS virus of choice are injected into the cerebellum of neonatal mice. *Nestin* expressing cells will be transduced, resulting in candidate gene expression driven by a constitutive retroviral promoter. Utilization of this model with overexpression of *Shh* alone or in combination with *Myc*, *MycN*, *HGF*, *IGF2*, *Akt*, and *Bcl-2* results in Shh subgroup MB(101-105). CRISPR/Cas9 knockout of *Ptch1* through PEI-mediated transfection or *in vivo* electroporation has also generated Shh MB(106). Additionally, isolated granule neuron precursor cells (GNPCs) from P6 *Ink4c*$^{-/-}$; *Trp53*$^{-/-}$ mice transduced with either *MycN* or *CyclinD1* form Shh MB when injected into immunocompromised mice(106). Lastly, *Sleeping Beauty* transposon mutagenesis has been used in several studies to identify drivers in Shh MB, as described in detail below(107-110).

iii. Wnt subgroup medulloblastoma

Wnt subgroup MB has been surprisingly difficult to model in the mouse; although activating *CTNNB1* mutations are present in the majority of human WNT MB, expression of a non-degradable form of β-Catenin (*Cttnb1*$^{lox(ex3)}$) in brain lipid-binding protein (*Blbp*) expressing progenitors does not result in MB in the mouse(76). Gibson *et al*. combined *Ctnnb1*$^{flox(ex3)}$ and *Trp53*$^{flox/flox}$ in *Blbp-Cre* transgenic mice to achieve tissue specific loss of *Ctnnb1* and *Trp53* in progenitor cell populations across the hindbrain. This resulted in low penetrance of MB (14%) that resembled the human WNT subgroup(76). Introduction of an additional activation mutation in the catalytic subunit of PI3K (*Pik3ca*) to *Cttnb1*$^{lox(ex3)}$ and p53 loss further promoted tumor formation, resulting in 100% penetrance within 3 months(53).

iv. Group 3 and 4 medulloblastoma

Several mouse models of Myc(N)-driven group 3 MB have been described. The only genetically engineered mouse model involves overexpression of *MycN* and luciferase under control of the *Glt-1* promoter (GTML)(111). *Glt-1* is expressed in the developing

posterior hindbrain from postnatal day 1 through adulthood in rodents(112). When *MycN* amplification is combined with dominant negative *Trp53* in this model, mice get group 3 MB with 100% penetrance(113). Group 3 MB has also been modeled using the RCAS/*tv-a* system to combine *Myc* amplification with loss of *Trp53* or *Bcl-2*. Mice form tumors with high incidence of leptomeningeal spread, a common and therapeutically important aspect of group 3 MBs(114). *in utero* electroporation has been used to create another set of models of group 3 MB, to deliver Cre-inducible Myc and DNp53 (dominant negative) constructs into the developing cerebellum with several different Cre lines (Blbp-Cre, Atoh-Cre, Gad2-IRES-Cre, Ptfa-Cre)(115). All promoters produced group 3 MB, implicating that group 3 MB can arise from multiple different progenitor cell populations.

Several cell line injection models, involving isolating cerebellar progenitor cells from P6-P7 mice, transducing them with viruses overexpressing oncogenes, and injecting them back into mice have been used to generate group 3 MB. Isolation of GNPCs from *Ink4c*$^{-/-}$; *Trp53*$^{-/-}$ mice, transduction with a *Myc* OE vector, and injection into mice results in 100% penetrance of group 3 MB(116). Isolation of a *CD133+*, *Lin-* stem cell population from the cerebellar white matter and transduction with stable *Myc* (*Myc*$^{T58A}$) and dominant negative *Trp53* results in high penetrance of MB (100%) (80). Isolation of *Math1+* cells and transduction of stable *Myc* and dominant negative *Trp53* results in approximately 32% incidence of MB(80). While these mouse injection models of group 3 MB are informative, they all involve a combination of *Myc* amplification and *Trp53* loss, which is uncommon in human MB. A potentially more relevant model involves isolation of *CD133+*, *Lin-* stem cells and transduction with *GFI1* or *GFI1b* and *MYC*, two genes predicted to cooperate in human MB. These mice have high incidence of MB formation (88% and 90%, respectively) with leptomeningeal spread(51). Currently there are no mouse models of group 4 MB, making this group exceptionally difficult to study.

2. Central nervous system primitive neuroectodermal tumors
    a. Overview

Central nervous system primitive neuroectodermal tumors (CNS-PNETs) represent a group of poorly differentiated embryonal tumors. Histologically, CNS-PNETs resemble MBs with densely-packed, small blue tumor cells and little cytoplasm. While MBs are mostly a cerebellar tumor, CNS-PNETs predominately occur in the cerebrum,

brain stem and spinal cord. Due to their low incidence and a lack of specific molecular knowledge, patients with CNS-PNET receive similar treatment as those with MB. These tumors are largely resistant to treatment, resulting in a reduced 5-year overall survival of 20 to 40% and similar life-long therapy-related side effects(2). In a recent study specifically looking at CNS-PNET, 73% (11/15) of treatment survivors had severe long-term neurocognitive toxicities requiring intensive physical and neurocognitive rehabilitation(117).

This tumor classification has slowly evolved over time with increased knowledge of the heterogeneous nature of embryonal tumors. The PNET concept initially related MB (primitive neuroectodermal tumor of the cerebellum) to embryonal tumors of the cerebrum (supratentorial PNET)(118,119). Supratentorial PNET was adjusted to the more general term, CNS-PNET, to include similar tumors located within the brain stem and spinal cord(15). As an umbrella term in the 2007 World Health Organization (WHO) classification of CNS tumors, CNS-PNET included 5 subgroups: CNS neuroblastoma (CNS-NB), ganglioneuroblastoma, medulloepithelioma (ME), ependymoblastoma (EB), and CNS-PNET, NOS (not otherwise specified)(15). These groups have been reclassified, driven by identification of a common amplification of the C19MC micro-RNA cluster in ME, EB and embryonal tumors with abundant neuropil and true rosettes (ETANTR)(120-124). The presence of C19MC amplification now results in diagnosis of embryonal tumor with multilayered rosettes (ETMR), *C19MC-altered*; those without C19MC amplification remain histologically identified as ME and ETMR, NOS(18). Remaining CNS-PNETs are now classified as CNS embryonal tumors, NOS. The molecularly heterogeneous group of CNS embryonal tumors, NOS was further classified by *Sturm et al.*, with identification of 4 new molecular entities associated with recurrent genetic alterations: CNS neuroblastoma with *FOXR2* activation (CNS NB-*FOXR2*), CNS Ewing sarcoma family tumor with *CIC* alteration (CNS EFT-*CIC*), CNS high-grade neuroepithelial tumor with *MN1* alteration (CNS HGNET-*MN1*) and CNS high-grade neuroepithelial tumor with *BCOR* alteration (CNS HGNET-*BCOR*)(125).

b. Known genetic drivers of CNS-PNET

In comparison to MB, the molecular drivers of CNS-PNET are much less clear. Two inherited disorders, Turcot syndrome Type I and Li-Fraumeni syndrome, are

associated with development of CNS-PNET(126,127). Turcot syndrome Type I is characterized by mutations in mismatch repair genes *MLH1*, *MSH2*, and *PMS2*; mutation in *PMS2* has been observed in human CNS-PNETs(126). Mutational inactivation of mismatch repair genes results in a progressive accumulation of mutations, some of which will provide a selective advantage to the cell and give rise to cancer. *MYCN*, *MYCC*, and *CDK4,* a cyclin-dependent kinase with a known oncogenic role, are amplified in a subset of CNS-PNETs(125,128,129). Focal deletion of chromosome 9 resulting in loss of *CDKN2A* is common in CNS-PNET(125,128,130). Somatic mutations in *TP53* have also been associated with adult CNS-PNETs(131-133), potentially acting as a cooperating factor with activated Ras signaling, as suggested in a CNS-PNET zebrafish model(134).

The recent study by Sturm *et al*. identified recurrent inter and intrachromosomal rearrangements defining the above mentioned molecular subgroups of CNS-PNET(125), implicating *FOXR2*, *CIC*, *MN1*, and *BCOR* as drivers in CNS-PNET. *FOXR2* has been identified as an oncogene in several cancer types, with potential mechanisms including interaction with MYC and activation of SHH signaling(110,135,136). *CIC* fusions are present in pediatric primitive round cell sarcoma and result in transcriptional activation in CNS EFT-*CIC*(125,137). *MN1* fusion proteins act as transcription factors and are transforming in myeloid leukemia(138). Internal tandem duplications of the 16$^{th}$ exon of *BCOR* was detected in 100% of CNS HGNET-*BCOR* tumors, driving increased *BCOR* expression and activating WNT signaling, although the mechanism by which this amplification drives CNS-PNET tumor formation is unclear(125).

c. Models of CNS-PNET

One of the most limiting factors to developing improved therapies for patients with CNS-PNET is a general lack of animal models. One mouse model has been established for CNS-PNET, which uses orthotopic transplantation of human radial glial cells into the subventricular zone of the 3$^{rd}$ ventricle of immunocompromised mice to achieve CNS-PNET formation(139). These radial glial cells are derived from human embryonic or human induced pluripotent stem cells and injected into adult (8 week old) NOD-SCID mice. After injection, these cells show stabilized HIF-1α and HIF-2α, up-regulation of *MYCC*, and accumulation of stabilized p53. In a second animal model of CNS-PNET, Modzelewska *et al*. injected *sox10*-driven *NRAS* and dominant negative $p53^{M214K}$ into

zebrafish embryos to functionally test if CNS-PNETs could originate from oligo-neural progenitor cells (OPCs) with Ras/MAPK activation and loss of p53(134). Fish developed CNS-PNETs with about 50% penetrance and both transgenes were necessary for tumor development (*p53* or *NRAS* expression alone were not sufficient)(134).

3. Neuroblastoma

    a. Overview

Neuroblastoma represents the most commonly occurring childhood extracranial tumor and is the most diagnosed cancer in the first year of life(140). It is primarily a disease of childhood, with 90% of neuroblastomas occurring before age 5. Although still relatively rare (it accounts for 5 to 10% of childhood malignancies)(141,142), neuroblastoma accounts for a disproportionate number of deaths (15% of cancer-related deaths in children)(143). Tumors occur in the sympathetic nervous system, commonly presenting in or around the adrenal glands and along the paravertebral ganglia. Based on primary tumor location and characteristic secretions, the cell of origin for neuroblastoma is thought to be a developing cell of the neural crest(140,144-147). Neuroblastoma has a large range of prognoses, ranging from localized disease and good prognoses to widespread metastasis and a survival rate of only 30%(148). A particular subtype of neuroblastoma is even known to present in a highly metastatic state only to spontaneously regress on its own(143). This heterogeneity in presentation and treatment response leads to frequent failures of therapy. Further molecular study of the disease is needed to identify novel therapeutic targets in neuroblastoma and investigate improved treatment strategies.

    b. Known drivers in neuroblastoma

Neuroblastomas present with a characteristically low number of mutations in comparison to other cancer types(149,150). Familial or inherited neuroblastoma is quite rare and accounts for less than 2% of cases(151-153). Despite their low incidence, these tumors have provided knowledge behind the genetic drivers of neuroblastoma. Activating mutations in anaplastic lymphoma kinase (ALK) occur in approximately 50% of inherited neuroblastoma(154-156) and more than 92% of sporadic neuroblastoma(157). ALK is a receptor tyrosine kinase with high expression in many different cancers, including glioma, melanoma, and breast cancer (158-162). ALK has been shown to form

a stable complex with ShcC and modify the responsiveness of the MAPK pathway to growth factors(163). Interestingly, expression changes in ALK have been correlated with expression changes in another gene mutated in familial neuroblastoma, *PHOX2B*(164). *PHOX2B* is an early transcription factor expressed in the development of the neural crest and differentiation of sympatho-adrenal precursors(165). Increased PHOX2B induces *ALK* expression, underscoring the role of ALK in promoting neuroblastoma tumorigenesis(166).

In sporadic neuroblastoma *MYCN* is the most well-characterized amplification. Approximately 25% of human neuroblastomas have amplification of the *MYCN* locus, and patients with this amplification suffer a poor prognosis with high incidence of metastasis(145). MYCN is a member of the MYC-family of basic helix-loop-helix transcription factors, which regulate a large variety of cellular processes. Specifically in the context of neuroblastoma, MYCN has roles in differentiation and proliferation during neural crest development(167). In neuroblastoma cell lines, knockdown of *MYCN* causes spontaneous differentiation, supporting the role of MYCN in maintaining a more "progenitor cell" state(168,169). Overexpression of *Mycn* alone under the *Th* promoter (sympathetic neuron promoter) is sufficient to cause neuroblastoma in the mouse(170). *ALK* mutations co-occur with *MYCN* mutations in approximately 10% of sporadic neuroblastoma which represents a particularly deadly form of neuroblastoma with very poor prognosis(171,172). Lastly, *ATRX*, a chromatin remodeler, is often mutated in "older" patients with neuroblastoma (44% of patients >12 years) and has been implicated in genetic instability and telomere maintenance(173).

While point mutations are less common in neuroblastoma, large chromosomal rearrangements occur frequently and are associated with poor prognosis. Chromothripsis, a pattern of localized chromosomal shredding and random reassembly, occurs in up to 20% of high-risk neuroblastoma(173). Loss of chromosomal regions 1p36 and 11q23 and gain of 17q22 occurs in approximately 30%, 40%, and 50% of sporadic neuroblastoma, respectively(141,174). Several genes within the 1p36 loss have been validated as tumor suppressors including *CAMTA1*, *CASZ1*, *CHD5*, *TP73*, and *KIF1B*, but it's unclear which are functionally most relevant to neuroblastoma development(175-

179). Loss of 11q often occurs in a mutually exclusive manner to *MYCN* amplification, though its function is also yet unclear(174).

4. *Sleeping Beauty* mutagenesis for use in cancer genetic screens

    a. Overview

*Sleeping Beauty* (*SB*) is a cut-and-paste transposon system containing a transposable element mobilized by the *SB* transposase enzyme. These two components were reconstructed from dormant *Tc1*/*Mariner* fish transposon genes by correcting mutations responsible for their inactivity(180). The transposon element can be modified to contain any DNA sequence of appropriate length flanked by *SB* inverted repeat/directed terminal repeat (IR/DR) sequences. The *SB* transposase enzyme recognizes these IR/DR sequences and catalyzes excision and reintegration of the transposon element at a new "TA" dinucleotide within the genome. *SB* transposition is supported in a wide range of vertebrate cells, including human and mouse(181).

    b. *Sleeping Beauty* forward genetic screens to model human cancer in mice

Forward genetic screens in model organisms are powerful tools in the discovery of gene function. Forward genetics is an approach of determining the genetic changes behind an observed phenotype. Insertional mutagenesis approaches, for example using the *SB* transposon system, are preferable to classic mutagenic approaches such as radiation or chemically-induced mutagenesis, due to the ease of identifying mutations caused by DNA insertion. In *SB* insertional mutagenesis cancer screens, the random mobilization and insertion of the *SB* transposon can increase expression of an oncogene or ablate expression of a tumor suppressor gene depending on the transposon orientation. *T2*/*Onc* is a mutagenic *SB* transposon engineered to drive gene expression through the use of a constitutively active murine stem cell virus promoter followed by a splice donor and disrupt gene expression with bidirectional splice acceptor sites followed by stop codons and polyadenylation sequences (Figure 1.1)(182). A proto-oncogene can be activated by increased expression or N or C-terminal truncation by *T2*/*Onc*. A tumor suppressor gene can by inactivated by splicing to a splice acceptor followed by a polyadenylation sequence.

The *SB* system has been used to generate many mouse models of human cancers, including carcinomas, sarcomas, and hematological malignancies. Transgenic mice

possessing a concatomer of approximately 25-300 copies of the *T2/Onc* transposon(182,183) were crossed to mice with ubiquitous expression of *SB* transposase under the *Rosa26* promoter resulting in robust tumor formation(183,184). The majority of tumors were hematopoietic malignancies, but some solid tumors occurred including medulloblastoma, glioma, prostate, intestinal, and pituitary tumors(184,185). *SB* can be targeted to a specific tissue type, which is critical to studying a particular cancer type and allows information regarding the cell of origin for an individual malignancy. This is possible using the Cre-lox technology. Dupuy *et al*. modified the *Rosa26-SB11* allele to include a lox-stop-lox cassette directly proceeding the *SB11* cDNA ($Rosa26^{lsl\text{-}SB11}$)(186). The floxed stop cassette prevents transposase expression until it is removed by Cre recombinase. Therefore, by controlling the tissue expressing Cre through tissue-specific promoters, one is able to direct transposition. *SB* has been used to drive medulloblastoma genesis by 4 different groups. This was done using whole body mutagenesis(107,108) and tissue-specific mutagenesis(109,110) to identify novel drivers of MB in the mouse.

5. Candidate oncogenes in medulloblastoma – *ARHGAP36* and *FOXR2*

    a. Overview

*ARHGAP36* and *FOXR2* were identified as candidate oncogenes in medulloblastoma by our lab and will be the subject of subsequent chapters in my thesis. The following section contains background information on the study of these genes by other groups.

    b. *ARHGAP36*

ARHGAP36 is a relatively mysterious member of the Rho GTPase activating family with roles implicated in several cancers, including phenochromocytoma, neuroblastoma, and medulloblastoma(109,187-189). ARHGAP36 is a member of the Rho GTPase activating protein (GAP) family. Rho GTPases regulate several cellular processes related to cancer, including cell cycle regulation, polarity establishment, migration, apoptosis, and angiogenesis(190,191). Most Rho GTPases are tightly regulated through a molecular switch from an inactive GDP-bound state to an active GTP-bound conformation (Figure 1.2). Their activation and inactivation are controlled by guanine nucleotide exchange factors (GEFs) and GTPase activating proteins (GAPs).

GEFs stimulate the exchange of GDP for GTP and GAPs catalyze the hydrolysis of GTP to GDP by Rho GTPases.

In an investigation of genes with altered expression in tumor versus normal tissue, Croise *et al*, found that 3 Rho GTPases, *RHOA*, *RAC1*, and *CDC42* have increased expression in pheochromocytoma, a type of neuroendocrine tumor arising from chromaffin cells of the adrenal medulla, compared to surrounding adrenal tissue(187). Interestingly, although their expression was increased, RAC1 and CDC42 were less active, indicating an increased presence of GDP-bound forms. They also found that *ARHGAP36* was highly expressed in tumor versus adjacent normal tissue, implicating the role of ARHGAP36 as a GAP in decreased GTP-bound RAC1 and CDC42. Despite this implied role in regulation of RAC1 and CDC42, ARHGAP36 is unlikely to function as a traditional GAP. ARHGAP36 lacks the "arginine finger" motif at AA246 which participates in Rho GTPase activity, suggesting that ARHGAP36 may not have GAP activity(192).

Two separate studies have identified ARHGAP36 as an *in vitro* activator of the sonic hedgehog (SHH) signaling pathway(188,189). SHH signaling is an evolutionarily conserved pathway which regulates embryonic patterning and tissue homeostasis(193,194). When SHH activation is left unchecked, it can lead to basal cell carcinoma, medulloblastoma, and other cancer types(195). In the off state, the 12 transmembrane receptor Patched (PTCH) prevents Smoothened (SMO) from entering the primary cilium, a structure present on most mammalian cell types specialized for SHH signaling transduction (Figure 1.3). Full forms of the Gli proteins (GLI2/3F) will be bound to the protein scaffold Suppressor of Fused (SUFU) and trafficked to the primary cilium where they are phosphorylated by protein kinase A (PKA) and targeted for proteolysis into their repressive forms (GLI2/3R)(196-200). GLI2/3R block transcription of SHH target genes. When SHH ligand is present, it binds PTCH and alleviates its repression of SMO, allowing SMO to accumulate within the primary cilium and induce dissociation of SUFU-GLIF complexes(196,197,201,202). Full length GLI2/3 are then converted to their transcriptionally active forms (GLI2/3A), which translocate to the nucleus and promote expression of SHH target genes(203).

Rack *et al*. identified *ARHGAP36* as a Shh pathway agonist using a flow cytometry-based screen of human cDNAs(189). Using a GFP Shh reporter 3T3 cell line, they found that full length mouse Arhgap36 activated Shh signaling in a Smo-independent, Gli2/3 dependent manner (Isoform 1, Figure 1.4). The activation of Shh signaling by Arhgap36 was dependent on primary cilia formation, as knockout of *Kif3a* or *Ift88* (two genes required for primary cilia formation), ablated Shh activation in the presence of Arhgap36. In a functional analysis study, Rack *et al*. mutated two other residues of Arhgap36 structurally equivalent to those necessary for Rho GAP function in GRAF. Mutation of these two residues did not affect Arhgap36's ability to activate Shh signaling, further supporting a non-GAP related role for Arhgap36. Additionally, they found that when transfected alone, the GAP domain (AA215-414) and C-terminus (AA415-590) did not affect Shh signaling. Interestingly, transfection of the N-terminus alone (AA1-214) inhibited Shh signaling when Shh ligand was present. This study hints at a possible role for the N-terminus of Arhgap36 in its regulation. Rack *et al*. identified a novel binding partner for Arhgap36: Sufu. As Sufu is a negative regulator of the Shh pathway, this interaction offers a mechanism in which Arhgap36 could be driving Shh activation. Lastly, they identified a role for *Arhgap36* in medulloblastoma; in mouse MB allografts from *Ptch1*$^{+/-}$; *Tp53*$^{-/-}$ mice propagated with or without LDE225 (a SMO antagonist), *Arhgap36* was the most upregulated gene in LDE225 resistant MB. Confusingly, they also found *ARHGAP36* to be significantly upregulated in a subset of group 3 and 4 human MB, which did not correlate with changes in *PTCH1* or *GLI1* expression.

The second group to identify *ARHGAP36* as a positive regulator of the SHH pathway did so in a study of protein kinase A catalytic subunit (PKAC) binding partners. PKA is a master negative regulator of the SHH pathway(204,205). The full forms of GLI proteins are trafficked by SUFU to the primary cilium where PKA phosphorylates them and targets them for proteolysis into their repressive forms (Figure 1.3) (196-200). PKA is a serine/threonine kinase and is a tetrameric holoenzyme comprised of a dimer of regulatory subunits (PKAR) which bind 2 catalytic subunits (PKAC). When PKA is activated, for example by cyclic AMP (cAMP), cAMP binds to PKAR and allows release of PKAC. Because PKA regulates several essential cellular processes it is tightly

controlled by several different mechanisms, including A-kinase-anchoring proteins (AKAPs) which serve as scaffolds to target PKA to distinct subcellular compartments and kinase inhibitor proteins (PKI) which bind PKAC and inhibit it competitively(206-208). Eccles *et al*. found that human ARHGAP36 inhibits PKA signaling by acting as a pseudosubstrate inhibitor, similar to PKIs (Figure 1.5, isoform 2)(188). They were able to pull down ARHGAP36 and PKAC together and determine the exact 25 AA responsible for the interaction (AA141-165). Within this 25 AA region, they identified a sequence fitting the PKAC substrate sequence (RRGAV) and were able to identify the PKAC/ARHGAP36 interaction with mutations of R153/R154/V157 on ARHGAP36. They found that the first 194 AA, AA118-194, and just the 25 AA portion of ARHGAP36 all bound PKAC with high affinity and drastically inhibited its catalytic activity. Similarly to Rack *et al*., they found that the full form of ARHGAP36 activated Shh in 3T3 cells, but their RRV mutant did not, implying the interaction with PKAC is responsible for ARHGAP36-mediated Shh activation. Lastly, they found that ARHGAP36 is expressed in 2 neuroblastoma (NB) lines (NGP and CLB-GA) and binds endogenous PKAC(188).

While some aspects of the Rack *et al*. and Eccles *et al*. papers are complimentary to each other, other aspects disagree. Binding to both major negative regulators of the Shh pathway (Sufu in Rack *et al*., PKA in Eccles *et al*.) provides a clear, dual-pronged approached to ARHGAP36-mediated Shh activation. However, the constructs used in these papers are of different species and make the results difficult to interpret (mouse in Rack *et al*., human in Eccles *et al*.)(188,189). In comparing the isoforms of mouse and human ARHGAP36 used (mouse isoform 1 in Rack *et al*., human isoform 2 in Eccles *et al*.), they have 70% identity (aligned using UniProt alignment software, Figure 1.6). Focusing specifically on the PKAC region, it is largely conserved between mouse and human, with just 3 residue mismatches in the mouse (A178, A181, and D182 in the mouse). The PKAC pseudosubstrate motif remains completely intact in both species (RRGAV).

Specifically, the conclusion of Eccles *et al*. is that PKAC binding is what drives the Shh activating capacity of ARHGAP36. However, when transfected alone, the N-terminus containing this binding site (AA1-214 mouse) by Rack *et al*. resulted in

inhibition of Shh pathway activation (Figure 1.7). Interestingly, in the exact same 3T3 GFP reporter cell line for Gli1 activation, Eccles *et al*. found that a small section of the N terminus (N2, AA118-194 human) activated Shh. This may be explained in several ways, including: human and mouse ARHGAP36 may act differently on the Shh pathway or the very N-terminal portion of ARHGAP36 (AA1-118) which was not assessed in Eccles *et al*. may be specifically inhibitory. Further study of the human and mouse ARHGAP36 isoforms is needed to answer these questions.

Lastly, there is some degree of disagreement in what cell type ARHGAP36 is able to activate Shh signaling in these two papers. PKA is a common negative regulator of Shh signaling in both developing neural and somitic (muscle) cells(209). Rack *et al*. specifically compared *Arhgap36*-mediated Shh activation in zebrafish embryos in comparison to a dominant negative PKA (dnPKA) construct. They found that *Arhgap36* activated Shh signaling in developing neural tissues, but not somitic cells(189). In contrast, the dnPKA construct activated Shh signaling in both tissues. Eccles *et al*. found that *Arhgap36* is expressed in mouse somitic tissue up until birth and then becomes undetectable(188). Combined, these results imply that ARHGAP36 is regulated from activating Shh signaling in developing somitic cells through its PKAC interaction, implicating the ARHGAP36→PKAC inhibition→Shh activation is not just a linear process. Further study of ARHGAP36 expression in developing and mature human tissue is needed to determine how this interaction occurs and is regulated in human tissue.

c. *FOXR2*

FOXR2 is a member of the Forkhead box (FOX) transcription factor family. The Forkhead gene (*fkh*) was originally identified in *Drosophila melanogaster* in a random mutagenesis screen(210). It was coined "forkhead" due to a characteristic "forked head" appearance which occurred in its absence. The forkhead box is a conserved DNA-binding domain shared by all 49 family members (FOXA1-FOXS1)(211,212). FOX genes contribute to a diverse variety of cellular functions, including gastrulation, stem cell maintenance, metabolism, cell cycle control, and tissue specification(213-217).

Mutation or misregulation of FOX genes has been associated with several diseases including cancer, acting as both oncogenes and tumor suppressors. For example, FOXM1 is an established oncogene in more than 20 different cancers and has roles in every

hallmark of cancer(218). FOXA2 is a pioneering transcription factor with tumor suppressive roles in lung cancer, HCC, and gastric cancer(219-222). FOXR1 is a close homologue to FOXR2 (57.7% identity)(223) and shares the ability of FOXR2 to bind MYC and MAX and promote MYC-dependent transcription(136). FOXR1 is recurrently activated in peripheral neuroblastoma by intrachromosomal deletion and fusion events resulting in its overexpression(224). Santo *et al*. also found that high FOXR1 expression could functionally replace MYC to drive proliferation in JoMa1, a neural crest stem cell line.

Forkhead box R2 (FOXR2) has been implicated as an oncogene in numerous cancers (Table 1.3, Figure 1.8), including non-small cell lung cancer (NSCLC), endometrial adenocarcinoma (EAC), hepatocellular carcinoma (HCC), colorectal cancer (CRC), prostate cancer, and breast cancer(136,225-230). Additionally, FOXR2 is associated with several cancers of neural origin, including glioma, CNS-PNET, malignant peripheral nerve sheath tumors (MPNSTs), and medulloblastoma(110,125,135,231). However, while FOXR2's role as an oncogene is relatively well-established, the molecular mechanism behind FOXR2-driven tumorigenesis is unclear. FOXR2 promotes several key pathways in cancer, including WNT signaling (NSCLC, prostate cancer, HCC), SHH signaling (CRC, HCC, MB), and EMT (CRC, prostate)(110,226-229). FOXR2 has also been shown to form a stable complex with MYC and MAX and drive expression of MYC target genes(136). Further study on FOXR2 is needed to determine which of these mechanisms are most relevant to cancer and potentially targetable.

MYC (C-MYC, cellular as opposed to viral) is a helix-loop-helix transcription factor that dimerizes with MAX to regulate gene transcription(232). MYC is the third most amplified gene in human cancers(233,234) and its overexpression in the mouse can drive tumorigenesis in many tissue types(235). MYC is highly regulated in the cell, both posttranscriptionally through miRNA and translation regulation and post translationally by kinases, ubiquitin ligases, acetyltransferases, and other binding partners(236-240). Due to its abundance in cancer and the "addiction" of MYC-driven tumors to continued MYC expression in the mouse, MYC is a strong therapeutic target in cancer(241-243). However, directly targeting MYC has been unsuccessful thus far. Therefore, targeting MYC interacting proteins, such as FOXR2, could have a large impact on a variety of

cancers. Additionally, the MYC family of transcription factors contains multiple members with distinct expression patterns, particularly when it comes to their expression in cancer (38,34,39,40). While C-MYC is broadly expressed in both blood and solid tumors, N-MYC is most frequently overexpressed in solid cancers of neural origin, and L-MYC is most associated with small cell lung cancer. If FOXR2 is capable of binding alternative forms of MYC, this could further expand its reach in cancer biology.

We have also found evidence for FOXR2 in activation of the focal adhesion kinase (FAK) signaling pathway. FAK is a cytoplasmic, highly conserved, non-receptor tyrosine kinase that associates with receptors at the plasma membrane and distinct protein complexes within the nucleus(244). FAK was initially identified in v-Src transformed chick embryo fibroblasts(245) and is ubiquitously expressed in all cells(246,247). FAK is highly expressed and activated in a variety of cancers and is correlated with poor prognosis and drug resistance(248-251). When FAK is activated (for example after integrin clustering upon cellular binding to the extracellular matrix (ECM)) FAK is autophosphorylated at Y397 which provides a binding site for SRC family kinases to bind and become activated. SRC then further phosphorylates FAK in its kinase domain (Y576 and Y577) resulting in formation of an activated FAK-SRC complex(252-254). FAK inhibitors have been sought after due to FAK's activation in so many cancers and effectiveness of FAK inhibition in mouse models to prevent tumor growth and metastasis(255). However, targeting FAK signaling remains a challenge, largely due its ubiquitous expression and the potential off-target effects of inhibitors(255). Therefore, targeting FAK-interacting proteins such as FOXR2 offers an alternative method to target FAK-mediated effects in cancer.

6. Hypotheses
    a. I hypothesize that *Sleeping Beauty* mutagenesis can be applied to the central nervous system to create a mouse model of medulloblastoma and CNS-PNETs that resemble human tumors at the gene expression level.
    b. I hypothesize that candidate genes identified using *Sleeping Beauty* mutagenesis will be important in CNS embryonal tumorigenesis, especially *Arhgap36*, *Foxr2*, and *Megf10*.

c. I hypothesize that *FOXR2* is a driver in neuroblastoma through its interaction with C-MYC and N-MYC.

7. Objectives
    a. Use *Sleeping Beauty* mutagenesis to model human medulloblastoma and CNS-PNETs in mice.
    b. Validate *Arhgap36*, *Foxr2*, and *Megf10* as oncogenes in medulloblastoma and CNS-PNET.
    c. Elucidate the mechanism of *Arhgap36* and *Foxr2*-driven transformation in neural cancers.

**Table 1.1. Mouse models of medulloblastoma.**

| **Genetically engineered mouse models** | | | | |
|---|---|---|---|---|
| **Subgroup** | **Genotype/description** | **MB %** | **Ref** | **Notes** |
| Shh | *Ptc*$^{+/-}$ | 14% | (82) | |
| Shh | *Ptc*$^{+/-}$; *Trp53*$^{-/-}$ | 95% | (83) | |
| Shh | *Ptc*$^{+/-}$; *Ink4c*$^{-/-}$ or $^{+/-(77,91)}$ | 30% | (84) | |
| Shh | *Ptc*$^{+/-}$; *Kip1*$^{-/-}$ or $^{+/-}$ | 65% | (85) | |
| Shh | *Ptc*$^{+/-}$; *Hic1*$^{-/-}$ | ~40% | (86) | |
| Shh | *Math1-Cre*; *Ptc*$^{flox/flox}$ | 100% | (78) | |
| Shh | *Gfap-Cre*; *Ptc*$^{flox/flox}$ | 100% | (78) | |
| Shh | *Sufu*$^{+/-}$; *Trp53*$^{-/-}$ | 58% | (87) | |
| Shh | Hemizygous *NeuroD2-SmoA1* (W539L) | 48% | (88) | |
| Shh | Homozygous *NeuroD2-SmoA1* (W539L) | 94% | (89) | Leptomeningeal spread |
| Shh | Homozygous *NeuroD2-SmoA2* (S537N) | 100% | (90) | |
| Shh | *CAGGS-CreER*; *Rosa26*$^{tdSmoM2-YFP}$ (W539L) | 40% | (91) | Postnatal Cre induction (P10) |
| Shh | *hGFAP-Cre*; *Rosa26*$^{tdSmoM2-YFP}$ (W539L) | 100% | (77) | |
| Shh | *Olig2-tva-Cre*; *Rosa26*$^{tdSmoM2-YFP}$ (W539L) | 100% | (77) | |
| Shh | *Tlx3-Cre*; *Rosa26*$^{tdSmoM2-YFP}$ (W539L) | 100% | (77) | |
| Shh | *Gfap-Cre*; *Rb*$^{flox/flox}$; *Trp53*$^{-/-\text{ or flox/flox}}$ | >84% | (92) | |
| Shh | *Lig4*$^{-/-}$; *Trp53*$^{-/-}$ | 100% | (93) | |
| Shh | *Nestin-Cre*; *Xrcc4*$^{flox/flox}$; *Trp53*$^{-/-}$ | 87% | (94) | |
| Shh | *Nestin-Cre*; *Xrcc2*$^{flox/flox}$; *Trp53*$^{-/-}$ | >90% | (95) | |
| Shh | *Nestin-Cre*; *Lig4*$^{flox/flox}$; *Trp53*$^{-/-}$ | >90% | (95) | |
| Shh | *Nestin-Cre*; *Brca2*$^{flox/flox}$; *Trp53*$^{-/-}$ | >90% | (95) | |
| Shh | *Parp1*$^{-/-}$; *Trp53*$^{-/-}$ | 49% | (96) | |
| Shh | *Ku80*$^{-/-}$; *Trp53*$^{-/-}$; *Rag1*$^{-/-}$ | 67% | (97) | |
| Shh | *GFAP-tTa*; *Tre-IFNγ* | >80% | (98) | Dox released on E16 |
| Shh | *GFAP-IFNα*; *Stat1*$^{-/-}$ | 50% | (99) | |
| Shh | *GFAP-IFNα*; *Stat2*$^{-/-}$ | 100% | (99) | |
| Wnt | *Blp-Cre*; *Ctnnb1*$^{+/flox}$; *Trp53*$^{flox/flox}$ | 14% | (76) | |
| Wnt | *Blp-Cre*; *Ctnnb1*$^{+/flox}$; *Trp53*$^{flox/flox}$; *Pik3ca*$^{E545K}$ | 100% | (53) | |
| Group 3 | *Glt1-tTA*; *TRE-MYCN-Luc* (GTML) - het | 40% | (111) | |
| Group 3 | *GTML* - homozygous | 75% | (111) | |
| Group 3 | *GTML*; *Tp53*$^{ki53ERTAM}$ | 100% | (113) | |
| **Somatic gene editing** | | | | |
| **Subgroup** | **Genotype/description** | **MB %** | **Ref** | **Notes** |
| Shh | *Nestin-TV-A* (*Ntv-a*); *RCAS-Shh* | 9-34% | (101-103) | |
| Shh | *Ntv-a*; *RCAS-Shh*, *RCAS-Myc* | 23% | (101) | |
| Shh | *Ntv-a*; *RCAS-Shh*, *RCAS-MycN* | 47% | (102) | |
| Shh | *Ntv-a*; *RCAS-Shh*, *RCAS-MycN*$^{T58A}$ | 78% | (102) | N-Myc w/increased stability |
| Shh | *Ntv-a*; *RCAS-Shh*, *RCAS-HGF* | 78% | (104) | |
| Shh | *Ntv-a*; *RCAS-Shh*, *RCAS-IGF2* | 39% | (105) | |
| Shh | *Ntv-a*; *RCAS-Shh*, *RCAS-Akt* | 48% | (105) | |
| Shh | *Ntv-a*; *RCAS-Shh*, *RCAS-Bcl-2* | 78% | (103) | |
| Shh | CRISPR/Cas9 *Ptch1* gRNA transfection in *Trp53*$^{-/-}$ | 80% | (106) | |
| Shh | CRISPR/Cas9 *Ptch1* gRNA | 92% | (106) | *in vivo* electroporation |
| Shh | *Ptch1*$^{tmMpz1}$; *T2Onc*; *Rosa26-SB11*$^{+/-}$ | ~23% | (107) | |
| Shh | *Ptch1*$^{loxP/+}$; *T2Onc3*; *Rosa26*$^{tdSB11/+}$; *β-Actin-Cre* | ~70% | (108) | |
| Shh | *Math1-SB11*; *T2Onc*; *Ptch1*$^{+/-}$ or *Trp53*$^{+/-}$ | 97/40% | (109) | |
| Shh | *Trp53*$^{tdR172H/+}$; *Nestin-Cre*; *T2Onc2*; *Rosa26*$^{tdSB11/+}$ | ~60% | (110) | |
| Shh/Grp3/4 | *Nestin-Cre*; *T2/Onc(2)*; *Rosa26*$^{tdSB11/+}$; *Pten*$^{flox/+}$ or *Trp53*$^{tdR270H/+}$ | 5/40% | (256) | Leptomeningeal spread |
| Group 3 | *LRL-Trp53DN*; *LRL-MycC*; *Blbp-Cre* | 57% | (115) | *in utero* electroporation E13.5 |
| Group 3 | *LRL-Trp53DN*; *LRL-MycC*; *Atoh-Cre* | 33% | (115) | *in utero* electroporation E13.5 |
| Group 3 | *LRL-Trp53DN*; *LRL-MycC*; *Gad2-IRES-Cre* | 36% | (115) | *in utero* electroporation E13.5 |
| Group 3 | *LRL-Trp53DN*; *LRL-MycC*; *Ptfa-Cre* | 43% | (115) | *in utero* electroporation E13.5 |
| Group 3/4? | *Ntv-a*; *Trp53*$^{-/-}$; *RCAS-Myc* | 50% | (114) | Leptomeningeal spread |
| Group 3/4? | *Ntv-a*; *RCAS-Myc*, *RCAS-BCl-2* | 87% | (114) | Leptomeningeal spread |
| **Cell line injection models** | | | | |
| **Subgroup** | **Genotype/description** | **MB %** | **Ref** | **Notes** |
| Shh | GNP from P6 *Ink4c*$^{-/-}$; *Trp53*$^{-/-}$, with *MycN* OE | 67% | (257) | |
| Shh | GNP from P6 *Ink4c*$^{-/-}$; *Trp53*$^{-/-}$, with *CyclinD1* OE | 40% | (257) | |
| Group 3 | GNP from P6 *Ink4c*$^{-/-}$; *Trp53*$^{-/-}$, with *Myc* OE | 100% | (116) | |
| Group 3 | CD133+, Lin- cells with *Myc*$^{T58A}$ and *DNTrp53* | 100% | (80) | |

| | | | | |
|---|---|---|---|---|
| Group 3 | Math1+ cells with *Myc*$^{T58A}$ and *DNTrp53* OE | 32% | (80) | |
| Group 3 | CD133+, Lin- cells with *GFI1(b)* and *Myc* OE | ~90% | (51) | Leptomeningeal spread |
| Group 3 | *Trp53*$^{fl/fl}$; *Atoh1-CreER* isolated at P7, transduced w/Myc | 86% | (115) | Tamoxifen at P0 or P1 |
| Group 3 | *Trp53*$^{fl/fl}$; *Prom11-CreER* isolated at P7, transduced w/Myc | 80% | (115) | Tamoxifen at P0 or P1 |

Table 1.2. Clinical trials of SHH inhibitors in medulloblastoma.

| Trial identifier Phase | Drug name | Target | Description |
|---|---|---|---|
| **Ongoing trials** | | | |
| NCT01878617 Phase 2 | GDC-0449 Vismodegib | SMO | Used in newly diagnosed SHH activated MB, in combination with surgery and irradiation |
| NCT01601184 Phase 1/2 | GDC-0449 Vismodegib | SMO | In combination with temozolomide, only in patients with activation SHH by IHC |
| NCT02624388 Phase 2 | Genistein | Gli1 | Used as supportive care in a variety of childhood cancers, including MB |
| **Completed trials** | | | |
| NCT00822458 Phase 1 | GDC-0449 Vismodegib | SMO | Done in children with recurrent or refractory MB to determine the best dose and side effects |
| NCT01239316 Phase 2 | GDC-0449 Vismodegib | SMO | Done in children with recurrent or refractory MB to determine efficacy in MB with and without SHH pathway activation |
| NCT00939484 Phase 2 | GDC-0449 Vismodegib | SMO | Done in adults with recurrent or refractory MB to determine efficacy in MB with and without SHH pathway activation |
| NCT01106508 Phase 1 | LEQ506 | SMO | Dose escalation study in adults with recurrent or refractory MB |
| NCT00880308 Phase 1 | LDE225 Sonidegib | SMO | Dose escalation study in adults with recurrent or refractory MB |
| NCT01208831 Phase 1 | LDE225 Sonidegib | SMO | Dose escalation study in adults with recurrent or refractory MB |
| NCT01125800 Phase 1/2 | LDE225 Sonidegib | SMO | Dose escalation study in children and phase 2 portion to assess efficacy in recurrent or refractory MB |
| NCT01708174 Phase 2 | LDE225 Sonidegib | SMO | Study done in children and adults with SHH MB |

| **Table 1.3. Published work on *FOXR2*-driven tumorigenesis** | | | |
|---|---|---|---|
| **Cancer type** | **Description** | **Mechanism** | **Ref** |
| Non-small cell lung cancer (NSCLC) | - Looked at 128 patient tumor versus adjacent tissue samples, found that FOXR2 was upregulated at mRNA and protein level<br>- Did KD (shRNA) experiments in human NSCLC line (A549), found that FOXR2 loss reduced proliferation (MTT) and invasion (transwell)<br>- FOXR2 KD also reduced flank tumor formation and metastasis to the lung after IV injection | **Wnt**<br>- KD of FOXR2 decreased protein levels of β-Catenin, Cyclin D1 and C-Myc | (226) |
| Glioma | - Compared FOXR2 expression in 33 human glioma samples to normal brain (N=8), found FOXR2 was upregulated in glioma<br>- Created GOF and LOF cell line models of FOXR2 in glioma (KO in U251, OE in U87).<br>- KO of FOXR2 resulted in decreased colony formation, cellular proliferation (EdU), migration (scratch assay), and invasion (transwell).<br>- OE of FOXR2 increased growth (EdU), colony formation, migration (scratch assay), and invasion (transwell) | **Cell cycle regulation**<br>- KO of FOXR2 induced G1 cell cycle arrest, FOXR2 KO increased protein levels of p21 (cell cycle inhibitor) and decreased cyclin D1, cyclin E and p-Rb.<br>- Inverse correlation with FOXR2 and p27 (tumor suppressor, negative regulator of the cell cycle)<br>**Invasion**<br>- Levels of MMP-2 (degrades ECM) correlate with FOXR2 expression levels (decrease with KO, increase with OE) | (231) |
| Endometrial adenocarcinoma (EAC) | - Compared FOXR2 and miR-202 expression in 90 EAC tissue with 40 control tissues, miR-202 is down in EAC, FOXR2 is up<br>- Binding site for miR-202 in the 3'UTR of FOXR2, confirmed that FOXR2 is a direct target of miR-202 through reporter assay and western blot analysis | **miR-202**<br>- Find that FOXR2 is a direct target of miR-202 and is negatively regulated by it<br>**AKT**<br>- Find that p-AKT levels correlate with FOXR2 expression | (225) |
| Colorectal cancer (CRC) | - Compared FOXR2 expression in 36 CRC tissue samples versus adjacent controls, found FOXR2 is increased in CRC at the mRNA and protein level<br>- Compared FOXR2 expression in 3 CRC cell lines (SW480, HT29, LOVO) to normal, colonic epithelial line (NCM460), FOXR2 is expressed higher in CRC lines<br>- KD (siRNA) of FOXR2 (SW480 and HT29) decreased proliferation (MTT) and invasion (transwell)<br>- KD of FOXR2 (SW480) reduced flank tumor formation in nude mice and decreased metastasis after IV injection in nude mice | **EMT**<br>- FOXR2 KD increased E-cadherin (epithelial marker) and decreased vimentin and N-cadherin (mesenchymal markers) in SW480<br>**SHH**<br>- FOXR2 KD reduced protein levels of SHH, GLI1, and PTCH1 in SW480 | (228) |

| | | | |
|---|---|---|---|
| Prostate cancer | - Evaluated FOXR2 expression in prostate cancer cell lines, found high expression in LNCaP, DU-145, and PC-3 by mRNA and protein compared to normal prostate epithelial line (RWPE-1)<br>- FOXR2 KD (shRNA) in DU-145 decreased proliferation (MTT) and invasion (transwell)<br>- KD of FOXR2 decreased tumor formation of DU-145 in the flank of nude mice | **EMT**<br>- FOXR2 KD increase E-Cadherin, decreased Vimentin and N-Cadherin<br>**Wnt**<br>- FOXR2 KD decreased β-catenin, cyclinD1 and C-Myc protein levels in DU-145 | (229) |
| Breast cancer | - FOXR2 is highly expressed in 13 breast cancer cell lines compared to normal controls<br>- FOXR2 is overexpressed in human breast (273), lung (145), and liver (210) cancer.<br>- FOXR2 MYC binding region is AA120-240 of MYC and AA80-100 of FOXR2<br>- OE of FOXR2 promoted colony formation on soft agar in MCF10A, FOXR2 without MYC binding formed reduced colonies<br>- FOXR2 KD in MDA-MB-468 reduced proliferation (Ki67 staining and BrdU) and tumor formation in nude mice | **Modulation of MYC target genes**<br>- FOXR2 binds the promoter regions of several MYC targets (ChIP)<br>- FOXR2 forms a stable complex with MYC and MAX (MDA-MB-468 breast cancer line)<br>- FOXR2 OE in MCF10A increased MYC target genes (*CCNA1* and *CCND1*) without changing MYC expression<br>- FOXR2 KD in MD-MB-468 reduced expression of MYC targets (*CCNA1*, *CCND1*, *p15*, *XRCC4*, *XRCC6*) | (136) |
| Central nervous system primitive neuroectodermal tumor (CNS-PNET) | - Identified new subgroup of CNS-PNET driven by FOXR2 activation (CNS NB-*FOXR2*)<br>- CNS NB-*FOXR2* express OLIG2 and Synaptophysin and are highly mitotic<br>- Genetic alterations include gain of chromosome 1q and 8, loss of 16q | - Complex inter- and intrachromosomal rearrangements converging on *FOXR2*, leading to increased *FOXR2* expression<br>- Fusion partners include: *JMJD1C*, *LOC550643*, *JPX*, *MAGEH1*, *MAGED2*, and *USP51* | (125) |
| Hepatocellular carcinoma (HCC) | - Compared FOXR2 expression in 42 patient HCC samples with normal liver controls, found high FOXR2 at protein and mRNA level in a subset of tumor samples<br>- Did GOF in 4 HCC lines (Hep3B, Huh7, YY-8103, and L02), FOXR2 increased proliferation and colony formation<br>- LOF (siRNA) in 2 HCC lines (WRL68 and HCC-LM3), loss of FOXR2 reduced cell viability and decreased soft agar colonies<br>- Increased FOXR2 promoted flank tumor formation (YY-8103, WRL68) | **WNT, SHH, and Skp2**<br>- Found that FOXR2 drove increased levels *β-Catenin*, *C-Myc*, *Gli1*, and *Skp2* (oncogene) by qPCR. | (227) |
| Breast cancer | - Compared FOXR2 expression in 25 patient breast cancer samples to normal | - None suggested | (230) |

| | | | |
|---|---|---|---|
| | tissue controls by qPCR, found increased FOXR2 in cancer tissues<br>- Compared FOXR2 expression in 203 breast cancer samples by IHC, found that increased FOXR2 expression correlated with poor prognosis | | |
| Medulloblastoma | - *SB* screen on WT or *Trp53*$^{R172H/+}$ background using *Nestin-Cre*, *Foxr2* was top CIS gene (7/17 WT, 15/27 p53 mut)<br>- FOXR2 transformed 3T3 cells (foci formation, growth in low-serum media)<br>- FOXR2 reduced senescence in MEFs and promoted their proliferation<br>- FOXR2 promoted growth in primary mouse cerebellar cells (increased colony size, express Ki67 | **SHH**<br>- Increased *FOXR2* in subset of SHH MB (microarray of 285 samples)<br>- FOXR2 drove expression of Gli1 reporter in HEK293 cells | (110) |
| Malignant peripheral nerve sheath tumors (MPNSTs) | - *SB* screen for MPNSTs, using *Nf1*$^{flox/flox}$; *Pten*$^{flox/+}$ backgrounds with *Cnp-Cre*<br>- GOF – FOXR2 OE in HSC1λ increased proliferation, soft agar colony formation, and flank tumor formation<br>- LOF – FOXR2 KO with TALENs (S462-TY and STS26T) reduced proliferation, soft agar colony formation, and flank tumor formation | - None suggested | (135) |

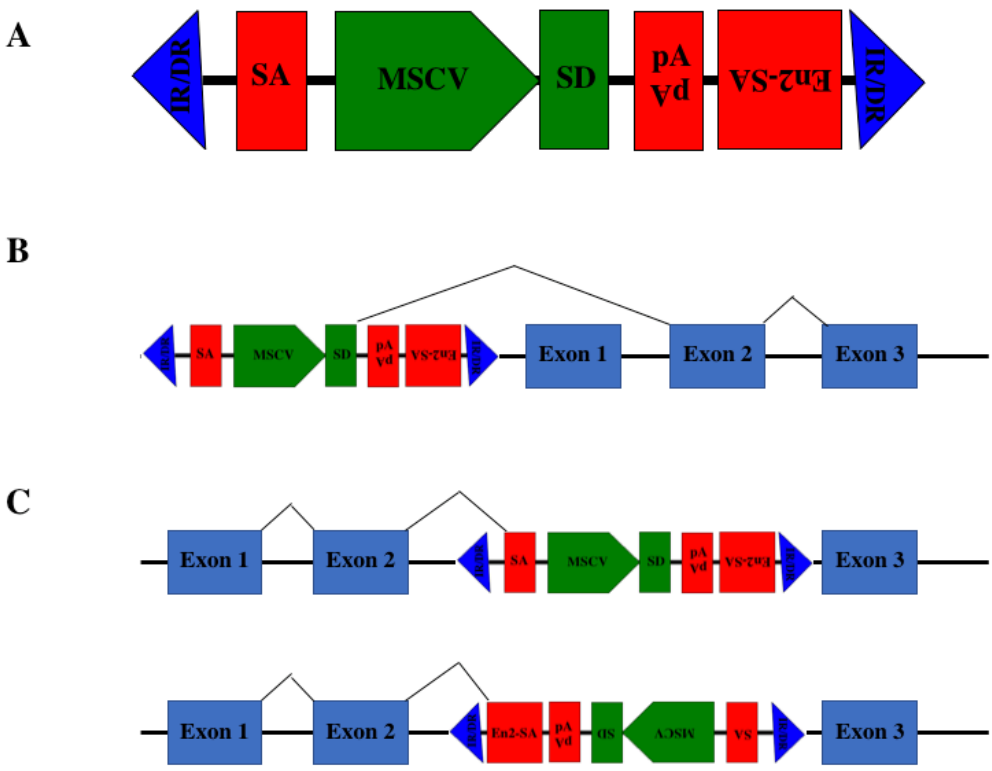


**Figure 1.1. *T2/Onc2* transposon for promotion and disruption of gene expression.** **A**, Schematic of the mutagenic *T2/Onc2* transposon. *T2/Onc2* contains two splice acceptors (SA) and a bi-directional polyadenylation sequence (pA). One splice acceptor is from the carp *β-Actin* gene (SA) and the other is derived from mouse *Engrailed 2* (En2-SA). *T2/Onc2* also contains the murine stem cell virus (MSCV) 5' long terminal repeat derived from the MSCVneo vector (Clontech) and a splice donor sequence (SD) derived from mouse *Foxf2*. The transposon is flanked by optimized binding sites for *Sleeping Beauty* transposase located within inverted repeat/directed terminal repeat (IR/DR) sequences (Collier *et al*. 2005). B, Promotion of gene expression by T2/Onc2 through the MSCV promoter, possibly driving N-terminal truncation of a gene if the start codon is within exon 1. C**,** Disruption of gene expression by T2/Onc2 by splicing to the bidirectional SA/pA sequences.

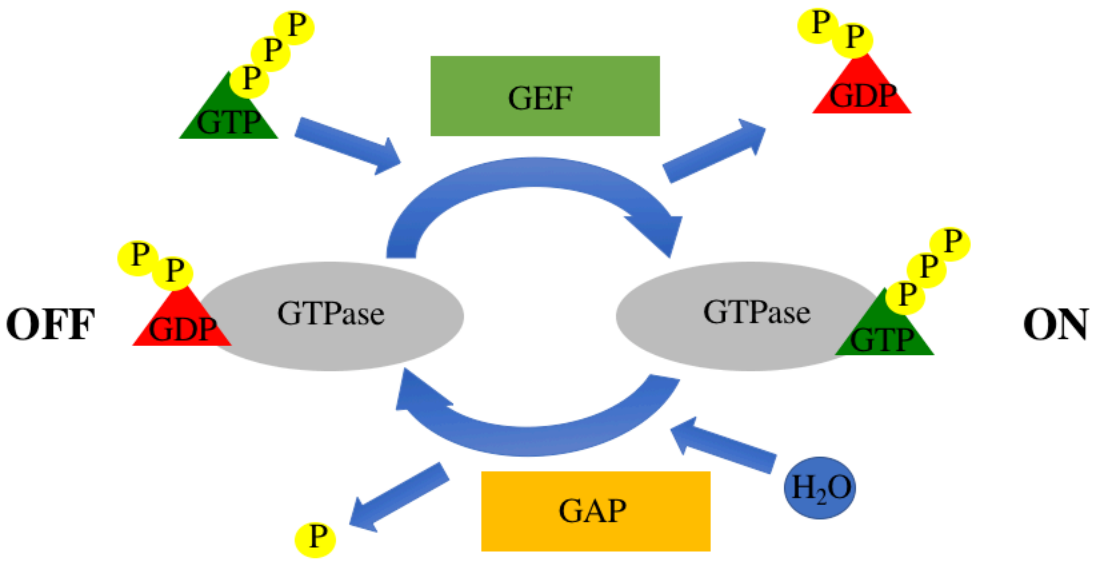


**Figure 1.2. Schematic of GTPase conversion from off (GDP-bound) to on (GTP-bound) state.**
GTPases are molecular switches within the cell which regulate many cellular processes. They are tightly regulated by guanine nucleotide exchange factors (GEFs) and GTPase activating proteins (GAPs). GEFs facilitate the exchange of GTP for GDP, turning GTPases "on." GAPs catalyze the hydrolysis reaction of GTP to GDP by the GTPase, turning them from "on" to "off."

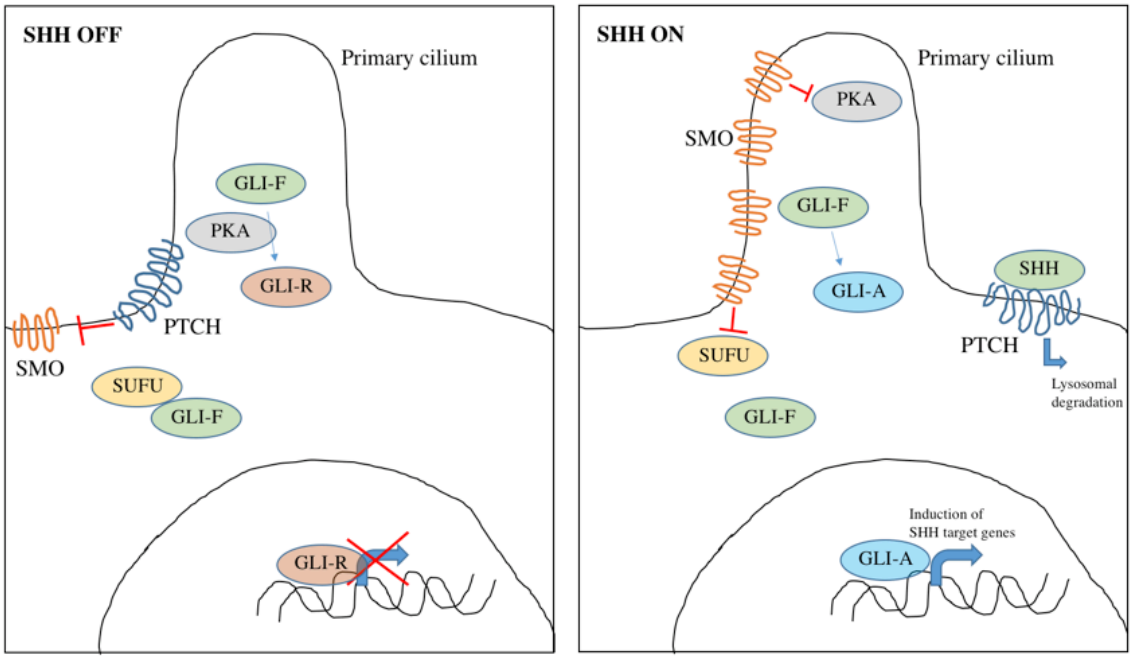


**Figure 1.3. Depiction of the SHH signaling pathway in its "off" and "on" states.** In the SHH off state, Patched (PTCH) prevents Smoothened (SMO) from entering the primary cilium. Full length GLI proteins (GLI-F) will be sequestered by Suppressor of fused (SUFU) and trafficked to the primary cilium. GLI-F are phosphorylated by Protein Kinase A (PKA) which targets them for proteolytic processing into their repressive forms (GLI-R). GLI-R blocks transcriptions of SHH target genes. In the presence of SHH ligand (SHH), SHH will bind PTCH and remove its negative pressure on SMO. This allows SMO to enter and accumulate in the primary cilium. SMO dissociates the SUFU/GLI-F complexes, allowing GLI to be converted to its active forms (GLI-A) which induce transcription of SHH target genes.

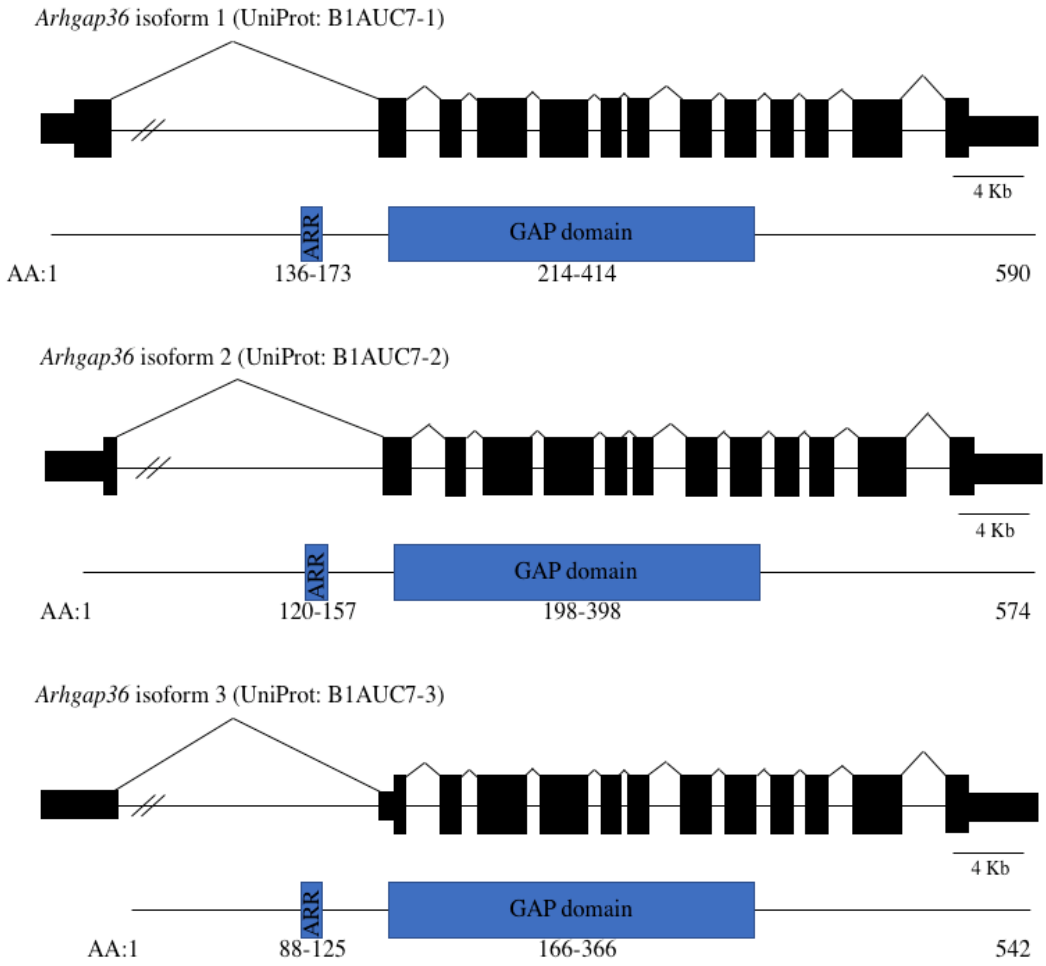


| Isoform | UniProt # | Length (AA) | Mass (kDa) | Description |
|---|---|---|---|---|
| Isoform 1 | B1AUC7-1 | 590 | 67 | Full length protein |
| Isoform 2 | B1AUC7-2 | 574 | 65 | 1-19: MAWMLDCLFASAFEPRPRR → MKL |
| Isoform 3 | B1AUC7-3 | 556 | 63 | 1-34: Missing |

**Figure 1.4. *Arhgap36* locus in the mouse.**
Arhgap36 has 3 isoforms expressed in the mouse. The predominant isoform (isoform 1, UniProt ID: B1AUC7-1) produces a 590 AA protein from a 3033 bp transcript. The second and third isoforms are 574 and 556, respectively, through N-terminal truncation. These isoforms are reported on UniProt under identifier (B1AUC7).

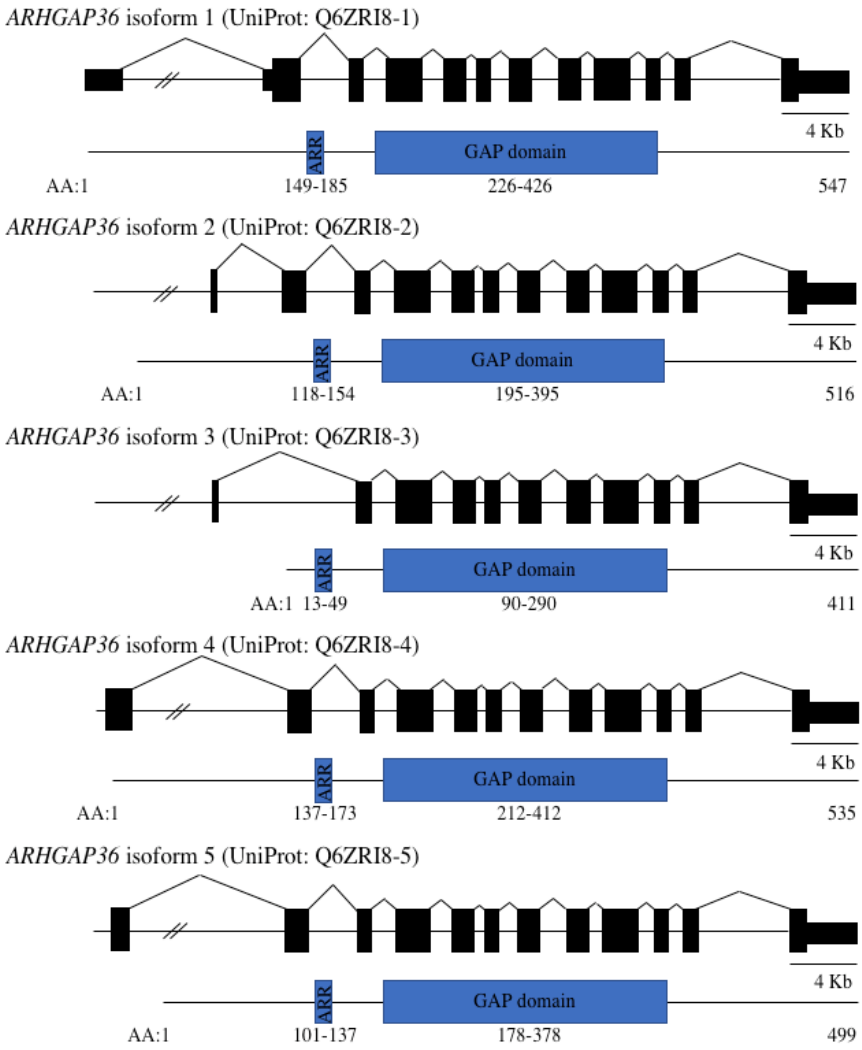


| Isoform | UniProt # | Length (AA) | Mass (kDa) | Description |
|---|---|---|---|---|
| Isoform 1 | Q6ZRI8-1 | 547 | 62 | Full length protein, Ensembl 201 |
| Isoform 2 | Q6ZRI8-2 | 516 | 58 | 1-32: MGGCIPFLKAARALCPRIMPPLLLLSAFIFLV → M, Ensembl 204 |
| Isoform 3 | Q6ZRI8-3 | 411 | 46 | 1-136: Missing, Ensembl 202 and 206 |
| Isoform 4 | Q6ZRI8-4 | 535 | 61 | 1-31: MGGCIPFLKAARALCPRIMPPLLLLSAFIFL → MAWILDCLFASAFEPRPRR, Ensembl 203 |
| Isoform 5 | Q6ZRI8-5 | 499 | 57 | 1-48: Missing, not represented on Ensembl |

**Figure 1.5. *ARHGAP36* isoforms expressed in humans.**
There are 5 isoforms of ARHGAP36 expressed in humans according to UniProt (identifier Q6ZRI8). Isoforms 2-5 differ in their N-terminus from the canonical isoform 1. The locus schematics show shorter boxes for untranslated regions of the mRNA, taller boxes for protein coding regions. Each protein product made from individual isoforms is shown below, depicting the Argine rich regions (ARR) and GTPase activation protein (GAP) domains. All 5 isoforms contain the two putative functional domains. The table depicts the exact protein coding changes in isoforms 2-5, as well as the corresponding sequence in Ensembl, if it exists.

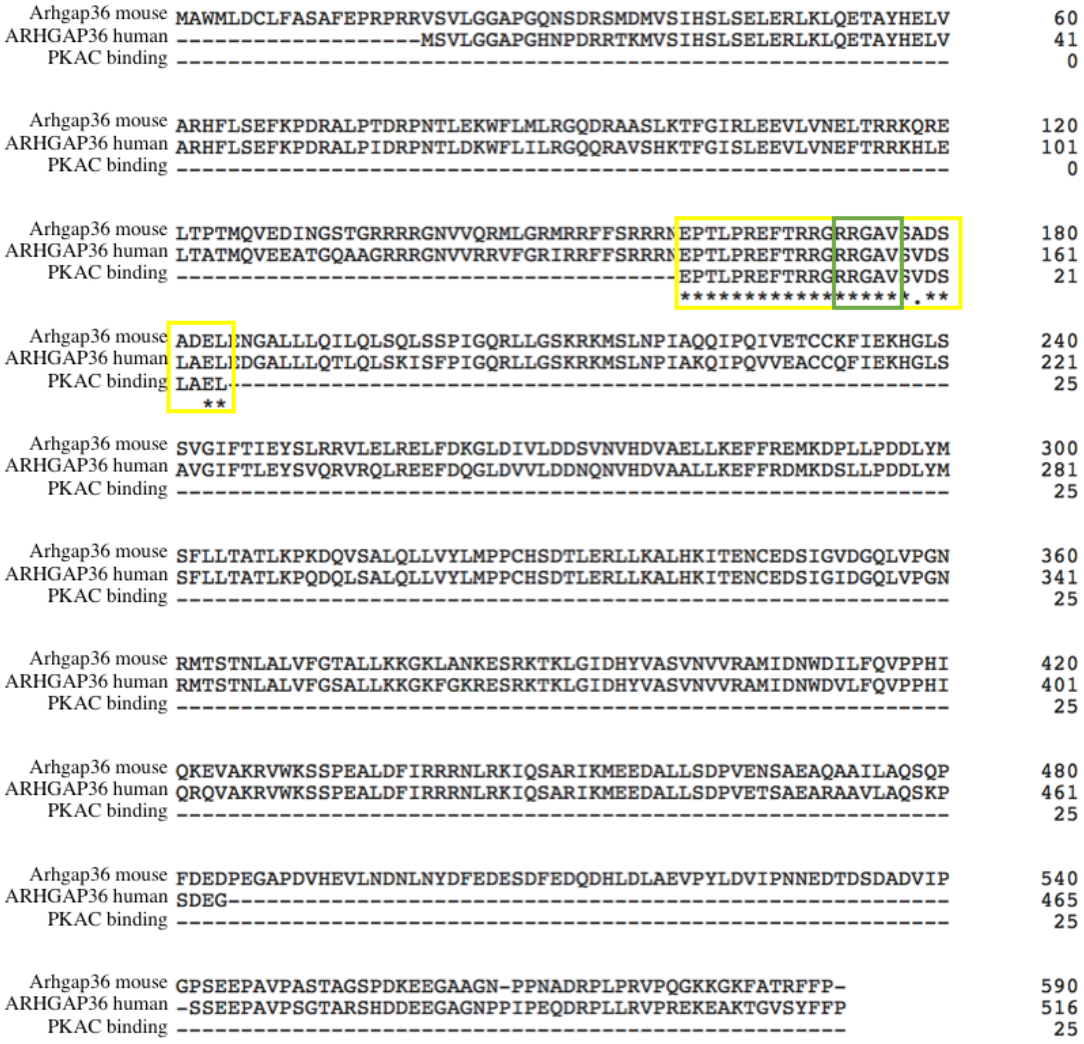


**Figure 1.6. Alignment of mouse and human ARHGAP36 with the PKAC interaction site noted.**

The isoforms of ARHGAP36 used in previous publications are shown for mouse (isoform 1, B1AUC7-1) and human (isoform 2, Q6ZRI8-2). The PKAC binding site is identified in Eccles et al. using human ARHGAP36. The yellow box shows the PKAC binding site and its alignment with both human and mouse ARHGAP36. The green box shows the specific RRGAV sequence identified as the interacting residues between ARHGAP36 and PKAC.

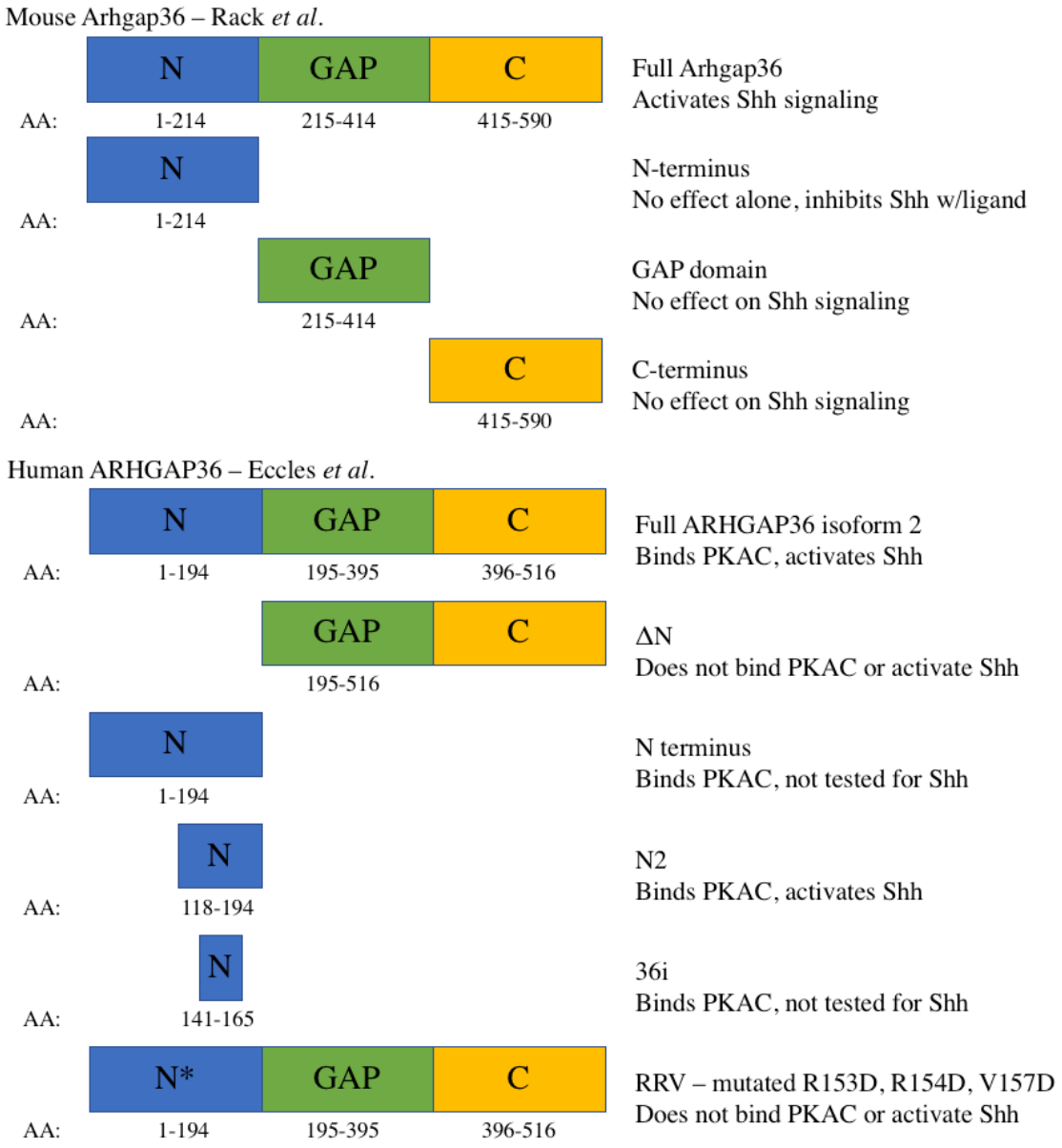


**Figure 1.7. ARHGAP36 constructs used in Rack et al. and Eccles et al.**
The canonical isoform of mouse Arhgap36 (B1AUC7-1) is shown for the functional analysis by Rack et al. and the second human isoform (Q6ZRI8-2) is shown for the functional analysis by Eccles *et al*. The reported results of Shh signaling activation in the 3T3 GFP cell line Gli1 reporter are shown along with binding capacity to the catalytic subunit of PKA (PKAC).

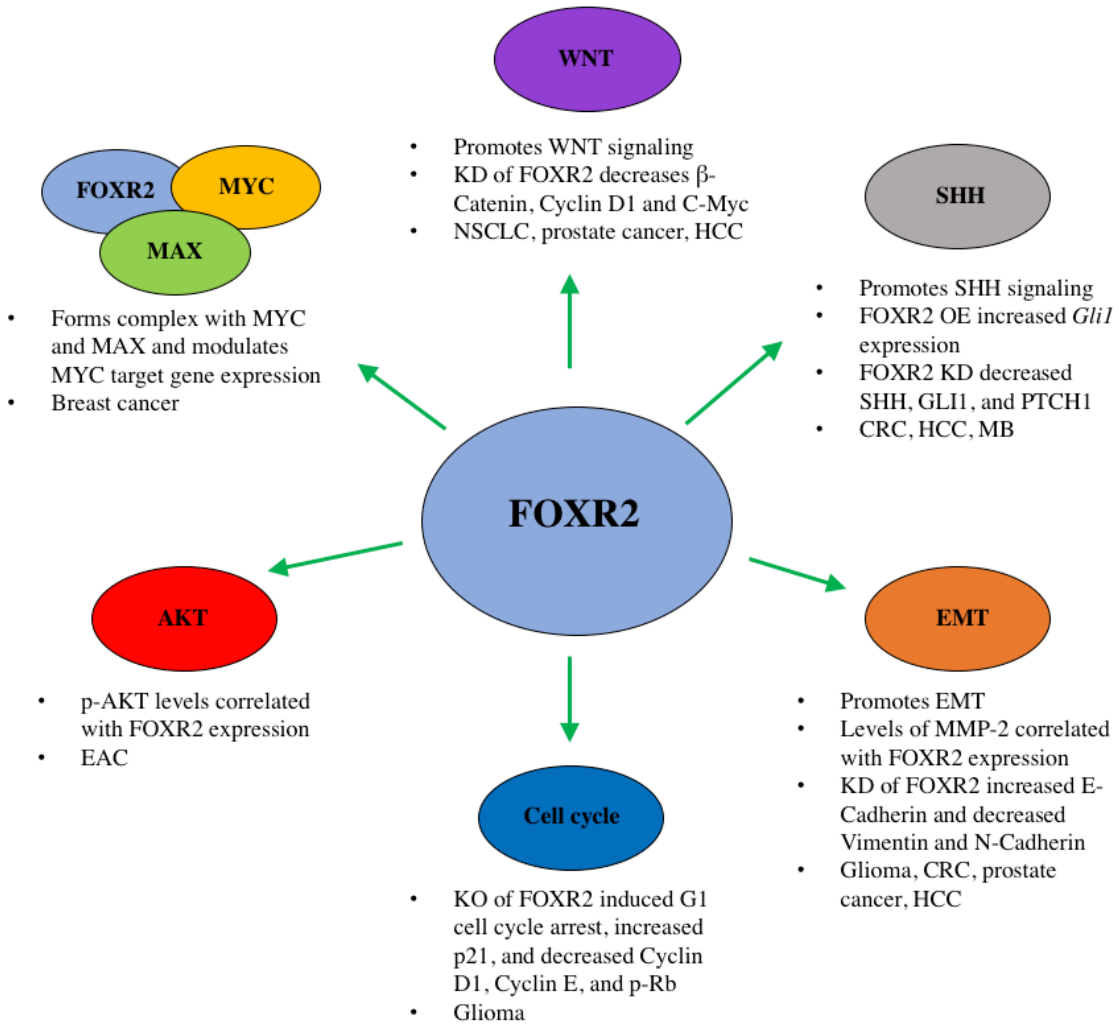


**Figure 1.8. Published mechanisms for *FOXR2*-driven oncogenesis**.
FOXR2 has been shown to promote tumorigenesis in many different cancer types through a variety of mechanisms. In breast cancer, FOXR2 forms a stable complex with MYC and MAX and promotes MYC-dependent transcription(Li *et al*. 2016). FOXR2 has been shown to promote WNT signaling in non-small cell lung cancer (NSCLC)(Wang *et al*. 2018), prostate cancer(Xu *et al*. 2017), and hepatocellular carcinoma (HCC)(Wang *et al*. 2016). FOXR2 has also been shown to promote SHH signaling in colorectal cancer (CRC)(Lu *et al*. 2017), HCC(Wang *et al*. 2016), and medulloblastoma (MB)(Koso *et al*. 2014). FOXR2 has reported roles in promoting epithelial mesenchymal transition (EMT) in glioma(Liu *et al*. 2017), CRC(Lu *et al*. 2017), prostate cancer(Xu *et al*. 2017), and HCC(Wang *et al*. 2016). Lastly, FOXR2 has reported roles in cell cycle regulation and activation of AKT in glioma(Liu *et al*. 2017) and endometrial adenocarcinoma (EAC)(Deng *et al*. 2017), respectively.

## Chapter 2:

*Sleeping Beauty* insertional mutagenesis reveals important drivers in central nervous system embryonal tumorigenesis

*The following chapter contains material from a manuscript under review:

**Beckmann, Pauline J**, Larson, Jon D, Larrson, Alex T, Ostergaard, Jason P, Wagner, Sandra, Rahrmann, Eric O, Shamsan, Ghaidan A, Otto, George M, Williams, Rory L, Tschida, Barbara R, Das, Paramita, Dubuc, Adrian M, Moriarity, Branden S, Picard, Daniel, Xiaochong, Wu, Rodriguez, Fausto J, Rosemarie, Quincy, Krebs, Ryan, Molan, Amy M, Demer, Addison M, Frees, Michelle M, Rizzardi, Anthony E, Schmechel, Stephen C, Eberhard, Charles G, Jenkins, Robert B, Odde, Dave J, Huang, Annie A, Taylor, Michael D, Sarver, Aaron L, Largaespada, David A. *Sleeping Beauty* insertional mutagenesis reveals important drivers in central nervous system embryonal tumorigenesis. Under review.

**Preface**

Medulloblastoma and primitive neuroectodermal tumors of the central nervous system (CNS-PNET) are aggressive, poorly differentiated brain tumors with limited effective targeted therapies. Using *Sleeping Beauty* (*SB*) transposon insertional mutagenesis we identified novel genetic drivers of medulloblastoma and CNS-PNET. Cross-species gene expression analyses classified the *SB*-driven tumors into distinct medulloblastoma and CNS-PNET molecular subgroups, indicating *SB*-derived medulloblastomas resemble human SHH and group 3 and 4 medulloblastomas, and a subset of *SB*-derived CNS-PNETs resemble the human FOXR2 neuroblastoma (NB-*FOXR2*) CNS-PNET subgroup. Importantly, this represents the first genetically-induced mouse model of CNS-PNET and provides a rare model of group 3 and 4 medulloblastoma. We identified several putative proto-oncogenes including *Arhgap36*, *Megf10*, and *Foxr2*. Genetic manipulation of these genes demonstrated a robust impact on CNS tumorigenesis *in vitro* and *in vivo*. Overexpression of *FOXR2*, *ARHGAP36*, or *Megf10* in neural precursors significantly increased anchorage-independent growth *in vitro* and tumor formation *in vivo*. Further dissection of the molecular pathways driving these phenotypes revealed that FOXR2 directly interacts with C-MYC and N-MYC, altering MYC signaling by increasing C-MYC protein stability. Additionally, *FOXR2* overexpression led to activated FAK signaling which was reduced with *FOXR2* knockout. Altogether, our study identified several promising therapeutic targets in medulloblastoma and CNS-PNET

**Implications**: This study describes a transposon mutagenesis-induced mouse model of non-Wnt medulloblastoma and CNS-PNET and highlights several novel therapeutic target candidates, including *Arhgap36*, *Foxr2,* and *Megf10*. New roles for FOXR2 in C-MYC stability and FAK/SRC activation are also described.

## Introduction

Embryonal tumors, including medulloblastoma and primitive neuroectodermal tumors of the central nervous system (CNS-PNET), are the most common malignant pediatric brain tumors, accounting for approximately 20% of primary brain malignancies in children(1). In this manuscript, CNS-PNET is used according to the 2007 World Health Organization CNS tumor classification and includes CNS neuroblastomas (NB), CNS ganglioneuroblastomas, medulloepitheliomas, and ependymoblastomas(15). Medulloblastoma and CNS-PNET have similar histology, with densely-packed, small tumor cells with hyperchromatic nuclei and little cytoplasm. Medulloblastomas are most commonly cerebellar, while CNS-PNETs occur predominantly in the cerebral hemispheres, brain stem and spinal cord. Although aggressive, multi-modality treatments improve survival, they produce lifelong side effects, and the 5-year overall survival rates remain 60-65% for medulloblastoma and 20-40% for CNS-PNET(2).

Recent work has provided insight into the heterogeneous nature of medulloblastoma and CNS-PNET. Medulloblastoma includes at least four molecular subgroups: WNT, SHH (*TP53* mutant and wildtype), group 3, and group 4. WNT and SHH subgroup medulloblastoma are associated with mutations activating those pathways, but groups 3 and 4 remain less defined(55). A large genomic study by Picard *et al*. identified three distinct subgroups of CNS-PNET: primitive-neural, oligo-neural, and mesenchymal(128). Using methylation and gene expression-based analysis, Sturm *et al*. identified significant overlap of CNS-PNET and a variety of other pediatric brain tumors and revealed 4 new molecular subgroups associated with gene fusions(125). While progress has been made to understand the biology of these tumors, a barrier to improving targeted therapies is the current lack of animal models and targetable oncogenic drivers, particularly in non-SHH medulloblastoma and CNS-PNET.

We used *Sleeping Beauty* (*SB*) transposon insertional mutagenesis to identify novel drivers of both medulloblastoma and CNS-PNET in an unbiased manner. This method has previously identified genetic drivers of brain tumors, including medulloblastoma(109,110). Here, we initiated transposition in neural progenitor cells using *Nestin*-driven Cre recombinase alone or in combination with dominant-negative *Trp53*$^{lsl\text{-}R270H/+}$ or *Pten*-deficiency to generate medulloblastomas and CNS-PNETs. These

tumors resembled human medulloblastoma and CNS-PNET histologically and transcriptionally. Three oncogenes, *Arhgap36*, *Foxr2*, and *Megf10*, were validated *in vitro* and *in vivo* and their mechanisms examined.

## Methods

### Generation of transgenic mice

All mice were bred and cared for under the guidelines of the University of Minnesota Animal Care and Use Committee. *Nestin-Cre* mice(258) were bred to either low-copy *T2/Onc* (chromosome 15 or 1)(182) or high-copy *T2/Onc2* (chromosome 4)(183) to generate *Nestin-Cre*:*T2/Onc(2)* double transgenic mice. *Rosa26*$^{lsl\text{-}SB11/+}$(186) were bred to either *Trp53*$^{lsl\text{-}R270H/+}$(259) or *Pten*$^{flox/flox}$(260) to generate *Rosa26*$^{lsl\text{-}SB11/+}$:*Pten*$^{flox/flox}$ or *Rosa26*$^{lsl\text{-}SB11/+}$: *Trp53*$^{lsl\text{-}R270H/+}$ double transgenic mice. *Nestin-Cre*:*T2/Onc(2)* mice were then bred to *Rosa26*$^{lsl\text{-}SB11/+}$:*Pten*$^{flox/flox}$ or *Rosa26*$^{lsl\text{-}SB11/+}$: *Trp53*$^{lsl\text{-}R270H/+}$ mice to generate mice with and without CNS-restricted insertional mutagenesis on wildtype (WT), *Trp53*$^{lsl\text{-}R270H/+}$ and *Pten*$^{flox/+}$ backgrounds. *T2/Onc(2)* excision PCR was performed as described(182). Primers are listed in Table 2.1.

### Immunohistochemistry, immunoprecipitation, and western blotting

Unstained tissue microarray (TMA) sections of formalin-fixed, paraffin-embedded (FFPE) human tumor specimens were obtained through the University of Minnesota Biological Materials Procurement Network (11 samples) and Johns Hopkins University (54 samples). FFPE mouse tissue slides were stained with Hematoxilin and Eosin (H&E) or immunohistochemistry (IHC) using standard methods. Immunoprecipitation (IP) assays were done using a Nuclear Complex CoIP Kit (Active Motif #54001). CoIP was done with 500 μg total protein and captured using Protein G Agarose Columns (Active Motif #53039). Protein for western blotting (non-CoIP) was detected in whole cell lysates harvested with RIPA buffer as described(135). Antibodies are listed in Table 2.2. Probing was done according to manufacturer's protocol. Target proteins were visualized using chemiluminescence (Advansta K-12042) and a LI-COR imaging system.

### DNA-Common insertion site (D-CIS) analysis

Linker-mediated PCR to identify transposon insertion sites was performed as described(135). Transposon insertion sites were annotated using the TAPDANCE software(261). Non-redundant insertion sites that represented greater than 0.1% of the mapped insertions from each tumor library were used to generate top candidate CIS (*P*-value < 0.05) for medulloblastoma and CNS-PNET.

**RNA-Sequencing (RNA-Seq)**

Upon necropsy, tumors were snap-frozen. Isolated RNA (RNA midi extraction kit, Qiagen) was assessed for quality using capillary electrophoresis (RIN>6.5, Agilent 2100 BioAnalyzer). Paired-end sequencing (30-40 million reads per sample) of TruSeq-prepared libraries was performed at the University of Minnesota Genomics Center (Illumina HiSeq 2000). Raw FASTQ files are available at the NCBI Sequence Read Archive and linked to Gene Expression Omnibus SuperSeries. FASTQ files were mapped to the MM10 genome (including *T2/Onc* and *Rosa26*$^{lsl\text{-}SB11/+}$ as additional chromosomes)(262) using STAR-Fusion (https://github.com/STAR-Fusion/STAR-Fusion/wiki). Transcript FPKM values were computed using cuffquant and cuffnorm and adjusted by +0.1(263).

***T2/Onc* fusion identification**

To identify *T2/Onc*:genome fusions, both the chimeric.out.junction and the chimeric.out.sam output files from STAR-Fusion were parsed to summarize the number of junction (one read contains the junction between the *T2/Onc* splice donor or acceptor and the genome) and bridge (one paired-end read maps to *T2/Onc* and the other to the genome) reads present within 1000 bp regions. Fusions supported by ≥ 1 junction read or ≥ 3 bridging reads were retained for analysis. Manual detection of *T2/Onc(2):Arhgap36* fusion transcripts was done using 500ng of purified mouse tumor RNA (TRIzol, Invitrogen 15596-018) reverse-transcribed (SuperScript III, Invitrogen 18080-051) and amplified using primers in Table 2.1.

**Gene cluster similarity (GC-SIM)**

GC-SIM was used to identify similar gene clusters across different transcriptional datasets in an unsupervised, unbiased manner. Transcriptional profile datasets were individually log transformed, mean centered, filtered for highly variant genes, and hierarchically clustered using average linkage and (1 – Pearson correlation) as the distance metric. Gene clusters with node correlation and size greater than respective thresholds were retained. Cross-dataset cluster pairs were tested for enrichment of common gene members (Fisher's Exact Test) to identify conserved transcriptional patterns across the datasets.

**RT-PCR and 5′-rapid amplification of cDNA ends (5'-RACE)**

For CNS-PNET expression analysis, cDNAs were synthesized using the High Capacity cDNA Reverse Transcription Kit (Applied Biosystems 4368814) per the manufacturer's instructions. qRT-PCR was performed using TaqMan® probes and Master Mix (Invitrogen 4369016). Two μg of purified cellular RNA (PureLink RNA Mini Kit, Ambion 12183025) was reverse transcribed (3 technical replicates) using the SuperScript VILO (Invitrogen 11755050) recommendations. qRT-PCR was performed in triplicate using FastStart SYBR Green Master Mix (Roche 4673492001). Shh pathway activation was done as described(189) for *Gli1* expression analysis. For 5'-RACE, total RNA was extracted from human medulloblastoma tumor samples using TRIzol (Invitrogen 15596-018). Normal human brain RNA was purchased from BioChain: fetal cerebellum (R1244039-50), fetal brain (R1244035-50), adult cerebellum (R1234040-10). 5'-RACE was conducted using the FirstChoice RLM-RACE Kit (Ambion AM1700). Subsequent detection of transcripts by RT-PCR was performed with 500 ng total RNA using SuperScript III (Invitrogen 18080-051). Primers and probes are listed in Table 2.1.

**Cell culture/assays**

Media components and cell line sources are described in Table 2.3. All cell lines were grown at 37°C in 5% $CO_2$. Proliferation and soft agar assays were done as described(135). Briefly, MTS assays (Promega G1111) were done following the manufacturer protocol with 1200 cells per well measured over 5 days. Soft agar assays were plated in 6 well plates with 10,000 cells/well; six plates were averaged for each condition. Transfections were

done as described(135). Stable lines transfected with cDNAs (*ARHGAP36* (Q6ZRI8-5), *FOXR2* (Q6PJQ5-1), *Megf10* (Q6DIB5-1)) were cultured as polyclonal populations after selection in Puromycin. Transient transfection in HEK293T was done using Lipofectamine 2000 (Invitrogen 11668019) per manufacture's protocol. CRISPR KO clones were isolated as described(135). Briefly, Daoy WT cells were transfected with PiggyBAC transposase and a Puromycin-selectable PiggyBAC transposon vector containing 2 *FOXR2* guide RNAs and Cas9. Clones were isolated under Puromycin and sequenced to identify changes in the *FOXR2* locus. Guide RNA sequences are listed in Table 2.1. Wound healing assays were performed as described(264).

***in vivo* assays**

Neonatal NRG mice (Jackson 007799) were injected as described(106). Briefly, C17.2 cells at 80% confluency were prepared in HBSS, counted, and stored on wet ice prior to injection ($2x10^5$ cells/2µl injection). P0 mice were anesthetized using hypothermia and injected in the fourth ventricle at stereotactic coordinates: 1.5mm anterior to Bregma, 1.5mm deep beyond the dura. Successful injection was verified on P1 by luciferase imaging as described(106). Adult intracranial injections were performed as described(78). Female NU/J mice (Jackson 002019, 6-8 weeks old) were anesthetized with 81 mg/kg ketamine, 13.8 mg/kg xylazine by intraperitoneal injection. $1x10^6$ cells (prepared as above) were injected in 5µl HBSS. For flank tumor assays, female NU/J mice (Jackson 002019, 6-8 weeks old) were injected with $1x10^6$ C17.2 cells (prepared as above) resuspended 1:1 in HBSS and Matrigel (Corning CB-40234C). Tumors were measured weekly using a digital caliper. Tumor volume = $(l \times w^2)/2$, $l$ = tumor length and $w$ = tumor width.

**Results**

***SB* Insertional Mutagenesis Promotes medulloblastoma and CNS-PNET Formation**

To identify genetic drivers of medulloblastoma and CNS-PNET, we targeted $Nestin^+$ neural and glial precursor cells with *SB* insertional mutagenesis on three genetic backgrounds: wildtype (WT), *Pten* heterozygous ($Pten^{flox/+}$) or *Trp53* mutant ($Trp53^{lsl\text{-}R270H/+}$). $Pten^{flox/+}$ and $Trp53^{lsl\text{-}R270H/+}$ were used as sensitizing backgrounds as they are commonly mutated in human medulloblastoma(54) and occur in CNS-PNET(133). SB expression in our target

cells was evaluated by IHC. SB was expressed throughout the developing brain, including granule cells, white matter cells, cells surrounding the fourth ventricle, subependymal midbrain, subventricular zone, and olfactory bulb (Figure 2.1A-G). To induce transposon mutagenesis, experimental cohorts harbored one of three mutagenic transposon concatomers (Figure 2.1H). *SB*-mutagenesis significantly reduced survival in combination with *Trp53*$^{lsl\text{-}R270H}$ (Figure 2.1I-K). At time of necropsy we observed masses in the brain, testicles, bone, peripheral lymph nodes, and spleen (Figure 2.1I-K, Table 2.4).

Histological analysis of *SB*-mutagenized brain masses revealed the presence of infratentorial medulloblastoma or supratentorial CNS-PNET. Macroscopic tumors were observed in mice undergoing *SB* mutagenesis (total of 22 medulloblastomas and 14 CNS-PNETs) with varying frequency depending on genetic background, with the highest frequency of medulloblastoma in mice carrying *Trp53*$^{lsl\text{-}R270H/+}$ (Figure 2.2A-B). No CNS-PNETs were recovered on the *Pten* deficient background. The high-copy transposon (*T2Onc2*, chromosome 4) produced the highest proportion of medulloblastoma, while the CNS-PNETs were equally derived from concatomers on chromosome 4 or 15 concatomers (Figure 2.2C). Tumors expressed nuclear SB by IHC and showed transposon mobilization by PCR (Figure 2.2D-E).

### *SB*-induced medulloblastoma and CNS-PNET Resemble Human Tumors Histologically

*SB*-induced medulloblastoma originated in the cerebellum and displayed morphology characteristic of human medulloblastoma, including small round cells with high nuclear:cytoplasmic ratios, Homer-Wright rosettes, vascularization, and mitotic figures (Figure 2.3A). *SB*-induced medulloblastomas expressed conventional markers of human medulloblastoma by IHC, including Synaptophysin, Ki67, and Nestin, markers of neuronal origin, proliferation, and neural progenitors, respectively, and were negative for the astrocytic marker Gfap (Figure 2.3A). Metastatic characteristics, including leptomeningeal spread and tumor cell infiltration into the parenchyma or brainstem, were observed in 50% (11/22) of medulloblastomas across all genetic backgrounds (Figure 2.3A, Table 2.4). *SB*-induced CNS-PNETs were found in the rostral portion of the brain, commonly overwhelming the olfactory bulbs, lateral ventricle and cortex (Figure 2.3B).

Tumors histopathologically resembled human CNS-PNETs, with small round cells with high nuclear:cytoplasmic ratios, Homer-Wright rosettes, vascularization and mitotic figures (Figure 2.3B). All CNS-PNETs showed cellular infiltration into the parenchyma, leptomeninges, and/or cortex (Table 2.4), expressed conventional markers used in human CNS-PNET diagnosis: Ki67, Synaptophysin and Nestin, and stained negative for Gfap, except for reactive astrocytes within the bulk tumor (Figure 2.3B). Leptomeningeal spread is of interest to us as it has been difficult to model in the mouse and is a deadly characteristic present in approximately one third of patients with medulloblastoma and CNS-PNET(109,128).

### *SB*-induced medulloblastomas resemble SHH and group 3 and 4 human medulloblastoma

To determine what subtypes of human medulloblastoma our *SB*-induced mouse tumors most closely represented, we used RNA-Sequencing (RNA-Seq) to compare our tumors to published human MB data sets. Transcriptional profiling of 18 *SB*-induced medulloblastomas revealed two clear subgroups (Figure 2.4A). The first subgroup (N=13) showed increased levels of *Gli1* and *Sfrp1*, genes canonically associated with human SHH medulloblastoma(17). The second subgroup (N=5) showed increased levels of *Kcna1*, a canonical marker for human group 4 medulloblastoma(17). When compared to a published medulloblastoma dataset(125), the *SB*-derived medulloblastoma gene set highly expressing *Gli1* and *Sfrp1* was significantly enriched for genes (N=48) that were highly expressed in the human SHH medulloblastoma subtype (Figure 2.4A, Table 2.5). Similarly, the *SB*-derived medulloblastoma gene set containing *Kcna1* was significantly enriched for genes (N=120) that were highly expressed in human group 3 and 4 medulloblastoma. No Wnt medulloblastoma signatures were identified in the *SB*-induced medulloblastoma.

### *SB*-induced CNS-PNET resemble human CNS neuroblastoma with *FOXR2* activation

Using the same approach to compare *SB*-induced mouse CNS-PNETs to human CNS-PNETs, transcriptional profiling of mouse *SB*-induced CNS-PNETs (N=5) and

published human CNS-PNETs (N=58) revealed two subgroups (Figure 2.4B)(125). A single cluster of co-varying genes (N=298) was significantly enriched in both human and mouse CNS-PNET and contained high levels of CNS NB-*FOXR2* enriched genes, including *MMP24*, *KCJN9*, and *CHGB* (Figure 2.4B, Table 2.6). In agreement with a CNS NB-*FOXR2* classification, *SB*-induced CNS-PNETs showed significantly increased *Olig1*, *Oli2*, and *Sox10* by qPCR (Figure 2.5A). The three remaining mouse CNS-PNETs had increased expression of some CNS EFT-*CIC* marker genes (*Shc4*, *Argdib*, and *Pole*) but did not correspond clearly to one subgroup of human CNS-PNET (Figure 2.4B).

**CIS reveal candidate cancer genes**

To identify novel genetic drivers of medulloblastoma and CNS-PNETs, we performed linker-mediated PCR on 22 medulloblastomas and 13 CNS-PNETs. A total of 390,000 and 155,000 non-redundant insertions for medulloblastoma and CNS-PNET, respectively, were sequenced. TAPDANCE analysis(261) identified 13 and 15 DNA-CIS (D-CIS) in medulloblastoma and CNS-PNET, respectively (Figure 2.6A, Table 2.7). We also identified RNA-CIS (R-CIS) in both tumor types, defined as transposon fusion transcripts present in more than 10% of cases and more than one tumor (Figure 2.6A, Tables 2.8 and 2.9). For several putative oncogenes, the presence of a *T2/Onc(2)* fusion transcript significantly increased expression (Figure 2.6B). We identified genes previously implicated in medulloblastoma, including *Gli1* and *Pten*; upregulation of *GLI1* expression and PI3K pathway activation through *PTEN* loss are observed in human medulloblastoma(54). Predicted transposon-mediated driving effects on Gli1 expression were confirmed by IHC (Figure 2.6C). We also confirmed a reduction in Pten and a corresponding increase in pAkt in mouse medulloblastoma with *Pten* insertions (Figure 2.6D).

We identified known and novel molecular events in *SB*-induced CNS-PNETs. *Pten* was predicted as a candidate tumor suppressor gene (TSG) and loss of *PTEN* through 10q copy loss or mutation has been observed in human CNS-PNET(133). Unique to this study, *NF1* was the most targeted CNS-PNET TSG. We identified several other genes with predicted effects on Ras signaling activation, including overexpression of *Eras* and disruption of *Erbb2ip* and *Rasa3* (Table 2.4). Collectively, tumors harboring

these insertions exhibited increased pErk (Figure 2.7A, Table 2.4) supporting Ras pathway activation. We also observed *NF1* locus deletion in a subset of human CNS-PNET (Figure 2.7B)(128).

Furthermore, several genes were identified as both D-CIS and R-CIS in *SB*-induced medulloblastoma and CNS-PNET. *Arhgap36* was the most frequently modified gene in our screen, with insertions identified in 14 and 13 medulloblastomas at the DNA and RNA level, respectively, and in 2 CNS-PNETs by RNA-Seq. *Foxr2*, a member of the forkhead box transcription factor family, was both a D and R-CIS and a predicted oncogene in medulloblastoma. *Enox2* (predicted *SB* oncogene), a tumor-associated NADH oxidase, was also a D and R-CIS in medulloblastoma. While *Enox2* is not currently implicated in medulloblastoma, it was shown to be involved in the growth of several cancer cell lines(265).

To determine the importance of our CIS genes in human tumors, we analyzed their expression in published human medulloblastoma and CNS-PNET transcriptomic data (Figure 2.8A-C)(125). Interestingly, *ARHGAP36* is expressed at high levels in group 3 and 4 human medulloblastoma, with low levels in the SHH subgroup. In the mouse, *Arhgap36* insertions occurred in Shh and group 3/4 tumors (7/12 Shh and 4/5 group 3/4 tumors with *Arhgap36* insertions, Table 2.4). *GRIA4* showed high expression in both SHH medulloblastoma and CNS NB-*FOXR2*. *FOXR2* is elevated in a subset of WNT medulloblastoma and CNS NB-*FOXR2*. *MEGF10* is upregulated in a small subset of non-SHH medulloblastoma.

**ARHGAP36 expression is associated with poor prognosis in human medulloblastoma**

Transposon location and orientation implicated *Arhgap36* as an oncogene, with insertions occurring upstream of the locus or within intron 1 and promoting gene expression (Figure 2.9A). Additionally, fusion transcripts led to significantly increased transcript expression (Figure 2.9B). *T2/Onc:Arhgap36* transcripts displayed precise fusion of the *T2/Onc* splice donor to the *Arhgap36* exon 2 splice acceptor (Figure 2.9C). This fusion generates a 15 amino acid N-terminal truncation, with translation from an in-frame ATG. Tumors with *Arhgap36* insertions showed high levels of cytoplasmic Arhgap36 by IHC compared to tumors without *Arhgap36* insertions, which displayed sparse nuclear

expression similar to normal granule cells (Figure 2.9D). Spatial and temporal analysis of ARHGAP36 expression in normal human and mouse cells of the developing cerebellum showed nuclear localization throughout the molecular layer (ML), Purkinje cell layer (PC) and internal granule cell layer (IGL); mature cerebella showed similar expression in the ML, PC and IGL (Figure 2.9E).

To determine the relevance of *ARHGAP36* in human medulloblastoma, we evaluated ARHGAP36 expression in two human tissue microarrays (TMAs). 37/65 (56%) tumors displayed cytoplasmic ARHGAP36 expression whereas 8/65 (12%) showed strong nuclear expression (Figure 2.10A). ARHGAP36 expression was observed across all four human subgroups (Figure 2.10B)(17) and overall and cytoplasmic ARHGAP36 expression correlated with accelerated mortality (Figure 2.10A-B). Four of five patients with confirmed metastatic disease also showed cytoplasmic ARHGAP36 expression.

We further investigated *ARHGAP36* transcript profiles in normal and malignant human brain tissue, using 5′-RACE on human group 3/4 medulloblastoma samples and cell lines and normal cerebellar cells. Several *ARHGAP36* amplification products were identified (Figure 2.11A-B) predicting expression of canonical isoform 1 (*), isoform 5 (**), and isoform 3 (***; ****). All 3 isoforms contained intact predicted functional domains for ARHGAP36, including an arginine-rich domain (ARR), nuclear localization sequence (NLS), and GTPase-activating protein domain (GAP). Interestingly, the 5' ends of *** and **** begin with distinct intron 2 sequences splicing to exon 3 and an in-frame ATG located in exon 4. Target-specific RT-PCR revealed these *ARHGAP36* sequences in additional tumor samples (Figure 2.11C). Canonical isoform 1 was the only isoform detected in normal fetal cerebellum. We predict that N-terminally truncated isoforms of *ARHGAP36* possess pathological function in human medulloblastoma similar to the N-terminally truncated *Arhgap36* transcript in *SB*-induced mouse tumors (Figure 2.9A).

**N-terminally truncated ARHGAP36 promotes tumor formation in neural progenitor cells through activation of Shh signaling**

To further characterize the role of ARHGAP36 in promoting medulloblastoma, we overexpressed truncated *ARHGAP36* (isoform 5) in the mouse neural progenitor cell line, C17.2, which models a medulloblastoma cell of origin(266) (Figure 2.12A).

Increased ARHGAP36 expression significantly enhanced soft agar colony formation but did not affect proliferation or collective cell migration rate (Figure 2.12B-D). C17.2 cells expressing ARHGAP36 formed tumors significantly faster in the flanks of NU/J mice than luciferase-transfected (C17.2 Luc) control cells, with 4/5 mice reaching tumor size endpoint (2 cm) by 10 weeks (Figure 2.12E). ARHGAP36 expression also reduced survival in adult NU/J and neonatal NRG mice orthotopically injected with C17.2 cells (median survival reduced from 99 to 71 days and from 180 to 104 days, respectively) (Figure 2.12F-G). As previously reported, ARHGAP36 strongly activated Shh signaling in a ligand independent manner (Figure 2.12H) (188,189). Additionally, *SB* transposon insertions in the *Arhgap36* locus were mutually exclusive with those in Shh signaling pathway activators, *Gli1* and *Gli2,* supporting that *Arhgap36* likely signals through this pathway (Figure 2.12I).

### *Megf10* promotes transformation *in vitro* and *in vivo*

*Megf10* (Multiple epidermal growth factor-like domains protein 10, predicted SB oncogene) was identified as an R-CIS, with fusion transcripts present in 3 medulloblastomas which significantly increased transcript expression (Figure 2.13A). We investigated *Megf10* as a candidate proto-oncogene as it is expressed throughout the CNS during development and is a positive regulator of Notch signaling(267). *Megf10* expression in C17.2 cells significantly enhanced colony formation in soft agar and proliferation *in vitro* and promoted tumor formation *in vivo* (Figure 2.13B-C). Megf10 did not promote Notch signaling in C17.2 cells by western blot, however, so the mechanism of transformation in these cells is unknown (Figure 2.13D).

### FOXR2 promotes tumor formation in human and mouse cells

Transposon position and orientation predict an oncogenic role for *Foxr2* in mouse medulloblastoma; all insertions were located upstream of the translation start site and in the forward orientation (Figure 2.14A). The presence of a *T2Onc:Foxr2* fusion transcript significantly increased *Foxr2* expression (Figure 2.14B). Mice with a transposon insertion in the *Foxr2* locus had significantly reduced survival compared to mice with tumors driven by other insertions (116.5 versus 166.5 days median survival, Figure

2.14C). Overexpression of *FOXR2* in C17.2 cells resulted in significantly increased soft agar colony formation and enhanced collective cell migration without increasing proliferation (Figure 2.14D-G). C17.2 FOXR2 cells formed flank tumors significantly faster than C17.2 Luc controls (Figure 2.15A). When injected orthotopically into adult NU/J mice, C17.2 FOXR2 cells migrated to the granule layer of the cerebellum and formed large, vascular tumors, reducing median survival from 99 to 43 days (Figure 2.15B-D). C17.2 FOXR2 cells injected orthotopically into neonatal NRG mice also significantly reduced median survival compared to C17.2 Luc (110 vs 183 days, Figure 2.15E). Using the CRISPR/Cas9 system, we knocked out *FOXR2* in Daoy, a human medulloblastoma cell line. Daoy clone #21 had a nonsense mutation in exon 1, resulting in significantly decreased proliferation and soft agar colony formation, which were rescued by expression of a *FOXR2* cDNA (Figure 2.16A-C).

**FOXR2 has a multi-faceted mechanism of tumorigenesis, including effects on MYC and FAK**

FOXR2 has many suggested oncogenic mechanisms, including interaction with C-MYC(136). We confirmed this interaction by CoIP in a human Schwann cell line, HSC1λ, and C17.2 cells stably expressing Flag-tagged *FOXR2* (Figure 2.16D-E). To determine if FOXR2 interacts with other forms of MYC, we transiently transfected HEK293T cells with V5-tagged *C-MYC*, *L-MYC* and *N-MYC*. We observed reduced interaction of FOXR2 and N-MYC and minimal interaction with L-MYC (Figure 2.16F). To determine if FOXR2 affects C-MYC stability, we treated HSC1λ and C17.2 cells with and without FOXR2 with cycloheximide (CHX) for up to 5 hours to inhibit translation. Almost all C-MYC protein was degraded in luciferase control HSC1λ cells, but C-MYC levels in the presence of FOXR2 were only reduced by half after 3 hours, indicating FOXR2 stabilizes C-MYC (Figure 2.17A). Interestingly, C-MYC was highly stable in C17.2 cells regardless of FOXR2 expression, likely due to their immortalization by V-Myc(266). This implies that FOXR2 promotes tumorigenesis through alternative mechanisms in C17.2 cells (Figure 2.17A).

To further characterize the oncogenic mechanism of FOXR2, we synthesized *FOXR2* cDNA constructs missing the following domains: the predicted

NLS(ΔNLS)(268), MYC interaction domain (ΔMYC)(136), predicted low complexity regions (ΔLC1, ΔLC2 and ΔLC1/2)(269) and forkhead box transcription factor domain (ΔTF)(269)(Figure 2.17B-C). We stably expressed each mutant and performed soft agar assays in C17.2 and HSC1λ cells. Surprisingly, no single deletion mutant completely ablated the colony formation promoting capacity of *FOXR2* in either line, but loss of the Myc interaction domain and low complexity region 2 both significantly reduced colony formation (Figure 2.17B-C). We verified that the *FOXR2ΔMYC* mutant did not bind C-Myc (Figure 2.18A). Given that no single domain loss completely ablates colony formation but some do reduce it, we conclude that FOXR2 likely has a multi-faceted mechanism. Upon observation of *FOXR2* expressing cells, we noticed a slight change in the actin cytoskeleton, encouraging us to assess focal adhesion kinase (Fak) activation in our cells (data not shown). C17.2 cells expressing FOXR2 displayed increased Fak phosphorylation at Y397, resulting in increased Src activation as evidenced by increased phosphorylation at Src Y416 (Figure 2.18B). This effect was independent of Myc, as the *FOXR2ΔMYC* mutant still activated Fak (Figure 2.18C). Correspondingly, loss of FOXR2 in Daoy cells resulted in decreased pFAK and pSRC, a phenotype rescued by expression of *FOXR2* cDNA (Figure 2.18B).

**Discussion**

We used *SB* transposon insertional mutagenesis and RNA-Seq to identify novel drivers of medulloblastoma and CNS-PNET. Over half of our D-CIS and several of our R-CIS genes were reported in previous SB medulloblastoma screens(107-110), including *Pten*, *Wac*, *Arid1b, Arhgap36*, *Foxr2*, and *Megf10*, making them especially compelling candidate genes (Table 2.10). Notably, several R-CIS genes are located on chromosomes 4 and 15, the locations of the *T2/Onc2* and *T2/Onc* concatomers, respectively. Although local hopping may account for bias toward genes on these chromosomes, several of these genes have been implicated in cancer, including *Tle1* and *Ptprd* (270,271). Our medulloblastoma R-CIS genes include several highly compelling targets, including *Megf10*(267). We identified a novel, tumor-promoting role for *Megf10* in neural progenitor cells, the mechanism for which warrants further study.

Ours is the first transposon screen to produce CNS-PNETs. We identified several genes with known roles in neural cancer not previously implicated in CNS-PNET, including *Setd2*, *Ambra1*, and *Usp9x*(272-274). Several Ras signaling pathway genes were mutated in our screen, including *Nf1*, *Eras*, *Pten*, and *Ras3*, suggesting an importance of Ras pathway activation in PNETagenesis and also a cooperation between Ras pathway activation and p53 loss in CNS-PNETs. We also identified *NF1* loss in human CNS-PNETs. Activated RAS/MAPK signaling has been shown to drive formation of CNS NB-*FOXR2* in zebrafish used in cooperation with p53 loss(134) and somatic *PTEN* loss is associated with human CNS-PNET(133). Interestingly, we did not recover any CNS-PNETs on the *Pten* deficient background, possibly indicating that loss of p53 creates a permissive cell for CNS-PNET formation with subsequent Ras activation.

*FOXR2* is a member of the forkhead-box (FOX) family of transcription factors, which contribute to a wide variety of cellular processes, including proliferation, differentiation, migration and apoptosis(275). Several FOX proteins have been identified as human cancer oncogenes and tumor suppressors. *FOXR2* has been implicated as an oncogene in many cancers of neuroectodermal origin, including: malignant peripheral nerve sheath tumors, glioma, CNS-PNET and medulloblastoma (110,125,135,231). Interestingly, although *FOXR2* has been shown to be upregulated in CNS NB-*FOXR2*(125), we did not recover *Foxr2* insertions in the *SB*-induced CNS-PNETs, including the 2 tumors that resembled CNS NB-*FOXR2* transcriptionally. It is possible that other insertions mimic the CNS NB-*FOXR2* phenotype; of the 5 CNS-PNETs sent for RNA-Seq, these 2 tumors exclusively harbored insertions and expressed high levels of *Epb4.1l1*, *Itpr1*, *Rbfox1* and *Sphkap*.

The mechanisms of FOXR2-driven tumorigenesis have proven diverse and elusive. FOXR2 can promote WNT signaling, activate SHH signaling, promote EMT, and affect cell cycle (110,227-229,231). We examined each of these pathways in C17.2 cells and found that FOXR2 did not affect B-catenin localization or *Axin2* mRNA expression, *Gli1* mRNA expression, N-Cadherin, E-Cadherin or Vimentin protein levels, or *p21* and *CyclinD1* mRNA levels (Figure 2.18D, data not shown). As previously reported, we found that FOXR2 binds C-MYC(136) and can promote C-MYC stability. C-MYC is a transcription factor that binds to thousands of promoters, differentially

activating or repressing target gene sets, partly in response to its association with various binding partners(276). Mouse models with C-MYC-driven tumors show an addiction to continued C-MYC expression, suggesting C-MYC is a strong therapeutic target in cancer(242). However, directly targeting C-MYC has been unsuccessful. Therefore, targeting C-MYC interacting proteins, such as FOXR2, may prove useful for cancer therapy.

FOXR2 promotes activation of the FAK/SRC signaling pathway. FAK is a highly conserved, non-receptor tyrosine kinase activated and associated with poor prognosis and drug resistance in a variety of cancers(255). The cause of FAK activation is often unclear and targeting FAK produces deleterious off-target effects. Interestingly, co-targeting of FAK and C-MYC was recently shown to have synergistic effects in ovarian cancer(250). Supporting independent activation of both pathways by FOXR2, the FOXR2ΔMYC mutant activates FAK and transforms C17.2 and HSC1λ cells. The ability of FOXR2 to activate both of these pathways makes it an excellent candidate for targeted therapy. Additionally, FOXR2 has minimal expression in adult tissues, making off-target toxicity risk low(135).

We identified *ARHGAP36* as an oncogene in both mouse and human medulloblastoma and associated its pathology with a truncated isoform. Truncated ARHGAP36 expression promoted anchorage independent growth, flank tumor formation, and reduced survival in two *in vivo* models. As previously described, *ARHGAP36* strongly activated the SHH pathway *in vitro*. *ARHGAP36* activates SHH signaling through direct interactions with two negative regulators of SHH signaling, Suppressor of Fused (SUFU), and Protein Kinase A (PKA)(188,189). Current SHH medulloblastoma therapies targeting an upstream pathway member, Smoothened (SMO), have been met with resistance through SMO mutations(277). Given that its interactions with PKA and SUFU are both downstream of SMO, ARHGAP36 poses a particularly good target for treatment-resistant, SHH-driven medulloblastoma. Additionally, *Arhgap36* was found to be the most up-regulated gene in mouse allografts propagated in the presence of a SMO antagonist(189). Interestingly, despite its clear ability to activate Shh signaling *in vitro*, *Arhgap36* insertions occurred in *SB*-induced Shh and group 3/4 tumors, and *ARHGAP36* is expressed at high levels in human group 3 and 4 medulloblastoma indicating

ARHGAP36 may have non-SHH dependent pro-tumorigenic effects. It is also worth noting that *Arhgap36* was an R-CIS in CNS-PNET and expressed at high levels in some human CNS-PNETs.

Using a *SB* forward genetic screen, we identified several candidate driver genes in medulloblastoma and CNS-PNET relevant to human cancer. To our knowledge, this is the first study to present a genetically-induced CNS-PNET mouse model, providing an opportunity for studying this rare and aggressive tumor. We also present tumors that resemble group 3 and 4 medulloblastoma with high incidence of leptomeningeal spread, again providing a needed mouse model for these tumors. Interestingly, the formation of these diverse tumors types occurred with the use of the same, *Nestin*-driven Cre recombinase, indicating that the cell of origin of non-Wnt medulloblastoma and CNS-PNET is Nestin positive or a close descendent. We used RNA-Seq data to both identify CIS genes and subtype mouse *SB*-induced tumors based on human expression data. *Arhgap36* was identified as our top CIS gene and shown to transform a mouse neuroblast line through Shh pathway activation. *Foxr2* was also identified as a proto-oncogene and shown to promote C-MYC stability and FAK pathway activation. Both of these genes offer promise as novel therapeutic targets in human medulloblastoma and warrant additional study. Further functional testing of additional CIS genes, particularly those identified in CNS-PNET, may reveal additional treatment options for embryonal tumors.

**Table 2.1 - Primers and probes**

| **Primers for SB screen genotyping** | **Forward (5' - 3')** | **Reverse (5' - 3')** |
|---|---|---|
| *Nestin-Cre* | CTGATGGACATGTTCAGGGATCG | CCCACCGTCAGTACGTGAGATATCT |
| *Rosa26*$^{lsl\text{-}SB11}$ | ATGTTTGGAGGAAGAAGGGG | CCATTTGCGACCAAGCTTTA |
| *T2/Onc* or *T2/Onc2* | CGCTTCTCGCTTCTGTTCGC | CCACCCCCAGCATTCTAGTT |
| *Pten*$^{flox}$ | AAAAGTTCCCCTGCTGATTTGT | TGTTTTTGACCAATTAAAGTAGGCTGT |
| *Trp53* (WT) | TTACACATCCAGCCTCTGTGG | CTTGGAGACATAGCCACACTG |
| *Trp53*$^{lsl\text{-}R270H}$ | AGCTAGCCACCATGGCTTGAGTAAGTCTGCA | CTTGGAGACATAGCCACACTG |
| **Excision PCR primers for *T2/Onc* and *T2/Onc2*** | **Forward (5' - 3')** | **Reverse (5' - 3')** |
| *T2/Onc* or *T2/Onc2* | TGTGCTGCAAGGCGATTA | ACCATGATTACGCCAAGC |
| **Primers for manual detection of *T2/Onc(2):Arhgap36* fusion transcripts** | **Forward (5' - 3')** | **Reverse (5' - 3')** |
| *T2/Onc(2)* splice donor forward | CTACTAGCACCAGAACGCCC | |
| Mouse *Arhgap36* Exon5 Reverse | | GATTTGTTGAGCAATTGGGTTGAGG |
| Mouse *β-Actin* (+) control | TGGGCCGCCCTAGGCACCA | CTCTTTGATGTCACGCACGA |
| **TaqMan probes for qPCR** | **Probe** | |
| *Olig1* | Mm00497537_s1 | |
| *Olig2* | Mm01210556_m1 | |
| *Sox10* | Mm01300162_m1 | |
| *Msx1* | Mm00440330_m1 | |
| *Foxj1* | Mm01267279_m1 | |
| *Igf2* | Mm00439564_m1 | |
| *Lin28a* | Mm00524077_m1 | |
| *Crabp1* | Mm00442776_m1 | |
| *Actb* | Mm00607939_s1 | |
| **qPCR primers for Shh pathway activation** | **Forward (5' - 3')** | **Reverse (5' - 3')** |
| Mouse - *Gapdh* | TTCCAGTATGACTCCACTCACGG | TGAAGACACCAGTAGACTCCACGAC |
| Mouse - *Gli1* | TTATGGAGCAGCCAGAGAGACCAG | ATGGAGAGAGCCCGCTTCTTT |
| **5' RACE primers** | | |
| Reverse gene-specific primers | **Reverse (5' - 3')** | |
| *ARHGAP36* Exon4 Reverse Outer | CCTGACCGGTGGCTTCTTCAACC | |
| *ARHGAP36* Exon4 Reverse Inner | ACTCGTTCACCAGGACCTCTTC | |
| Target PCR gene-specific primers | **Forward (5' - 3')** | |
| Canonical ATG *ARHGAP36* | ATGGGTGGCTGCATTCCTTTTCTG | |
| ** Outer | TGGCTGCCGGGGAGCGAGCAGGAC | |
| ** Inner | CGAGGTTCGAGTGCACCAGGGAATC | |
| *** Outer | TGGCGTCTGGGGAACTGAAGAAG | |
| *** Inner | GAGTTGAAGGCTGTTTGTTGAATTG | |
| *ARHGAP36* Exon2 | TCTCTGAGCTGGAGCGTCTGAAG | |
| Positive control primers | **Forward (5' - 3')** | **Reverse (5' - 3')** |
| *β-ACTIN* | CACAGGGGAGGTGATAGCAT | CTCAAGTTGGGGGACAAAAA |
| **Guide RNA sequences for FOXR2 KO** | **Forward (5' - 3')** | |
| FOXR2 Exon1 gRNA | TCTCCATGGCCAGGTCCCAgttttagagctagaaatagc | |
| FOXR2 3' UTR gRNA | GTTGCATGAAAAAAAGCAGgttttagagctagaaatagc | |

**Table 2.2 - Antibodies used for IHC, CoIP and Western blotting**

| Antibody | Company | ID # | Use |
|---|---|---|---|
| SB | R&D Systems | MAB2798 | IHC |
| Ki67 | Leica | NCL-L-Ki67-MM1 | IHC |
| Synaptophysin | ICN Biomedicals | Clone SY38 | IHC |
| Nestin | Santa Cruz Biotechnology | SC-33677 | IHC |
| GFAP | Dako | Z0334 | IHC |
| Gli1 | Millipore | AB3444 | IHC |
| Arhgap36 | Sigma | HPA002064 | IHC |
| p-Akt (Ser473) | Cell Signaling Technologies | 4060 | IHC |
| Pten | Cell Signaling Technologies | 9559 | IHC |
| p-ERK (Thr202/Tyr204) | Cell Signaling Technologies | 4370 | IHC |
| Olig1 | Millipore | AB15620 | IHC |
| Olig2 | Millipore | AB9610 | IHC |
| Rreb1 | Sigma | HPA001756 | IHC |
| FOXR2 | Proteintech | 14111-1-AP | Western |
| ARHGAP36 | Abcam | AB84010 | Western |
| Megf10 | Sigma | ABC10 | Western |
| GAPDH | Cell Signaling Technologies | 5174S | Western |
| Flag | Cell Signaling Technologies | 2368 | Western/CoIP |
| C-MYC | Cell Signaling Technologies | 5605S | Western |
| C-MYC | Cell Signaling Technologies | 9402 | CoIP |
| V5 | Cell Signaling Technologies | 13202S | Western/CoIP |
| β-ACTIN | Cell Signaling Technologies | 8457S | Western |
| α-Tubulin | Cell Signaling Technologies | 2144 | Western |
| FAK | Cell Signaling Technologies | 3285 | Western |
| pFAK (Y397) | Cell Signaling Technologies | 3283S | Western |
| SRC | Cell Signaling Technologies | 2123S | Western |
| pSRC (pY416) | Cell Signaling Technologies | 6943 | Western |
| MAML1 | Cell Signaling Technologies | 12166 | Western |
| RBPSUH | Cell Signaling Technologies | 5313 | Western |
| HES1 | Cell Signaling Technologies | 11988 | Western |
| NCID | Cell Signaling Technologies | 4147 | Western |
| CCND3 | Cell Signaling Technologies | 2936 | Western |
| p21 Waf1/Cip1 | Cell Signaling Technologies | 2947 | Western |

**Table 2.3 - Cell sources, media components, and testing**

| **Cell line** | **Base media** | **Additional supplements** | **Source** | **Mycoplasma testing - last** (test once/year) | **Cell line authentication** |
|---|---|---|---|---|---|
| C17.2 | DMEM | 5% HS, 10% FBS, 2 mM L-glutamine, 100 U penicillin/ml and 100 µg streptomycin/ml | Gift - Dr. Connie Cepko - 2014 | April of 2018 | April of 2018, all C17.2 lines authenticated with IDEXX, validated as mouse without other species, and of the same origin between transfected lines compared to controls |
| Daoy | DMEM | 20% FBS, 100 U penicillin/ml and 100 µg streptomycin/ml | ATCC - HTB-186 - 2014 | April of 2018 | August of 2017, all Daoy cell lines authenticated as Daoy without contamination through UAGC |
| Med8A | DMEM | 20% FBS, 100 U penicillin/ml and 100 µg streptomycin/ml | Gift - Dr. Michael Taylor - 2012 | February of 2015, not used further | April of 2018, authenticated as human without contamination through UAGC (no reference line) |
| Ons76 | DMEM | 10% FBS, 100 U penicillin/ml and 100 µg streptomycin/ml | Gift - Dr. Michael Taylor - 2012 | February of 2015, not used further | April of 2018, authenticated as Ons76 without contamination through UAGC |
| HSC1λ | DMEM | 10% FBS, 100 U penicillin/ml and 100 µg streptomycin/ml | Gift - Dr. Margaret Wallace - 2011 | April of 2018 | April of 2018, all HSC1λ cell lines authenticated as human without contamination through UAGC (no reference line) |
| HEK293T | DMEM | 10% FBS, 100 U penicillin/ml and 100 µg streptomycin/ml | ATCC - CRL-11268 - 2017 | April of 2018 | April of 2018, authenticated as HEK293T without contamination through UAGC |
| | | *Generally cells are passaged Monday, Wednesday and Friday to avoid over confluent plates. Cell lines are thawed, grown up for experiments and then discarded to avoid high passage numbers | | | |
| | | *UAGC = University of Arizona Genetics Core | | | |
| | | *IDEXX = IDEXX Laboratories | | | |

**Table 2.4 - Medulloblastoma and CNS-PNET Characteristics**

| **Medulloblastoma** | **Sex** | **Age (days)** | **Histology** | **Subgroup designation by RNA-Seq** | **Observed metastasis** | ***Arhgap36* insertion** | ***Foxr2* insertion** | ***Megf10* insertion** |
|---|---|---|---|---|---|---|---|---|
| Transposition only | | | | | | | | |
| WT22 | F | 120 | Classic | | None | X | | |
| WT363 | F | 181 | Classic | Shh | Leptomeningial spread | X | | |
| WT459 | F | 219 | Classic | Shh | None | | | |
| WT523 | F | 87 | Classic | Shh | None | | | |
| WT701 | M | 111 | Classic | Grp 3/4 | None | X | | |
| WT724 | F | 169 | Classic | Grp 3/4 | Parenchyma infiltration | X | X | |
| Transposition and *Pten*$^{flox/+}$ | | | | | | | | |
| Pten49 | F | 190 | Classic | Grp 3/4 | Leptomeningial spread | X | | |
| Pten164 | M | 214 | Classic with nodular region | Shh | None | X | | |
| Pten241 | F | 185 | Classic with nodular region | Grp 3/4 | Parenchyma infiltration | X | | |
| Pten468 | F | 191 | Classic | Shh | None | X | | |
| Transposition and *Trp53*$^{lsl\text{-}R270H/+}$ | | | | | | | | |
| P53184 | F | 133 | Classic | Shh | Leptomeningial spread | X | X | X |
| P53176? | M | 129 | Classic | Shh | None | X | | |
| P53272 | M | 142 | Classic | Shh | Leptomeningial spread | X | | |
| P53531 | M | 239 | Classic | Shh | None | | | X |
| P53546 | M | 104 | Classic | Shh | None | | X | |
| P53586 | M | 90 | Classic | | None | | X | |
| P53593 | F | 82 | Classic | Grp 3/4 | Brainstem infiltration | | | |
| P53634 | F | 73 | Classic | Shh | None | X | X | X |
| P53690 | F | 133 | Classic | Shh | Leptomeningial spread | | X | |
| P53691? | F | 77 | Classic | Shh | Leptomeningial spread | X | X | |
| P53720 | F | 129 | Classic | | Leptomeningial spread | X | X | |
| P53812 | M | 152 | Classic | | Parenchyma infiltration | | | |

| **CNS-PNET** | **Sex** | **Age (days)** | **Histology and location** | **Subgroup designation by RNA-Seq** | **Observed metastasis** | ***Nf1* insertion** | ***Pten* insertion** | ***Erbb2ip* insertion** | ***Eras* insertion** | ***Rasa3* insertion** | **pERK by IHC** |
|---|---|---|---|---|---|---|---|---|---|---|---|
| *Nestin-Cre* ; *Trp53*$^{lsl\text{-}R270H/+}$ | | | | | | | | | | | |
| P53198 | M | 333 | Esthesioneuroblastoma - olfactory bulb | | None | N/A | N/A | | | | - |
| Tranposition only | | | | | | | | | | | |
| WT722 | M | 499 | CNS-PNET - olfactory bulb, cortex | | Leptomeningial spread | X | | | | X | Nuclear + |
| Transposition and *Trp53*$^{lsl\text{-}R270H/+}$ | | | | | | | | | | | |
| P53163 | M | 319 | CNS-PNET - cortex, lateral ventricle | | Parenchyma infiltration | | | | | | - |
| P53209 | F | 332 | CNS-PNET - cortex, lateral ventricle | | Parenchyma infiltration, leptomeningial spread | | | | | | Nuclear + |
| P53301 | M | 381 | CNS-PNET with nodular areas - olfactory bulb, cortex | CNS-PNET, other | Cortex infiltration | X | X | | | X | Localized Nuclear + |
| P53308 | M | 471 | CNS-PNET - olfactory bulb, cortex | CNS NB-*Foxr2* | Cortex infiltration | X | | | | | Nuclear + |
| P53323 | M | 513 | CNS-PNET - olfactory bulb, cortex | | Cortex infiltration | X | | X | X | | Localized Nuclear + |
| P53434 | M | 507 | CNS-PNET - olfactory bulb, cortex | | Cortex infiltration | | | | X | | Nuclear + |
| P53528 | F | 377 | CNS-PNET with nodular areas - olfactory bulb, cortex | | Leptomeningial spread | X | | | | | Localized Nuclear + |
| P53566 | F | 591 | CNS-PNET - lateral ventricle | CNS NB-*Foxr2* | Parenchyma infiltration | X | | | | | Nuclear + |
| P53579 | M | 575 | CNS-PNET - olfactory bulb, cortex | CNS-PNET, other | Leptomeningial spread | | X | | | | - |
| P53581 | M | 528 | CNS-PNET - olfactory bulb, lateral ventricle | CNS-PNET, other | Parenchyma infiltration | X | | | X | | Localized Nuclear + |
| P53714 | F | 249 | CNS-PNET - olfactory bulb, cortex | | Cortex infiltration | | | | | | - |
| P53819 | F | 439 | CNS-PNET - cortex | | Cortex infiltration | X | | X | | | Nuclear + |

**Table 2.5 - Gene lists comparing SB-induced mouse medulloblastoma (MB) and human MB**

| | | **Total overlap** | | | |
|---|---|---|---|---|---|
| **List name** | **Total number of genes** | All mouse MB | Mouse MB1 | Mouse MB2 | Mouse MB3 |
| All mouse MB | 10367 | 10367 | 2868 | 5183 | 507 |
| Mouse MB1 (red) | 2868 | 2868 | 2868 | 0 | 0 |
| Mouse MB2 (green) | 5182 | 5182 | 0 | 5182 | 0 |
| Mouse MB3 | 507 | 507 | 0 | 0 | 507 |
| All human MB | 963 | 684 | 127 | 396 | 45 |
| Human MB1 | 88 | 73 | 15 | 42 | 2 |
| Human MB2 | 213 | 155 | 27 | 92 | 9 |
| Human MB3 (green) | 269 | 200 | 22 | 141 | 10 |
| Human MB4 (red) | 224 | 163 | 48 | 73 | 13 |
| **Lists compared** | ***P* - value** (Fisher's Exact Test) | | | | |
| Human MB1: mouse MB1 | 0.3901 | | | | |
| Human MB1: mouse MB2 | 0.5749 | | | | |
| Human MB1: mouse MB3 | 0.9537 | | | | |
| Human MB2: mouse MB1 | 0.6684 | | | | |
| Human MB2: mouse MB2 | 0.4053 | | | | |
| Human MB2: mouse MB3 | 0.695 | | | | |
| Human MB3: mouse MB1 | 0.9967 | | | | |
| Human MB3: mouse MB2 | 0.0007715 | | | | |
| Human MB3: mouse MB3 | 0.8362 | | | | |
| Human MB4: mouse MB1 | 0.001907 | | | | |
| Human MB4: mouse MB2 | 0.9991 | | | | |
| Human MB4: mouse MB3 | 0.3137 | | | | |
| | | | | | |
| | *significant after Bonferroni correction | | | | |

**Table 2.6 - Gene lists comparing SB-induced mouse CNS-PNET and human CNS-PNET**

| | | Total overlap | | | | |
|---|---|---|---|---|---|---|
| **List name** | **Total number of genes** | All mouse CNS-PNET | Mouse CNS-PNET1 | Mouse CNS-PNET2 | Mouse CNS-PNET3 | Mouse CNS-PNET4 |
| All mouse CNS-PNET | 12359 | 12359 | 4863 | 1081 | 5425 | 900 |
| Mouse CNS-PNET1 (blue box) | 4863 | 4863 | 4863 | 0 | 0 | 0 |
| Mouse CNS-PNET2 | 1081 | 1081 | 0 | 1081 | 0 | 0 |
| Mouse CNS-PNET3 | 5425 | 5425 | 0 | 0 | 5425 | 0 |
| Mouse CNS-PNET4 | 900 | 900 | 0 | 0 | 0 | 900 |
| All human CNS-PNET | 1735 | 1274 | 606 | 93 | 476 | 87 |
| Human CNS-PNET1 | 98 | 64 | 19 | 9 | 29 | 7 |
| Human CNS-PNET2 (blue box) | 633 | 482 | 298 | 33 | 127 | 24 |
| Human CNS-PNET3 | 34 | 21 | 8 | 2 | 8 | 3 |
| Human CNS-PNET4 | 59 | 31 | 7 | 0 | 22 | 2 |
| Human CNS-PNET5 | 40 | 33 | 23 | 0 | 6 | 4 |
| Human CNS-PNET6 | 63 | 54 | 34 | 3 | 17 | 0 |
| Human CNS-PNET7 | 100 | 82 | 29 | 3 | 35 | 10 |
| Human CNS-PNET8 | 86 | 65 | 14 | 12 | 35 | 3 |
| Human CNS-PNET9 | 35 | 29 | 9 | 1 | 16 | 3 |
| **Lists compared** | ***P* - value** (Fisher's Exact Test) | | | | | |
| Human CNS-PNET1: mouse CNS-PNET1 | 0.9985 | | | | | |
| Human CNS-PNET1: mouse CNS-PNET2 | 0.04869 | | | | | |
| Human CNS-PNET1: mouse CNS-PNET3 | 0.126 | | | | | |
| Human CNS-PNET1: mouse CNS-PNET4 | 0.1563 | | | | | |
| Human CNS-PNET2: mouse CNS-PNET1 | 5.72E-08 | | | | | |
| Human CNS-PNET2: mouse CNS-PNET2 | 0.6631 | | | | | |
| Human CNS-PNET2: mouse CNS-PNET3 | 1 | | | | | |
| Human CNS-PNET2: mouse CNS-PNET4 | 0.9399 | | | | | |
| Human CNS-PNET3: mouse CNS-PNET1 | 0.8607 | | | | | |
| Human CNS-PNET3: mouse CNS-PNET2 | 0.4638 | | | | | |
| Human CNS-PNET3: mouse CNS-PNET3 | 0.5554 | | | | | |
| Human CNS-PNET3: mouse CNS-PNET4 | 0.1747 | | | | | |
| Human CNS-PNET4: mouse CNS-PNET1 | 0.9988 | | | | | |
| Human CNS-PNET4: mouse CNS-PNET2 | 1 | | | | | |
| Human CNS-PNET4: mouse CNS-PNET3 | 0.0001835 | | | | | |
| Human CNS-PNET4: mouse CNS-PNET4 | 0.6374 | | | | | |
| Human CNS-PNET5: mouse CNS-PNET1 | 0.00934 | | | | | |
| Human CNS-PNET5: mouse CNS-PNET2 | 1 | | | | | |
| Human CNS-PNET5: mouse CNS-PNET3 | 0.9948 | | | | | |
| Human CNS-PNET5: mouse CNS-PNET4 | 0.1928 | | | | | |
| Human CNS-PNET6: mouse CNS-PNET1 | 0.0186 | | | | | |
| Human CNS-PNET6: mouse CNS-PNET2 | 0.7643 | | | | | |
| Human CNS-PNET6: mouse CNS-PNET3 | 0.8463 | | | | | |
| Human CNS-PNET6: mouse CNS-PNET4 | 1 | | | | | |
| Human CNS-PNET7: mouse CNS-PNET1 | 0.9886 | | | | | |
| Human CNS-PNET7: mouse CNS-PNET2 | 0.9412 | | | | | |
| Human CNS-PNET7: mouse CNS-PNET3 | 0.1981 | | | | | |
| Human CNS-PNET7: mouse CNS-PNET4 | 0.06149 | | | | | |
| Human CNS-PNET8: mouse CNS-PNET1 | 1 | | | | | |
| Human CNS-PNET8: mouse CNS-PNET2 | 0.003376 | | | | | |
| Human CNS-PNET8: mouse CNS-PNET3 | 0.006137 | | | | | |
| Human CNS-PNET8: mouse CNS-PNET4 | 0.8279 | | | | | |
| Human CNS-PNET9: mouse CNS-PNET1 | 0.976 | | | | | |
| Human CNS-PNET9: mouse CNS-PNET2 | 0.8888 | | | | | |
| Human CNS-PNET9: mouse CNS-PNET3 | 0.04076 | | | | | |
| Human CNS-PNET9: mouse CNS-PNET4 | 0.3238 | | | | | |
| | *significant after Bonferroni correction | | | | | |

**Table 2.7 - D-CIS lists for medulloblastoma and CNS-PNET**

| **D-CIS - Medulloblastoma** | | | | |
|---|---|---|---|---|
| Candidate Gene | Chromosome | Tumor Count | Predicted Effect | *P*-Value |
| *Arhgap36* | X | 14 | N-terminal truncation | 6.10E-16 |
| *Foxr2* | X | 3 | Overexpress | 1.10E-05 |
| *Ddx19a* | 8 | 3 | Overexpress, C-terminal truncation | 5.79E-03 |
| *Gli1* | 10 | 3 | N-terminal truncation | 8.00E-03 |
| *Zmynd11* | 13 | 2 | Disrupt | 1.17E-05 |
| *Enox2* | X | 2 | Disrupt | 7.99E-03 |
| *Chl1* | 6 | 2 | N-terminal truncation | 7.99E-03 |
| *Dlg1* | 16 | 2 | Disrupt | 7.99E-03 |
| *Pten* | 19 | 2 | Disrupt | 7.99E-03 |
| *Dusp14* | 11 | 2 | Disrupt | 7.99E-03 |
| *Rreb1* | 13 | 2 | Overexpress | 3.18E-02 |
| *Dyrk1a* | 16 | 2 | Disrupt | 3.18E-02 |
| *Vsp45* | 3 | 2 | Overexpress, N-terminal truncation | 3.18E-02 |
| **D-CIS - CNS-PNET** | | | | |
| Candidate Gene | Chromosome | Tumor Count | Predicted Effect | *P*-Value |
| *Nf1* | 11 | 7 | Disrupt | 1.04E-16 |
| *Ambra1* | 2 | 5 | Disrupt | 7.61E-06 |
| *Erbb2ip* | 13 | 3 | Disrupt | 4.53E-03 |
| *Eras* | X | 3 | Overexpress | 9.11E-06 |
| *Setd5* | 6 | 3 | Overexpress | 9.11E-06 |
| *Rfwd2* | 1 | 2 | Disrupt | 9.11E-06 |
| *Npas3* | 12 | 2 | Disrupt | 9.11E-06 |
| *Ube2d3* | 3 | 2 | Disrupt | 6.64E-03 |
| *Qk* | 17 | 2 | Disrupt | 6.64E-03 |
| *Pten* | 19 | 2 | Disrupt | 6.64E-03 |
| *Agap1* | 1 | 2 | N-terminal truncation | 2.65E-02 |
| *Rasa3* | 8 | 2 | Disrupt | 2.65E-02 |
| *Clcn3* | 8 | 2 | Disrupt | 2.65E-02 |
| *Setd2* | 9 | 2 | Disrupt | 2.65E-02 |
| *Usp9x* | X | 2 | Disrupt | 2.65E-02 |
| *CIS listed in order of significance | | | | |

**Table 2.8 - R-CIS list for medulloblastoma**

| **R-CIS - Medulloblastoma** | | | |
|---|---|---|---|
| Candidate Gene | Chromosome | Tumor Count | Predicted Effect |
| *Arhgap36* | X | 13 | Overexpress |
| *Ptprd* | 4 | 10 | Disrupt |
| *Tle1* | 4 | 10 | Disrupt |
| *Megf9* | 4 | 7 | Disrupt |
| *Cdk5rap2* | 4 | 6 | Disrupt |
| *9530051G07Rik* | X | 6 | Disrupt |
| *Foxr2* | X | 6 | Overexpress |
| *Brinp1* | 4 | 5 | Overexpress |
| *Cdkn2a* | 4 | 5 | Overexpress |
| *Kdm4c* | 4 | 5 | Disrupt |
| *Nfia* | 4 | 5 | Overexpress |
| *Zic4* | 9 | 5 | Overexpress |
| *Enox2* | X | 5 | Overexpress |
| *Oxr1* | 15 | 4 | Premature truncation |
| *Vps13b* | 15 | 4 | Disrupt |
| *Arid1b* | 17 | 4 | Overexpress |
| *Dpy30* | 17 | 4 | Overexpress |
| *Gli2* | 1 | 4 | Overexpress |
| *Gm5860* | 4 | 4 | Overexpress |
| *Hivep3* | 4 | 4 | Overexpress |
| *Kdm1a* | 4 | 4 | Disrupt |
| *Kif1b* | 4 | 4 | Disrupt |
| *Padi2* | 4 | 4 | Overexpress |
| *Sh3gl2* | 4 | 4 | Overexpress |
| *Samd4b* | 7 | 4 | Overexpress |
| *Jmjd1c* | 10 | 3 | Disrupt |
| *Spag9* | 11 | 3 | Overexpress |
| *Xpo1* | 11 | 3 | Disrupt |
| *Nln* | 13 | 3 | Overexpress |
| *Atp8a2* | 14 | 3 | Overexpress |
| *Asap1* | 15 | 3 | Disrupt |
| *Cdh10* | 15 | 3 | Disrupt |
| *Csmd3* | 15 | 3 | Disrupt |
| *Ctnnd2* | 15 | 3 | Disrupt |
| *Rad21* | 15 | 3 | Disrupt |
| *Sybu* | 15 | 3 | Premature truncation |
| *Ubr5* | 15 | 3 | Disrupt |
| *Dyrk1a* | 16 | 3 | Disrupt |
| *Megf10* | 18 | 3 | Overexpress |
| *Wac* | 18 | 3 | Disrupt |
| *Zfp521* | 18 | 3 | Disrupt |
| *Mreg* | 1 | 3 | Overexpress |
| *Ckap5* | 2 | 3 | Disrupt |
| *Sp9* | 2 | 3 | Overexpress |
| *Atp6v1g1* | 4 | 3 | Overexpress |
| *Cdc42* | 4 | 3 | Overexpress |
| *Chd7* | 4 | 3 | Overexpress |
| *Cntln* | 4 | 3 | Overexpress |
| *Eif2b3* | 4 | 3 | Overexpress |
| *Elavl2* | 4 | 3 | Disrupt |
| *Epb4.1l4b* | 4 | 3 | Overexpress |
| *Eps15* | 4 | 3 | Disrupt |
| *Faf1* | 4 | 3 | Disrupt |
| *Lrp8* | 4 | 3 | Overexpress |
| *Mmp16* | 4 | 3 | Premature truncation |
| *Nfib* | 4 | 3 | Overexpress |
| *Pdik1l* | 4 | 3 | Overexpress |
| *Svep1* | 4 | 3 | Overexpress |
| *Ttc22* | 4 | 3 | Overexpress |
| *Ube2r2* | 4 | 3 | Disrupt |
| *Whrn* | 4 | 3 | Disrupt |
| *Fbxw8* | 5 | 3 | Disrupt |
| *Ppfia1* | 7 | 3 | Overexpress |
| *Snrpn* | 7 | 3 | Disrupt |
| *Coro2b* | 9 | 3 | Disrupt |
| *Setd2* | 9 | 3 | Disrupt |
| *Eras* | X | 3 | Overexpress |

*CIS listed in order of tumor count followed by chromosomal location

**Table 2.9 - R-CIS list for medulloblastoma**

| **R-CIS - CNS-PNET** | | | |
|---|---|---|---|
| Candidate Gene | Chromosome | Tumor Count | Predicted Effect |
| *Nf1* | 11 | 4 | Disrupt |
| *Auts2* | 5 | 3 | Disrupt |
| *Grid2* | 6 | 3 | Disrupt |
| *Micu1* | 10 | 2 | Disrupt |
| *Agtpbp1* | 13 | 2 | Disrupt |
| *Oxr1* | 15 | 2 | Disrupt |
| *Trio* | 15 | 2 | Disrupt |
| *Zfpm2* | 15 | 2 | Disrupt |
| *Zfr* | 15 | 2 | Disrupt |
| *App* | 16 | 2 | Disrupt |
| *Igsf11* | 16 | 2 | Overexpress |
| *Rbfox1* | 16 | 2 | Disrupt |
| *Ankhd1* | 18 | 2 | Disrupt |
| *Dtna* | 18 | 2 | Disrupt |
| *Pten* | 19 | 2 | Disrupt |
| *Sphkap* | 1 | 2 | Disrupt |
| *Epb4.1l1* | 2 | 2 | Disrupt |
| *Ralgapb* | 2 | 2 | Disrupt |
| *Slc23a2* | 2 | 2 | Disrupt |
| *Ywhab* | 2 | 2 | Disrupt |
| *Unc5c* | 3 | 2 | Disrupt |
| *Akr1a1* | 4 | 2 | Disrupt |
| *Astn2* | 4 | 2 | Disrupt |
| *Kdm4a* | 4 | 2 | Disrupt |
| *Megf9* | 4 | 2 | Disrupt |
| *Sdcbp* | 4 | 2 | Disrupt |
| *Ube4b* | 4 | 2 | Disrupt |
| *Ankrd17* | 5 | 2 | Disrupt |
| *Cttnbp2* | 6 | 2 | Disrupt |
| *Itpr1* | 6 | 2 | Disrupt |
| *Tubb3* | 8 | 2 | Overexpress |
| *Gria4* | 9 | 2 | Disrupt |
| *Ncam1* | 9 | 2 | Disrupt |
| *Nptn* | 9 | 2 | Disrupt |
| *Sik3* | 9 | 2 | Disrupt |
| *Sorl1* | 9 | 2 | Disrupt |
| *Arhgap36* | X | 2 | Overexpress |
| *Gpm6b* | X | 2 | Disrupt |
| *Hprt* | X | 2 | Disrupt |

*CIS listed in order of tumor count followed by chromosomal location

**Table 2.10 - CIS comparison between *SB* medulloblastoma (MB) and CNS-PNET screens**

| | Beckmann/Larson et al. | | | | Koso et al. | Wu et al. | | | Lastowska et al. | Genovesi et al. | Wu et al. | | | |
|---|---|---|---|---|---|---|---|---|---|---|---|---|---|---|
| **Transgenes used** | *Nestin-Cre , T2/Onc(2) x Rosa26$^{lsl\text{-}SB11/+}$ , Pten$^{fl/+}$ , Trp53$^{lsl\text{-}R270H/+}$ | | | | *Trp53$^{lsl\text{-}R172H/+}$ , Nestin-Cre x T2Onc2 , Rosa26$^{lsl\text{-}SB11/+}$ | *Math1-SB11 , T2Onc , Trp53$^{mut}$ | | | *Ptch1$^{tm1Mpu1}$ , T2Onc, Rosa26$^{SB11/+}$ | *Ptch1$^{loxP/+}$ , T2Onc3, Rosa26$^{lsl\text{-}SB11/+}$ , B-Actin-Cre | *Math1-SB11, T2Onc, Ptch$^{+/-}$ | | | |
| **CIS identification** | *TAPDANCE for D-CIS | | | | *Guassian kernel convolution | *gCIS | | | *Guassian kernel convolution | *Guassian kernel convolution | *gCIS | | | |
| **Gene name** | **MB - D-CIS** | **MB - R-CIS** | **CNS-PNET - D-CIS** | **CNS-PNET - R-CIS** | **Primary MB** | **Primary MB** | **Mets only** | **Both** | **Primary MB** | **Primary MB** | **Primary MB** | **Mets** | **Both** | **Overlap** |
| *Pten* | X | | X | X | | | X | | X | X | | | X | 7 |
| *Wac* | | X | | | X | | | X | | X | X | | | 5 |
| *Crebbp* | | | | | X | | | | X | X | | | X | 4 |
| *Arhgap36* | X | X | | X | | | | X | | | | | | 4 |
| *Arid1b* | | X | | | X | | | | | X | | | X | 4 |
| *Nfia* | | X | | | | | | | X | X | | | X | 4 |
| *Setd2* | | X | X | | | X | | | | | | | X | 4 |
| *Zmynd11* | X | | | | | | X | | | | | | X | 3 |
| *Foxr2* | X | X | | | X | | | | | | | | | 3 |
| *Eras* | | X | X | | | | | | | | | | X | 3 |
| *Dyrk1a* | X | X | | | | | | | | X | | | | 3 |
| *Nfib* | | X | | | | | | | X | | | | X | 3 |
| *Trim33* | | | | | X | | | | | X | | X | | 3 |
| *Sfi1* | | | | | | | X | | X | | | | X | 3 |
| *App* | | | | X | | | | | | | X | | | 2 |
| *Auts2* | | | | X | | | | | | X | | | | 2 |
| *Gli1* | X | | | | X | | | | | | | | | 2 |
| *Chl1* | X | | | | | | X | | | | | | | 2 |
| *Enox2* | X | X | | | | | | | | | | | | 2 |
| *Cdk5rap2* | | X | | | | | | | | | | X | | 2 |
| *Hivep3* | | X | | | X | | | | | | | | | 2 |
| *Megf10* | | X | | | | | | | | | | | X | 2 |
| *Erbb2ip* | | | X | | | | | | | | X | | | 2 |
| *Ube2d3* | | | X | | | | | | | X | | | | 2 |
| *Megf9* | | X | | X | | | | | | | | | | 2 |
| *Oxr1* | | X | | X | | | | | | | | | | 2 |
| *Cdkn2a* | | X | | | | | | | | X | | | | 2 |
| *Kdm1a* | | X | | | | | | | | X | | | | 2 |
| *Nfl* | | | X | X | | | | | | | | | | 2 |
| *Xpo1* | | X | | | | | X | | | | | | | 2 |
| *Csmd3* | | X | | | | | | | | | X | | | 2 |
| *Zfp521* | | X | | | | | | | | X | | | | 2 |
| *Ubr5* | | X | | | | | | | | X | | | | 2 |
| *Tgif2* | | | | | X | | | | X | | | | | 2 |
| *Akap6* | | | | | X | | | | | X | | | | 2 |
| *Map2k4* | | | | | X | | | | | | X | | | 2 |
| *Map3k1* | | | | | | | | | | X | | | X | 2 |
| *Nfix* | | | | | | | | | | X | X | | | 2 |
| *Edil3* | | | | | | | | | | X | | | X | 2 |
| *3110070M22Rik* | | | | | | | | | | X | | | X | 2 |
| *Zbtb20* | | | | | | | | | | X | X | | | 2 |
| *5033411D12Rik* | | | | | | | | | | X | X | | | 2 |
| *Brd4* | | | | | | | | | | X | X | | | 2 |
| *Rab3c* | | | | | | | | | | X | X | | | 2 |
| *Akap6* | | | | | X | | | | | X | | | | 2 |
| *BC003993* | | | | | | | X | | | | X | | | 2 |
| *Evl* | | | | | | X | | | | | X | | | 2 |
| *Mtr* | | | | | | | X | | | | X | | | 2 |
| *Ptch1* | | | | | | | | X | | | X | | | 2 |
| *Rfxdc2* | | | | | | X | | | | | X | | | 2 |
| *Tox3* | | | | | | X | | | | | X | | | 2 |
| *Zfp516* | | | | | | X | | | | | X | | | 2 |
| *BC016423* | | | | | | X | | | | | | X | | 2 |
| *Arid4b* | | | | | | X | | | | | | | X | 2 |
| *Edil3* | | | | | | | | | | X | | | X | 2 |

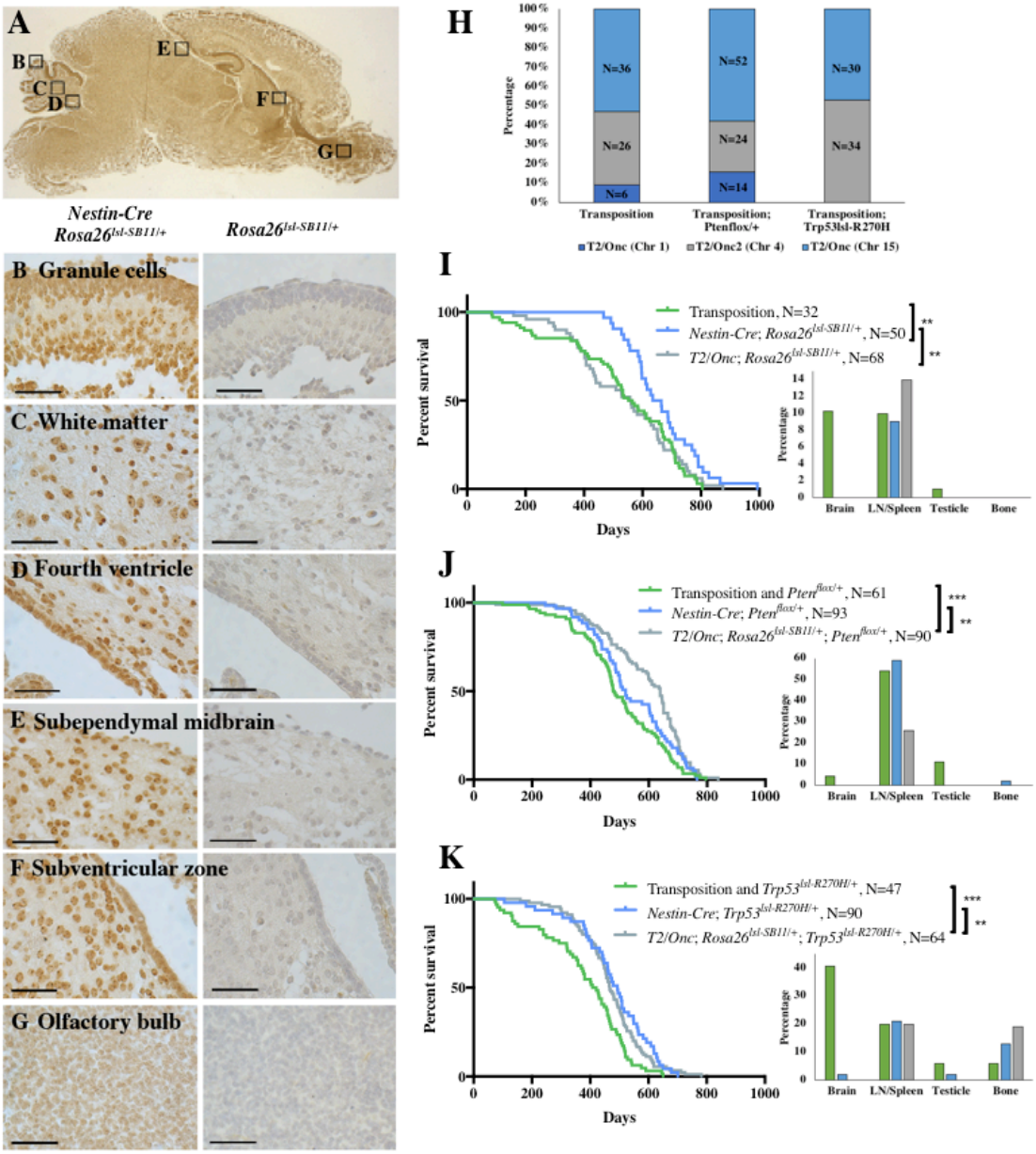


**Figure 2.1. Characterization of *SB* mutagenesis cohorts**

**A – G**, SB transposase IHC. **A**, Sagittal section of *Nestin-Cre*; *Rosa26*$^{lsl\text{-}SB11/+}$ mouse at P2. **B-G**, High-power magnification of specific areas in (**A**) demonstrating nuclear SB expression. **H**, Transposon distribution across WT, *Pten*$^{flox/+}$, and *Trp53*$^{lslR270H/+}$ backgrounds. **I-K**, Kaplan-Meier survival curves (left) and tumor burden (right) of experimental cohorts on WT (**I**), *Pten*$^{flox/+}$(**J**), and *Trp53*$^{lsl\text{-}R270H/+}$(**K**) backgrounds. Statistical significance: $^{**}P<0.05$, $^{***}P<0.001$ (Log rank Mantel-Cox Test).

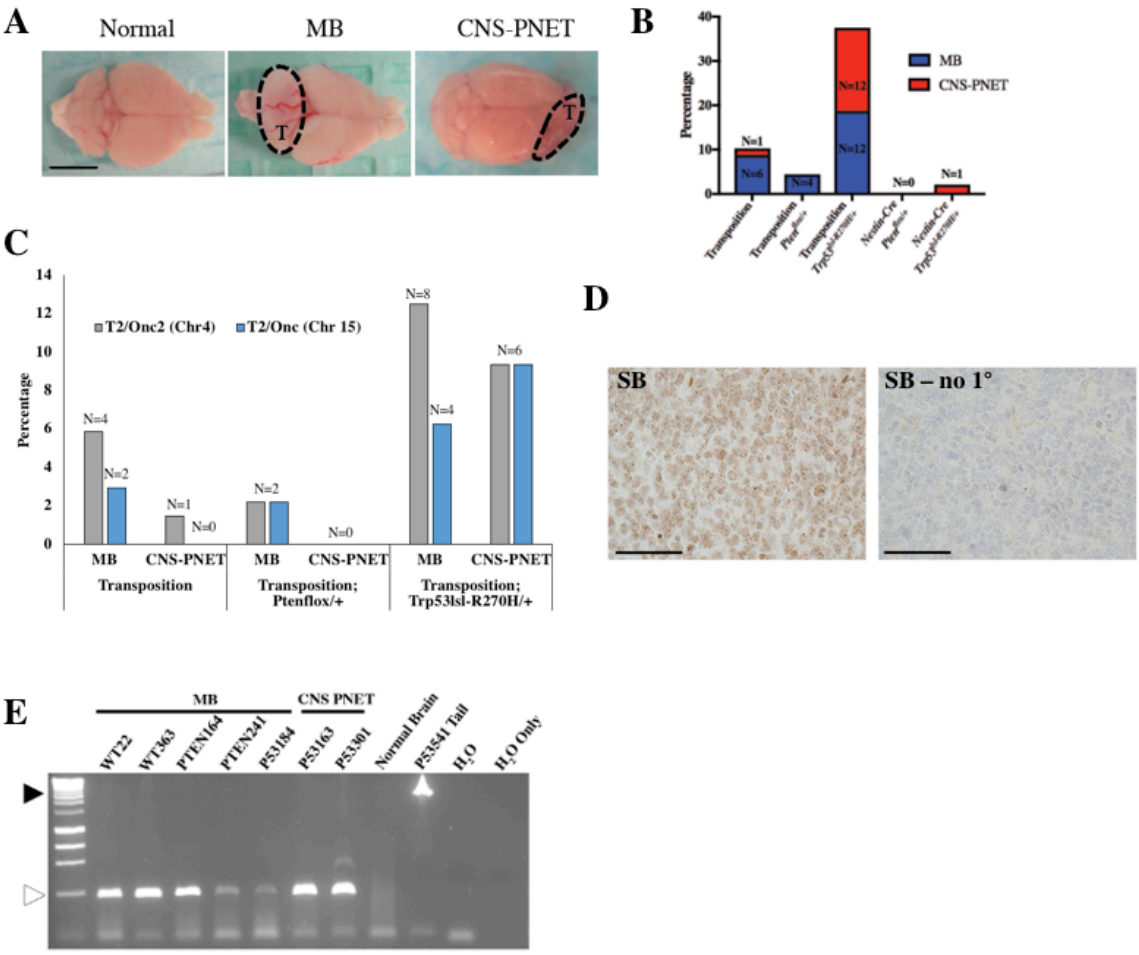


**Figure 2.2. *SB*-induced medulloblastoma and CNS-PNET occur across genetic backgrounds.**
**A,** Macroscopic images of normal brain and brains with *SB*-induced medulloblastoma in the cerebellum and CNS-PNET in the cerebral cortex and olfactory bulbs. T=tumor with outline. **B,** Frequency of macroscopic medulloblastoma and CNS-PNET across genetic backgrounds. **C**, Medulloblastoma (MB) and CNS-PNET occurrence with *T2/Onc2* and *T2/Onc*(Chr 15) across WT, $Pten^{flox/+}$, and $Trp53^{lsl\text{-}270H/+}$ backgrounds with transposition. No brain tumors were observed with *T2/Onc*(Chr 1). **D**, SB transposase IHC on CNS-PNET with and without primary antibody. **E**, Excision PCR in MB and CNS-PNET tissue (white arrowhead at 225 bp) compared to control tissue lacking *Cre* recombinase (black arrowhead at 2200 bp). $H_2O$ = water plus master mix, $H_2O$ only = water. Tumor numbers at the top depict genetic background.

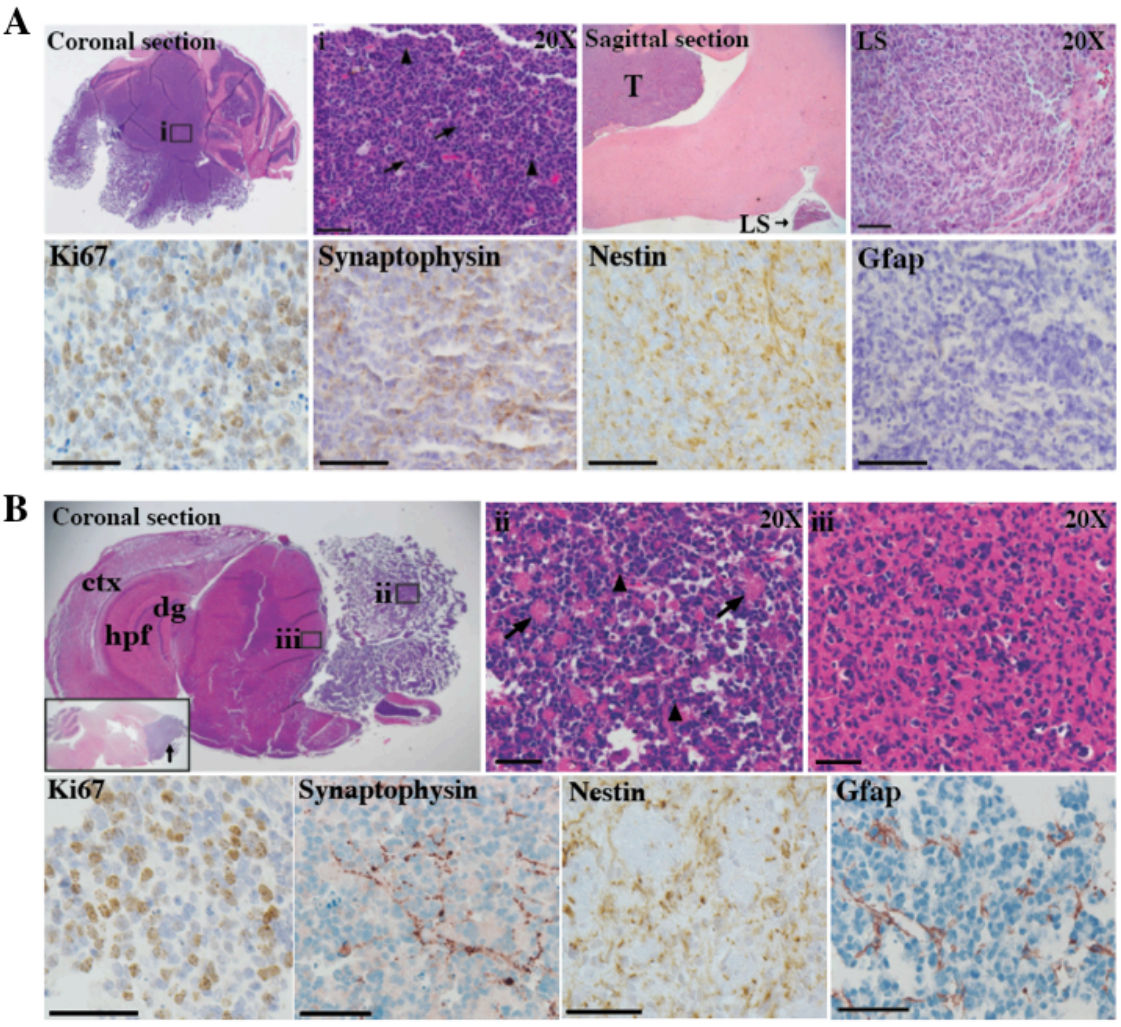


**Figure 2.3. *SB*-induced medulloblastoma and CNS-PNET resemble human tumors**
**A**, Upper panels: H&E staining of medulloblastoma. **i**, Rosettes (arrows), mitotic nuclei (arrowheads). Primary medulloblastoma (T) with leptomeningeal spread (LS). Lower panels: IHC on *SB*-driven medulloblastoma. **B**, Upper panels: H&E-stained CNS-PNET. Cerebral cortex (ctx), hippocampal formation (hpf), dentate gyrus (dg). Inset: sagittal section of CNS-PNET, olfactory bulb (arrow). **ii**, Bulk tumor with rosette formations (arrows) and mitotic nuclei (arrowheads). **iii**, Tumor cell parenchyma infiltration. Lower panels: show IHC on CNS-PNET. Scale bars = 50 μm.

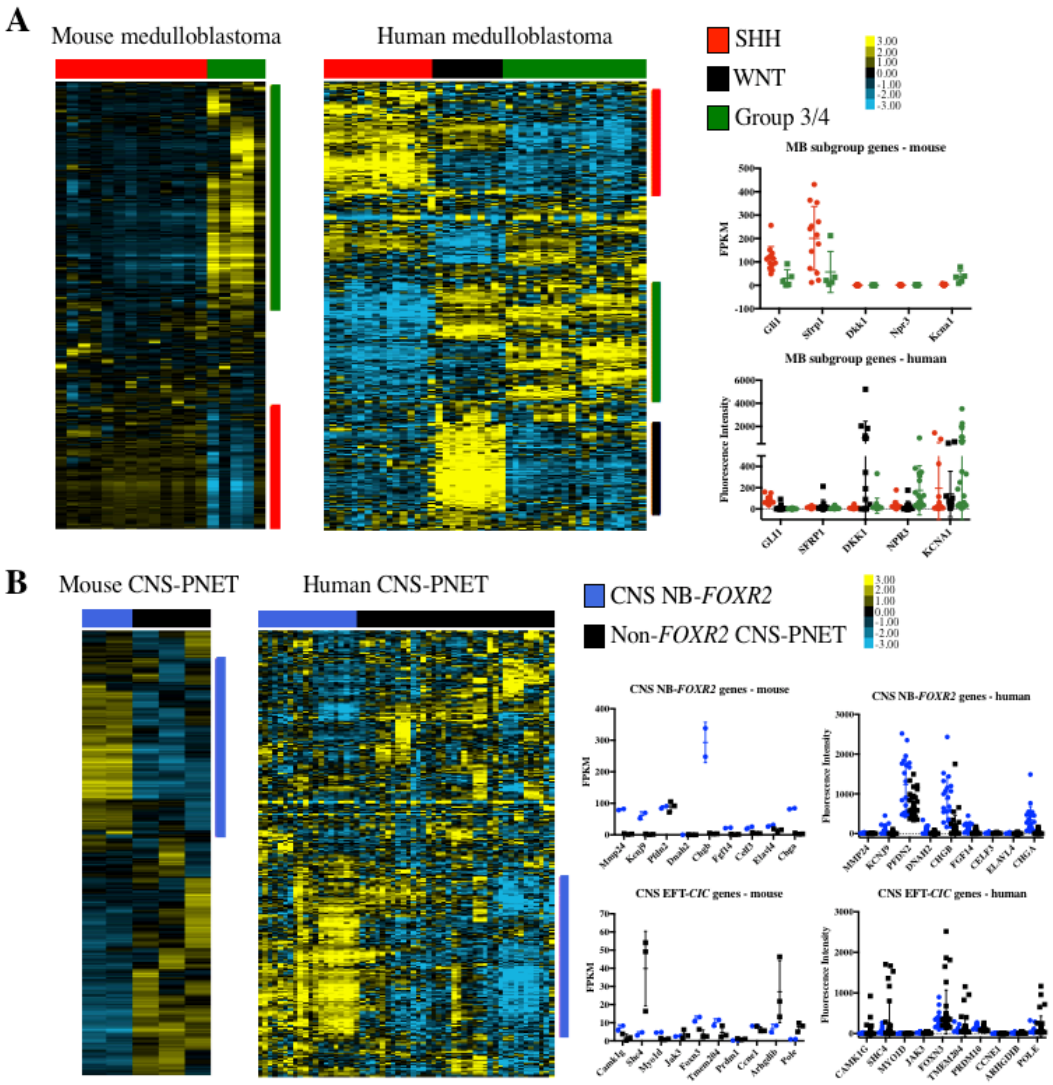


**Figure 2.4. *SB*-induced mouse tumors resemble human non-WNT medulloblastoma and CNS-PNET transcriptionally.**

**A**, Hierarchical clustering of *SB*-induced mouse and human medulloblastoma transcription profiles(6). Red boxes denote transcripts in SHH medulloblastoma (*P*-value <0.002, Fisher's Exact Test); green boxes denote transcripts in group 3/4 medulloblastoma (*P*-value <0.001, Fisher's Exact Test). SHH, WNT, and group 3/4 subgroup designation are indicated with red, black, and green toebars, respectively. Select subgroup specific genes are shown on the right for both mouse and human medulloblastoma. **B**, Hierarchical clustering of *SB*-induced mouse and human CNS-PNET transcription profiles(6) analyzed using GC-SIM. Blue boxes correspond with transcripts in CNS NB-*FOXR2* (*P*-value <1.0e-8, Fisher's Exact Test). CNS NB-*FOXR2* and non-*FOXR2* CNS-PNET designation are shown with blue and black toebars, respectively. Select subgroup specific genes are shown on the right for both mouse and human CNS-PNET. For inclusion in the heatmaps, log-transformed and mean-centered data with variance > 0.5 for the murine RNA-Seq datasets and variance > 2.0 for the human array datasets were clustered using average linkage clustering. Clusters were systematically identified with node correlation > 0.2 and cross species subtype cluster association was assessed by Fisher's Exact Test.

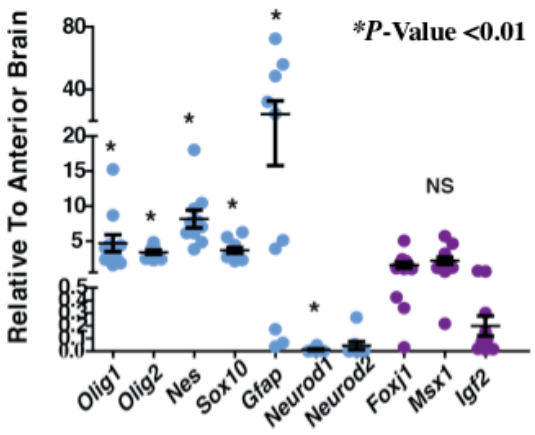


**Figure 2.5. Characterization of *SB*-induced CNS-PNET.**
qRT-PCR analysis of oligo neural cell lineage markers performed on *SB*-induced CNS-PNETs. Gene expression is shown relative to control fore brain; data points represent SEM (N=2 replicas). Scale bars = 50μm.

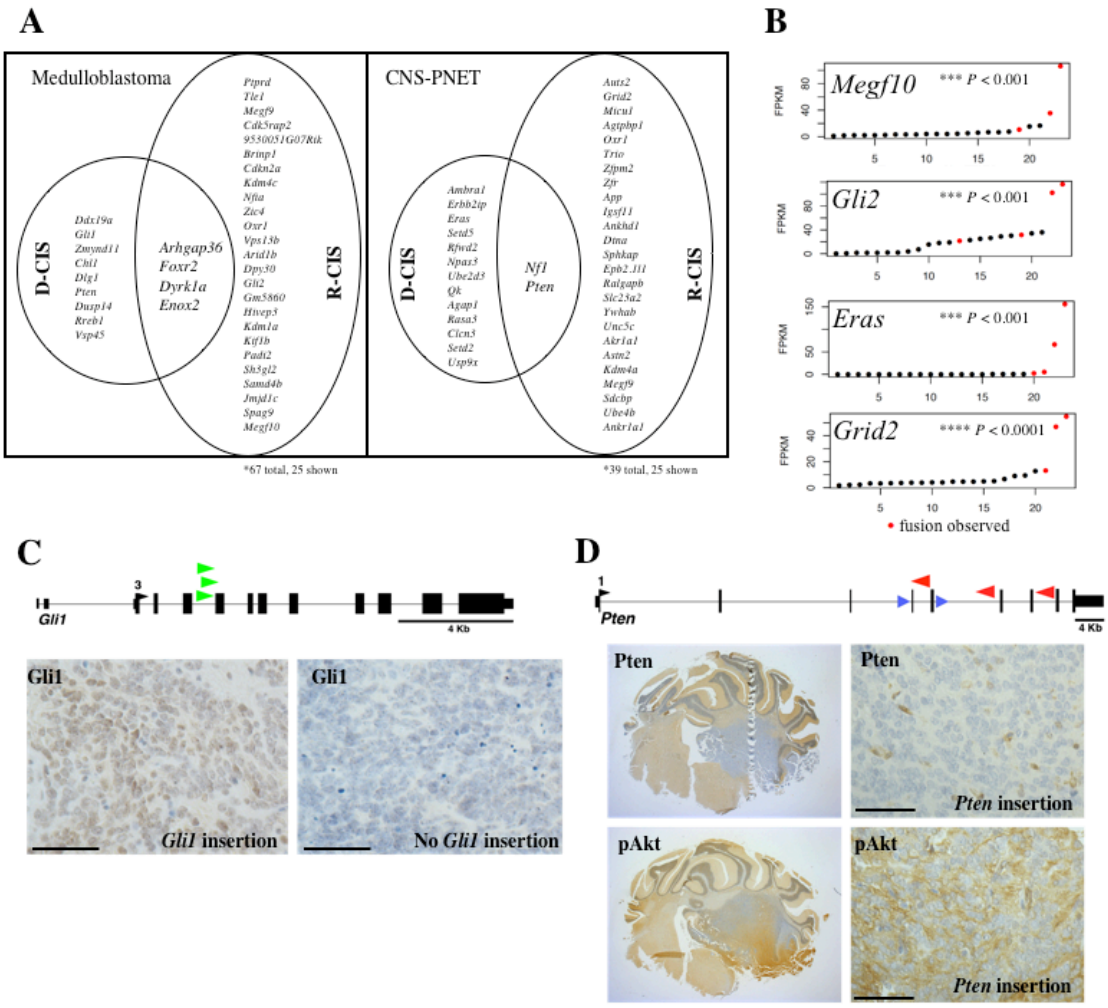


**Figure 2.6. CIS gene identification and expression analysis in mouse *SB*-induced tumors.**
**A**, CIS genes identified in medulloblastoma (MB) and CNS-PNET. **B**, RNA-Seq expression levels of *Megf10*, *Gli2*, *Eras* and *Grid2* in *SB*-induced tumors with transposon fusions shown (red dots). *P*-Value represents comparison of transcripts with and without *T2/Onc(2)* fusion using a Student *t* test, two-tailed. **C-D**, Top: schematics of *Gli1* and *Pten* loci indicating the position and orientation of transposon insertions. Endogenous translation start (black arrowheads), LoxP (blue arrowheads), and transposon directionality (green = sense, red = anti-sense) are shown. **C**, IHC for Gli1 in *SB*-induced medulloblastoma with and without *Gli1* insertion. **D**, IHC for Pten and pAKT in *SB*-induced MB with a *Pten* insertion.

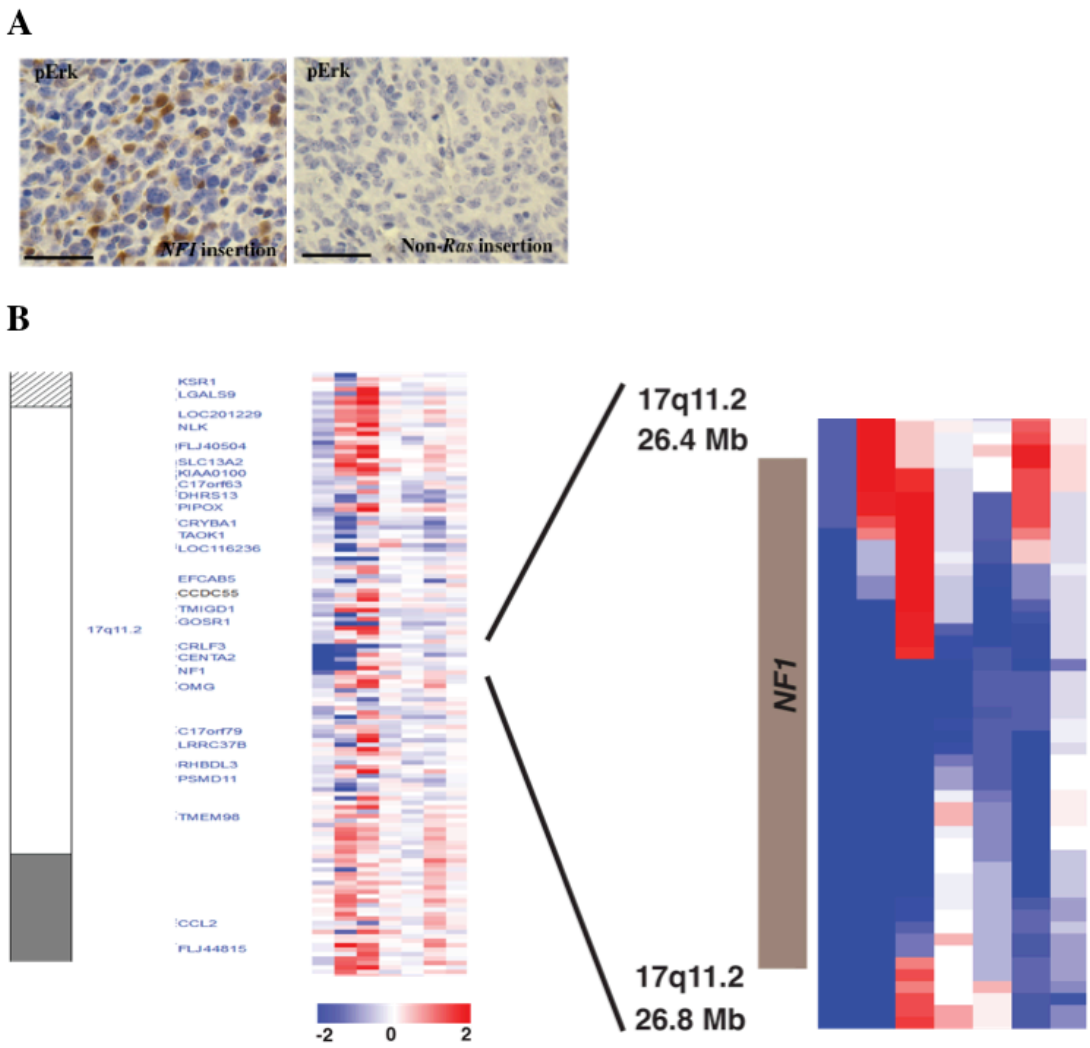


**Figure 2.7. Transposon-mediated effects on Ras pathway activation.**
**A**, IHC for pErk in CNS-PNET with an *Nf1* insertion compared to one without insertions that affect Ras-pathway activation. **B**, DNA copy number profiles of 7 primary human CNS-PNETs (Human Omni 2.5 Quad SNP array(Picard *et al*. 2012). Scale bars = 50μm.

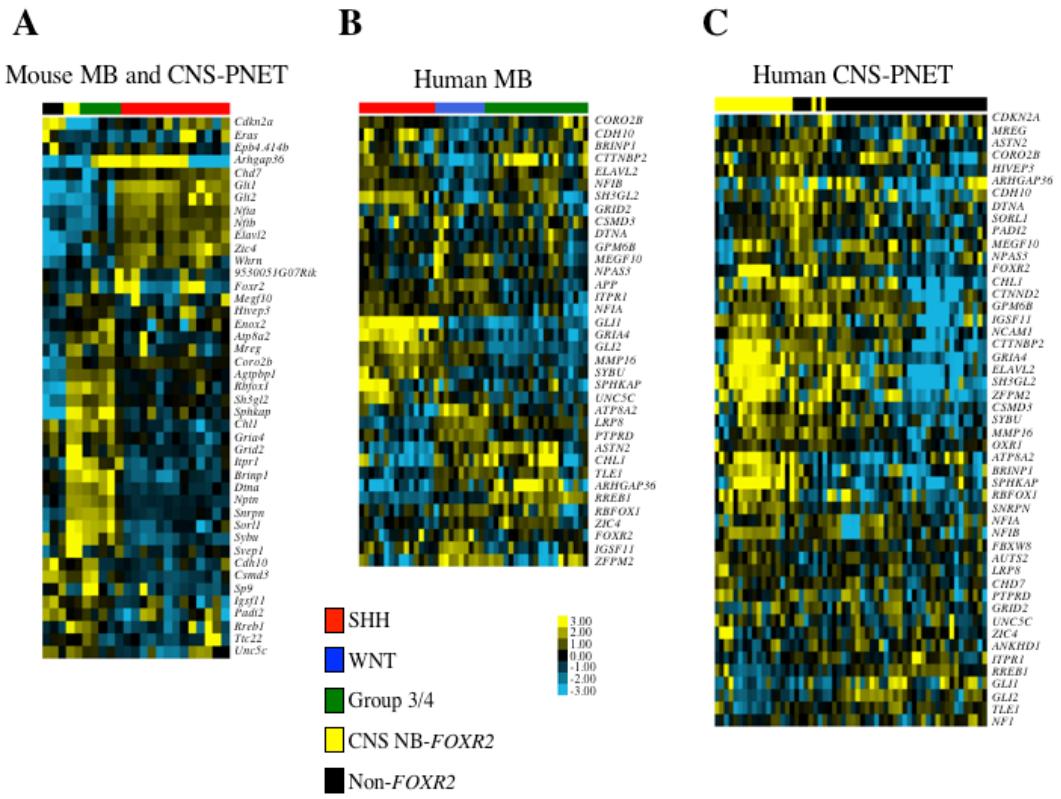


**Figure 2.8. Analysis of CIS gene expression in mouse and human medulloblastoma and CNS-PNET.** **A-C**, Expression of CIS genes with highest variability in *SB*-induced tumors (**A**), human medulloblastoma(**B**) and human CNS-PNET (**C**) (Sturm *et al*. 2016). For the heatmaps, log-transformed and mean-centered data with variance > 1.0 for were clustered using average linkage clustering. Multiple probes to human genes corresponding to CIS were averaged to obtain a single value.

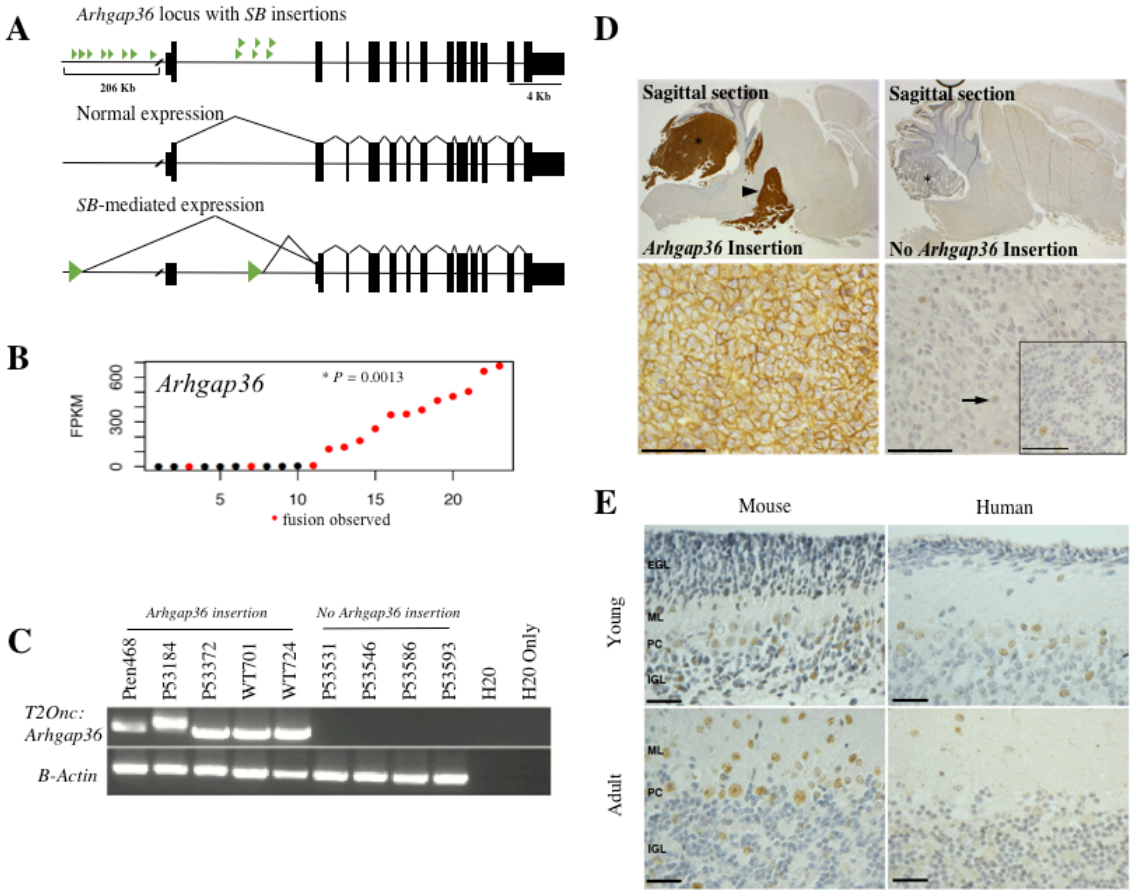


**Figure 2.9. *Arhgap36* transposon insertion and expression analysis.**
**A**, *Arhgap36* locus with transposon insertions (green arrowheads) indicated. **B**, *Arhgap36* expression by RNA-Seq (*P*-Value: Student *t* test, two-tailed). **C**, RT-PCR for *T2Onc:Arhgap36* fusion transcript in tumors with and without *Arhgap36* insertion. *β-Actin* included as loading control. Tumor numbers at the top depict genetic background. **D**, IHC for Arhgap36 expression in *SB*-induced medulloblastoma. Primary tumor (*), leptomeningeal spread (arrowhead). Nuclear expression in control tumor (arrow) compared to normal granule neural cells of the same brain (inset). **E**, IHC for ARHGAP36 expression in cerebella of mouse (Age: 7 and 63 days) and human (Age: 32-week and adult). The molecular layer (ML), Purkinje cell layer (PC) and internal granule cell layer (IGL) are shown. Scale bars = 50μm.

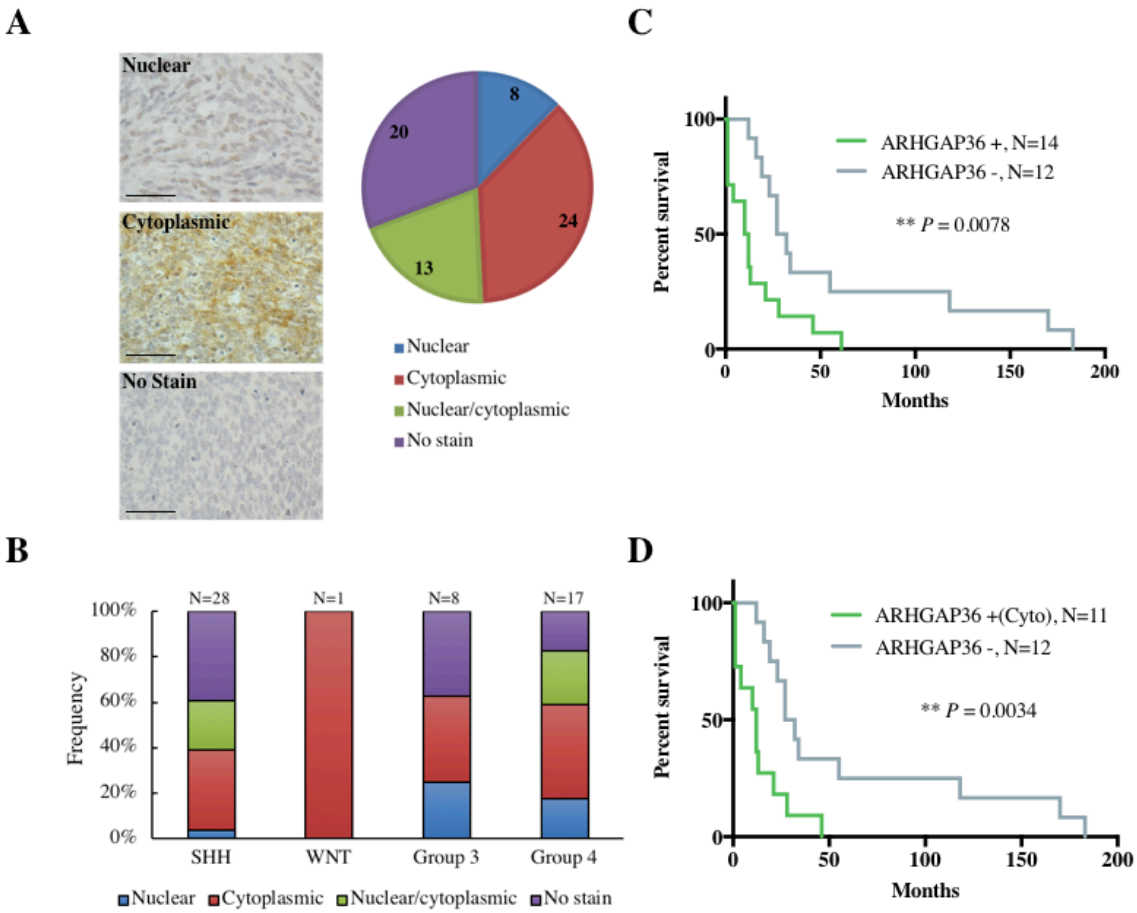


**Figure 2.10. *Arhgap36* expression dysregulation is associated with poor prognosis human medulloblastoma.**

**A**, Combined tissue microarrays (TMAs) analyzed for ARHGAP36 expression by IHC. **B**, ARHGAP36 positivity by IHC across sub-grouped TMA from John's Hopkins. **C**, Kaplan-Meier analysis of patients from the John's Hopkins TMA with and without ARHGAP36 protein expression (*P*-value: log rank Mantel-Cox test). **D**, Kaplan-Meier analysis of deceased patients in the John's Hopkins TMA with and without cytoplasmic ARHGAP36 protein expression specifically (*P*-Value: log rank Mantel-Cox test). Scale bars = 50mm.

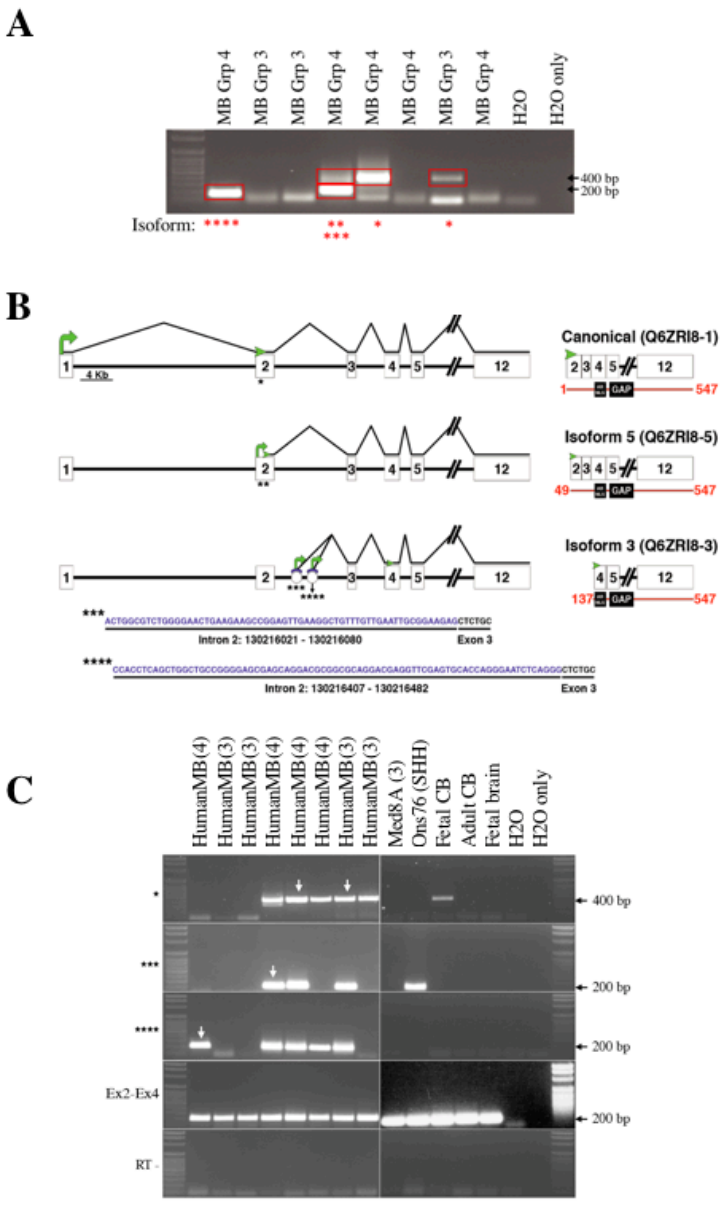


**Figure 2.11. *ARHGAP36* isoform expression characterization by 5'RACE.**
**A-B**, 5'-RACE PCR conducted on human medulloblastoma samples using *ARHGAP36* exon 4-specific reverse primers. Isoforms predicted include: * = canonical (UniProt Q6ZRI8-1), ** = Isoform 5 (UniProt Q6ZRI8-5), *** and **** = Isoform 3 (UniProt Q6ZRI8-3). **C**, Target-specific RT-PCR to capture *ARHGAP36* sequences derived from 5'RACE. Subgroup is noted with human MB or cell line samples (Med8a and Ons76). CB = cerebellum. White arrows indicate samples found to contain described transcript in the original 5'RACE. * = canonical sequence (UniProt Q6ZRI8-1), *** = *intron2:exon3* fusion sequences, **** = *intron2:exon3* fusion sequences. A control, exon 2 – exon 4 PCR of the canonical sequence is included. $H_2O$ = water plus master mix, $H_2O$ only = water.

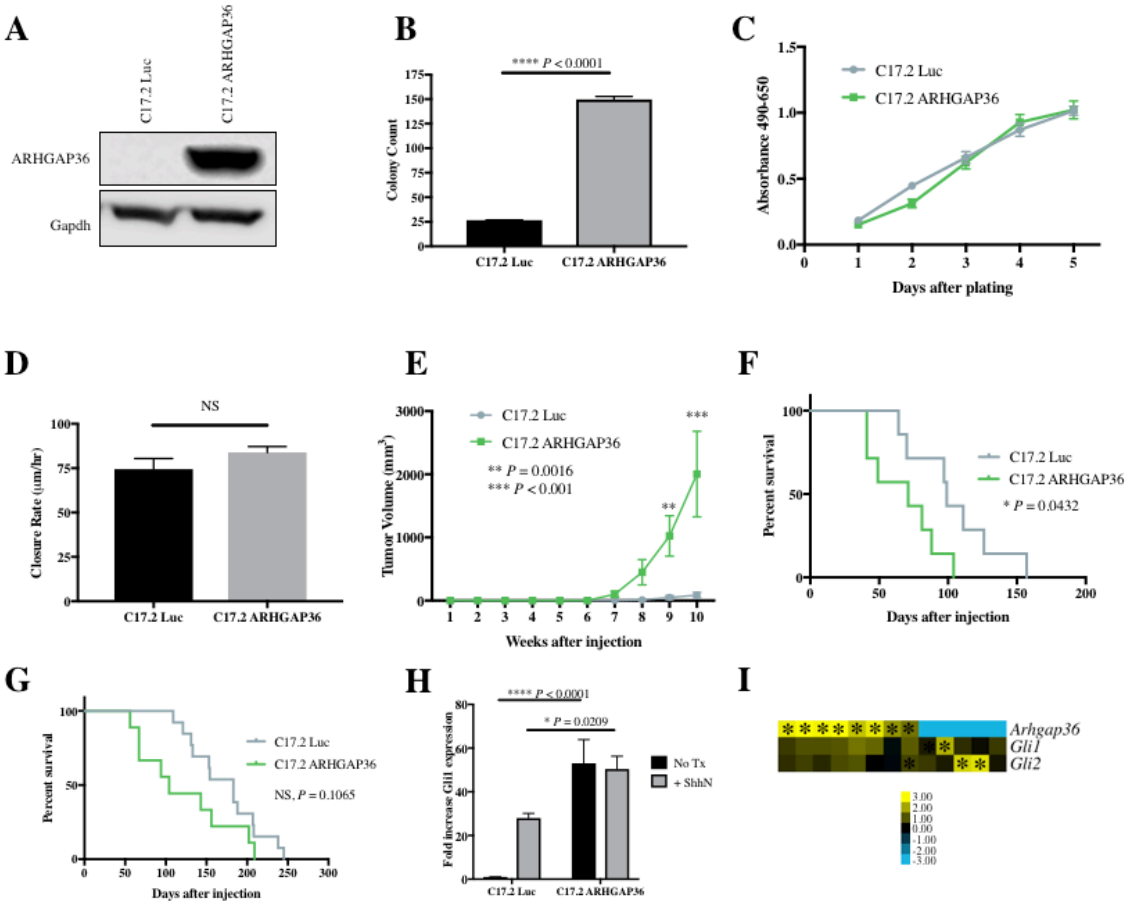


**Figure 2.12. *ARHGAP36* promotes transformation of C17.2 cells.**
**A**, Western blot analysis of ARHGAP36 in transfected C17.2 cells. **B**, Soft agar colony formation assay comparing luciferase control and *ARHGAP36* expressing C17.2 cells (*P*-value: Student *t* test, two-tailed). **C,** MTS assay of C17.2 Luc and C17.2 ARHGAP36 cells. **D**, Wound closure rate of C17.2 Luc (N=14) and C17.2 ARHGAP36 (N=14) cells on tissue culture plastic dishes. **E**, Flank tumor volume of NU/J mice injected with C17.2 Luc or C17.2 ARHGAP36 cells (N=5, *P*-value: Sidak's multiple comparisons test). **F**, NU/J mice injected intracranially with C17.2 Luc or C17.2 ARHGAP36 cells (N=7, *P*-Value: log rank Mantel-Cox test). **G**, Neonatal injections of NRG mice with C17.2 Luc (N=13) or C17.2 ARHGAP36 (N=9) cells (*P*-value: log rank Mantel-Cox test). **H**, qRT-PCR for *Gli1* in C17.2 Luc and C17.2 ARHGAP36. Cells are serum starved with or without treatment of exogenous ShhN ligand. *Gli1* expression is normalized to *Gapdh* (*P*-Values: Sidak's multiple comparison's test). **I**, RNA-Seq of *SB*-induced MB showing expression of indicated genes. Transposon insertion in the respective gene locus is shown as an asterisk (*). Error bars are SEM.

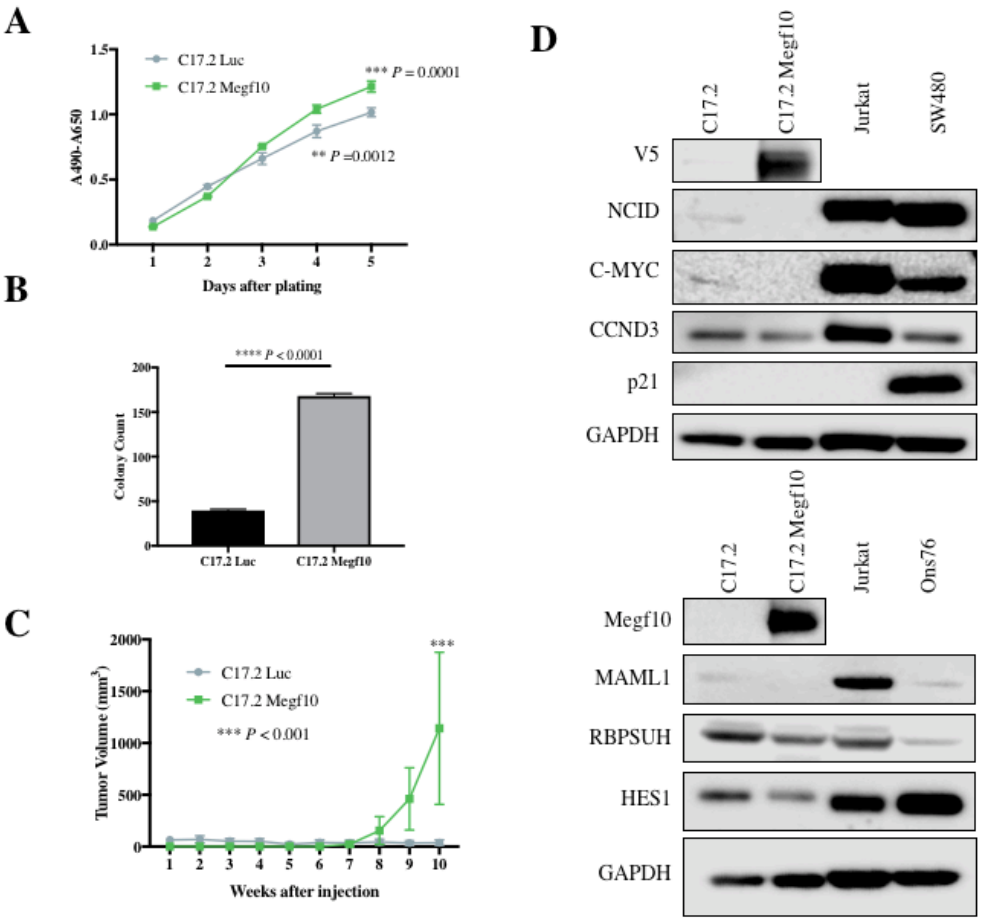


**Figure 2.13.** ***Megf10*** **promotes transformation of C17.2 cells but does not activate Notch signaling.** **A,** MTS assay of C17.2 Luc and C17.2 Megf10 cells (*P*-value: Sidak's multiple comparisons test). **B**, Soft agar colony formation assay of C17.2 Luc and C17.2 Megf10 cells (*P*-value: Student *t* test, two-tailed). **C**, Flank tumor volume of NU/J mice injected with C17.2 Luc (N=7) or C17.2 Megf10 (N=8) cells (*P*-values: Sidak's multiple comparisons test). **D**, Western blot analysis of the effect of *Megf10* on Notch signaling pathway activation in C17.2 cells. Jurkat, Ons76 and SW480 cells are included as controls. Error bars are SEM.

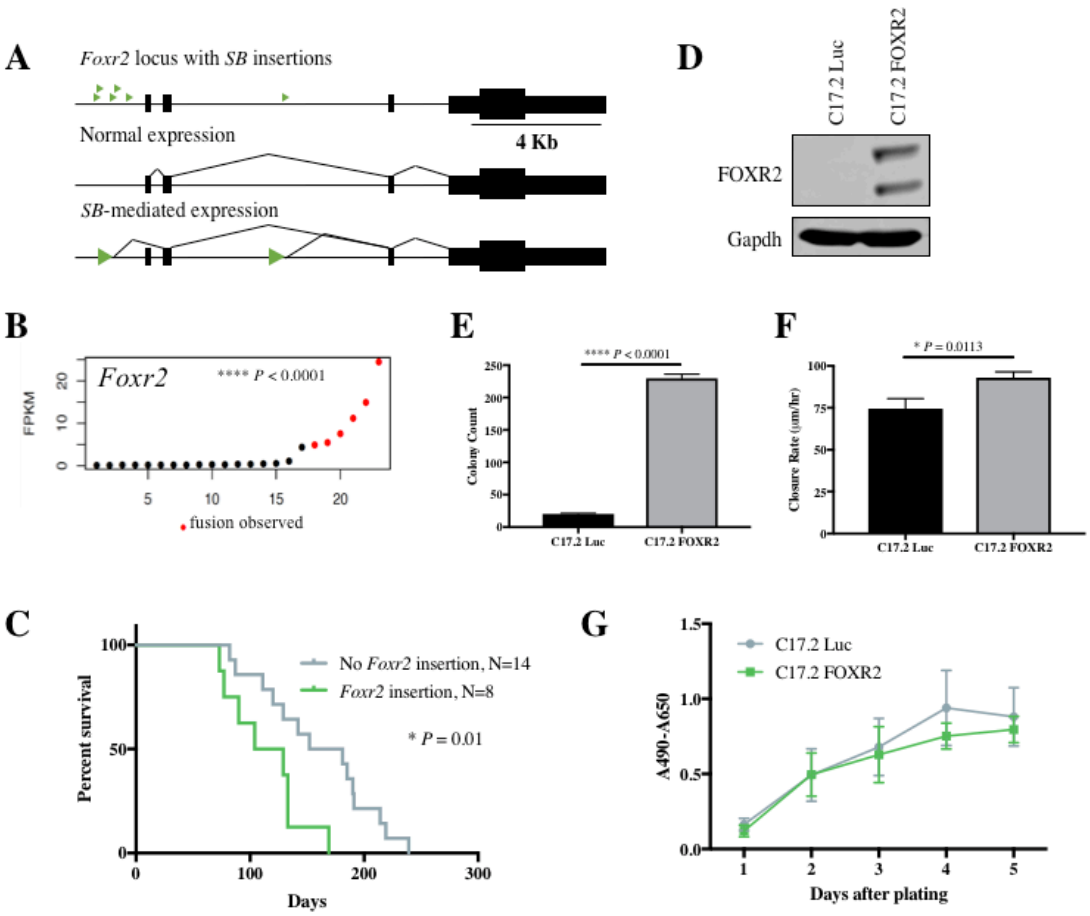


**Figure 2.14. *FOXR2* transposon insertion analysis and *in vitro* characterization in C17.2 cells.**
**A**, Transposon insertions (green arrowheads) in the *Foxr2* locus. **B**, *Foxr2* expression by RNA-Seq in *SB*-induced medulloblastoma with *T2/Onc:Foxr2* fusions noted (red dots). *P*-Value: Student *t* test, two-tailed. **C**, Kaplan-Meier analysis of mice with *SB*-induced medulloblastoma with and without *Foxr2* insertions (*P*-Value: log rank Mantel-Cox test). **D**, Western blot showing FOXR2 expression in C17.2 Luc and C17.2 FOXR2 cells. **E**, Soft agar colony formation assay comparing C17.2 Luc and C17.2 FOXR2 cells (*P*-value: Student *t* test, two-tailed). **F**, Wound closure rate of C17.2 Luc (N=14) and C17.2 FOXR2 (N=15) cells on tissue culture plastic dishes (*P*-value: Student *t* test, two-tailed). **G**, MTS assay of C17.2 Luc and C17.2 FOXR2 cells. Error bars are SEM.

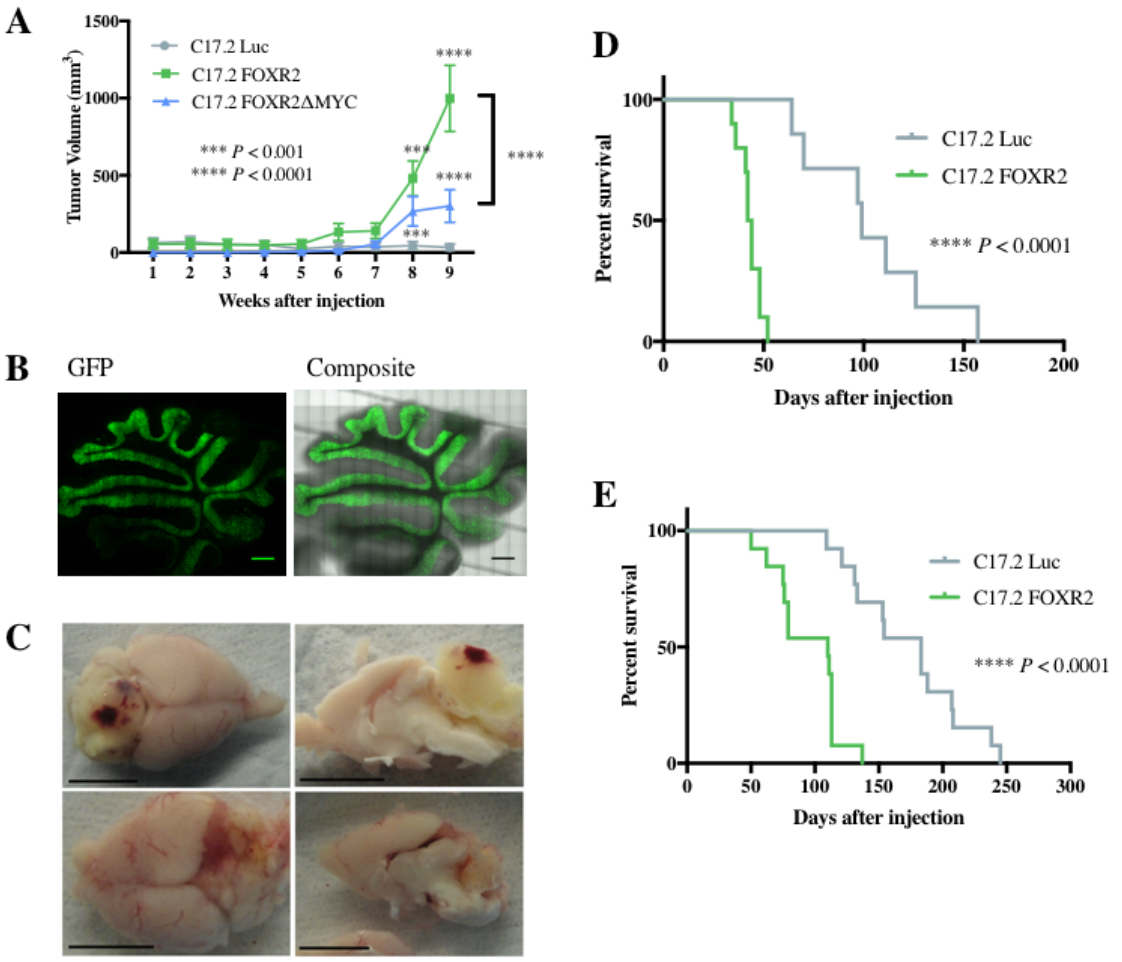


**Figure 2.15. FOXR2 promotes tumor formation in nude mice.**
**A**, Flank tumor volume of NU/J mice injected with C17.2 Luc (N=7) or C17.2 FOXR2 (N=8) cells (*P*-value: Sidak's multiple comparison's test). **B**, Fluorescence tile scan images of sagittal live-brain slice of mouse cerebellum injected with C17.2 FOXR2 cells. Left image shows GFP from C17.2 FOXR2 cells, right image is composite image of GFP and transmitted channels. Scale bars = 500 μm. **C**, Macroscopic images of whole and halved brains from NU/J mice injected with C17.2 FOXR2 cell injections. Scale bars = 1 cm. **D**, Survival of NU/J mice injected intracranially with C17.2 Luc (N=7) or C17.2 FOXR2 (N=10) cells (*P*-value: log rank Mantel-Cox test). **E**, Survival of NRG mice injected intracranially at P0 with C17.2 Luc or C17.2 FOXR2 (N=13) cells (*P*-value: log rank Mantel-Cox test). Error bars are SEM.

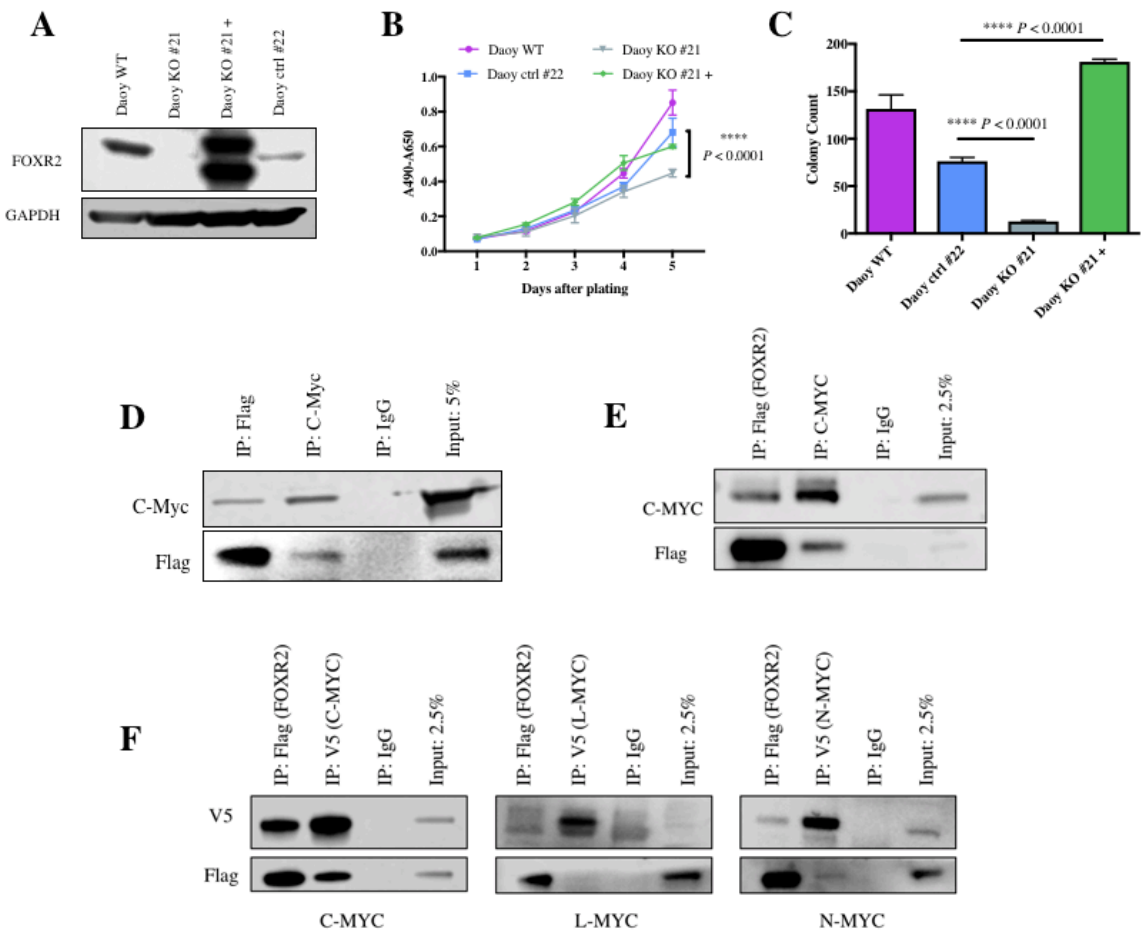


**Figure 2.16. *FOXR2* loss reduces proliferation and colony formation in Daoy. FOXR2 binds C-MYC and N-MYC.**

**A**, Western blot of Daoy WT, Daoy #21 (FOXR2 KO), Daoy #21+ (FOXR2 KO with rescue *FOXR2* cDNA), and Daoy #22 (has integrated *FOXR2 CRISPR/Cas9* vector but no alteration in the *FOXR2* locus). **B**, MTS assay of Daoy WT, Daoy #21, Daoy #21+ and Daoy ctrl #22 (*P*-value: Dunnett's multiple comparison's test). **C**, Soft agar colony formation assay of Daoy WT, Daoy #21, Daoy #21+ and Daoy ctrl #22 (*P*-value: Dunnett's multiple comparison's test). **D**, CoIP analysis in C17.2 cells of endogenous C-Myc with exogenous flag-tagged FOXR2 using flag and C-Myc antibodies. Input and IgG controls are included. **E**, CoIP of endogenous C-MYC with exogenous flag-tagged FOXR2 performed in nuclear extracts of HSC1λ cells stably expressing FOXR2 using flag and C-MYC antibodies. **F**, CoIP of exogenous V5-tagged C-MYC, L-MYC and N-MYC with exogenous flag-tagged FOXR2 performed in nuclear extracts of HEK293T cells 48 hours after transient transfection. Error bars are SEM.

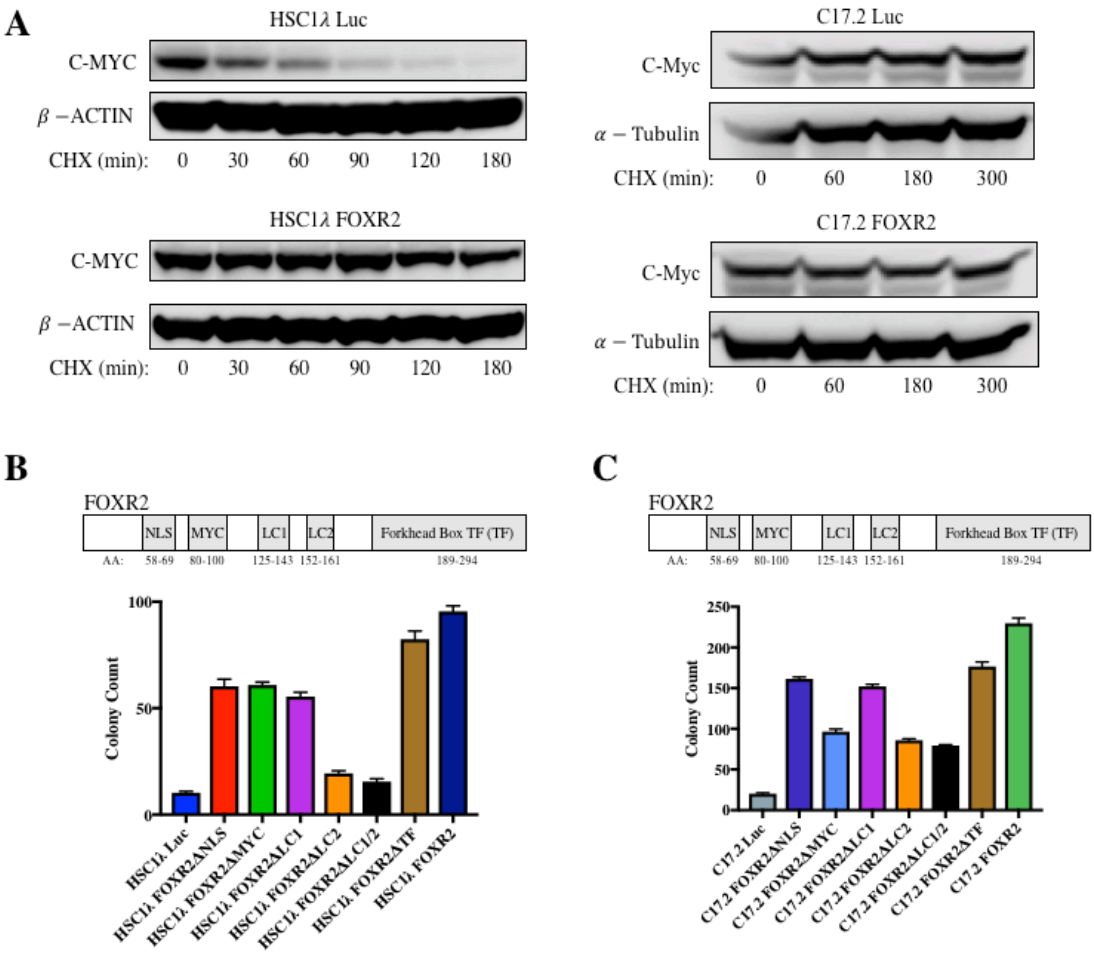


**Figure 2.17. Functional analysis of FOXR2 in C17.2 and HSC1λ cells.**
**A**, Western blot showing the effects of cycloheximide (CHX) treatment on C-MYC protein levels in HSC1λ (left panel) and C17.2 (right panel) cells with and without *FOXR2* expression. Cells were treated with CHX (100 ug/ml, resuspended in DMSO) for the time indicated and harvested for protein. **B**, Upper panel: diagram indicating locations of putative domains in the FOXR2 protein. Lower panel: soft agar analysis of HSC1λ cells stably transfected with full length FOXR2 or FOXR2 with the denoted partial deletions. **C**, Upper panel: diagram indicating locations of putative domains in the FOXR2 protein. Lower panel: soft agar colony formation assays performed on C17.2 cells stably expressing luciferase or the indicated *FOXR2* deletion mutant. Error bars are SEM.

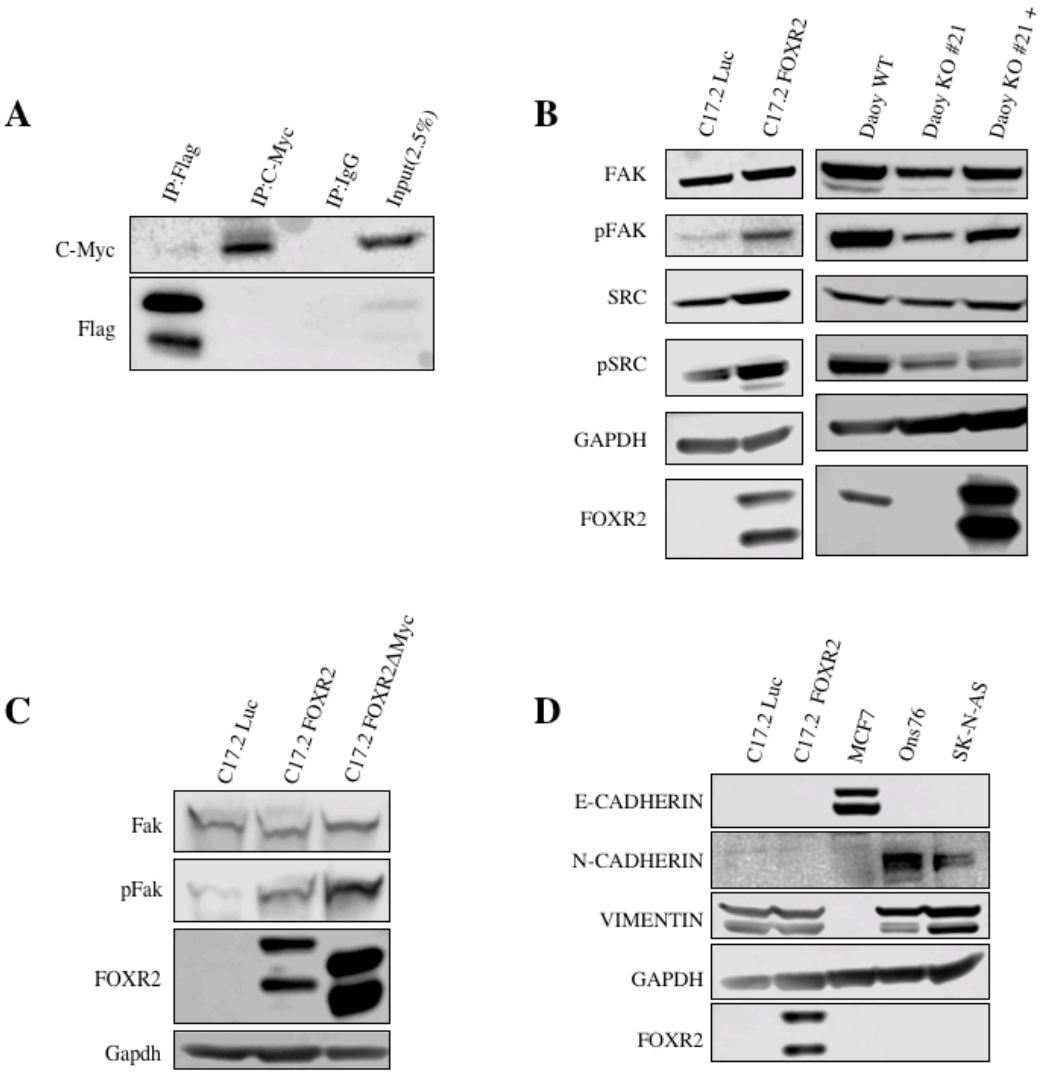


**Figure 2.18. FOXR2 activates FAK/SRC signaling independent of MYC**
**A**, CoIP of endogenous C-Myc with exogenous flag-tagged FOXR2ΔMYC in C17.2 cells. IP and western analysis was done with flag and C-MYC antibodies. Input and IgG controls are shown. **B**, Western blot showing the effects of changes in FOXR2 expression on FAK/SRC signaling. **C**, Western of C17.2 Luc, C17.2 FOXR2, and C17.2 FOXR2ΔMYC cells for Fak activation (Y397). **D**, Western blot analysis of proteins affected by epithelial-mesenchymal transition. MCF7, Ons76 and SK-N-AS are included as controls.

## Chapter 3:

Functional analysis of SB oncogenes *ARHGAP36* and *FOXR2*.

**Introduction**

ARHGAP36 (RhoGTPase activating protein 36) and FOXR2 (Forkhead box R2) have been implicated as oncogenes in several cancers, but their mechanisms of action are not completely understood. ARHGAP36 has been implicated as a regulator of the RhoGTPases CDC42, RAC1, and RHOA in pheochromocytoma, but this has not been functionally validated(187). ARHGAP36 has been shown to bind the catalytic subunit of protein kinase A (PKA, PKAC), inhibiting PKA signaling(188). ARHGAP36 has also been shown to activate sonic hedgehog (SHH) signaling(189). As PKA is a negative regulator of SHH signaling, the inhibition of ARHGAP36 on PKA provides a straight-forward mechanism to ARHGAP36-mediated SHH activation. However, there is disagreement in the literature regarding the binding-site of ARHGAP36 to PKA and its connection to SHH signaling. Also, although ARHGAP36 has been shown to be a SHH activator *in vitro*, there is little *in vivo* evidence for this. ARHGAP36 is upregulated in group 3 and group 4 human medulloblastoma and has no correlation with *Gli1* and *Ptch1* expression, two target genes activated by the SHH pathway (Figure 2.8)(189). Therefore, it is possible that the effects of ARHGAP36 *in vivo* are outside its ability to activate SHH signaling, and more functional studies are needed to further elucidate its mechanism.

In the literature, FOXR2 has many suggested mechanisms of action (Figure 1.8). We have validated the interaction of FOXR2 with C-MYC and shown a novel interaction between FOXR2 and N-MYC and a role of FOXR2 in C-MYC stability (Figure 2.16F, 2.17A). We also found the FOXR2 promotes activation of the FAK/SRC signaling pathway in a MYC-interaction independent manner (Figure 2.18). However, the importance of FAK/SRC activation on FOXR2-driven transformation has not been confirmed.

In this chapter, we further dissect the actions of ARHGAP36 as a RhoGAP and find that it does not affect the activation status of RhoA in NIH3T3 cells. We also show that when expressed individually, the 5 human isoforms of ARHGAP36 have differential effects on SHH signaling and cellular proliferation, soft agar colony formation, and tumor formation *in vivo*. The truncated isoform of ARHGAP36 (isoform 5) was found to work in cooperation with p53 loss to promote tumor formation. Lastly, we tested the effects of Dasatinib, a SRC family kinase inhibitor, on FOXR2 high versus FOXR2 low cells in a

soft agar colony assay. FOXR2 expression was found to result in Dasatinib resistance in a MYC-dependent manner.

**Methods**

**G-LISA assay for RhoA activation**

The activation status of RhoA was detected per manufacturer's protocol (Cytoskeleton G-LISA RhoA Activation Assay Biochem Kit, #BK124). Briefly, NIH3T3 cells(ATCC CRL-1658) were plated at 30% confluency ($1x10^4$ cells in a 10 cm plate) and grown for 3 days in complete media. Cells were serum starved (1% FBS for 24 hours, 0% FBS for 24 hours) to remove background RhoA activation. Cells were then treated with serum free media containing either DMSO or a RhoA activator, Calpeptin, at 0.1 mg/ml final concentration, Cytoskeleton #CN01) for 30 min at 37°C. Cells were lysed and their protein quantified. Analysis was done immediately without freezing. 1 mg/ml total protein was added to a GTP-RhoA specific 96 well plate. A490 was read on a plate reader, using the kit lysis buffer as a blank.

**Vector construction (ARHGAP36 isoforms and DNp53R270H)**

V5-tagged ARHGAP36 isoforms were constructed as GeneArt constructs through Invitrogen. Each construct was synthesized with all downstream in-frame ATG's mutated to ATC's to maintain similar amino acid charge in the protein products but eliminate usage of downstream start codons (ATG→ATC results in methionine → isoleucine). The dominant negative p53R270H construct was synthesized as a GeneArt construct through Invitrogen. Upon arrival, constructs were cloned in a pENTR vector using BP Clonase (Invitrogen #11789-100) and sequenced and digested to verify construct integrity. Subsequently, constructs were transferred to a destination vector using LR Clonase II (Invitrogen #11791). The destination vector has an internal ribosomal entry site (IRES) followed by a GFP coding sequence to facilitate *in vivo* detection. Final constructs were transfected into C17.2 and Ons76 cells and selected in Puromycin (ARHGAP36 isoforms) or Hygromycin (p53). Polyclonal lines were subjected to analysis.

**RT-PCR to show isoform expression**

Cellular RNA was purified using a PureLink RNA Mini Kit (Ambion #12183025). cDNA synthesis was done using the SuperScript VILO (Invitrogen #11755050)

recommendations. GoTaq DNA Polymerase mix (Promega #M3001) was used to amplify a common sequence among all *ARHGAP36* isoforms with primers listed in Table 3.1.

**Western blotting to show isoform expression**

Protein for western blotting was detected in whole cell lysates harvested with RIPA buffer as described(135). Antibodies are listed in Table 3.2. Probing was done according to manufacturer's protocol. Target proteins were visualized using chemiluminescence (Advansta K-12042) and a LI-COR imaging system.

**qPCR for Gli1 activation**

Cellular RNA was purified using a PureLink RNA Mini Kit (Ambion #12183025). cDNA synthesis was done using the SuperScript VILO (Invitrogen #11755050) recommendations. qRT-PCR was done using primers listed in Table 3.1 and FastStart SYBR Green Master Mix (Roche Life Science #4673492001). The $\Delta\Delta C_t$ method was used to calculate mRNA expression levels. 3 technical replicates were analyzed in triplicate for each mean with standard error of the mean (SEM) shown.

**Cell culture and *in vitro* assays**

Media components and cell line sources are described in Supplementary Table 3. All cell lines were grown at 37°C in 5% $CO_2$. Proliferation and soft agar assays were done as described(135). Briefly, MTS assays (Promega G1111) were done following the manufacturer protocol with 1200 cells per well measured over 5 days. Soft agar assays were plated in 6 well plates with 10,000 cells/well; six plates were averaged for each condition. Dasatinib (Sigma #CDS023389) was dissolved in DMSO and resuspended in complete media at the desired concentrations. Dasatinib was included in the top layer of soft agar as well as the liquid media layer. Liquid media containing Dasatinib was changed 3 days a week due to its short half-life. Transfections were done as described(135). Stable lines transfected with cDNAs were cultured as polyclonal populations after selection in Puromycin.

***in vivo* assays**

Neonatal NRG mice (Jackson 007799) were injected as described(106). Briefly, C17.2 cells at 80% confluency were prepared in HBSS, counted, and stored on wet ice prior to injection ($2x10^5$ cells/2µl injection). P0 mice were anesthetized using hypothermia and injected in the fourth ventricle at stereotactic coordinates: 1.5mm anterior to Bregma,

1.5mm deep beyond the dura. Successful injection was verified on P1 by luciferase imaging as described(106). Adult intracranial injections were performed as described(78). Female NU/J mice (Jackson 002019, 6 to8 weeks old) were anesthetized with 81 mg/kg ketamine, 13.8 mg/kg xylazine by intraperitoneal injection. $1x10^5$ cells (prepared as above) were injected in 5µl HBSS. For flank tumor assays, female NU/J mice (Jackson 002019, 6 to 8 weeks old) were injected with $1x10^6$ C17.2 cells (prepared as above) resuspended 1:1 in HBSS and Matrigel (Corning CB-40234C). Tumors were measured weekly using a digital caliper. Tumor volume = $(l \times w^2)/2$, $l$ = tumor length and $w$ = tumor width.

**Results**

**ARHGAP36 does not affect the activation status of RhoA**

To assess the role of ARHGAP36 on RhoA activation status, we used a G-LISA kit. The kit contains a RhoA-GTP binding protein coating the wells of a 96 well plate. GTP-bound RhoA will bind the wells while inactive (GDP-bound) RhoA will be removed during washes. The bound active RhoA can then be detected using a RhoA primary antibody followed by a horseradish peroxidase (HRP) conjugated secondary antibody and HRP detection using a plate reader. NIH3T3 cells stably expressing two isoforms of human ARHGAP36 (isoform 1, Q6ZRI8-1, and isoform 5, Q6ZRI8-5) or a GFP transfection control were serum starved followed by treatment with either vehicle (DMSO) or a RhoA activation control (Calpeptin). Stable expression of ARHGAP36 had no effect on baseline RhoA activation or relative RhoA activation in the presence of Calpeptin (Figure 3.1).

***ARHGAP36* isoform 1, 3, and 4 promote soft agar colony formation**

To assess the effects of each ARHGAP36 isoform individually on its transformative capacity, we transfected C17.2 and Ons76 cells with cDNA constructs with all downstream ATGs mutated to ATC, unmutated constructs expressed multiple isoforms (Figures 1.5). We were interested in dissecting the capabilities of each ARHGAP36 isoform individually, as there is disagreement regarding the effects of the N-terminal portion on Protein Kinase A (PKA) and Sonic Hedgehog (SHH) signaling(188,189). Each isoform was constructed with a V5 tag to facilitate detection

and protein-protein interactions. All 5 isoforms in both C17.2 and Ons76 were detectable by RT-PCR and western blot (Figure 3.2A-C). Interestingly, while the full and truncated isoforms of ARHGAP36 (isoform 1 and 5, respectively) activate SHH strongly in C17.2, the 5 mutated isoform constructs had much lower activation capacity (Figure 2.12H, Figure 3.3). The mutated isoform 3 and 4 constructs (mIso3 and mIso4) still significantly increase *Gli1* expression relative to *Gapdh*, but it was only ~1.5 to 2 fold compared to the ~15 to 20 fold activation by unmutated Iso5. mIso3 expression promoted proliferation as measured by an MTS assay (Figure 3.4A). mIso1, mIso3, and mIso4 all promoted soft agar colony formation close to the level of the non-mutated isoform 5 (Figure 3.4B, Figure 2.12B).

***ARHGAP36* mIso2 promotes tumor formation in the flank**

Interestingly, although mIso1, 3, and 4 promoted soft agar colony formation, mIso2 was the only construct to promote tumor formation *in vivo*. We assessed the ability of the mIsos to promote tumor formation in the flanks of nude mice in comparison to luciferase control cells (Figure 3.5A-B). mIso2 significantly promoted tumor formation in the flank, but the others did not. None of the isoforms were able to promote tumor formation alone in two orthotopic models, a neonatal injection model in NRG mice and an adult intracranial model in nude mice (Figure 3.5C-D).

***ARHGAP36* works in combination with dominant negative p53 to decrease survival**

As *ARHGAP36* and *FOXR2* were CIS genes identified in an *SB* screen using a dominant negative p53 background (p53R270H), we assessed the flank tumor formation capacity of C17.2 cells transfected with the combination of FOXR2 or two *ARHGAP36* constructs (full and truncated, isoform 1 and 5). Expression of the DNp35R270H construct did not enhance tumor volume, but it did significantly reduce survival of the mice (Figure 3.6). In comparison to C17.2 Luc, the median survival was reduced from 104 to 69 days ($P < 0.0001$, Log-Rank Mantel-Cox test). The decrease in survival with the addition of the dominant negative p53 construct was due to greatly increased necrosis in the tumors, resulting in euthanasia of the animals. When used in combination with FOXR2 or ARHGAP36, FOXR2 had no effect, but truncated ARHGAP36 significantly decreased survival further (69 to 58 days median survival, $P = 0.0035$, Log-Rank Mantel-Cox test).

**FOXR2 expression conveys a resistance to Dasatinib that is dependent on FOXR2's interaction with MYC**

In order to determine the importance of FAK/SRC signaling in FOXR2-driven transformation, we challenged FOXR2 expressing C17.2 cells with Dasatinib and assessed their colony formation capacity. Dasatinib is a tyrosine kinase inhibitor that potently inhibits BCR-ABL and SRC family kinases (SRC, LCK, YES, FYN). We also included ARHGAP36 expressing C17.2 cells, as Dasatinib should not affect SHH signaling. Our hypothesis was that if C17.2 FOXR2 cells are dependent on SRC signaling activation, they would be exquisitely sensitive to Dasatinib treatment. Surprisingly, C17.2 FOXR2 cells were less sensitive to Dasatinib treatment that ARHGAP36 expressing cells and this resistance was dependent on the interaction between FOXR2 and MYC (Figure 3.7A). The FOXR2ΔMYC cDNA is a FOXR2 cDNA that does not bind MYC (Figure 2.17-18). In addition to inhibition of colony number, colony size was also reduced in the FOXR2ΔMYC expressing C17.2 cells (Figure 3.7B).

**Discussion**

In this study, we further dissected the mechanisms of ARHGAP36-driven transformation. Although *ARHGAP36* expression correlated with a change in RHOA activation status in human pheochromocytoma, we did not find an effect of ARHGAP36 on RhoA activation in NIH3T3 cells(187). It is possible that ARHGAP36 may affect activation of other small RhoGTPases like CDC42 or RAC1, or that ARHGAP36 lacks GAP activity entirely. Alternatively, ARHGAP36 may have more effect in a different cellular context or effect interaction with RhoA effector proteins.

When individually expressed, we found that the 5 ARHGAP36 isoforms had a much-reduced ability to activate SHH signaling. This could be due to several factors. When these isoform cDNAs were constructed, all downstream ATG codons were mutated to ATC. This results in an amino acid change from methionine to isoleucine. Although mutation from methionine to isoleucine is generally considered "safe," this could have affected the conformation of ARHGAP36 or its ability to bind other proteins, including the two negative regulators of the SHH pathway it is known to bind: Suppressor of Fused and PKA(188,189). Alternatively, a protein produced using a

downstream ATG could be responsible for the effects of ARHGAP36 on the SHH pathway.

The individually expressed isoforms of ARHGAP36 also had variable effects on proliferation, soft agar colony formation, and tumor formation *in vivo*. mIso3 (mutated to only express isoform 3) promoted proliferation, while mIso1, mIso3, and mIso4 all promoted colony formation in soft agar. Interestingly, although it had little effect on SHH signaling, proliferation, or colony formation, mIso2 was the only isoform to promote any tumor formation *in vivo*. All of the constructed *ARHGAP36* isoforms maintain intact arginine rich regions (ARR), GTPase activating protein (GAP) domains, and binding sites to PKAC(188). Therefore, it's difficult to explain the correlation with SHH activation and soft agar colony formation and the apparent discrepancy in tumor promoting capacity. The lack of SHH activation by mIso2 and its solo ability to promote tumor formation in the flank may suggest an alternative mechanism of ARHGAP36 in oncogenesis.

We assessed the ability of ARHGAP36 to cooperate with p53 deficiency. The truncated form of ARHGAP36 was shown to cooperate with p53 to reduce survival in nude mice when injected in the flank. This suggests that further *in vivo* studies, including creation of an ARHGAP36 expressing transgenic mouse model, may benefit from use of a p53 deficient background. Interestingly, *Arhgap36* insertions in *Sleeping Beauty*-induced mouse tumors correlated with an incidence of metastasis, and SHH subgroup medulloblastoma with a p53 mutation represent a particularly aggressive and invasive tumor type (Table 2.4)(278).

Additionally, in order to study the effects of *ARHGAP36* loss in the context of medulloblastoma, we attempted to knockout ARHGAP36 in several medulloblastoma cell lines (Ons76, Daoy, and Med8A). Unfortunately, although we tried many different tools (TALENs, CRISPR/Cas9, siRNA, shRNA) to create a loss of function model, we were unable to create bi-allelic, frameshift changes in the *ARHGAP36* locus or successfully knock it down (data not shown). The only modifications achieved were either heterozygous or in multiples of 3, presumably leaving the protein intact (data not shown). This implicates *ARHGAP36* as an essential gene in these medulloblastoma cell lines.

Lastly, we assessed the effects of a SRC family kinase inhibitor, Dasatinib, on FOXR2-driven colony formation. Surprisingly, FOXR2 expressing C17.2 cells were more resistant than ARHGAP36 expressing counterparts, and this effect was dependent on the interaction between MYC and FOXR2. This is surprising in several ways. First of all, we expected that if ARHGAP36-driven transformation was dependent on SHH signaling, a tyrosine kinase inhibitor should have little effect on its transforming capacity. This suggests that an alternative mechanism for ARHGAP36-driven tumorigenesis, if it exists, could be through a SRC family kinase. Secondly, we expected FOXR2 expressing cells to be dependent on SRC activation and thus more sensitive to Dasatinib. An alternative explanation could be that because more activated SRC is present with FOXR2 expression, more inhibitor is required to achieve the same loss of colony formation. And lastly, the MYC interaction mutant of FOXR2 was still shown to promote SRC activation in C17.2, so its individual response to Dasatinib is surprising (Figure 2.18C). Inhibition of SRC blocks C-MYC translation. Therefore, if FOXR2 binding to MYC is promoting MYC stability, the consequence of MYC translation inhibition could be reduced(279). This could explain the reduction of colony formation in the MYC binding mutant expressing cells. To address this, MYC protein levels need to be assessed in the presence of Dasatinib in each of these lines to determine if MYC levels are being affected. In addition, treatment with a targeted inhibitor of MYC and FAK, both individually and together, would provide more insight.

**Table 3.1. - Primers**

| **Primers for RT-PCR of ARHGAP36 mIso constructs** | **Forward (5' - 3')** | **Reverse (5' - 3')** |
|---|---|---|
| ARHGAP36cDNA-F1/R1 | Caactttccgtaccacttcctaccc | cgctttacttgtacctgagcgcg |
| **qPCR primers for Shh pathway activation** | **Forward (5' - 3')** | **Reverse (5' - 3')** |
| Mouse - *Gapdh* | TTCCAGTATGACTCCACTCACGG | TGAAGACACCAGTAGACTCCACGAC |
| Mouse - *Gli1* | TTATGGAGCAGCCAGAGAGACCAG | ATGGAGAGAGCCCGCTTCTTT |

**Table 3.2. - Antibodies used for western blotting**

| Antibody | Company | ID # | Use |
|---|---|---|---|
| GAPDH | Cell Signaling Technologies | 5174S | Western |
| V5 | Cell Signaling Technologies | 13202S | Western/CoIP |
| ARHGAP36 | Abcam | AB84010 | Western |

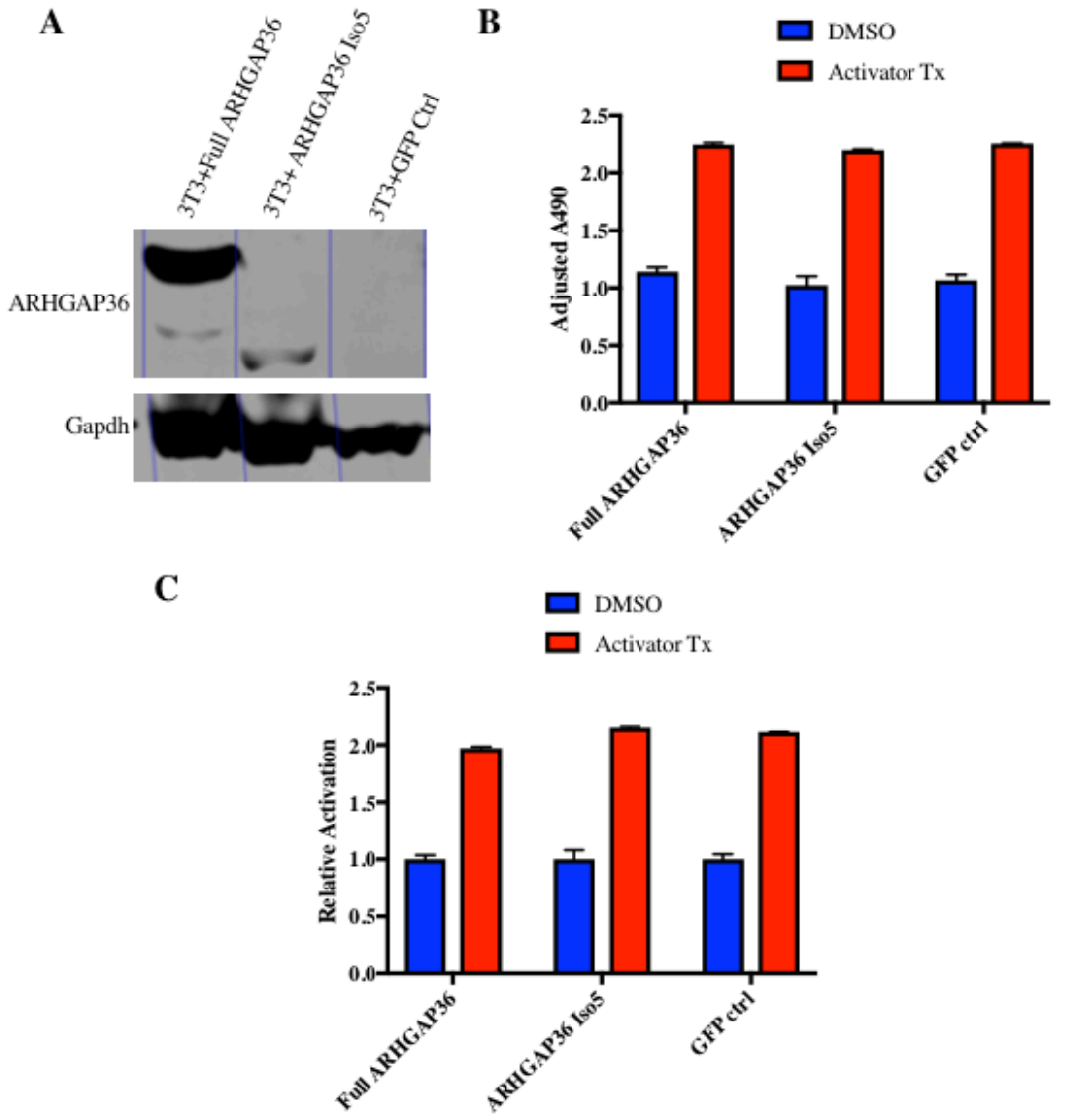


**Figure 3.1. *ARHGAP36* does not affect RhoA activation in NIH3T3 cells.**
**A**, Western blot showing ARHGAP36 expression in NIH3T3 cells stably expressing either full ARHGAP36 (isoform 1,Q6ZRI8-1), truncated ARHGAP36 (isoform 5, Q6ZRI8-5), or a GFP control vector . **B-C,** Activation of RhoA shown as detected by a G-LISA plate reader assay. 3T3 cells with GFP or two forms of ARHGAP36 were serum starved for 48 hours followed by DMSO or a RhoA activator treatment (Calpeptin, 0.1 mg/ml, #CN01, 30 min). **B**, A490 values of each samples adjusted to subtract a blank sample. **C**, RhoA activation relative to the vehicle (DMSO) control.

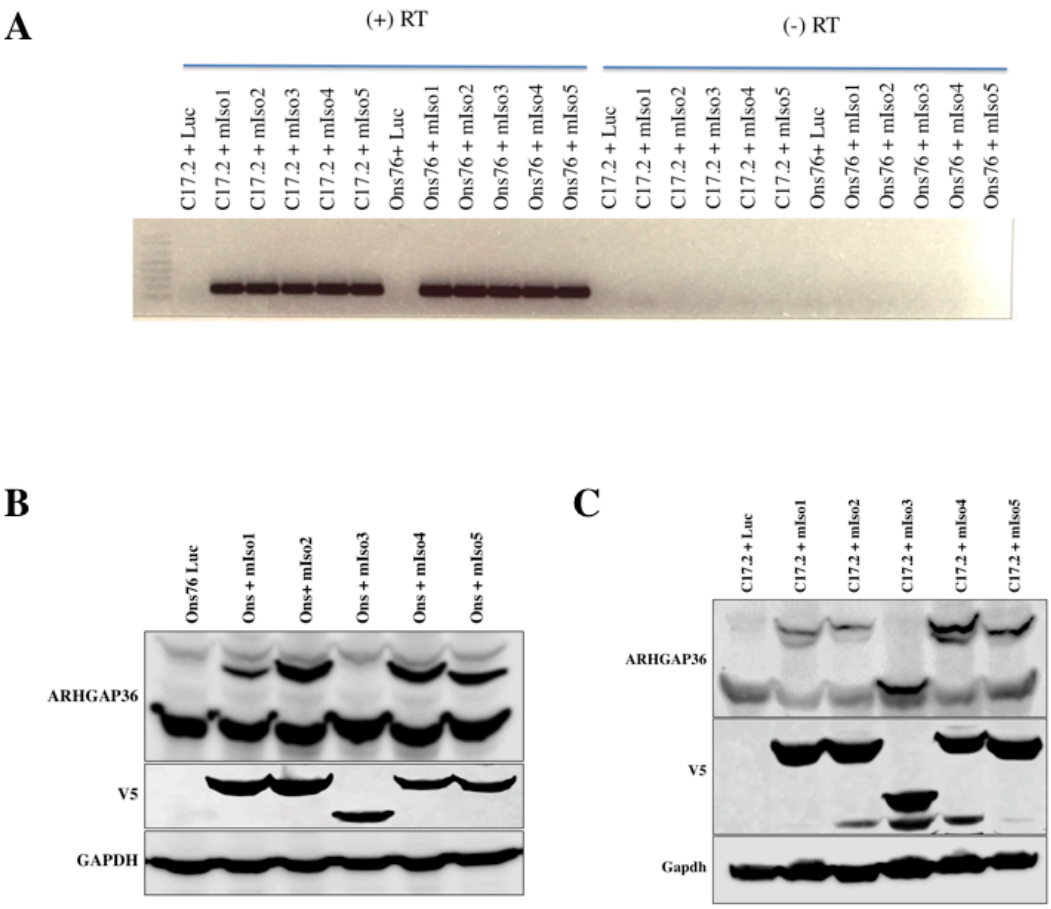


**Figure 3.2. All 5 human isoforms of *ARHGAP36* express individually in Ons76 and C17.2.**
**A**, Reverse transcriptase PCR (RT-PCR) of 5 *ARHGAP36* isoforms mutated to only allow expression from the appropriate ATG. No reverse transcriptase (-RT) control samples are show on the right side. **B-C**, Western blot showing expression of all 5 isoforms of ARHGAP36 in Ons76 (**B**) and C17.2 (**C**). Size of isoforms – 62, 58, 46, 61, 57kDa, respectively. All isoforms are V5-tagged.

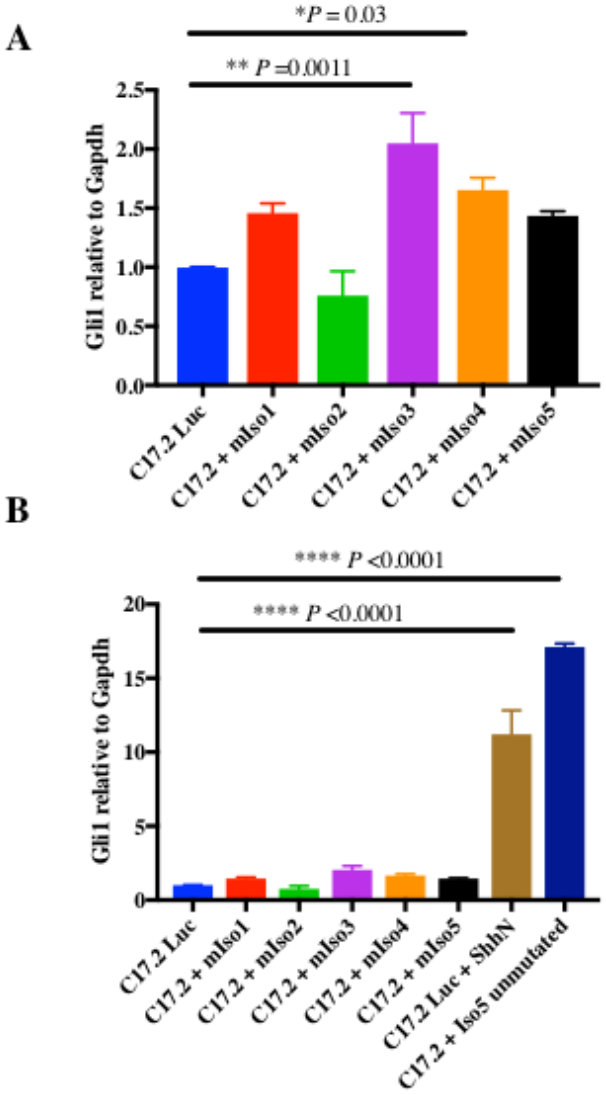


**Figure 3.3. Mutated ARHGAP36 isoforms activate SHH signaling but at a much lower level than unmutated forms.**

**A-B**, qRT-PCR for *Gli1* in C17.2 cells stably expressing ARHGAP36 constructs for each isoform in humans. These constructs have been mutated to only express a single isoform. Cells are serum starved with or without treatment of exogenous ShhN ligand. *Gli1* expression is normalized to *Gapdh* (*P*-Values: Dunnett's multiple comparison's test). Error bars are SEM.

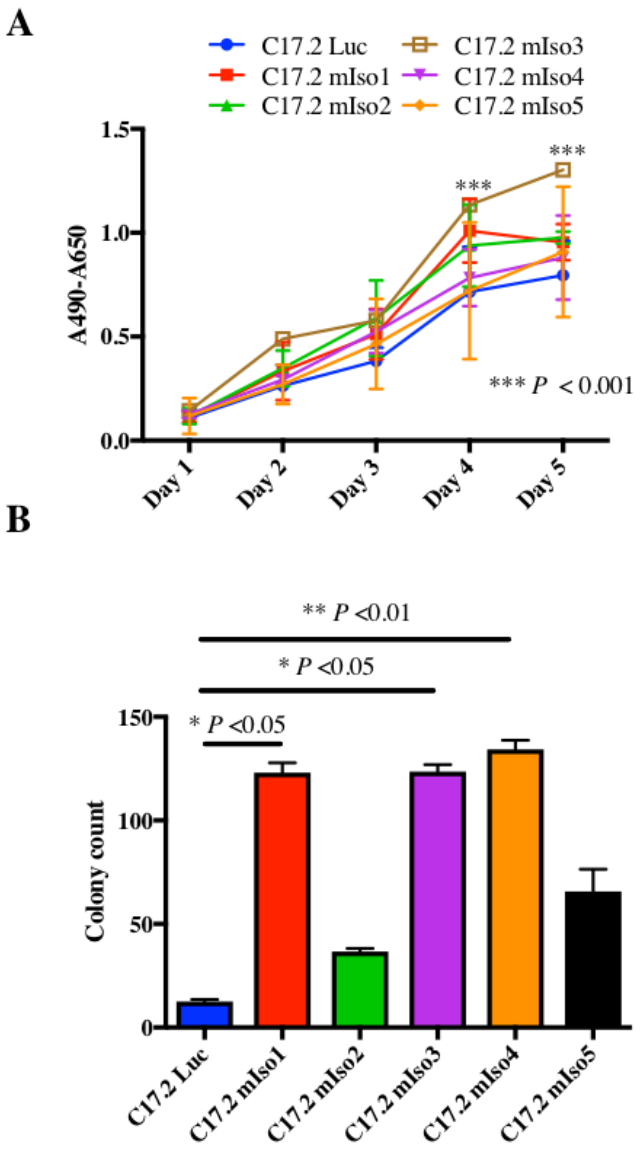


**Figure 3.4. Some *ARHGAP36* isoforms promote proliferation and soft agar colony formation.** **A**, MTS assay for C17.2 cells stably expressing luciferase or individual *ARHGAP36* isoforms. *P*-Value shown is between C17.2 Luc and C17.2 mIso3 (Dunnett's multiple comparisons test).**B**, Soft agar assays of C17.2 cells stably expressing luciferase or one of 5 *ARHGAP36* isoforms. (*P*-Values: Dunnett's multiple comparison's test). Error bars are SEM.

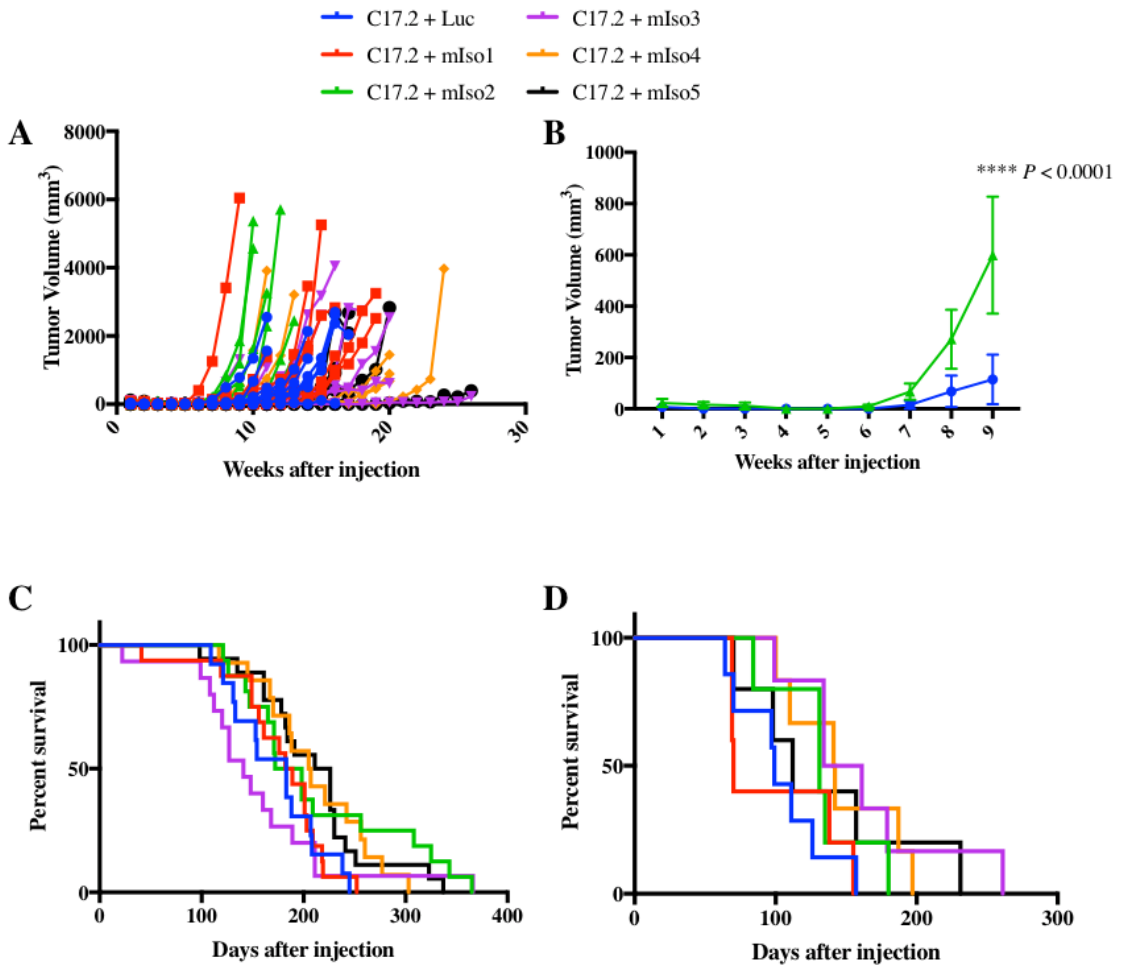


**Figure 3.5. *ARHGAP36* mIso2 promotes flank but not orthotopic tumor formation.**
**A**, Flank tumor volume of NU/J mice injected with C17.2 Luc (N=9) or C17.2 expressing individual *ARHGAP36* isoforms (N=10,8,10,8,7). **B**, Averaged flank tumor volumes for C17.2 Luc and C17.2 mIso2 (*P*-value: Sidak's multiple comparisons test). **C**, Neonatal injections of NRG mice with C17.2 Luc (N=14) or C17.2 expressing individual *ARHGAP36* isoforms (N=16,16,15,14, and 22 for isoform 1,2,3,4, and 5, respectively). **D**, NU/J mice injected intracranially with C17.2 Luc (N=5) or C17.2 expressing individual *ARHGAP36* isoforms (N=5 for each).

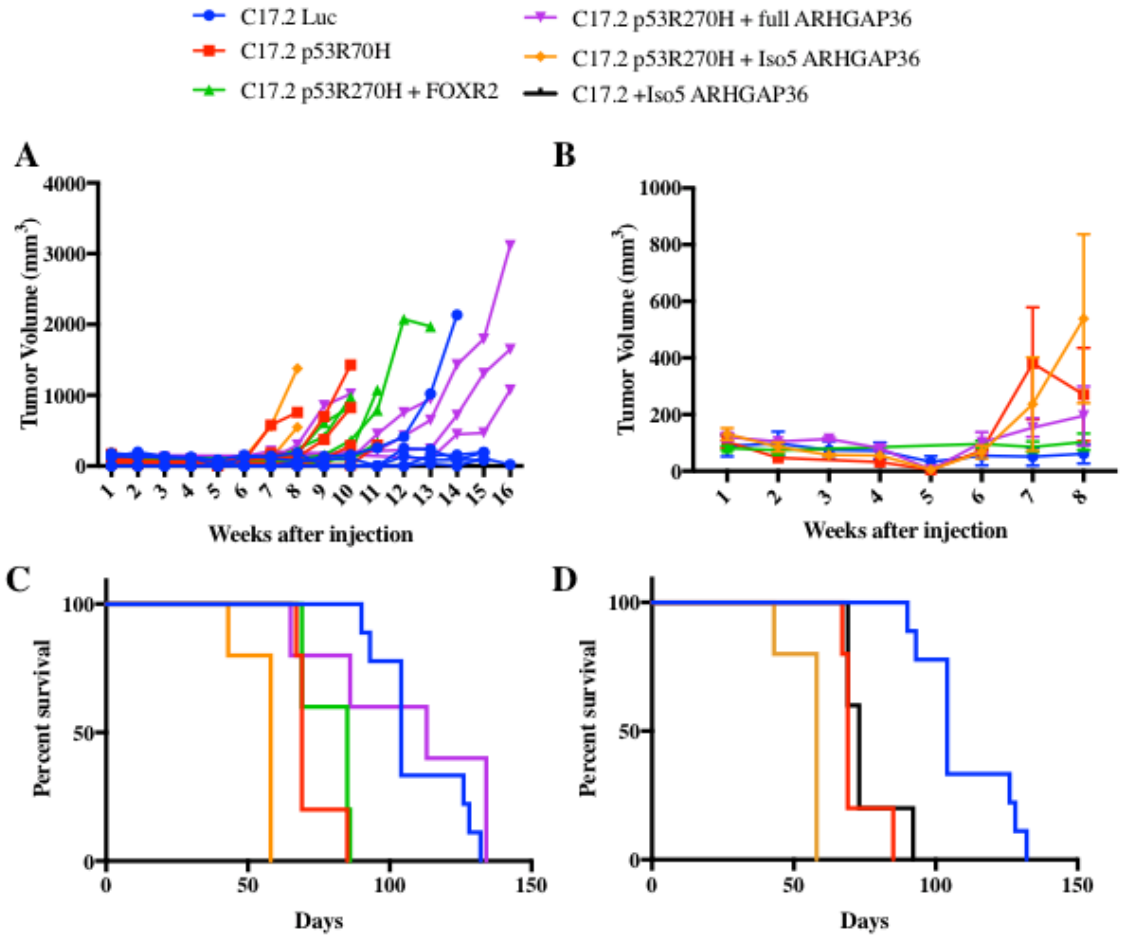


**Figure 3.6. Truncated *ARHGAP36* works in cooperation with DNp52R270H to reduce survival.** **A**, Flank tumor volume of NU/J mice injected with C17.2 cells expressing luciferase, dominant negative p53 (p53DN270H) or p53DN270H in combination with full or truncated ARHGAP36 (isoform 1 and 5, respectively) or FOXR2 (N=5 for all). **B**, Averaged flank tumor volumes for all cell lines up to week 8. **C**, Kaplan Meier analysis of mice injected with the above mentioned cell lines. **D**, Kaplan Meier analysis of mice injected with C17.2 Luc, C17.2 p53DN270H, C17.2 p53DN270H + Iso5 ARHGAP36, and C17.2 Iso5 ARHGAP36.

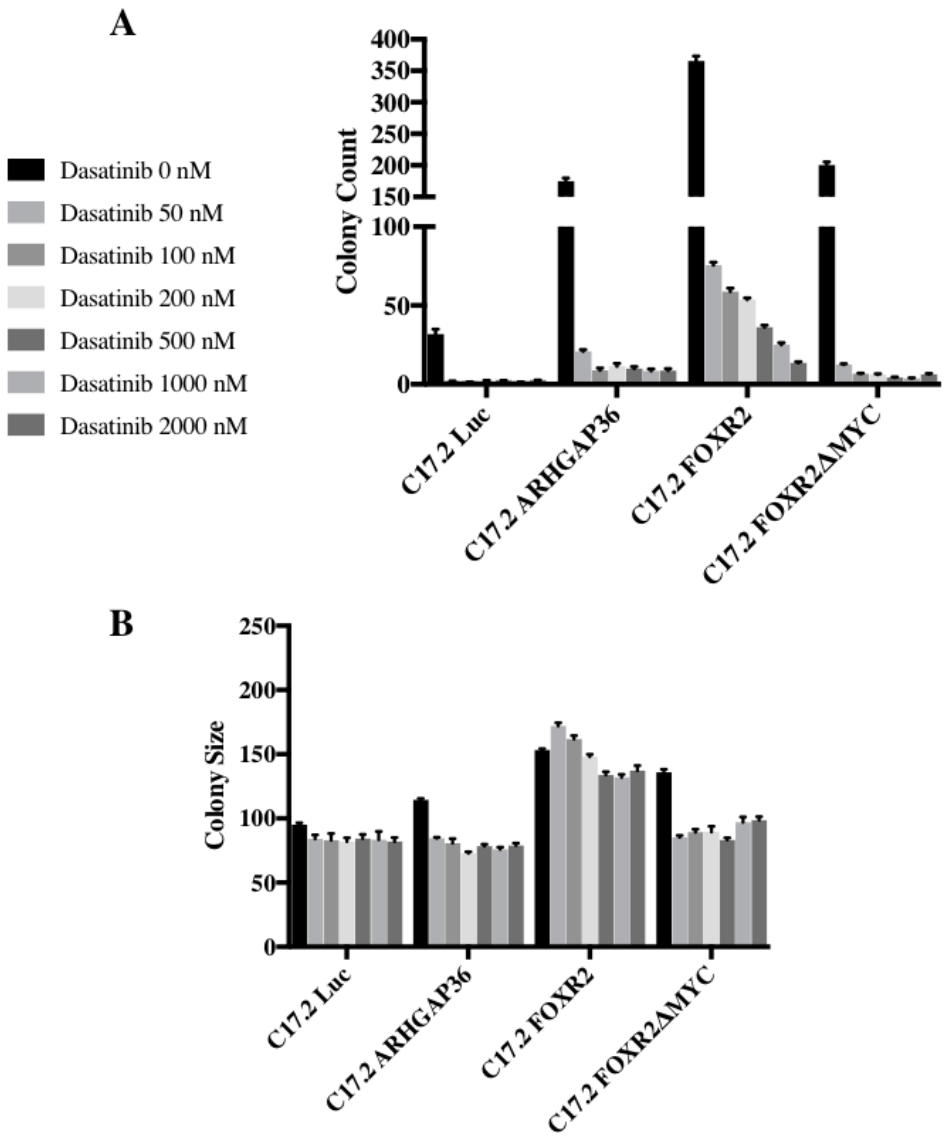


**Figure 3.7. FOXR2 expression conveys a resistance to Dasatinib that is MYC-dependent.**
**A**, Soft agar colony formation of C17.2 cells expression luciferase, ARHGAP36 (isoform 5), FOXR2, or C17.2FOXR2ΔMYC with increasing concentrations of Dasatinib. **B**, Colony size of the above cell lines and conditions.

# Chapter 4:

Characterization of *FOXR2* as a novel oncogene in neuroblastoma.

**Introduction**

FOXR2 (Forkhead box R2) has been identified as an oncogene in many cancers of neural origin, including glioma, malignant peripheral nerve sheath tumors (MPNSTs), central nervous system neuroblastoma (CNS NB-*FOXR2*) and medulloblastoma(110,125,135,231). Specifically in CNS NB-*FOXR2*, complex inter- and intra-chromosomal re-arrangements converging on *FOXR2* resulted in increased *FOXR2* expression and the formation of fusion transcripts(125). In 8 samples analyzed, *FOXR2* had the following fusion partners: *JMJD1C* (complex interchromosomal translocation involving chromosome 10, 1 sample), *LOC550643* (tandem duplications on chromosome X, 1 sample), *JPX* (tandem duplications on chromosome X, 1 sample), *MAGEH1* (large deletion between genes, 2 samples), and *USP51* (insertion of mitochondrial DNA to form novel FOXR2 promoter). One sample with no change in the *FOXR2* locus and low *FOXR2* expression was the only sample analyzed found to have a focal amplification in *MYC* with increased *MYC* expression. This mutual exclusivity implicates that *FOXR2* and *MYC* may be acting together.

Our lab is interested in further characterizing the presence of *FOXR2* fusion transcripts in peripheral neuroblastoma, which may result in increased *FOXR2* expression and tumorigenesis. Peripheral neuroblastoma (NB) is known to have large chromosomal rearrangements(173). *FOXR1*, a *FOXR2* homolog, is recurrently activated in NB through intra-chromosomal fusion events(224). Our hypothesis is that *FOXR2* fusion transcripts and increased expression will be mutually exclusive with *MYCN* amplification. *MYCN* is amplified in approximately 25% of human neuroblastoma and is associated with increased metastasis(145). As we have shown FOXR2 is able to bind N-MYC (Figure 2.16F) and increase C-MYC protein stability (Figure 2.17A), we hypothesize that FOXR2 is binding to and stabilizing N-MYC, increasing the N-MYC protein presence without increasing N-MYC at the transcript level. Alternatively, FOXR2-mediated C-MYC stability could act as an alternative MYC source in N-MYC low NB.

To address these hypotheses, we first determined if *FOXR2* fusion transcripts occur in human NB and if they occur in the presence or absence of *MYCN* amplification. We also created gain and loss of function models in human NB cell lines to determine if *FOXR2* is an important oncogene in NB.

## Methods

### *FOXR2* and *MYCN* analysis in human neuroblastoma tumors and cell lines

Primary tumor gene expression profiles were organized by the TARGET (Therapeutically Applicable Research to Generate Effective Treatments) consortium. Profiles were obtained using Affymetrix arrays Human Exon 1.0ST platform. Gene expression intensities were normalized using Robust Multi-array Average implemented in the Affymetrix Power Tools suite using the "-rma-sketch" option over the core probe set annotation. A panel of 25 neuroblastoma cell line expression profiles was obtained using HuGene-1_0-st Affymetrix Human Gene 1.0 ST Arrays (GeneOmnibus GSE78061). Gene expression intensities were normalized using Robust Multi-array Average implemented in the Affymetrix Power Tools suite using the "-rma-sketch"and transcript level summarization.Kaplan-Meier representation and Log-rank statistical analyses was implemented in the R "survival" package (http://cran.rproject.org/web/packages/survival/index.html).

### Cell line culture and *in vitro* assays

Cell line sources and media components are listed in Table 4.1. All cell lines not acquired within 1 year from ATCC were authenticated through the University of Arizona Genetics Core. All cell lines were grown at 37°C in 5% $CO_2$. Proliferation and soft agar assays were done as described(135). Briefly, MTS assays (Promega G1111) were done following the manufacturer protocol with 1200 or 1400 cells per well measured over 5 days (1200 cells/well for NB16 and SK-N-SH, 1400 cells/well for IMR32). Soft agar assays were plated in 6 well plates with 10,000 cells/well; six plates were averaged for each condition.

### 5' RACE

Cellular RNA was isolated (PureLink RNA Mini Kit, Ambion 12183025) and treated with DNase (Invitrogen CX27091). 5'RACE (rapid amplification of cDNA ends) using 2 $\mu$g of purified RNA was done according to the manufacture's protocol using gene specific primers in Table 4.2 (Invitrogen 18374058). The identified fusion product was re-amplified using primers in Table 4.2 and GoTaq Master Mix according to the manufacture's protocol (Promega M7123).

### Western blotting

Protein for western blotting (non-CoIP) was detected in whole cell lysates harvested with RIPA buffer as described(135). Antibodies are listed in Table 4.3. Probing was done according to manufacturer's protocol. Target proteins were visualized using chemiluminescence (Advansta K-12042) and a LI-COR imaging system.

**Flank tumor injections and measurement**

For flank tumor assays, female NU/J mice (Jackson 002019, 6-8 weeks old) were injected with $1x10^7$ cells resuspended 1:1 in HBSS and Matrigel and stored on wet ice prior to injection (Corning CB-40234C). Tumors were measured weekly using a digital caliper. Tumor volume = $(l \times w^2)/2$, $l$ = tumor length and $w$ = tumor width.

**Results**

To determine if *FOXR2* is important in human neuroblastoma (NB), we analyzed *FOXR2* expression in low and high-risk human NB assembled by the NCI TARGET (Therapeutically Applicable Research to Generate Effective Treatments) initiative(280). These are Affymetrix-based Human Exon 1.0 ST Arrays (HuEx) which show exon expression levels of *FOXR2* in different clinical stages of NB with and without *NMYC* amplification. We found that *FOXR2* expression is dichotomic, with high expression in a subset of non-*MYCN* amplified tumors and low expression in *MYCN* amplified and low-risk tumors (Figure 4.1A). In the high-risk, non-amplified group alone, high *FOXR2* expression correlated with decreased survival (Figure 4.1B-C).

We also analyzed *FOXR2* expression levels and *MYCN* amplification status in a panel of human NB cell lines. Aside from NLF and NB69, NB cell lines with *MYCN* amplification had lower levels of *FOXR2* than non-amplified cell lines (Figure 4.2A). Interestingly, the only *MYCN* amplified line with high *FOXR2* expression (NLF) has a relatively low level of *NMYC* expression for a *MYCN* amplified NB line (Figure 4.2B). Additionally, NB69 has low levels of both *N-MYC* and *FOXR2*, but extremely high levels of *C-MYC* (Figure 4.2C).

In order to determine if *FOXR2* fusion events are occurring in human NB, we performed 5'RACE (rapid amplification of cDNA ends) on one *FOXR2* low cell line (CHP212) and two *FOXR2* high cell lines (SK-N-AS and SK-N-SH, Table 4.1, Figure 4.3A). No *FOXR2* expression was detected in the *FOXR2* low cell line, CHP212. Six different transcripts were visible in the *FOXR2* high cell lines (a-f, Figure 4.3A). These

bands were purified and sequenced to determine if any fusion sequences were present at the 5' end of *FOXR2*. One fusion product in SK-N-AS contained sequence from exon 1 of *KLHL13* (Figure 4.3B). This fusion of exon 1 of *KLHL13* with exons 3-5 of *FOXR2* results in production of the full length FOXR2 protein. This full FOXR2 protein product will not contain any of KLHL13, as the start site of translation for KLHL13 is within exon 2. Therefore, the fusion transcript should efficiently translate to make a full length FOXR2 protein. Subsequently, we were able to amplify this fusion product in SK-N-AS using gene specific primers within *KLHL13* exon 1 and *FOXR2* exon 3 (Figure 4.3C, primers listed in Table 4.2). Both *KLHL13* and *FOXR2* are located on the X chromosome, so in order to create the *KLHL13*:*FOXR2* fusion transcript, all that is needed is 2 chromosomal breaks and an inversion (Figure 4.4).

We created gain of function models of FOXR2 in 2 neuroblastoma cell lines with low endogenous *FOXR2* expression (IMR32 and NB16) to determine if increased FOXR2 affects tumor promoting properties in these lines (Figure 4.5A). IMR32 has low *FOXR2* expression and *MYCN* amplification (Table 4.1). NB16 has low to medium *FOXR2* expression without *MYCN* amplification (Table 4.1, Figure 4.2A). Increased FOXR2 expression increased colony formation in soft agar but did not affect proliferation in an MTS assay (Figure 4.5).

Additionally, we created loss of function models in neuroblastoma lines expressing high levels of *FOXR2*. FOXR2 was knocked down with shRNA constructs (Dharmacon, Figure 4.6A). Knock down of FOXR2 resulted in a decrease in C-MYC protein and FAK (focal adhesion kinase) activation as measured by phosphorylation at Y397 (Figure 4.6A). Upon observation of the cell lines, it became clear that the wildtype populations were a heterogenous population consisting of cells with varying shape and size, a known phenomenon for SK-N-SH and SK-N-AS cell lines(281). We isolated single cell clones of SK-N-AS and found varying levels of MYC and FOXR2 which followed similar patterns as the knockdown lines, with lower C-MYC expression in lines expressing low FOXR2 (Figure 4.7).

**Discussion**

We identified a novel role for *FOXR2* as an oncogene in peripheral neuroblastoma (NB). High levels of *FOXR2* drove colony formation in soft agar. A subset of high-risk human NBs express a high level of *FOXR2* and this is mutually exclusive to *MYCN* amplification. We also found the same mutual exclusivity between high *FOXR2* expression and *MYCN* amplification in a panel of NB cell lines. Interestingly, 2 cell lines did not fit this pattern and provide additional information. NLF was the only *MYCN* amplified line to have high *FOXR2* expression, but *N-MYC* expression levels were comparable to non-*MYCN* amplified cell lines. NB69 was the only line with low levels of *N-MYC* and *FOXR2*, but it had extremely high levels of *C-MYC*. These data imply that N-MYC, C-MYC, and FOXR2 are working together in the context of neuroblastoma. FOXR2 binds C-MYC and increases its protein stability (Figure 2.16D-F, 2.17A) and is capable of binding N-MYC (Figure 2.16F). Therefore, increased FOXR2 expression could be affecting N-MYC stability as well, or increased C-MYC stability in the presence of FOXR2 may provide another mechanism for MYC-driven transformation. FOXR2-mediated effects on C-MYC stability in NB are supported by decreases in C-MYC protein levels with decreased expression of FOXR2 (Figure 4.6, Figure 4.7). However, further experiments are needed to elucidate the mechanism of FOXR2 in NB.

We also identified a novel fusion partner for *FOXR2*, *KLHL13*. Kelch like family member 13 is located on the X chromosome and encodes a BTB (Bric-a-brac-Tram-track-Broad complex) and kelch domain-containing protein(282) and has been implicated in inherited neuropathies(283) but is relatively unstudied. KLHL13 is expressed in the brain and nerves, making it likely to be expressed in the neural crest and progenitor cells for neuroblastoma (www.genecards.org, www.proteinatlas.org). *KLHL13* is also highly expressed in NB cell lines without changes in copy number (Figure 4.8). The identification of a *KLHL13*:*FOXR2* fusion warrants further study, as it provides a mechanism by which FOXR2 is expressed at high levels in neuroblastoma. These data suggest that increased FOXR2 expression may be the result of translocations, but other mechanisms may also come into play.

**Table 4.1. Human neuroblastoma cell lines**

| Cell line | FOXR2 status | MYCN status | Media | Cell line source | Validation status |
|---|---|---|---|---|---|
| CHP212 | Low | Yes | 1:1 mix of EMEM and F12 media with 10% FBS | ATCC-CRL-2273, aquired 2017 | Verified as CHP212 October 2017 |
| IMR32 | Low | Yes | 1:1 mix of EMEM and F12 media with 10% FBS | ATCC-CCL-127, aquired 2017 | Verified as IMR32 October 2017 |
| NB16 | Medium | No | RPMI with 10% FBS, 1% P/S, and 2mM L-Glutamine | John Maris lab, aquired 2017 | 80% match to TE-671 (DSMZ), October 2017 |
| SK-N-AS | High | No | 1:1 mix of EMEM and F12 media with 10% FBS and 0.1 mM NEAA | ATCC-CRL-2137, aquired 2017 | Not authenticated, acquired from ATCC within a year of analysis |
| SK-N-SH | High | No | 1:1 mix of EMEM and F12 media with 10% FBS and 1% P/S | ATCC-HTB-11, aquired 2017 | Not authenticated, acquired from ATCC within a year of analysis |
| SK-N-Fl | High | No | 1:1 mix of EMEM and F12 media with 10% FBS and 0.1 mM NEAA | ATCC-CRL-2142, aquired 2017 | Not authenticated, acquired from ATCC within a year of analysis |
| SH-SY5Y | High | No | 1:1 mix of EMEM and F12 media with 10% FBS | ATCC-CRL-2266, aquired 2017 | Not authenticated, acquired from ATCC within a year of analysis |
| NLF | High | Yes | RPMI with 10% FBS, 1% P/S, and 2mM L-Glutamine | John Maris lab, aquired 2017 | No reference sample available, found to be human without contamination, October 2017 |

**Table 4.2. Primers**

| **5' RACE primers** | **Forward (5' - 3')** | **Reverse (5' - 3')** |
|---|---|---|
| FOXR2 RACE GSP1 | TTATCTTCATCCTTAAGG | |
| FOXR2 RACE GSP2 | TGTCCCAGTCCAGCAGCCCT | |
| FOXR2 RACE GSP3 | CCTGGGACCTGGCCATGGAGA | |
| **Gene specific primers to amplify KLHL13:FOXR2 fusion** | **Forward (5' - 3')** | **Reverse (5' - 3')** |
| KLHL13_F1 | GCTCAGCTCCTATTCCTGGG | |
| KLHL13_F2 | GACTCCCTCTTTGGCCCTC | |
| FOXR2_R | | ACCCGGCGGACAAGC |

**Table 4.3. Antibodies used for western blotting.**

| Antibody | Company | ID # |
|---|---|---|
| HSP90 | Cell Signaling Technologies | 4874S |
| FOXR2 | Proteintech | 14111-1-AP |
| C-MYC | Cell Signaling Technologies | 5605S |
| FAK | Cell Signaling Technologies | 3285 |
| pFAK (Y397) | Cell Signaling Technologies | 3283S |

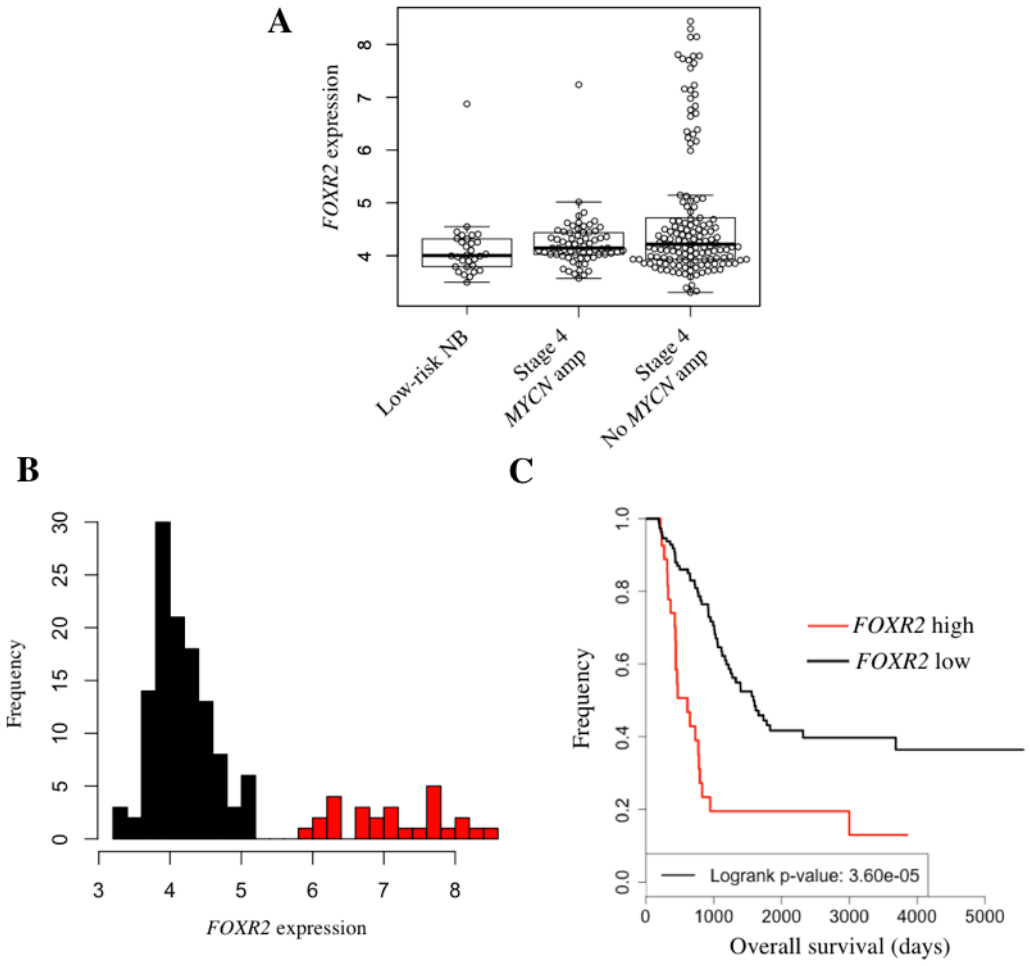


**Figure 4.1. *FOXR2* is expressed in a subset of non-*MYCN* amplified neuroblastoma and associated with poor survival.**

**A**, *FOXR2* expression in human neuroblastoma according to clinical stage and *MYCN* amplification status. This data was assembled by the NCI TARGET (Therapeutically Applicable Research to Generate Effective Treatments) initiative. **B**, *FOXR2* expression in non-*MYCN* amplified, high-risk tumors. **C**, Kaplan Meier analysis of *FOXR2* high and low tumors in **B**.

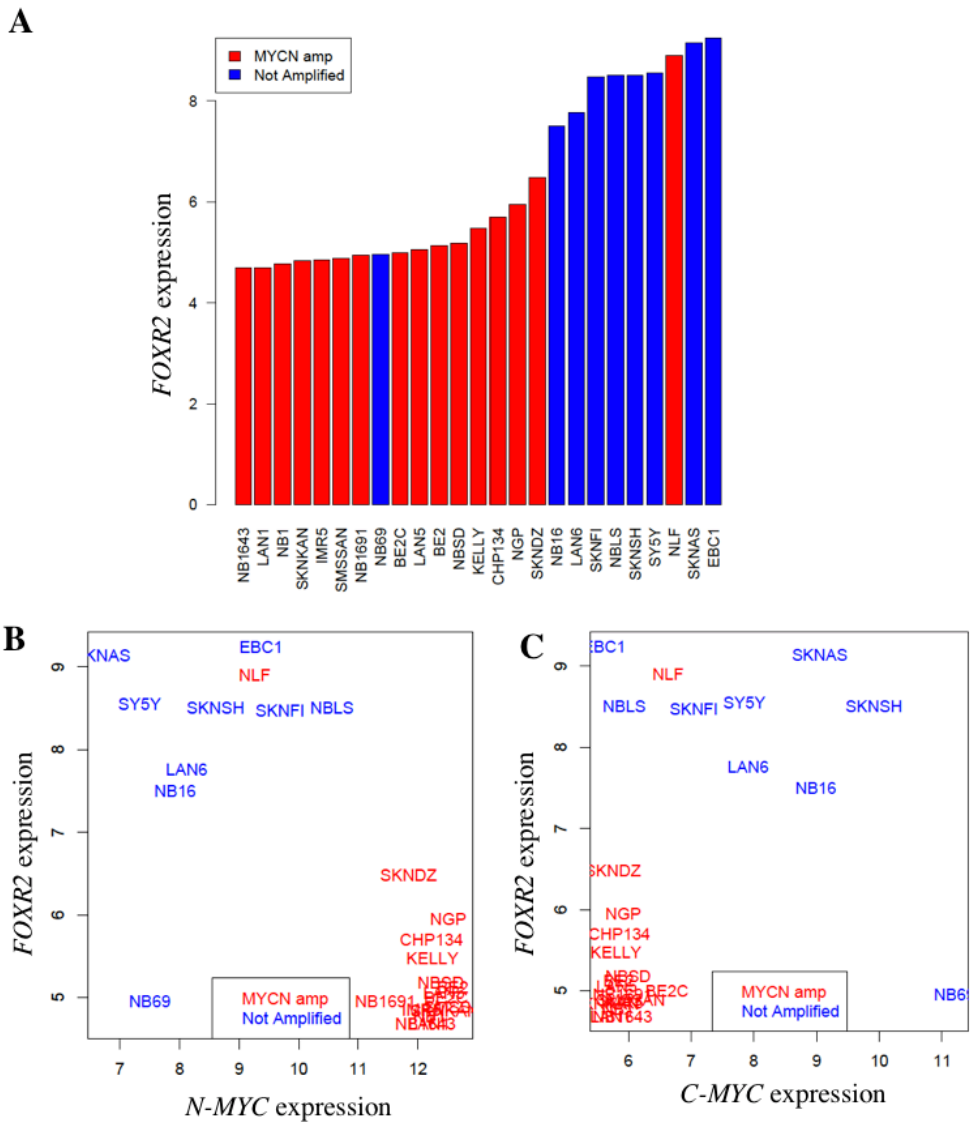


**Figure 4.2. *FOXR2* is expressed at high levels in non-*MYCN* amplified neuroblastoma cell lines.**
**A**, *FOXR2* expression in human neuroblastoma (NB) cell lines with and without *MYCN* amplification. This data is based on U133 Affymetrix arrays. **B**, FOXR2 versus N-MYC expression in human NB cell lines. **C**, FOXR2 versus C-MYC expression in human NB cell lines.

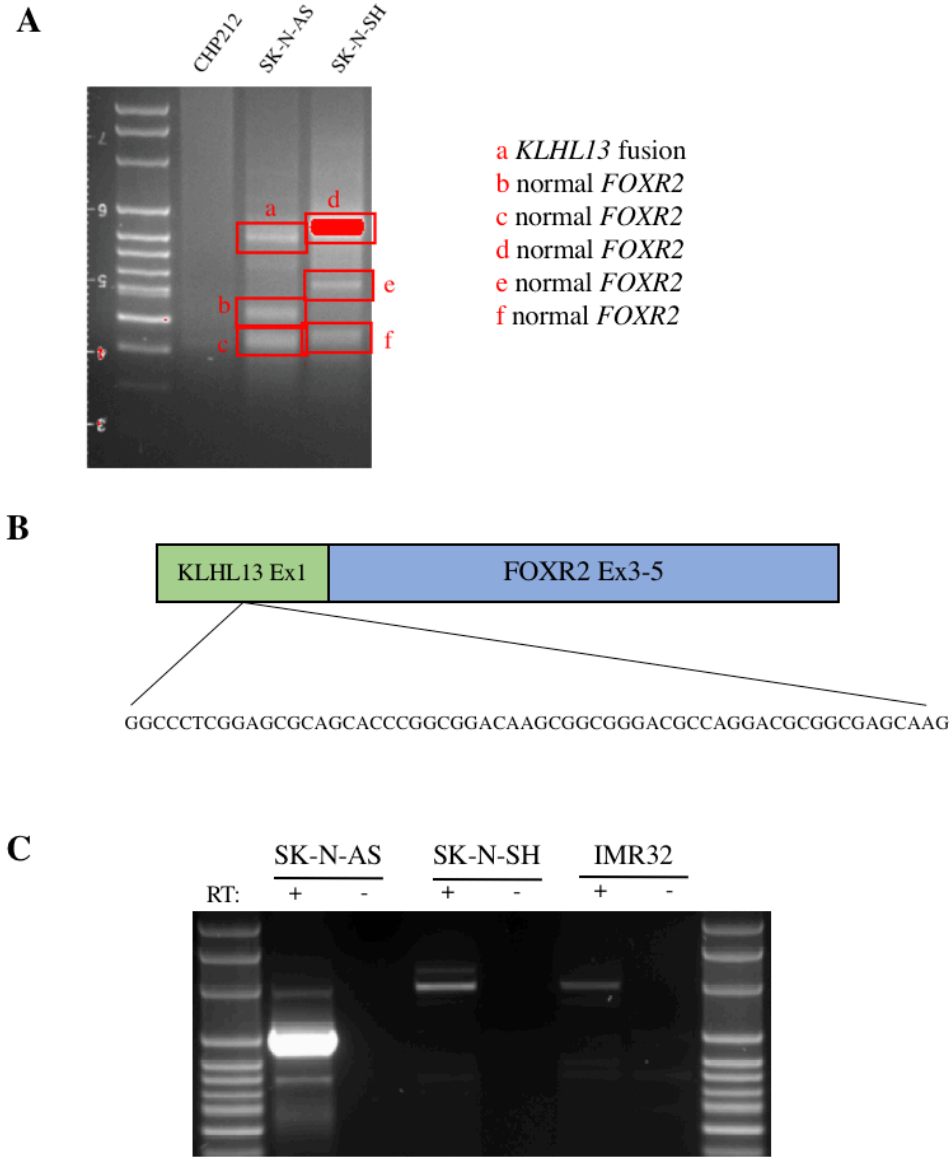


**Figure 4.3. *FOXR2* fusion products in neuroblastoma.**
**A**, *FOXR2* 5'RACE products from 3 neuroblastoma cell lines. CHP212 has low *FOXR2* expression and *MYCN* amplification. SK-N-AS and SK-N-SH have high *FOXR2* expression and no *MYCN* amplification. PCR products that were purified and sequenced are boxed in with red boxes and labeled with letters corresponding to the fusion partners found 5' of *FOXR2*. **B**, FOXR2 fusion product diagram with KLHL13. **C**, Reamplification of *KLHL13*:*FOXR2* fusion product in SK-N-AS, SK-N-SH, and IMR32. With and without reverse transcriptase (RT) reactions are shown.

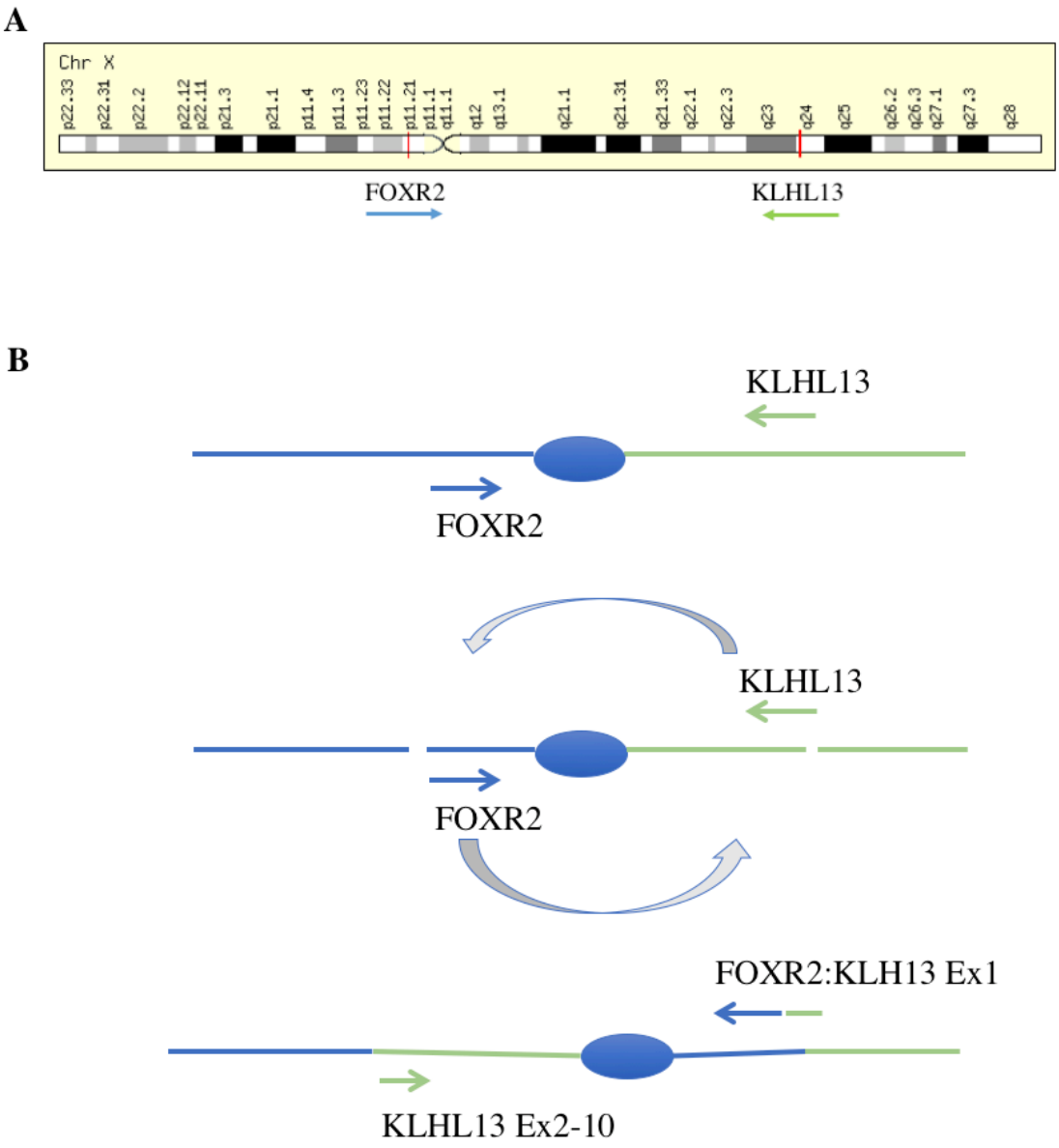


**Figure 4.4. Putative mechanism for *KLHL13*:*FOXR2* fusion.**
**A**, Schematic of chromosome X with the *FOXR2* and *KLHL13* loci shown with directionality indicated. **B**, Putative mechanism for creating a *KLHL13*:*FOXR2* fusion gene. This mechanism indicates 2 chromosomal breaks and an inversion to create the fusion transcript.

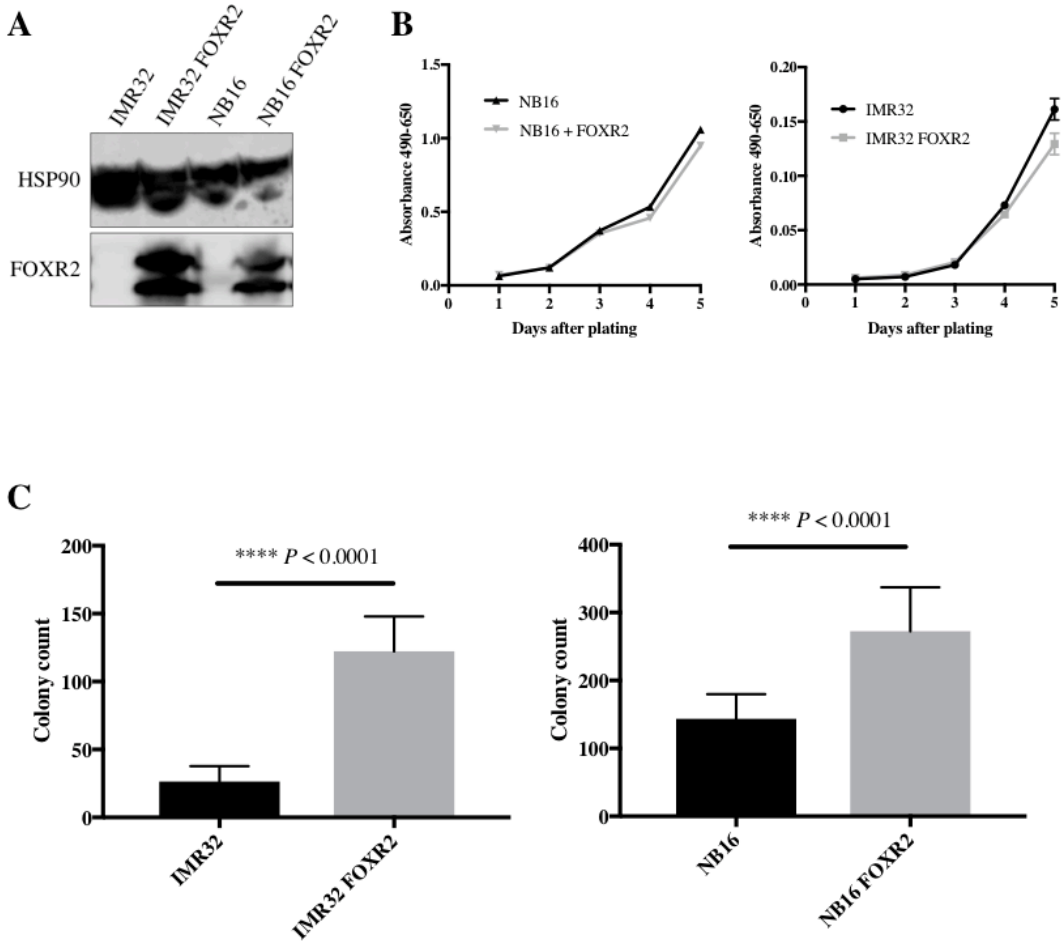


**Figure 4.5. *FOXR2* expression promotes colony formation but does not affect proliferation in IMR32 and NB16.**

**A**, Western blot showing FOXR2 expression in IMR32 and NB16 neuroblastoma cell lines with and without a *FOXR2* overexpression construct. HSP90 is shown as a loading control. **B**, MTS assay with low *FOXR2* expressing lines NB16 and IMR32 with and without a *FOXR2* overexpression construct. 1200 cells/well were used for NB16 and 1400 cells/well were used with IMR32. **C**, Soft agar analysis in neuroblastoma cell lines with FOXR2 OE (*P*-Value: T test, two-tailed).

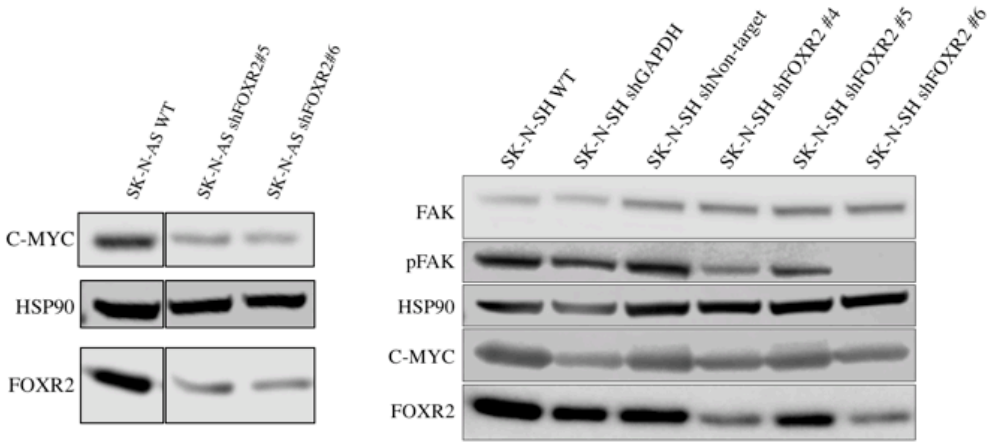


**Figure 4.6. *FOXR2* shRNA knockdown reduces MYC expression and FAK activation.**
Western blot showing changes in MYC expression and FAK activation with FOXR2 knockdown. HSP90 is shown as the loading control.

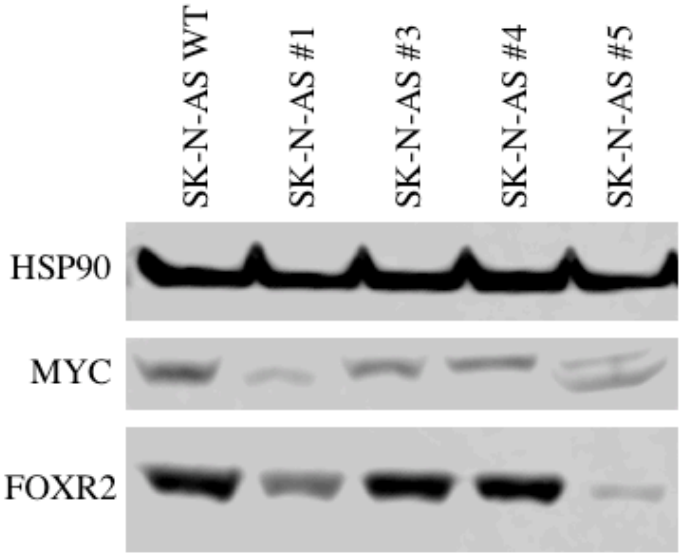


**Figure 4.7. Variation in C-MYC and FOXR2 expression in single cell clones isolated from SK-N-AS.**
Western blot showing changes in MYC and FOXR2 expression in single cell isolates of SK-N-AS. HSP90 is shown as the loading control.

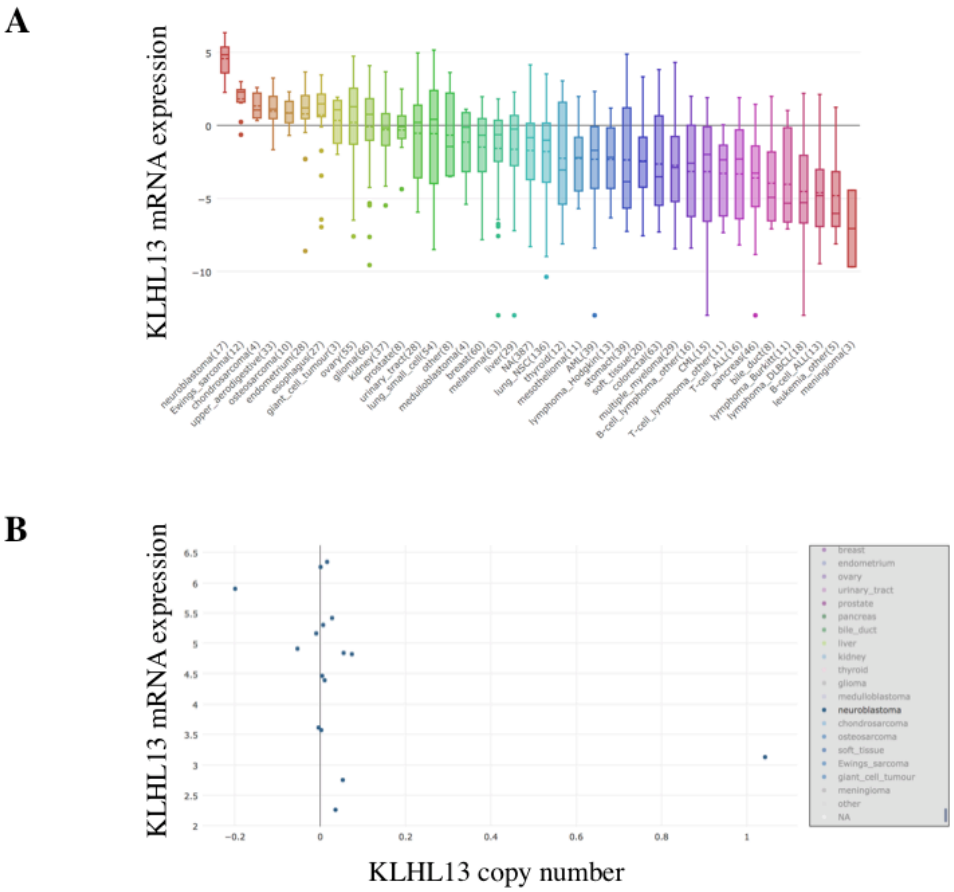


**Figure 4.8. *KLHL13* is highly expressed in human neuroblastoma cell lines.**
**A-B**, *KLHL13* expression data as references from the Cancer Cell Line Encyclopedia (www.broadinstitute.org/ccle). **A**, *KLHL13* mRNA expression in a variety of human cell lines in the Cancer Cell Line Encyclopedia. **B**, *KLHL13* mRNA expression versus copy number changes in neuroblastoma cell lines on the Cancer Cell Line Encyclopedia.

# Chapter 5:

Conclusions and significance

Medulloblastoma, central nervous system primitive neuroectodermal tumors (CNS-PNETs), and neuroblastoma are all cancers of the nervous system that predominantly affect children. Research continues to add to the knowledge behind the genetics and epigenetics driving these tumors, but survival rates and long-term treatment-related side effects remain a challenge for patients facing these diseases. Molecularly targeted therapies represent one method of increasing efficacy of treatments while reducing associated side effects.

In order to identify novel therapeutic targets in medulloblastoma and CNS-PNETs, we used *Sleeping Beauty* (*SB*) transposon-mediated mutagenesis to create tumors in mice. These tumors resembled human medulloblastoma and CNS-PNET at the histological and transcriptome levels. Using RNA-Sequencing to characterize the mouse tumors, we were able to identify which types of human medulloblastoma and CNS-PNET they most closely resemble. Our *SB*-induced tumors most closely represented human non-WNT medulloblastoma (SHH, group 3, and group 4) and a subgroup of CNS-PNET with *FOXR2* activation (CNS NB-*FOXR2*). This represents the first mouse model of CNS-PNET and a rare mouse model of group 3 and 4 medulloblastoma.

We identified over 100 candidate genes as drivers in medulloblastoma and CNS-PNET using traditional DNA-based CIS (common insertion site) identification and more novel methods using RNA-Sequencing-based identification of transposon:gene fusions. Of the CIS genes identified in CNS-PNET, we identified several with effects on Ras signaling activation (*Eras*, *Erbb2ip*, *Ras3*, *NF1*), suggesting an importance of Ras pathway activation in CNS-PNET and a cooperation between Ras pathway activation and p53 loss. In medulloblastoma, we identified 3 oncogenes of interest and validated their transforming potential in a neural progenitor cell line (*Megf10*, *Arhgap36*, and *Foxr2*).

Megf10 (multiple epidermal growth factor-like domains protein 10) was identified as an R-CIS gene (RNA-based CIS) in medulloblastoma. Mice with *Megf10* insertions expressed significantly higher levels of *Megf10*, implicating it as an oncogene. Increased *Megf10* in a mouse neural progenitor cell line (C17.2) promoted proliferation, soft agar colony formation, and tumor formation *in vivo*. However, the mechanism of Megf10-driven tumorigenesis is still unclear and warrants further study.

Arhgap36 (RhoGTPase activating protein 36) was the most mutated gene in our mouse screen and identified as both an R-CIS and a D-CIS. Insertions in the *Arhgap36* drove its expression and occurred mutually exclusively with members of sonic hedgehog (Shh) signaling pathway, suggesting *Arhgap36* is an oncogene in mouse medulloblastoma that acts through Shh signaling. We also found increased expression of ARHGAP36 in a subset of human medulloblastoma. Overexpression of *ARHGAP36* in C17.2 cells promoted soft agar colony formation, *in vivo* tumor formation, and Shh pathway activation. Interestingly, while *ARHGAP36* is clearly an activator of Shh signaling *in vitro*, its role in Shh signaling in the bulk tumor is less clear. *Arhgap36* insertions in *SB*-induced mouse tumors did not correlate with increase Shh target gene expression and human tumors with high levels of *ARHGAP36* expression are in group 3 and 4, not SHH subgroup medulloblastoma. Therefore, the relevance of ARHGAP36-mediated SHH activation is yet to be determined. It is plausible that ARHGAP36 has an alternative mechanism *in vivo* and its effects on SHH activation are context dependent. Further study into this protein is warranted to determine if it represents a strong therapeutic target in medulloblastoma.

Foxr2 (forkhead box R2) was identified as a D-CIS and R-CIS in medulloblastoma and insertion in the *Foxr2* locus drove its expression in the mouse. Overexpression in C17.2 cells enhanced cell migration, soft agar colony formation, and tumor formation *in vivo*. Knockout of *FOXR2* in a human medulloblastoma cell line (Daoy) reduced soft agar colony formation and proliferation. In our studies of the mechanism behind FOXR2-driven tumorigenesis, we identified a novel binding partner for FOXR2 (N-MYC) and determined that FOXR2 enhances C-MYC stability. FOXR2 also promotes activation of the FAK/SRC signaling pathway independently of its interaction with C-MYC. Interestingly, increased FOXR2 expression resulted in Dasatinib (SRC family kinase inhibitor) resistance, and this effect was dependent on the interaction between FOXR2 and C-MYC. Therefore, it is clear that FOXR2's mechanism of transformation is multi-faceted, and its roles in MYC stability and FAK/SRC activation are important to its effects on tumorigenesis.

We identified a novel role for *FOXR2* as an oncogene in neuroblastoma. Increased *FOXR2* expression was associated with poor survival in high-risk

neuroblastoma and found to be mutually exclusive to *MYCN* amplification. Overexpression of *FOXR2* increased colony formation in two low expression neuroblastoma cell lines (IMR32 and NB16) and knock down of *FOXR2* expression decreased cellular proliferation and tumor formation capacity in a high FOXR2 expressing neuroblastoma cell line (SK-N-SH). We also found effects on C-MYC protein levels and FAK activation with changes in FOXR2 expression in the context of neuroblastoma. Lastly, we identified a potential mechanism of increased *FOXR2* expression in neuroblastoma by formation of a fusion gene between *KLHL13* and *FOXR2* in the FOXR2 high neuroblastoma cell line, SK-N-AS.

With dual roles in FAK/SRC signaling activation and MYC stability, FOXR2 represents a strong therapeutic target in medulloblastoma and neuroblastoma. Simultaneous targeting of both pathways has precedent in cancer(250) and may indicate that targeting FOXR2 will have a critical effect on tumor growth. Further study is needed to identify inhibitors of FOXR2-driven cancers. Potential candidates include SRC, FAK, and MYC inhibitors used in combination in FOXR2-high cell lines and mouse models of cancer. Additionally, more mechanistic study of how FOXR2 promotes both FAK/SRC and MYC signaling will allow design of additional drugs to target the activation by FOXR2 on those signaling pathways.

Bibliography


1. Ostrom QT, Gittleman H, Farah P, Ondracek A, Chen Y, Wolinsky Y*, et al.* CBTRUS statistical report: Primary brain and central nervous system tumors diagnosed in the United States in 2006-2010. Neuro Oncol **2013**;15 Suppl 2:ii1-56 doi 10.1093/neuonc/not151.
2. Chan TSY, Wang, X., Spence, T., Taylor, M.D., Huang, A. Embryonal brain tumors. New York: Springer

**2015**.
3. Paterson E, Farr RF. Cerebellar medulloblastoma: treatment by irradiation of the whole central nervous system. Acta radiol **1953**;39(4):323-36.
4. Jenkin D, Danjoux C, Greenberg M. Subsequent quality of life for children irradiated for a brain tumor before age four years. Med Pediatr Oncol **1998**;31(6):506-11.
5. Schmahmann JD, Caplan D. Cognition, emotion and the cerebellum. Brain **2006**;129(Pt 2):290-2 doi 10.1093/brain/awh729.
6. Steinlin M. The cerebellum in cognitive processes: supporting studies in children. Cerebellum **2007**;6(3):237-41 doi 10.1080/14734220701344507.
7. Merchant TE, Wang MH, Haida T, Lindsley KL, Finlay J, Dunkel IJ*, et al.* Medulloblastoma: long-term results for patients treated with definitive radiation therapy during the computed tomography era. Int J Radiat Oncol Biol Phys **1996**;36(1):29-35.
8. Packer RJ, Gajjar A, Vezina G, Rorke-Adams L, Burger PC, Robertson PL*, et al.* Phase III study of craniospinal radiation therapy followed by adjuvant chemotherapy for newly diagnosed average-risk medulloblastoma. J Clin Oncol **2006**;24(25):4202-8 doi 10.1200/JCO.2006.06.4980.
9. Edelstein K, Spiegler BJ, Fung S, Panzarella T, Mabbott DJ, Jewitt N*, et al.* Early aging in adult survivors of childhood medulloblastoma: long-term neurocognitive, functional, and physical outcomes. Neuro Oncol **2011**;13(5):536-45 doi 10.1093/neuonc/nor015.
10. Kieffer-Renaux V, Bulteau C, Grill J, Kalifa C, Viguier D, Jambaque I. Patterns of neuropsychological deficits in children with medulloblastoma according to craniospatial irradiation doses. Dev Med Child Neurol **2000**;42(11):741-5.
11. Maddrey AM, Bergeron JA, Lombardo ER, McDonald NK, Mulne AF, Barenberg PD*, et al.* Neuropsychological performance and quality of life of 10 year survivors of childhood medulloblastoma. J Neurooncol **2005**;72(3):245-53 doi 10.1007/s11060-004-3009-z.
12. Palmer SL, Goloubeva O, Reddick WE, Glass JO, Gajjar A, Kun L*, et al.* Patterns of intellectual development among survivors of pediatric medulloblastoma: a longitudinal analysis. J Clin Oncol **2001**;19(8):2302-8 doi 10.1200/JCO.2001.19.8.2302.
13. Lafay-Cousin L, Bouffet E, Hawkins C, Amid A, Huang A, Mabbott DJ. Impact of radiation avoidance on survival and neurocognitive outcome in infant medulloblastoma. Curr Oncol **2009**;16(6):21-8.

14. Bailey P, Cushing H. Medulloblastoma cerebelli a common type of midcerebellar glioma of childhood. Archives of Neurologic Psychiatry **19999**;14:192-224.
15. Louis DN, Ohgaki H, Wiestler OD, Cavenee WK, Burger PC, Jouvet A*, et al.* The 2007 WHO classification of tumours of the central nervous system. Acta Neuropathol **2007**;114(2):97-109 doi 10.1007/s00401-007-0243-4.
16. Gilbertson RJ, Ellison DW. The origins of medulloblastoma subtypes. Annu Rev Pathol **2008**;3:341-65 doi 10.1146/annurev.pathmechdis.3.121806.151518.
17. Northcott PA, Korshunov A, Witt H, Hielscher T, Eberhart CG, Mack S*, et al.* Medulloblastoma comprises four distinct molecular variants. J Clin Oncol **2011**;29(11):1408-14 doi 10.1200/JCO.2009.27.4324.
18. Louis DN, Perry A, Reifenberger G, von Deimling A, Figarella-Branger D, Cavenee WK*, et al.* The 2016 World Health Organization Classification of Tumors of the Central Nervous System: a summary. Acta Neuropathol **2016**;131(6):803-20 doi 10.1007/s00401-016-1545-1.
19. Taylor MD, Northcott PA, Korshunov A, Remke M, Cho YJ, Clifford SC*, et al.* Molecular subgroups of medulloblastoma: the current consensus. Acta Neuropathol **2012**;123(4):465-72 doi 10.1007/s00401-011-0922-z.
20. Schwalbe EC, Lindsey JC, Nakjang S, Crosier S, Smith AJ, Hicks D*, et al.* Novel molecular subgroups for clinical classification and outcome prediction in childhood medulloblastoma: a cohort study. Lancet Oncol **2017**;18(7):958-71 doi 10.1016/S1470-2045(17)30243-7.
21. Gailani MR, Bale SJ, Leffell DJ, DiGiovanna JJ, Peck GL, Poliak S*, et al.* Developmental defects in Gorlin syndrome related to a putative tumor suppressor gene on chromosome 9. Cell **1992**;69(1):111-7.
22. Hahn H, Wicking C, Zaphiropoulous PG, Gailani MR, Shanley S, Chidambaram A*, et al.* Mutations of the human homolog of Drosophila patched in the nevoid basal cell carcinoma syndrome. Cell **1996**;85(6):841-51.
23. Kimonis VE, Goldstein AM, Pastakia B, Yang ML, Kase R, DiGiovanna JJ*, et al.* Clinical manifestations in 105 persons with nevoid basal cell carcinoma syndrome. Am J Med Genet **1997**;69(3):299-308.
24. Evans DG, Farndon PA, Burnell LD, Gattamaneni HR, Birch JM. The incidence of Gorlin syndrome in 173 consecutive cases of medulloblastoma. Br J Cancer **1991**;64(5):959-61.
25. Reinders MG, van Hout AF, Cosgun B, Paulussen AD, Leter EM, Steijlen PM*, et al.* New mutations and an updated database for the patched-1 (PTCH1) gene. Mol Genet Genomic Med **2018** doi 10.1002/mgg3.380.
26. Katoh Y, Katoh M. Hedgehog target genes: mechanisms of carcinogenesis induced by aberrant hedgehog signaling activation. Curr Mol Med **2009**;9(7):873-86.
27. Taylor MD, Mainprize TG, Rutka JT. Molecular insight into medulloblastoma and central nervous system primitive neuroectodermal tumor biology from hereditary syndromes: a review. Neurosurgery **2000**;47(4):888-901.

28. Hamilton SR, Liu B, Parsons RE, Papadopoulos N, Jen J, Powell SM*, et al.* The molecular basis of Turcot's syndrome. N Engl J Med **1995**;332(13):839-47 doi 10.1056/NEJM199503303321302.
29. Munemitsu S, Albert I, Souza B, Rubinfeld B, Polakis P. Regulation of intracellular B-catenin levels by the adenomatous polyposis coli (APC) tumor-suppressor protein. Proc Natl Acad Sci U S A **1995**;92:3046-50.
30. He TC, Sparks AB, Rago C, Hermeking H, Zawel L, da Costa LT*, et al.* Identification of c-MYC as a target of the APC pathway. Science **1998**;281(5382):1509-12.
31. Tetsu O, McCormick F. Beta-catenin regulates expression of cyclin D1 in colon carcinoma cells. Nature **1999**;398(6726):422-6 doi 10.1038/18884.
32. He TC, Chan TA, Vogelstein B, Kinzler KW. PPARdelta is an APC-regulated target of nonsteroidal anti-inflammatory drugs. Cell **1999**;99(3):335-45.
33. Yamada T, Takaoka AS, Naishiro Y, Hayashi R, Maruyama K, Maesawa C*, et al.* Transactivation of the multidrug resistance 1 gene by T-cell factor 4/beta-catenin complex in early colorectal carcinogenesis. Cancer Res **2000**;60(17):4761-6.
34. Kim PJ, Plescia J, Clevers H, Fearon ER, Altieri DC. Survivin and molecular pathogenesis of colorectal cancer. Lancet **2003**;362(9379):205-9 doi 10.1016/S0140-6736(03)13910-4.
35. Crawford HC, Fingleton BM, Rudolph-Owen LA, Goss KJ, Rubinfeld B, Polakis P*, et al.* The metalloproteinase matrilysin is a target of beta-catenin transactivation in intestinal tumors. Oncogene **1999**;18(18):2883-91 doi 10.1038/sj.onc.1202627.
36. Brabletz T, Jung A, Dag S, Hlubek F, Kirchner T. beta-catenin regulates the expression of the matrix metalloproteinase-7 in human colorectal cancer. Am J Pathol **1999**;155(4):1033-8.
37. Zhang X, Gaspard JP, Chung DC. Regulation of vascular endothelial growth factor by the Wnt and K-ras pathways in colonic neoplasia. Cancer Res **2001**;61(16):6050-4.
38. Varley JM, Evans DG, Birch JM. Li-Fraumeni syndrome--a molecular and clinical review. Br J Cancer **1997**;76(1):1-14.
39. Pearson AD, Craft AW, Ratcliffe JM, Birch JM, Morris-Jones P, Roberts DF. Two families with the Li-Fraumeni cancer family syndrome. J Med Genet **1982**;19(5):362-5.
40. Giaccia AJ, Kastan MB. The complexity of p53 modulation: emerging patterns from divergent signals. Genes Dev **1998**;12(19):2973-83.
41. Hu W, Feng Z, Levine AJ. The Regulation of Multiple p53 Stress Responses is Mediated through MDM2. Genes Cancer **2012**;3(3-4):199-208 doi 10.1177/1947601912454734.
42. Vogelstein B, Lane D, Levine AJ. Surfing the p53 network. Nature **2000**;408(6810):307-10 doi 10.1038/35042675.
43. Laptenko O, Prives C. Transcriptional regulation by p53: one protein, many possibilities. Cell Death Differ **2006**;13(6):951-61 doi 10.1038/sj.cdd.4401916.
44. Bieging KT, Mello SS, Attardi LD. Unravelling mechanisms of p53-mediated tumour suppression. Nat Rev Cancer **2014**;14(5):359-70 doi 10.1038/nrc3711.

45. Taylor MD, Mainprize TG, Rutka JT, Becker L, Bayani J, Drake JM. Medulloblastoma in a child with Rubenstein-Taybi Syndrome: case report and review of the literature. Pediatr Neurosurg **2001**;35(5):235-8 doi 10.1159/000050428.
46. Miller RW, Rubinstein JH. Tumors in Rubinstein-Taybi syndrome. Am J Med Genet **1995**;56(1):112-5 doi 10.1002/ajmg.1320560125.
47. Dixon ZA, Nicholson L, Zeppetzauer M, Matheson E, Sinclair P, Harrison CJ*, et al.* CREBBP knockdown enhances RAS/RAF/MEK/ERK signaling in Ras pathway mutated acute lymphoblastic leukemia but does not modulate chemotherapeutic response. Haematologica **2017**;102(4):736-45 doi 10.3324/haematol.2016.145177.
48. Pasqualucci L, Dominguez-Sola D, Chiarenza A, Fabbri G, Grunn A, Trifonov V*, et al.* Inactivating mutations of acetyltransferase genes in B-cell lymphoma. Nature **2011**;471(7337):189-95 doi 10.1038/nature09730.
49. Jones DT, Jager N, Kool M, Zichner T, Hutter B, Sultan M*, et al.* Dissecting the genomic complexity underlying medulloblastoma. Nature **2012**;488(7409):100-5 doi 10.1038/nature11284.
50. Kool M, Jones DT, Jager N, Northcott PA, Pugh TJ, Hovestadt V*, et al.* Genome sequencing of SHH medulloblastoma predicts genotype-related response to smoothened inhibition. Cancer Cell **2014**;25(3):393-405 doi 10.1016/j.ccr.2014.02.004.
51. Northcott PA, Lee C, Zichner T, Stutz AM, Erkek S, Kawauchi D*, et al.* Enhancer hijacking activates GFI1 family oncogenes in medulloblastoma. Nature **2014**;511(7510):428-34 doi 10.1038/nature13379.
52. Rausch T, Jones DT, Zapatka M, Stutz AM, Zichner T, Weischenfeldt J*, et al.* Genome sequencing of pediatric medulloblastoma links catastrophic DNA rearrangements with TP53 mutations. Cell **2012**;148(1-2):59-71 doi 10.1016/j.cell.2011.12.013.
53. Robinson G, Parker M, Kranenburg TA, Lu C, Chen X, Ding L*, et al.* Novel mutations target distinct subgroups of medulloblastoma. Nature **2012**;488(7409):43-8 doi 10.1038/nature11213.
54. Northcott PA, Shih DJ, Peacock J, Garzia L, Morrissy AS, Zichner T*, et al.* Subgroup-specific structural variation across 1,000 medulloblastoma genomes. Nature **2012**;488(7409):49-56 doi 10.1038/nature11327.
55. Northcott PA, Buchhalter I, Morrissy AS, Hovestadt V, Weischenfeldt J, Ehrenberger T*, et al.* The whole-genome landscape of medulloblastoma subtypes. Nature **2017**;547(7663):311-7 doi 10.1038/nature22973.
56. Lindsey JC, Schwalbe EC, Potluri S, Bailey S, Williamson D, Clifford SC. TERT promoter mutation and aberrant hypermethylation are associated with elevated expression in medulloblastoma and characterise the majority of non-infant SHH subgroup tumours. Acta Neuropathol **2014**;127(2):307-9 doi 10.1007/s00401-013-1225-3.

57. Zhukova N, Ramaswamy V, Remke M, Pfaff E, Shih DJ, Martin DC*, et al.* Subgroup-specific prognostic implications of TP53 mutation in medulloblastoma. J Clin Oncol **2013**;31(23):2927-35 doi 10.1200/JCO.2012.48.5052.
58. Tas S, Avci O. Rapid clearance of psoriatic skin lesions induced by topical cyclopamine. A preliminary proof of concept study. Dermatology **2004**;209(2):126-31 doi 10.1159/000079596.
59. Mimeault M, Batra SK. Frequent deregulations in the hedgehog signaling network and cross-talks with the epidermal growth factor receptor pathway involved in cancer progression and targeted therapies. Pharmacol Rev **2010**;62(3):497-524 doi 10.1124/pr.109.002329.
60. Molckovsky A, Siu LL. First-in-class, first-in-human phase I results of targeted agents: highlights of the 2008 American society of clinical oncology meeting. J Hematol Oncol **2008**;1:20 doi 10.1186/1756-8722-1-20.
61. Rudin CM, Hann CL, Laterra J, Yauch RL, Callahan CA, Fu L*, et al.* Treatment of medulloblastoma with hedgehog pathway inhibitor GDC-0449. N Engl J Med **2009**;361(12):1173-8 doi 10.1056/NEJMoa0902903.
62. Von Hoff DD, LoRusso PM, Rudin CM, Reddy JC, Yauch RL, Tibes R*, et al.* Inhibition of the hedgehog pathway in advanced basal-cell carcinoma. N Engl J Med **2009**;361(12):1164-72 doi 10.1056/NEJMoa0905360.
63. Stanton BZ, Peng LF. Small-molecule modulators of the Sonic Hedgehog signaling pathway. Mol Biosyst **2010**;6(1):44-54 doi 10.1039/b910196a.
64. Robinson GW, Orr BA, Wu G, Gururangan S, Lin T, Qaddoumi I*, et al.* Vismodegib Exerts Targeted Efficacy Against Recurrent Sonic Hedgehog-Subgroup Medulloblastoma: Results From Phase II Pediatric Brain Tumor Consortium Studies PBTC-025B and PBTC-032. J Clin Oncol **2015**;33(24):2646-54 doi 10.1200/JCO.2014.60.1591.
65. Novartis. 2017, March 13 A Phase II, multi-center, open-label, single-arm study of the efficacy and safety of oral LDE225 in patients with Hh-pathway activated relapsed medulloblastoma. <https://www.novctrd.com/CtrdWeb/displaypdf.nov?trialresultid=16148>.
66. Laukkanen MO, Castellone MD. Hijacking the Hedgehog Pathway in Cancer Therapy. Anticancer Agents Med Chem **2016**;16(3):309-17.
67. Robinson GW, Kaste SC, Chemaitilly W, Bowers DC, Laughton S, Smith A*, et al.* Irreversible growth plate fusions in children with medulloblastoma treated with a targeted hedgehog pathway inhibitor. Oncotarget **2017**;8(41):69295-302 doi 10.18632/oncotarget.20619.
68. Buonamici S, Williams J, Morrissey M, Wang A, Guo R, Vattay A*, et al.* Interfering with resistance to smoothened antagonists by inhibition of the PI3K pathway in medulloblastoma. Sci Transl Med **2010**;2(51):51ra70 doi 10.1126/scitranslmed.3001599.
69. Dijkgraaf GJ, Alicke B, Weinmann L, Januario T, West K, Modrusan Z*, et al.* Small molecule inhibition of GDC-0449 refractory smoothened mutants and downstream mechanisms of drug resistance. Cancer Res **2011**;71(2):435-44 doi 10.1158/0008-5472.CAN-10-2876.

70. Friedel RH, Wurst W, Wefers B, Kuhn R. Generating conditional knockout mice. Methods Mol Biol **2011**;693:205-31 doi 10.1007/978-1-60761-974-1_12.
71. Walrath JC, Hawes JJ, Van Dyke T, Reilly KM. Genetically engineered mouse models in cancer research. Adv Cancer Res **2010**;106:113-64 doi 10.1016/S0065-230X(10)06004-5.
72. Metzger D, Chambon P. Site- and time-specific gene targeting in the mouse. Methods **2001**;24(1):71-80 doi 10.1006/meth.2001.1159.
73. Dahlstrand J, Lardelli M, Lendahl U. Nestin mRNA expression correlates with the central nervous system progenitor cell state in many, but not all, regions of developing central nervous system. Developmental Brain Research **1994**;84:109-29.
74. Machold R, Fishell G. Math1 is expressed in temporally discrete pools of cerebellar rhombic-lip neural progenitors. Neuron **2005**;48(1):17-24 doi 10.1016/j.neuron.2005.08.028.
75. Huang X, Liu J, Ketova T, Fleming JT, Grover VK, Cooper MK*, et al.* Transventricular delivery of Sonic hedgehog is essential to cerebellar ventricular zone development. Proc Natl Acad Sci U S A **2010**;107(18):8422-7 doi 10.1073/pnas.0911838107.
76. Gibson P, Tong Y, Robinson G, Thompson MC, Currle DS, Eden C*, et al.* Subtypes of medulloblastoma have distinct developmental origins. Nature **2010**;468(7327):1095-9 doi 10.1038/nature09587.
77. Schuller U, Heine VM, Mao J, Kho AT, Dillon AK, Han YG*, et al.* Acquisition of granule neuron precursor identity is a critical determinant of progenitor cell competence to form Shh-induced medulloblastoma. Cancer Cell **2008**;14(2):123-34 doi 10.1016/j.ccr.2008.07.005.
78. Yang ZJ, Ellis T, Markant SL, Read TA, Kessler JD, Bourboulas M*, et al.* Medulloblastoma can be initiated by deletion of Patched in lineage-restricted progenitors or stem cells. Cancer Cell **2008**;14(2):135-45 doi 10.1016/j.ccr.2008.07.003.
79. Lee A, Kessler JD, Read TA, Kaiser C, Corbeil D, Huttner WB*, et al.* Isolation of neural stem cells from the postnatal cerebellum. Nat Neurosci **2005**;8(6):723-9 doi 10.1038/nn1473.
80. Pei Y, Moore CE, Wang J, Tewari AK, Eroshkin A, Cho YJ*, et al.* An animal model of MYC-driven medulloblastoma. Cancer Cell **2012**;21(2):155-67 doi 10.1016/j.ccr.2011.12.021.
81. Lin CY, Erkek S, Tong Y, Yin L, Federation AJ, Zapatka M*, et al.* Active medulloblastoma enhancers reveal subgroup-specific cellular origins. Nature **2016**;530(7588):57-62 doi 10.1038/nature16546.
82. Goodrich LV, Milenkovic L, Higgins KM, Scott MP. Altered neural cell fates and medulloblastoma in mouse patched mutants. Science **1997**;277(5329):1109-13.
83. Wetmore C, Eberhart DE, Curran T. Loss of p53 but not ARF accelerates medulloblastoma in mice heterozygous for patched. Cancer Res **2001**;61(2):513-6.

84. Uziel T, Zindy F, Xie S, Lee Y, Forget A, Magdaleno S*, et al.* The tumor suppressors Ink4c and p53 collaborate independently with Patched to suppress medulloblastoma formation. Genes Dev **2005**;19(22):2656-67 doi 10.1101/gad.1368605.
85. Ayrault O, Zindy F, Rehg J, Sherr CJ, Roussel MF. Two tumor suppressors, p27Kip1 and patched-1, collaborate to prevent medulloblastoma. Mol Cancer Res **2009**;7(1):33-40 doi 10.1158/1541-7786.MCR-08-0369.
86. Briggs KJ, Corcoran-Schwartz IM, Zhang W, Harcke T, Devereux WL, Baylin SB*, et al.* Cooperation between the Hic1 and Ptch1 tumor suppressors in medulloblastoma. Genes Dev **2008**;22(6):770-85 doi 10.1101/gad.1640908.
87. Lee Y, Kawagoe R, Sasai K, Li Y, Russell HR, Curran T*, et al.* Loss of suppressor-of-fused function promotes tumorigenesis. Oncogene **2007**;26(44):6442-7 doi 10.1038/sj.onc.1210467.
88. Hallahan AR, Pritchard JI, Hansen S, Benson M, Stoeck J, Hatton BA*, et al.* The SmoA1 mouse model reveals that notch signaling is critical for the growth and survival of sonic hedgehog-induced medulloblastomas. Cancer Res **2004**;64(21):7794-800 doi 10.1158/0008-5472.CAN-04-1813.
89. Hatton BA, Villavicencio EH, Tsuchiya KD, Pritchard JI, Ditzler S, Pullar B*, et al.* The Smo/Smo model: hedgehog-induced medulloblastoma with 90% incidence and leptomeningeal spread. Cancer Res **2008**;68(6):1768-76 doi 10.1158/0008-5472.CAN-07-5092.
90. Dey J, Ditzler S, Knoblaugh SE, Hatton BA, Schelter JM, Cleary MA*, et al.* A distinct Smoothened mutation causes severe cerebellar developmental defects and medulloblastoma in a novel transgenic mouse model. Mol Cell Biol **2012**;32(20):4104-15 doi 10.1128/MCB.00862-12.
91. Mao J, Ligon KL, Rakhlin EY, Thayer SP, Bronson RT, Rowitch D*, et al.* A novel somatic mouse model to survey tumorigenic potential applied to the Hedgehog pathway. Cancer Res **2006**;66(20):10171-8 doi 10.1158/0008-5472.CAN-06-0657.
92. Marino S, Vooijs M, van Der Gulden H, Jonkers J, Berns A. Induction of medulloblastomas in p53-null mutant mice by somatic inactivation of Rb in the external granular layer cells of the cerebellum. Genes Dev **2000**;14(8):994-1004.
93. Lee Y, McKinnon PJ. DNA ligase IV suppresses medulloblastoma formation. Cancer Res **2002**;62(22):6395-9.
94. Yan CT, Kaushal D, Murphy M, Zhang Y, Datta A, Chen C*, et al.* XRCC4 suppresses medulloblastomas with recurrent translocations in p53-deficient mice. Proc Natl Acad Sci U S A **2006**;103(19):7378-83 doi 10.1073/pnas.0601938103.
95. Frappart PO, Lee Y, Russell HR, Chalhoub N, Wang YD, Orii KE*, et al.* Recurrent genomic alterations characterize medulloblastoma arising from DNA double-strand break repair deficiency. Proc Natl Acad Sci U S A **2009**;106(6):1880-5 doi 10.1073/pnas.0806882106.
96. Wang ZQ, Auer B, Stingl L, Berghammer H, Haidacher D, Schweiger M*, et al.* Mice lacking ADPRT and poly(ADP-ribosyl)ation develop normally but are susceptible to skin disease. Genes Dev **1995**;9(5):509-20.

97. Holcomb VB, Vogel H, Marple T, Kornegay RW, Hasty P. Ku80 and p53 suppress medulloblastoma that arise independent of Rag-1-induced DSBs. Oncogene **2006**;25(54):7159-65 doi 10.1038/sj.onc.1209704.
98. Lin W, Kemper A, McCarthy KD, Pytel P, Wang JP, Campbell IL*, et al.* Interferon-gamma induced medulloblastoma in the developing cerebellum. J Neurosci **2004**;24(45):10074-83 doi 10.1523/JNEUROSCI.2604-04.2004.
99. Wang J, Pham-Mitchell N, Schindler C, Campbell IL. Dysregulated Sonic hedgehog signaling and medulloblastoma consequent to IFN-alpha-stimulated STAT2-independent production of IFN-gamma in the brain. J Clin Invest **2003**;112(4):535-43 doi 10.1172/JCI18637.
100. Federspiel MJ, Bates P, Young JA, Varmus HE, Hughes SH. A system for tissue-specific gene targeting: transgenic mice susceptible to subgroup A avian leukosis virus-based retroviral vectors. Proc Natl Acad Sci U S A **1994**;91(23):11241-5.
101. Weiner HL, Bakst R, Hurlbert MS, Ruggiero J, Ahn E, Lee WS*, et al.* Induction of medulloblastomas in mice by sonic hedgehog, independent of Gli1. Cancer Res **2002**;62(22):6385-9.
102. Browd SR, Kenney AM, Gottfried ON, Yoon JW, Walterhouse D, Pedone CA*, et al.* N-myc can substitute for insulin-like growth factor signaling in a mouse model of sonic hedgehog-induced medulloblastoma. Cancer Res **2006**;66(5):2666-72 doi 10.1158/0008-5472.CAN-05-2198.
103. McCall TD, Pedone CA, Fults DW. Apoptosis suppression by somatic cell transfer of Bcl-2 promotes Sonic hedgehog-dependent medulloblastoma formation in mice. Cancer Res **2007**;67(11):5179-85 doi 10.1158/0008-5472.CAN-06-4177.
104. Binning MJ, Niazi T, Pedone CA, Lal B, Eberhart CG, Kim KJ*, et al.* Hepatocyte growth factor and sonic Hedgehog expression in cerebellar neural progenitor cells costimulate medulloblastoma initiation and growth. Cancer Res **2008**;68(19):7838-45 doi 10.1158/0008-5472.CAN-08-1899.
105. Rao G, Pedone CA, Del Valle L, Reiss K, Holland EC, Fults DW. Sonic hedgehog and insulin-like growth factor signaling synergize to induce medulloblastoma formation from nestin-expressing neural progenitors in mice. Oncogene **2004**;23(36):6156-62 doi 10.1038/sj.onc.1207818.
106. Zuckermann M, Hovestadt V, Knobbe-Thomsen CB, Zapatka M, Northcott PA, Schramm K*, et al.* Somatic CRISPR/Cas9-mediated tumour suppressor disruption enables versatile brain tumour modelling. Nat Commun **2015**;6:7391 doi 10.1038/ncomms8391.
107. Lastowska M, Al-Afghani H, Al-Balool HH, Sheth H, Mercer E, Coxhead JM*, et al.* Identification of a neuronal transcription factor network involved in medulloblastoma development. Acta Neuropathol Commun **2013**;1:35 doi 10.1186/2051-5960-1-35.
108. Genovesi LA, Ng CG, Davis MJ, Remke M, Taylor MD, Adams DJ*, et al.* Sleeping Beauty mutagenesis in a mouse medulloblastoma model defines networks that discriminate between human molecular subgroups. Proc Natl Acad Sci U S A **2013**;110(46):E4325-34 doi 10.1073/pnas.1318639110.

109. Wu X, Northcott PA, Dubuc A, Dupuy AJ, Shih DJ, Witt H*, et al.* Clonal selection drives genetic divergence of metastatic medulloblastoma. Nature **2012**;482(7386):529-33 doi 10.1038/nature10825.
110. Koso H, Tsuhako A, Lyons E, Ward JM, Rust AG, Adams DJ*, et al.* Identification of FoxR2 as an oncogene in medulloblastoma. Cancer Res **2014**;74(8):2351-61 doi 10.1158/0008-5472.CAN-13-1523.
111. Swartling FJ, Grimmer MR, Hackett CS, Northcott PA, Fan QW, Goldenberg DD*, et al.* Pleiotropic role for MYCN in medulloblastoma. Genes Dev **2010**;24(10):1059-72 doi 10.1101/gad.1907510.
112. Furuta A, Rothstein JD, Martin LJ. Glutamate transporter protein subtypes are expressed differentially during rat CNS development. J Neurosci **1997**;17(21):8363-75.
113. Hill RM, Kuijper S, Lindsey JC, Petrie K, Schwalbe EC, Barker K*, et al.* Combined MYC and P53 defects emerge at medulloblastoma relapse and define rapidly progressive, therapeutically targetable disease. Cancer Cell **2015**;27(1):72-84 doi 10.1016/j.ccell.2014.11.002.
114. Jenkins NC, Rao G, Eberhart CG, Pedone CA, Dubuc AM, Fults DW. Somatic cell transfer of c-Myc and Bcl-2 induces large-cell anaplastic medulloblastomas in mice. J Neurooncol **2016**;126(3):415-24 doi 10.1007/s11060-015-1985-9.
115. Kawauchi D, Ogg RJ, Liu L, Shih DJH, Finkelstein D, Murphy BL*, et al.* Novel MYC-driven medulloblastoma models from multiple embryonic cerebellar cells. Oncogene **2017**;36(37):5231-42 doi 10.1038/onc.2017.110.
116. Kawauchi D, Robinson G, Uziel T, Gibson P, Rehg J, Gao C*, et al.* A mouse model of the most aggressive subgroup of human medulloblastoma. Cancer Cell **2012**;21(2):168-80 doi 10.1016/j.ccr.2011.12.023.
117. de Rojas T, Bautista F, Flores M, Igual L, Rubio R, Bardon E*, et al.* Management and outcome of children and adolescents with non-medulloblastoma CNS embryonal tumors in Spain: room for improvement in standards of care. J Neurooncol **2018**;137(1):205-13 doi 10.1007/s11060-017-2713-4.
118. Rorke LB. The cerebellar medulloblastoma and its relationship to primitive neuroectodermal tumors. J Neuropathol Exp Neurol **1983**;42(1):1-15.
119. Kleihues P, Sobin LH. World Health Organization classification of tumors. Cancer **2000**;88(12):2887.
120. Korshunov A, Remke M, Gessi M, Ryzhova M, Hielscher T, Witt H*, et al.* Focal genomic amplification at 19q13.42 comprises a powerful diagnostic marker for embryonal tumors with ependymoblastic rosettes. Acta Neuropathol **2010**;120(2):253-60 doi 10.1007/s00401-010-0688-8.
121. Spence T, Sin-Chan P, Picard D, Barszczyk M, Hoss K, Lu M*, et al.* CNS-PNETs with C19MC amplification and/or LIN28 expression comprise a distinct histogenetic diagnostic and therapeutic entity. Acta Neuropathol **2014**;128(2):291-303 doi 10.1007/s00401-014-1291-1.
122. Li M, Lee KF, Lu Y, Clarke I, Shih D, Eberhart C*, et al.* Frequent amplification of a chr19q13.41 microRNA polycistron in aggressive primitive neuroectodermal brain tumors. Cancer Cell **2009**;16(6):533-46 doi 10.1016/j.ccr.2009.10.025.

123. Korshunov A, Sturm D, Ryzhova M, Hovestadt V, Gessi M, Jones DT*, et al.* Embryonal tumor with abundant neuropil and true rosettes (ETANTR), ependymoblastoma, and medulloepithelioma share molecular similarity and comprise a single clinicopathological entity. Acta Neuropathol **2014**;128(2):279-89 doi 10.1007/s00401-013-1228-0.
124. Eberhart CG, Brat DJ, Cohen KJ, Burger PC. Pediatric neuroblastic brain tumors containing abundant neuropil and true rosettes. Pediatr Dev Pathol **2000**;3(4):346-52.
125. Sturm D, Orr BA, Toprak UH, Hovestadt V, Jones DTW, Capper D*, et al.* New Brain Tumor Entities Emerge from Molecular Classification of CNS-PNETs. Cell **2016**;164(5):1060-72 doi 10.1016/j.cell.2016.01.015.
126. De Vos M, Hayward BE, Picton S, Sheridan E, Bonthron DT. Novel PMS2 pseudogenes can conceal recessive mutations causing a distinctive childhood cancer syndrome. Am J Hum Genet **2004**;74(5):954-64 doi 10.1086/420796.
127. Orellana C, Martinez F, Hernandez-Marti M, Castel V, Canete A, Prieto F*, et al.* A novel TP53 germ-line mutation identified in a girl with a primitive neuroectodermal tumor and her father. Cancer Genet Cytogenet **1998**;105(2):103-8.
128. Picard D, Miller S, Hawkins CE, Bouffet E, Rogers HA, Chan TS*, et al.* Markers of survival and metastatic potential in childhood CNS primitive neuro-ectodermal brain tumours: an integrative genomic analysis. Lancet Oncol **2012**;13(8):838-48 doi 10.1016/S1470-2045(12)70257-7.
129. Behdad A, Perry A. Central nervous system primitive neuroectodermal tumors: a clinicopathologic and genetic study of 33 cases. Brain Pathol **2010**;20(2):441-50 doi 10.1111/j.1750-3639.2009.00314.x.
130. Pfister S, Remke M, Toedt G, Werft W, Benner A, Mendrzyk F*, et al.* Supratentorial primitive neuroectodermal tumors of the central nervous system frequently harbor deletions of the CDKN2A locus and other genomic aberrations distinct from medulloblastomas. Genes Chromosomes Cancer **2007**;46(9):839-51 doi 10.1002/gcc.20471.
131. Eberhart CG, Chaudhry A, Daniel RW, Khaki L, Shah KV, Gravitt PE. Increased p53 immunopositivity in anaplastic medulloblastoma and supratentorial PNET is not caused by JC virus. BMC Cancer **2005**;5:19 doi 10.1186/1471-2407-5-19.
132. Ho YS, Hsieh LL, Chen JS, Chang CN, Lee ST, Chiu LL*, et al.* p53 gene mutation in cerebral primitive neuroectodermal tumor in Taiwan. Cancer Lett **1996**;104(1):103-13.
133. Kraus JA, Felsberg J, Tonn JC, Reifenberger G, Pietsch T. Molecular genetic analysis of the TP53, PTEN, CDKN2A, EGFR, CDK4 and MDM2 tumour-associated genes in supratentorial primitive neuroectodermal tumours and glioblastomas of childhood. Neuropathol Appl Neurobiol **2002**;28(4):325-33.
134. Modzelewska K, Boer EF, Mosbruger TL, Picard D, Anderson D, Miles RR*, et al.* MEK Inhibitors Reverse Growth of Embryonal Brain Tumors Derived from Oligoneural Precursor Cells. Cell Rep **2016**;17(5):1255-64 doi 10.1016/j.celrep.2016.09.081.

135. Rahrmann EP, Watson AL, Keng VW, Choi K, Moriarity BS, Beckmann DA*, et al.* Forward genetic screen for malignant peripheral nerve sheath tumor formation identifies new genes and pathways driving tumorigenesis. Nat Genet **2013**;45(7):756-66 doi 10.1038/ng.2641.
136. Li X, Wang W, Xi Y, Gao M, Tran M, Aziz KE*, et al.* FOXR2 Interacts with MYC to Promote Its Transcriptional Activities and Tumorigenesis. Cell Rep **2016**;16(2):487-97 doi 10.1016/j.celrep.2016.06.004.
137. Haidar A, Arekapudi S, DeMattia F, Abu-Isa E, Kraut M. High-grade undifferentiated small round cell sarcoma with t(4;19)(q35;q13.1) CIC-DUX4 fusion: emerging entities of soft tissue tumors with unique histopathologic features--a case report and literature review. Am J Case Rep **2015**;16:87-94 doi 10.12659/AJCR.892551.
138. Buijs A, van Rompaey L, Molijn AC, Davis JN, Vertegaal AC, Potter MD*, et al.* The MN1-TEL fusion protein, encoded by the translocation (12;22)(p13;q11) in myeloid leukemia, is a transcription factor with transforming activity. Mol Cell Biol **2000**;20(24):9281-93.
139. Malchenko S, Sredni ST, Hashimoto H, Kasai A, Nagayasu K, Xie J*, et al.* A mouse model of human primitive neuroectodermal tumors resulting from microenvironmentally-driven malignant transformation of orthotopically transplanted radial glial cells. PLoS One **2015**;10(3):e0121707 doi 10.1371/journal.pone.0121707.
140. Maris JM. Recent advances in neuroblastoma. N Engl J Med **2010**;362(23):2202-11 doi 10.1056/NEJMra0804577.
141. Jiang M, Stanke J, Lahti JM. The connections between neural crest development and neuroblastoma. Curr Top Dev Biol **2011**;94:77-127 doi 10.1016/B978-0-12-380916-2.00004-8.
142. Zhang J, Walsh MF, Wu G, Edmonson MN, Gruber TA, Easton J*, et al.* Germline Mutations in Predisposition Genes in Pediatric Cancer. N Engl J Med **2015**;373(24):2336-46 doi 10.1056/NEJMoa1508054.
143. Maris JM, Hogarty MD, Bagatell R, Cohn SL. Neuroblastoma. Lancet **2007**;369(9579):2106-20 doi 10.1016/S0140-6736(07)60983-0.
144. De Preter K, Vandesompele J, Heimann P, Yigit N, Beckman S, Schramm A*, et al.* Human fetal neuroblast and neuroblastoma transcriptome analysis confirms neuroblast origin and highlights neuroblastoma candidate genes. Genome Biol **2006**;7(9):R84 doi 10.1186/gb-2006-7-9-r84.
145. Brodeur GM. Neuroblastoma: biological insights into a clinical enigma. Nat Rev Cancer **2003**;3(3):203-16 doi 10.1038/nrc1014.
146. Anderson DJ, Axel R. A bipotential neuroendocrine precursor whose choice of cell fate is determined by NGF and glucocorticoids. Cell **1986**;47(6):1079-90.
147. Anderson DJ, Carnahan JF, Michelsohn A, Patterson PH. Antibody markers identify a common progenitor to sympathetic neurons and chromaffin cells in vivo and reveal the timing of commitment to neuronal differentiation in the sympathoadrenal lineage. J Neurosci **1991**;11(11):3507-19.

148. Cohn SL, Pearson AD, London WB, Monclair T, Ambros PF, Brodeur GM*, et al.* The International Neuroblastoma Risk Group (INRG) classification system: an INRG Task Force report. J Clin Oncol **2009**;27(2):289-97 doi 10.1200/JCO.2008.16.6785.
149. Cheung NK, Zhang J, Lu C, Parker M, Bahrami A, Tickoo SK*, et al.* Association of age at diagnosis and genetic mutations in patients with neuroblastoma. JAMA **2012**;307(10):1062-71 doi 10.1001/jama.2012.228.
150. Pugh TJ, Morozova O, Attiyeh EF, Asgharzadeh S, Wei JS, Auclair D*, et al.* The genetic landscape of high-risk neuroblastoma. Nat Genet **2013**;45(3):279-84 doi 10.1038/ng.2529.
151. Clausen N, Andersson P, Tommerup N. Familial occurrence of neuroblastoma, von Recklinghausen's neurofibromatosis, Hirschsprung's agangliosis and jaw-winking syndrome. Acta Paediatr Scand **1989**;78(5):736-41.
152. Knudson AG, Jr., Strong LC. Mutation and cancer: neuroblastoma and pheochromocytoma. Am J Hum Genet **1972**;24(5):514-32.
153. Maris JM, Weiss MJ, Mosse Y, Hii G, Guo C, White PS*, et al.* Evidence for a hereditary neuroblastoma predisposition locus at chromosome 16p12-13. Cancer Res **2002**;62(22):6651-8.
154. Mosse YP, Laudenslager M, Longo L, Cole KA, Wood A, Attiyeh EF*, et al.* Identification of ALK as a major familial neuroblastoma predisposition gene. Nature **2008**;455(7215):930-5 doi 10.1038/nature07261.
155. Janoueix-Lerosey I, Lequin D, Brugieres L, Ribeiro A, de Pontual L, Combaret V*, et al.* Somatic and germline activating mutations of the ALK kinase receptor in neuroblastoma. Nature **2008**;455(7215):967-70 doi 10.1038/nature07398.
156. Caren H, Abel F, Kogner P, Martinsson T. High incidence of DNA mutations and gene amplifications of the ALK gene in advanced sporadic neuroblastoma tumours. Biochem J **2008**;416(2):153-9.
157. Lamant L, Pulford K, Bischof D, Morris SW, Mason DY, Delsol G*, et al.* Expression of the ALK tyrosine kinase gene in neuroblastoma. Am J Pathol **2000**;156(5):1711-21 doi 10.1016/S0002-9440(10)65042-0.
158. Powers C, Aigner A, Stoica GE, McDonnell K, Wellstein A. Pleiotrophin signaling through anaplastic lymphoma kinase is rate-limiting for glioblastoma growth. J Biol Chem **2002**;277(16):14153-8 doi 10.1074/jbc.M112354200.
159. Lu KV, Jong KA, Kim GY, Singh J, Dia EQ, Yoshimoto K*, et al.* Differential induction of glioblastoma migration and growth by two forms of pleiotrophin. J Biol Chem **2005**;280(29):26953-64 doi 10.1074/jbc.M502614200.
160. Dirks WG, Fahnrich S, Lis Y, Becker E, MacLeod RA, Drexler HG. Expression and functional analysis of the anaplastic lymphoma kinase (ALK) gene in tumor cell lines. Int J Cancer **2002**;100(1):49-56 doi 10.1002/ijc.10435.
161. Li XQ, Hisaoka M, Shi DR, Zhu XZ, Hashimoto H. Expression of anaplastic lymphoma kinase in soft tissue tumors: an immunohistochemical and molecular study of 249 cases. Hum Pathol **2004**;35(6):711-21.
162. Perez-Pinera P, Garcia-Suarez O, Menendez-Rodriguez P, Mortimer J, Chang Y, Astudillo A*, et al.* The receptor protein tyrosine phosphatase (RPTP)beta/zeta is

expressed in different subtypes of human breast cancer. Biochem Biophys Res Commun **2007**;362(1):5-10 doi 10.1016/j.bbrc.2007.06.050.
163. Osajima-Hakomori Y, Miyake I, Ohira M, Nakagawara A, Nakagawa A, Sakai R. Biological role of anaplastic lymphoma kinase in neuroblastoma. Am J Pathol **2005**;167(1):213-22 doi 10.1016/S0002-9440(10)62966-5.
164. Trochet D, Bourdeaut F, Janoueix-Lerosey I, Deville A, de Pontual L, Schleiermacher G*, et al.* Germline mutations of the paired-like homeobox 2B (PHOX2B) gene in neuroblastoma. Am J Hum Genet **2004**;74(4):761-4 doi 10.1086/383253.
165. Goridis C, Rohrer H. Specification of catecholaminergic and serotonergic neurons. Nat Rev Neurosci **2002**;3(7):531-41 doi 10.1038/nrn871.
166. Bachetti T, Di Paolo D, Di Lascio S, Mirisola V, Brignole C, Bellotti M*, et al.* PHOX2B-mediated regulation of ALK expression: in vitro identification of a functional relationship between two genes involved in neuroblastoma. PLoS One **2010**;5(10) doi 10.1371/journal.pone.0013108.
167. Grimmer MR, Weiss WA. Childhood tumors of the nervous system as disorders of normal development. Curr Opin Pediatr **2006**;18(6):634-8 doi 10.1097/MOP.0b013e32801080fe.
168. Smith AG, Popov N, Imreh M, Axelson H, Henriksson M. Expression and DNA-binding activity of MYCN/Max and Mnt/Max during induced differentiation of human neuroblastoma cells. J Cell Biochem **2004**;92(6):1282-95 doi 10.1002/jcb.20121.
169. Nara K, Kusafuka T, Yoneda A, Oue T, Sangkhathat S, Fukuzawa M. Silencing of MYCN by RNA interference induces growth inhibition, apoptotic activity and cell differentiation in a neuroblastoma cell line with MYCN amplification. Int J Oncol **2007**;30(5):1189-96.
170. Weiss WA, Aldape K, Mohapatra G, Feuerstein BG, Bishop JM. Targeted expression of MYCN causes neuroblastoma in transgenic mice. EMBO J **1997**;16(11):2985-95 doi 10.1093/emboj/16.11.2985.
171. Zhu S, Lee JS, Guo F, Shin J, Perez-Atayde AR, Kutok JL*, et al.* Activated ALK collaborates with MYCN in neuroblastoma pathogenesis. Cancer Cell **2012**;21(3):362-73 doi 10.1016/j.ccr.2012.02.010.
172. Berry T, Luther W, Bhatnagar N, Jamin Y, Poon E, Sanda T*, et al.* The ALK(F1174L) mutation potentiates the oncogenic activity of MYCN in neuroblastoma. Cancer Cell **2012**;22(1):117-30 doi 10.1016/j.ccr.2012.06.001.
173. Molenaar JJ, Koster J, Zwijnenburg DA, van Sluis P, Valentijn LJ, van der Ploeg I*, et al.* Sequencing of neuroblastoma identifies chromothripsis and defects in neuritogenesis genes. Nature **2012**;483(7391):589-93 doi 10.1038/nature10910.
174. Schleiermacher G, Janoueix-Lerosey I, Ribeiro A, Klijanienko J, Couturier J, Pierron G*, et al.* Accumulation of segmental alterations determines progression in neuroblastoma. J Clin Oncol **2010**;28(19):3122-30 doi 10.1200/JCO.2009.26.7955.
175. Egan CM, Nyman U, Skotte J, Streubel G, Turner S, O'Connell DJ*, et al.* CHD5 is required for neurogenesis and has a dual role in facilitating gene expression and

polycomb gene repression. Dev Cell **2013**;26(3):223-36 doi 10.1016/j.devcel.2013.07.008.
176. Henrich KO, Bauer T, Schulte J, Ehemann V, Deubzer H, Gogolin S*, et al.* CAMTA1, a 1p36 tumor suppressor candidate, inhibits growth and activates differentiation programs in neuroblastoma cells. Cancer Res **2011**;71(8):3142-51 doi 10.1158/0008-5472.CAN-10-3014.
177. Ichimiya S, Nimura Y, Kageyama H, Takada N, Sunahara M, Shishikura T*, et al.* p73 at chromosome 1p36.3 is lost in advanced stage neuroblastoma but its mutation is infrequent. Oncogene **1999**;18(4):1061-6 doi 10.1038/sj.onc.1202390.
178. Liu Z, Yang X, Li Z, McMahon C, Sizer C, Barenboim-Stapleton L*, et al.* CASZ1, a candidate tumor-suppressor gene, suppresses neuroblastoma tumor growth through reprogramming gene expression. Cell Death Differ **2011**;18(7):1174-83 doi 10.1038/cdd.2010.187.
179. Munirajan AK, Ando K, Mukai A, Takahashi M, Suenaga Y, Ohira M*, et al.* KIF1Bbeta functions as a haploinsufficient tumor suppressor gene mapped to chromosome 1p36.2 by inducing apoptotic cell death. J Biol Chem **2008**;283(36):24426-34 doi 10.1074/jbc.M802316200.
180. Ivics Z, Hackett PB, Plasterk RH, Izsvak Z. Molecular reconstruction of Sleeping Beauty, a Tc1-like transposon from fish, and its transposition in human cells. Cell **1997**;91(4):501-10.
181. Izsvak Z, Ivics Z, Plasterk RH. Sleeping Beauty, a wide host-range transposon vector for genetic transformation in vertebrates. J Mol Biol **2000**;302(1):93-102 doi 10.1006/jmbi.2000.4047.
182. Collier LS, Carlson CM, Ravimohan S, Dupuy AJ, Largaespada DA. Cancer gene discovery in solid tumours using transposon-based somatic mutagenesis in the mouse. Nature **2005**;436(7048):272-6 doi 10.1038/nature03681.
183. Dupuy AJ, Akagi K, Largaespada DA, Copeland NG, Jenkins NA. Mammalian mutagenesis using a highly mobile somatic Sleeping Beauty transposon system. Nature **2005**;436(7048):221-6 doi 10.1038/nature03691.
184. Collier LS, Adams DJ, Hackett CS, Bendzick LE, Akagi K, Davies MN*, et al.* Whole-body sleeping beauty mutagenesis can cause penetrant leukemia/lymphoma and rare high-grade glioma without associated embryonic lethality. Cancer Res **2009**;69(21):8429-37 doi 10.1158/0008-5472.CAN-09-1760.
185. Rahrmann EP, Collier LS, Knutson TP, Doyal ME, Kuslak SL, Green LE*, et al.* Identification of PDE4D as a proliferation promoting factor in prostate cancer using a Sleeping Beauty transposon-based somatic mutagenesis screen. Cancer Res **2009**;69(10):4388-97 doi 10.1158/0008-5472.CAN-08-3901.
186. Dupuy AJ, Rogers LM, Kim J, Nannapaneni K, Starr TK, Liu P*, et al.* A modified sleeping beauty transposon system that can be used to model a wide variety of human cancers in mice. Cancer Res **2009**;69(20):8150-6 doi 10.1158/0008-5472.CAN-09-1135.
187. Croise P, Houy S, Gand M, Lanoix J, Calco V, Toth P*, et al.* Cdc42 and Rac1 activity is reduced in human pheochromocytoma and correlates with FARP1 and

ARHGEF1 expression. Endocr Relat Cancer **2016**;23(4):281-93 doi 10.1530/ERC-15-0502.
188. Eccles RL, Czajkowski MT, Barth C, Muller PM, McShane E, Grunwald S*, et al.* Bimodal antagonism of PKA signalling by ARHGAP36. Nat Commun **2016**;7:12963 doi 10.1038/ncomms12963.
189. Rack PG, Ni J, Payumo AY, Nguyen V, Crapster JA, Hovestadt V*, et al.* Arhgap36-dependent activation of Gli transcription factors. Proc Natl Acad Sci U S A **2014**;111(30):11061-6 doi 10.1073/pnas.1322362111.
190. Ellenbroek SI, Collard JG. Rho GTPases: functions and association with cancer. Clin Exp Metastasis **2007**;24(8):657-72 doi 10.1007/s10585-007-9119-1.
191. Vega FM, Ridley AJ. Rho GTPases in cancer cell biology. FEBS Lett **2008**;582(14):2093-101 doi 10.1016/j.febslet.2008.04.039.
192. Rittinger K, Walker PA, Eccleston JF, Nurmahomed K, Owen D, Laue E*, et al.* Crystal structure of a small G protein in complex with the GTPase-activating protein rhoGAP. Nature **1997**;388(6643):693-7 doi 10.1038/41805.
193. Hui CC, Angers S. Gli proteins in development and disease. Annu Rev Cell Dev Biol **2011**;27:513-37 doi 10.1146/annurev-cellbio-092910-154048.
194. Zacharias WJ, Madison BB, Kretovich KE, Walton KD, Richards N, Udager AM*, et al.* Hedgehog signaling controls homeostasis of adult intestinal smooth muscle. Dev Biol **2011**;355(1):152-62 doi 10.1016/j.ydbio.2011.04.025.
195. Teglund S, Toftgard R. Hedgehog beyond medulloblastoma and basal cell carcinoma. Biochim Biophys Acta **2010**;1805(2):181-208 doi 10.1016/j.bbcan.2010.01.003.
196. Tukachinsky H, Lopez LV, Salic A. A mechanism for vertebrate Hedgehog signaling: recruitment to cilia and dissociation of SuFu-Gli protein complexes. J Cell Biol **2010**;191(2):415-28 doi 10.1083/jcb.201004108.
197. Humke EW, Dorn KV, Milenkovic L, Scott MP, Rohatgi R. The output of Hedgehog signaling is controlled by the dynamic association between Suppressor of Fused and the Gli proteins. Genes Dev **2010**;24(7):670-82 doi 10.1101/gad.1902910.
198. Liu A, Wang B, Niswander LA. Mouse intraflagellar transport proteins regulate both the activator and repressor functions of Gli transcription factors. Development **2005**;132(13):3103-11 doi 10.1242/dev.01894.
199. Chen MH, Wilson CW, Li YJ, Law KK, Lu CS, Gacayan R*, et al.* Cilium-independent regulation of Gli protein function by Sufu in Hedgehog signaling is evolutionarily conserved. Genes Dev **2009**;23(16):1910-28 doi 10.1101/gad.1794109.
200. Wang B, Fallon JF, Beachy PA. Hedgehog-regulated processing of Gli3 produces an anterior/posterior repressor gradient in the developing vertebrate limb. Cell **2000**;100(4):423-34.
201. Corbit KC, Aanstad P, Singla V, Norman AR, Stainier DY, Reiter JF. Vertebrate Smoothened functions at the primary cilium. Nature **2005**;437(7061):1018-21 doi 10.1038/nature04117.
202. Rohatgi R, Milenkovic L, Scott MP. Patched1 regulates hedgehog signaling at the primary cilium. Science **2007**;317(5836):372-6 doi 10.1126/science.1139740.

203. Wilson CW, Chuang PT. Mechanism and evolution of cytosolic Hedgehog signal transduction. Development **2010**;137(13):2079-94 doi 10.1242/dev.045021.
204. Briscoe J, Therond PP. The mechanisms of Hedgehog signalling and its roles in development and disease. Nat Rev Mol Cell Biol **2013**;14(7):416-29 doi 10.1038/nrm3598.
205. Niewiadomski P, Kong JH, Ahrends R, Ma Y, Humke EW, Khan S*, et al.* Gli protein activity is controlled by multisite phosphorylation in vertebrate Hedgehog signaling. Cell Rep **2014**;6(1):168-81 doi 10.1016/j.celrep.2013.12.003.
206. Skroblin P, Grossmann S, Schafer G, Rosenthal W, Klussmann E. Mechanisms of protein kinase A anchoring. Int Rev Cell Mol Biol **2010**;283:235-330 doi 10.1016/S1937-6448(10)83005-9.
207. Scott JD, Dessauer CW, Tasken K. Creating order from chaos: cellular regulation by kinase anchoring. Annu Rev Pharmacol Toxicol **2013**;53:187-210 doi 10.1146/annurev-pharmtox-011112-140204.
208. Taylor SS, Kim C, Vigil D, Haste NM, Yang J, Wu J*, et al.* Dynamics of signaling by PKA. Biochim Biophys Acta **2005**;1754(1-2):25-37 doi 10.1016/j.bbapap.2005.08.024.
209. Hammerschmidt M, Bitgood MJ, McMahon AP. Protein kinase A is a common negative regulator of Hedgehog signaling in the vertebrate embryo. Genes Dev **1996**;10(6):647-58.
210. Weigel D, Jurgens G, Kuttner F, Seifert E, Jackle H. The homeotic gene fork head encodes a nuclear protein and is expressed in the terminal regions of the Drosophila embryo. Cell **1989**;57(4):645-58.
211. Jackson BC, Carpenter C, Nebert DW, Vasiliou V. Update of human and mouse forkhead box (FOX) gene families. Hum Genomics **2010**;4(5):345-52.
212. Myatt SS, Lam EW. The emerging roles of forkhead box (Fox) proteins in cancer. Nat Rev Cancer **2007**;7(11):847-59 doi 10.1038/nrc2223.
213. Ang SL, Rossant J. HNF-3 beta is essential for node and notochord formation in mouse development. Cell **1994**;78(4):561-74.
214. Weinstein DC, Ruiz i Altaba A, Chen WS, Hoodless P, Prezioso VR, Jessell TM*, et al.* The winged-helix transcription factor HNF-3 beta is required for notochord development in the mouse embryo. Cell **1994**;78(4):575-88.
215. Aoki R, Shoshkes-Carmel M, Gao N, Shin S, May CL, Golson ML*, et al.* Foxl1-expressing mesenchymal cells constitute the intestinal stem cell niche. Cell Mol Gastroenterol Hepatol **2016**;2(2):175-88 doi 10.1016/j.jcmgh.2015.12.004.
216. Hannenhalli S, Kaestner KH. The evolution of Fox genes and their role in development and disease. Nat Rev Genet **2009**;10(4):233-40 doi 10.1038/nrg2523.
217. Zhu H. Forkhead box transcription factors in embryonic heart development and congenital heart disease. Life Sci **2016**;144:194-201 doi 10.1016/j.lfs.2015.12.001.
218. Halasi M, Gartel AL. FOX(M1) news--it is cancer. Mol Cancer Ther **2013**;12(3):245-54 doi 10.1158/1535-7163.MCT-12-0712.

219. Halmos B, Basseres DS, Monti S, D'Alo F, Dayaram T, Ferenczi K*, et al.* A transcriptional profiling study of CCAAT/enhancer binding protein targets identifies hepatocyte nuclear factor 3 beta as a novel tumor suppressor in lung cancer. Cancer Res **2004**;64(12):4137-47 doi 10.1158/0008-5472.CAN-03-4052.
220. Li CM, Gocheva V, Oudin MJ, Bhutkar A, Wang SY, Date SR*, et al.* Foxa2 and Cdx2 cooperate with Nkx2-1 to inhibit lung adenocarcinoma metastasis. Genes Dev **2015**;29(17):1850-62 doi 10.1101/gad.267393.115.
221. Wang J, Zhu CP, Hu PF, Qian H, Ning BF, Zhang Q*, et al.* FOXA2 suppresses the metastasis of hepatocellular carcinoma partially through matrix metalloproteinase-9 inhibition. Carcinogenesis **2014**;35(11):2576-83 doi 10.1093/carcin/bgu180.
222. Zhu CP, Wang J, Shi B, Hu PF, Ning BF, Zhang Q*, et al.* The transcription factor FOXA2 suppresses gastric tumorigenesis in vitro and in vivo. Dig Dis Sci **2015**;60(1):109-17 doi 10.1007/s10620-014-3290-4.
223. Katoh M, Katoh M. Identification and characterization of human FOXN5 and rat Foxn5 genes in silico. Int J Oncol **2004**;24(5):1339-44.
224. Santo EE, Ebus ME, Koster J, Schulte JH, Lakeman A, van Sluis P*, et al.* Oncogenic activation of FOXR1 by 11q23 intrachromosomal deletion-fusions in neuroblastoma. Oncogene **2012**;31(12):1571-81 doi 10.1038/onc.2011.344.
225. Deng X, Hou C, Liang Z, Wang H, Zhu L, Xu H. miR-202 Suppresses Cell Proliferation by Targeting FOXR2 in Endometrial Adenocarcinoma. Dis Markers **2017**;2017:2827435 doi 10.1155/2017/2827435.
226. Wang XH, Cui YX, Wang ZM, Liu J. Down-regulation of FOXR2 inhibits non-small cell lung cancer cell proliferation and invasion through the Wnt/beta-catenin signaling pathway. Biochem Biophys Res Commun **2018**;500(2):229-35 doi 10.1016/j.bbrc.2018.04.046.
227. Wang X, He B, Gao Y, Li Y. FOXR2 contributes to cell proliferation and malignancy in human hepatocellular carcinoma. Tumour Biol **2016**;37(8):10459-67 doi 10.1007/s13277-016-4923-3.
228. Lu SQ, Qiu Y, Dai WJ, Zhang XY. FOXR2 Promotes the Proliferation, Invasion, and Epithelial-Mesenchymal Transition in Human Colorectal Cancer Cells. Oncol Res **2017**;25(5):681-9 doi 10.3727/096504016X14771034190471.
229. Xu W, Chang J, Liu G, Du X, Li X. Knockdown of FOXR2 suppresses the tumorigenesis, growth and metastasis of prostate cancer. Biomed Pharmacother **2017**;87:471-5 doi 10.1016/j.biopha.2016.12.120.
230. Song H, He W, Huang X, Zhang H, Huang T. High expression of FOXR2 in breast cancer correlates with poor prognosis. Tumour Biol **2016**;37(5):5991-7 doi 10.1007/s13277-015-4437-4.
231. Liu X, Liu N, Yue C, Wang D, Qi Z, Tu Y*, et al.* FoxR2 promotes glioma proliferation by suppression of the p27 pathway. Oncotarget **2017**;8(34):56255-66 doi 10.18632/oncotarget.17447.
232. Conacci-Sorrell M, McFerrin L, Eisenman RN. An overview of MYC and its interactome. Cold Spring Harb Perspect Med **2014**;4(1):a014357 doi 10.1101/cshperspect.a014357.

233. Zack TI, Schumacher SE, Carter SL, Cherniack AD, Saksena G, Tabak B*, et al.* Pan-cancer patterns of somatic copy number alteration. Nat Genet **2013**;45(10):1134-40 doi 10.1038/ng.2760.
234. Dang CV. MYC on the path to cancer. Cell **2012**;149(1):22-35 doi 10.1016/j.cell.2012.03.003.
235. Morton JP, Sansom OJ. MYC-y mice: from tumour initiation to therapeutic targeting of endogenous MYC. Mol Oncol **2013**;7(2):248-58 doi 10.1016/j.molonc.2013.02.015.
236. Lal A, Navarro F, Maher CA, Maliszewski LE, Yan N, O'Day E*, et al.* miR-24 Inhibits cell proliferation by targeting E2F2, MYC, and other cell-cycle genes via binding to "seedless" 3'UTR microRNA recognition elements. Mol Cell **2009**;35(5):610-25 doi 10.1016/j.molcel.2009.08.020.
237. Kim HH, Kuwano Y, Srikantan S, Lee EK, Martindale JL, Gorospe M. HuR recruits let-7/RISC to repress c-Myc expression. Genes Dev **2009**;23(15):1743-8 doi 10.1101/gad.1812509.
238. Wall M, Poortinga G, Hannan KM, Pearson RB, Hannan RD, McArthur GA. Translational control of c-MYC by rapamycin promotes terminal myeloid differentiation. Blood **2008**;112(6):2305-17 doi 10.1182/blood-2007-09-111856.
239. Tseng YY, Moriarity BS, Gong W, Akiyama R, Tiwari A, Kawakami H*, et al.* PVT1 dependence in cancer with MYC copy-number increase. Nature **2014**;512(7512):82-6 doi 10.1038/nature13311.
240. Farrell AS, Sears RC. MYC degradation. Cold Spring Harb Perspect Med **2014**;4(3) doi 10.1101/cshperspect.a014365.
241. Boxer RB, Jang JW, Sintasath L, Chodosh LA. Lack of sustained regression of c-MYC-induced mammary adenocarcinomas following brief or prolonged MYC inactivation. Cancer Cell **2004**;6(6):577-86 doi 10.1016/j.ccr.2004.10.013.
242. D'Cruz CM, Gunther EJ, Boxer RB, Hartman JL, Sintasath L, Moody SE*, et al.* c-MYC induces mammary tumorigenesis by means of a preferred pathway involving spontaneous Kras2 mutations. Nat Med **2001**;7(2):235-9 doi 10.1038/84691.
243. Soucek L, Whitfield JR, Sodir NM, Masso-Valles D, Serrano E, Karnezis AN*, et al.* Inhibition of Myc family proteins eradicates KRas-driven lung cancer in mice. Genes Dev **2013**;27(5):504-13 doi 10.1101/gad.205542.112.
244. Frame MC, Patel H, Serrels B, Lietha D, Eck MJ. The FERM domain: organizing the structure and function of FAK. Nat Rev Mol Cell Biol **2010**;11(11):802-14 doi 10.1038/nrm2996.
245. Schaller MD, Borgman CA, Cobb BS, Vines RR, Reynolds AB, Parsons JT. pp125FAK a structurally distinctive protein-tyrosine kinase associated with focal adhesions. Proc Natl Acad Sci U S A **1992**;89(11):5192-6.
246. Schaller MD, Hildebrand JD, Shannon JD, Fox JW, Vines RR, Parsons JT. Autophosphorylation of the focal adhesion kinase, pp125FAK, directs SH2-dependent binding of pp60src. Mol Cell Biol **1994**;14(3):1680-8.
247. Zachary I. Focal adhesion kinase. Int J Biochem Cell Biol **1997**;29(7):929-34.

248. Miyazaki T, Kato H, Nakajima M, Sohda M, Fukai Y, Masuda N*, et al.* FAK overexpression is correlated with tumour invasiveness and lymph node metastasis in oesophageal squamous cell carcinoma. Br J Cancer **2003**;89(1):140-5 doi 10.1038/sj.bjc.6601050.
249. Itoh S, Maeda T, Shimada M, Aishima S, Shirabe K, Tanaka S*, et al.* Role of expression of focal adhesion kinase in progression of hepatocellular carcinoma. Clin Cancer Res **2004**;10(8):2812-7.
250. Xu B, Lefringhouse J, Liu Z, West D, Baldwin LA, Ou C*, et al.* Inhibition of the integrin/FAK signaling axis and c-Myc synergistically disrupts ovarian cancer malignancy. Oncogenesis **2017**;6(1):e295 doi 10.1038/oncsis.2016.86.
251. Kanteti R, Batra SK, Lennon FE, Salgia R. FAK and paxillin, two potential targets in pancreatic cancer. Oncotarget **2016**;7(21):31586-601 doi 10.18632/oncotarget.8040.
252. Parsons JT. Focal adhesion kinase: the first ten years. J Cell Sci **2003**;116(Pt 8):1409-16.
253. Schaller MD. Cellular functions of FAK kinases: insight into molecular mechanisms and novel functions. J Cell Sci **2010**;123(Pt 7):1007-13 doi 10.1242/jcs.045112.
254. Zhao J, Guan JL. Signal transduction by focal adhesion kinase in cancer. Cancer Metastasis Rev **2009**;28(1-2):35-49 doi 10.1007/s10555-008-9165-4.
255. Sulzmaier FJ, Jean C, Schlaepfer DD. FAK in cancer: mechanistic findings and clinical applications. Nat Rev Cancer **2014**;14(9):598-610 doi 10.1038/nrc3792.
256. Beckmann PJ, Larson JD, Larrson AT, Ostergaard JP, Wagner S, Rahrmann EO*, et al. Sleeping Beauty* insertional mutagenesis reveals important drivers in central nervous system embryonal tumorigenesis. Submitted **2018**.
257. Zindy F, Uziel T, Ayrault O, Calabrese C, Valentine M, Rehg JE*, et al.* Genetic alterations in mouse medulloblastomas and generation of tumors de novo from primary cerebellar granule neuron precursors. Cancer Res **2007**;67(6):2676-84 doi 10.1158/0008-5472.CAN-06-3418.
258. Tronche F, Kellendonk C, Kretz O, Gass P, Anlag K, Orban PC*, et al.* Disruption of the glucocorticoid receptor gene in the nervous system results in reduced anxiety. Nat Genet **1999**;23(1):99-103 doi 10.1038/12703.
259. Olive KP, Tuveson DA, Ruhe ZC, Yin B, Willis NA, Bronson RT*, et al.* Mutant p53 gain of function in two mouse models of Li-Fraumeni syndrome. Cell **2004**;119(6):847-60 doi 10.1016/j.cell.2004.11.004.
260. Xiao A, Yin C, Yang C, Di Cristofano A, Pandolfi PP, Van Dyke T. Somatic induction of Pten loss in a preclinical astrocytoma model reveals major roles in disease progression and avenues for target discovery and validation. Cancer Res **2005**;65(12):5172-80 doi 10.1158/0008-5472.CAN-04-3902.
261. Sarver AL, Erdman J, Starr T, Largaespada DA, Silverstein KA. TAPDANCE: an automated tool to identify and annotate transposon insertion CISs and associations between CISs from next generation sequence data. BMC Bioinformatics **2012**;13:154 doi 10.1186/1471-2105-13-154.

262. Temiz NA, Moriarity BS, Wolf NK, Riordan JD, Dupuy AJ, Largaespada DA*, et al.* RNA sequencing of Sleeping Beauty transposon-induced tumors detects transposon-RNA fusions in forward genetic cancer screens. Genome Res **2016**;26(1):119-29 doi 10.1101/gr.188649.114.
263. Scott MC, Temiz NA, Sarver AE, LaRue RS, Rathe SK, Varshney J*, et al.* Comparative Transcriptome Analysis Quantifies Immune Cell Transcript Levels, Metastatic Progression, and Survival in Osteosarcoma. Cancer Res **2018**;78(2):326-37 doi 10.1158/0008-5472.CAN-17-0576.
264. Marko TA, Shamsan GA, Edwards EN, Hazelton PE, Rathe SK, Cornax I*, et al.* Slit-Robo GTPase-Activating Protein 2 as a metastasis suppressor in osteosarcoma. Sci Rep **2016**;6:39059 doi 10.1038/srep39059.
265. Lin MH, Lee YH, Cheng HL, Chen HY, Jhuang FH, Chueh PJ. Capsaicin Inhibits Multiple Bladder Cancer Cell Phenotypes by Inhibiting Tumor-Associated NADH Oxidase (tNOX) and Sirtuin1 (SIRT1). Molecules **2016**;21(7) doi 10.3390/molecules21070849.
266. Snyder EY, Deitcher DL, Walsh C, Arnold-Aldea S, Hartweieg EA, Cepko CL. Multipotent Neural Cell Lines Can Engraft and Participate in Development of Mouse Cerebellum. Cell **1992**;68:33-51.
267. Holterman CE, Le Grand F, Kuang S, Seale P, Rudnicki MA. Megf10 regulates the progression of the satellite cell myogenic program. J Cell Biol **2007**;179(5):911-22 doi 10.1083/jcb.200709083.
268. Lin JR, Mondal AM, Liu R, Hu J. Minimalist ensemble algorithms for genome-wide protein localization prediction. BMC Bioinformatics **2012**;13:157 doi 10.1186/1471-2105-13-157.
269. Zerbino DR, Achuthan P, Akanni W, Amode MR, Barrell D, Bhai J*, et al.* Ensembl 2018. Nucleic Acids Res **2018**;46(D1):D754-D61 doi 10.1093/nar/gkx1098.
270. Ortiz B, Fabius AW, Wu WH, Pedraza A, Brennan CW, Schultz N*, et al.* Loss of the tyrosine phosphatase PTPRD leads to aberrant STAT3 activation and promotes gliomagenesis. Proc Natl Acad Sci U S A **2014**;111(22):8149-54 doi 10.1073/pnas.1401952111.
271. Dali R, Verginelli F, Pramatarova A, Sladek R, Stifani S. Characterization of a FOXG1:TLE1 transcriptional network in glioblastoma initiating cells. Mol Oncol **2018** doi 10.1002/1878-0261.12168.
272. Fontebasso AM, Schwartzentruber J, Khuong-Quang DA, Liu XY, Sturm D, Korshunov A*, et al.* Mutations in SETD2 and genes affecting histone H3K36 methylation target hemispheric high-grade gliomas. Acta Neuropathol **2013**;125(5):659-69 doi 10.1007/s00401-013-1095-8.
273. Murtaza M, Jolly LA, Gecz J, Wood SA. La FAM fatale: USP9X in development and disease. Cell Mol Life Sci **2015**;72(11):2075-89 doi 10.1007/s00018-015-1851-0.
274. Cianfanelli V, Fuoco C, Lorente M, Salazar M, Quondamatteo F, Gherardini PF*, et al.* AMBRA1 links autophagy to cell proliferation and tumorigenesis by promoting c-Myc dephosphorylation and degradation. Nat Cell Biol **2015**;17(1):20-30 doi 10.1038/ncb3072.

275. Katoh M, Igarashi M, Fukuda H, Nakagama H, Katoh M. Cancer genetics and genomics of human FOX family genes. Cancer Lett **2013**;328(2):198-206 doi 10.1016/j.canlet.2012.09.017.
276. Walz S, Lorenzin F, Morton J, Wiese KE, von Eyss B, Herold S*, et al.* Activation and repression by oncogenic MYC shape tumour-specific gene expression profiles. Nature **2014**;511(7510):483-7 doi 10.1038/nature13473.
277. Dong X, Wang C, Chen Z, Zhao W. Overcoming the resistance mechanisms of Smoothened inhibitors. Drug Discov Today **2018** doi 10.1016/j.drudis.2018.01.012.
278. Ramaswamy V, Remke M, Bouffet E, Bailey S, Clifford SC, Doz F*, et al.* Risk stratification of childhood medulloblastoma in the molecular era: the current consensus. Acta Neuropathol **2016**;131(6):821-31 doi 10.1007/s00401-016-1569-6.
279. Jain S, Wang X, Chang CC, Ibarra-Drendall C, Wang H, Zhang Q*, et al.* Src Inhibition Blocks c-Myc Translation and Glucose Metabolism to Prevent the Development of Breast Cancer. Cancer Res **2015**;75(22):4863-75 doi 10.1158/0008-5472.CAN-14-2345.
280. Rajbhandari P, Lopez G, Capdevila C, Salvatori B, Yu J, Rodriguez-Barrueco R*, et al.* Cross-Cohort Analysis Identifies a TEAD4-MYCN Positive Feedback Loop as the Core Regulatory Element of High-Risk Neuroblastoma. Cancer Discov **2018**;8(5):582-99 doi 10.1158/2159-8290.CD-16-0861.
281. Boeva V, Louis-Brennetot C, Peltier A, Durand S, Pierre-Eugene C, Raynal V*, et al.* Heterogeneity of neuroblastoma cell identity defined by transcriptional circuitries. Nat Genet **2017**;49(9):1408-13 doi 10.1038/ng.3921.
282. Sumara I, Quadroni M, Frei C, Olma MH, Sumara G, Ricci R*, et al.* A Cul3-based E3 ligase removes Aurora B from mitotic chromosomes, regulating mitotic progression and completion of cytokinesis in human cells. Dev Cell **2007**;12(6):887-900 doi 10.1016/j.devcel.2007.03.019.
283. Schabhuttl M, Wieland T, Senderek J, Baets J, Timmerman V, De Jonghe P*, et al.* Whole-exome sequencing in patients with inherited neuropathies: outcome and challenges. J Neurol **2014**;261(5):970-82 doi 10.1007/s00415-014-7289-8.